NEUTRON SCATTERING STUDIES OF LOCAL MOTIONS IN POLYMER CHAINS

A thesis submitted for the Degree of Doctor of Philosophy of the University of London and for the Diploma of Imperial College

by

Karen Talya Ma B.Sc(Hons) Imperial College

Department of Chemical Engineering
and Chemical Technology,
Imperial College of Science and Technology,
London SW7.

June 1981

Abstract

The work presented in this thesis provides an example of how inelastic and quasi-elastic neutron scattering techniques may be used to give detailed information about the local dynamics of polymer chains.

The vibrational and rotational motion of the side groups in poly(methyl methacrylate) have been studied at some length,and values of torsional frequencies and rotational frequencies obtained for both the α-methyl and ester methyl group.These have been related to activation energies and barrier heights to rotation, leading to a discussion of the possibility of quantum mechanical tunnelling.The effect of stereoregularity on the values of these parameters is also considered,with reference to measurements made on stereoregular samples.The concept on the elastic incoherent structure factor(EISF) as a means of characterising completely the geometry of the methyl group rotation is discussed in great detail for both methyl groups.A series of supplementary experiments concerned with the measurement of coherent scattering from poly(methyl methacrylate) has given useful information about local structure in the amorphous material.

Results obtained from neutron scattering experiments have been useful in leading to a greater understanding of the dynamics of polymer networks.Quasi-elastic scattering experiments from modified samples of natural rubber have shown the effectiveness of hydrogen bonds in forming a high degree of crosslinking, and thus a totally hydrogen-bonded network.Measurements on polyester networks containing permanent chemical crossslinks have been made to investigate the relative motion of the crosslink points and chains between crosslinks.It is found that the crosslinks are moving at about half the rate of the chains, and furthermore, that the chains between crosslink points are observed to behave exactly as free chains in the melt.

TABLE OF CONTENTS

		Page
Abstract		2
Table of Contents		3
List of Tables		6
List of Figures		6
Acknowledgements		9
Chapter 1	Introduction	10
Chapter 2	General Neutron Scattering	17
2.1	Basic Principles of Neutron Scattering Theory	17
2.1.1	Energy and Momentum Transfer in the Scattering Process	17
2.1.2	Scattering from a Single Nucleus	18
2.1.3	Scattering from an Array of Nuclei-Coherent and Incoherent Scattering	19
2.1.4	The Double Differential Cross-section	20
2.1.5	The Scattering Law, $S(Q,\omega)$ and the van Hove Correlation Functions	22
2.2	Experimental Techniques and Instrumentation	25
2.2.1	Use of a Cold Source	26
2.2.2	The Backscattering Spectrometer, IN10	26
2.2.3	The Time-of-Flight Spectrometer, IN5	29
2.2.4	The Time-of-Flight Spectrometer, IN6	31
2.2.5	The Time-of-Flight Spectrometer, 4H5	32
2.2.6	The Powder Diffractometer, 10H	34
2.2.7	Use of Vanadium as a Standard	36
2.2.8	Sample Heating during Experiments	36
2.2.9	Sample Containers	36
2.3	Data Analysis	39
2.3.1	Analysis of Quasi-elastic data from IN10	39
2.3.2	Analysis of Quasi-elastic data from IN5	42
2.3.3	Analysis of Inelastic data from 4H5	47
2.3.4	Analysis of IN6 data	49
2.3.5	Analysis of 10H data	49
Chapter 3	Application of Neutron Scattering to the Study of Sidechain Motion in PMMA	50
3.1	Theoretical Considerations	50

TABLE OF CONTENTS(cont.)

3.1.1	Theory of Incoherent Scattering from a Polymer Molecule	50
3.1.2	The Scattering Law for Molecular Vibrations, $S_{inc}^{vib}(Q,\omega)$	53
3.1.3	Calculation of Barrier Height from Inelastic Data	57
3.1.4	The Rotational Scattering Law, $S_{inc}^{rot}(Q,\omega)$	59
3.1.5	Rotational Motion Between N equivalent Sites on a Circle of Radius r	63
3.1.6	Calculation of the EISF for Complex Rotations	65
3.1.7	Temperature Dependence of the Mean Jump Time,and Calculation of the Activation Energy	70
3.1.8	Relationship between E_a and V_3	72
3.1.9	The Question of Quantum Mechanical Tunnelling	72
3.2	Sample Preparation	73
3.3	Experimental Results and Interpretation	81
3.3.1	Inelastic Scattering Results	81
3.3.2	Consideration of Errors in extacting $\rho(\omega)$	87
3.3.3	Interpretation of Inelastic Measurements and assignment of peaks in $\rho(\omega)$	88
3.3.4	Quasi-elastic Scattering Results relating to the Rotational Motion of the ester-methyl group in PMMA	95
3.3.5	Corrections to the Calculated EISF for Comparison with Experimental Values	98
3.3.6	Experimental Values of the EISF and the Problem of Coherent Scattering	102
3.3.7	Experimental Values of Rotational Frequencies and Activation Enegries for the ester-methyl Group	123
3.3.8	Results relating to the Rotational Motion of the α-methyl Group in PMMA	125
3.3.9	Consideration of Errors for Quasi-elastic Data	128
3.3.10	The Structure Factor,S(Q)	130

TABLE OF CONTENTS(cont.)

	3.3.11	Discussion and Comparison of E_a and V_3	133
	3.4	Final Discussion of Results and the Application of Neutron Scattering to the Investigation of Sidegroup Motion in PMMA	142
Chapter 4		Application of Quasi-elastic Neutron Scattering to the Observation of the Dynamics of Polymer Networks	146
	4.1	Theoretical Considerations	147
	4.2	Sample Preparation	149
	4.2.1	Preparation of Modified Natural Rubber Samples	149
	4.2.2	Preparation of Polyester Networks	150
	4.2.3	Measurement of the Shear Modulus, G_0	151
	4.2.4	Preparation of Polypropylene Oxide Chains	153
	4.3	Quasi-elastic Scattering Results from Polymer Networks	154
	4.3.1	Results Obtained from Modified Natural Rubber in the Bulk	154
	4.3.2	Results obtained from Dilute Solutions of the Natural Rubber Samples	154
	4.3.3	Results Obtained from the Polyester Networks	158
	4.3.4	Results obtained from the Low Molecular Weight Polypropylene Oxide Chains	163
	4.4	Consideration of Errors	163
	4.5	Discussion of Results	169
	4.5.1	Discussion of Results Obtained from Modified Natural Rubber Samples	169
	4.5.2	Discussion of Polyester Network Results	170
Chapter 5		Conclusions and Aims for Future Work	176
	5.1	Conclusions from the Investigation of poly(methyl methacrylate)	176
	5.2	Conclusions from the Investigation of the Local Dynamics of Rubber Networks	178
	5.3	Concluding Remarks	180
References			182

LIST OF TABLES

		Page
Table 1.1	Application of Neutron Scattering to the Investigation of Polymer Systems	11
2.1	Scattering Cross-sections for some Common Elements	19
3.1	Assignment of Bands in Inelastic Neutron Scattering Spectra	94
3.2	Torsional Frequencies and Barrier Heights Obtained from Inelastic Measurements	95
3.3	Variation of the Width of the Quasi-elastic Component with Temperature for PMMA3	123
3.4	Variation of the Width of the Quasi-elastic Component for Stereoregular PMMA	123
3.5	Variation of the Width of the Quasi-elastic Component for PMMA1	128
3.6	Comparison of V_3 and E_a from various sources for the α-methyl Group in PMMA	135
3.7	Comparison of V_3 and E_a for the ester-methyl Group in PMMA	135

LIST OF FIGURES

Figure 2.1	The Backscattering Spectrometer,IN10	27
2.2	The Time-of-Flight Spectrometer.IN5	30
2.3	The Time-of-Flight Spectrometer,4H5	33
2.4	10H,Powder Diffractometer	35
3.1	EISF for Random Jump Between 3 Sites	66
3.2	EISF for Random Jump Between 2 and 4 sites	66
3.3	EISF for Complex Rotation	71
3.4	Variation of Torsional Frequency with Temperature for Different Barriers	74
3.5	NMR Spectrum for PMMA2	76
3.6	NMR Spectrum for ISOT1	77
3.7	NMR Spectrum for SYNDIO1	80
3.8	Frequency Distribution Function for PMMA1	83
3.9	Sum of $g(\omega)$ for PMMA1 (4H5)	83
3.10	$\rho(\omega)$ for PMMA2 (4H5)	84
3.11	Sum of $g(\omega)$ for PMMA2 (4H5)	84
3.12	$\rho(\omega)$ for PMMA3 (4H5)	85
3.13	Sum of $g(\omega)$ for PMMA3 (4H5)	85

LIST OF FIGURES (cont.)

Figure 3.14	$\rho(\omega)$ for ISOT1 (IN6)	86
3.15	$\rho(\omega)$ for PMMA3 (IN6)	87
3.16	$\rho(\omega)$ for SYNDIO1 (IN6)	87
3.17	$S(Q,\omega)$ for PMMA3, $\theta=43^0$, $T=47^0C$ (IN5)	96
3.18	$S(Q,\omega)$ for PMMA3, $\theta=62^0$, $T=47^0C$ (IN5)	96
3.19	$S(Q,\omega)$ for PMMA3, $\theta=82^0$, $T=47^0C$ (IN5)	97
3.20	$S(Q,\omega)$ for PMMA3, $\theta=119^0$, $T=47^0C$ (IN5)	97
3.21	$S(Q,\omega)$ for ISOT1, $\theta=62^0$, $T=25^0C$ (IN5)	99
3.22	$S(Q,\omega)$ for ISOT1, $\theta=102^0$, $T=25^0C$ (IN5)	100
3.23	Corrected EISF for Rotation of ester-methyl group in PMMA	103
3.24	3-fold Jump Model fitted to PMMA3, $Q=1.166\text{Å}^{-1}$, and $Q=2.056\text{Å}^{-1}$, $T=47^0C$	105
3.25	3-fold Jump Model fitted to PMMA3 $Q=1.166\text{Å}^{-1}$, $T=60^0C$ and $Q=1.362\text{Å}^{-1}$, $T=88^0C$	106
3.26	3-fold Jump Model fitted to PMMA3, $Q=1.166\text{Å}^{-1}$, and $Q=1.55\text{Å}^{-1}$, $T=118^0C$	107
3.27	3-fold Jump Model fitted to PMMA3, $Q=1.362\text{Å}^{-1}$ and $Q=2.056\text{Å}^{-1}$, $T=25^0C$	108
3.28	δ-function+single Lorentzian fit to PMMA3	109
3.29	3-fold Jump Model fit to ISOT1 $Q=1.55\text{Å}^{-1}$ and $Q=2.056\text{Å}^{-1}$, $T=25^0C$	110
3.30	Experimental Values of the EISF for PMMA3 (IN5) at different Temperatures	112
3.31	Comparison of the Experimental Values of the EISF obtained from IN5 and IN6	113
3.32	Experimental Values of the EISF for Stereoregular PMMA	115
3.33	Coherent Scattering from PMMA3	117
3.34	Wide angle X-ray Scattering from PMMA	118
3.35	Structure Factor, S(Q), for PMMA	121
3.36	Arrhenius Plot for ester-methyl group in PMMA	124
3.37	Experimental Values of the EISF for PMMA1	126
3.38	Experimental Values of the EISF for PMMA1 (combination of IN5 and IN10 data)	127
3.39	Arrhenius Plot for α-methyl rotation	129
3.40	Proposed Model of PMMA	132

LIST OF FIGURES (cont.)

Figure 4.1	Polyester Networks	152
4.2	Raw Data from R1	155
4.3	Raw Data from R7	156
4.4	Results from R1,R5 and R7	157
4.5	Results from R1,R5 and R7 in solution	159
4.6	$S(Q,\omega)$ for N2 ($Q=0.19\text{Å}^{-1}$ and 0.31Å^{-1})	160
4.7	$S(Q,\omega)$ for N2 ($Q=0.59\text{Å}^{-1}$ and 0.97Å^{-1})	161
4.8	Logarithmic Plot of FWHM against Q for Polyester Networks	162
4.9	Variation of $\Delta E/Q^2$ with Q for Polyester Networks	164
4.10	Double Logarithmic Plot of FWHM against Q for (N1-N2), and a High Molecular Weight Sample of Pure PPO	165
4.11	Comparison of Variation of FWHM with Q for PPO1 and PPO2	166
4.12	Variation of $\Delta E/Q^2$ with Q for PPO chains	167
4.13	Comparison of Spectrum obtained from (N1-N2) with Vanadium	168
4.14	Comparison of Low and High Molecular Weight PPO	174

Acknowledgements

I would like to offer thanks to my supervisor,Dr.J.S.Higgins, for her continual support and encouragement during this project.

Thanks are due to all my friends and colleagues at the ILL,Grenoble,and,in particular,to Dr.R.Ghosh,Dr.G.Jenkin, Dr.J.Hayter,Dr.C.Poinsignon,Dr.A.Heidemann,Dr.J.Beaufils and Mr.J.Bauchat.

I would like to thank everyone at the Materials Physics Division,AERE,Harwell,for their unremitting help during experiments,and particularly to Mr.V.Rainey,Mr.D.H.Harris, Mr.D.Cummings,Mrs.O.Price,Mr.J.Seymour,Mr.G.Proudfoot,Mr.G. Haines,Mr.S.Stevens,Mr.A.Baston and Mr.S.Sinclair.

Thanks are due to all my friends at the Rutherford Laboratory,for their help with data analysis,and I would like to thank,in particular,Dr.R.Richardson,Dr.M.Johnson, Dr.A.Taylor and Dr.S.Howells.

Acknowledgement is due to Dr.R.H.Hall,for his time and trouble taken in preparing the samples.

Thanks are due to workers at the Malaysian Rubber Producers' Research Association,for both supplying samples, and providing useful discussion.

I am grateful to all my friends here at Imperial College,and,in particular,to Dr.M.Letherby,Dr.C.L.Chong, Mr.A.Carter,Ms.A.Hill,Dr.A.Maconnachie,Dr.L.K.Nicholson, Dr.D.A.Young and Dr.J.Davis,for their helpful advice and comments.I would like to thank members of the workshop for their ready willingness to help whenever required.

I would like to thank my husband for his eternal optimism,and my parents,without whom,none of this would have been possible.

I acknowledge the financial support of the SRC.

Chapter 1. Introduction

The application of neutron scattering to the study of the structure and dynamics of polymers has become a widely established technique in recent years[1,2,3].The main area to benefit from the introduction of neutron scattering is in the understanding of amorphous polymers, since considerable information about the crystalline state may be obtained using X-ray diffraction and other conventional spectroscopic techniques.

Thermal neutrons have wavelengths in the range 2-20$\AA^{-1}$ and energies between 400 and 0.4 J/mol.It is this combination which makes the neutron such a valuable tool in the study of the structure and dynamics of matter, since the neutron wavelengths are of a magnitude approximately equal to that of interatomic separations, whilst the energies involved are of the same order as molecular vibrations.In addition, since the neutron is an uncharged particle, it can penetrate deeply into matter, and as it possesses a magnetic moment it can interact with unpaired electrons present to give detailed information about the magnetic properties of the system.

Broadly speaking, neutron scattering experiments performed on polymers may be divided into two categories- measurement of coherent scattering (which gives information about the relative positions of different nuclei) and incoherent scattering (giving details about individual atoms) -this distinction is discussed in greater depth in section 2.1.3.The scattering may then be further subdivided into elastic and inelastic scattering.

The following table summarises the various neutron scattering techniques, and their applicability to obtaining specific information about polymer systems (from 3).

Table 1.1 Application of Neutron Scattering to the Investigation of Polymer Systems.

Type of Experiment	Apparatus Used	Sample Form	Information Obtained
Elastic coherent	Diffract-ometer	Polymer crystals	Short-range structure
	Small-angle scattering spectrometer	Rubbers, melts, glasses, solutions	Molecular dimensions &conformation
Quasielastic coherent & incoherent	High resolution T.O.F and backscattering	Melts, solutions, glasses	Molecular dynamics
Inelastic coherent	Triple axis and T.O.F	Poly-crystals, single crystals	Dispersion curves,elastic constants and intermolecular potentials
Inelastic incoherent	T.O.F	Rubbers & glasses	Molecular spectra and lattice vibrations -inter & intra molecular potentials

Having outlined the general usefulness of neutron scattering for obtaining information about polymer systems, the following discussion will be confined to the application of the technique to studying local dynamics only, and with particular reference to the main chain dynamics of polymer networks, and sidechain motions of poly(methyl methacrylate) (PMMA).From table 1.1 it is clear that the most useful technique for studying these systems will be the measurement of quasi-elastic coherent and incoherent scattering, and inelastic incoherent scattering.Consequently, the work presented in this thesis has been almost exclusively involved with these aspects of neutron scattering.

The aims of the series of experiments performed on the networks were two-fold.Firstly, it was hoped to obtain detailed information about the contribution of hydrogen-bonding in forming temporary crosslink points in natural rubber samples which had been modified to have highly polar sidegroups.This investigation arose as a result of collaboration with workers from the Malaysian Rubber Producers Research Association (MRPRA), who were interested in modifications to natural rubber which would decrease the rate of crystallisation at low temperatures (below 0^0C), and thus improve the storage properties of the material before processing.In interpreting the results relating to the degree of crystallisation,it is difficult to know to what extent loss of stereoregularity, steric hindrance due to the size of the modifying groups and interactions between neighbouring chains contribute to the observed effect.Consequently,conclusive neutron scattering results confirming the effect of at least one of these (in this case the effect on chain mobility of hydrogen bonding between neighbouring chains) would be of some use in interpreting the rate of crystallisation data.

The aim of the second series of experiments was to observe the difference (if any) between the motion of the crosslink points and chains between crosslink points in a network.To date, no experiments have been reported which can successfully separate the motion of the two components of the system, so conclusive information obtained using neutron scattering could be most useful.

The use of quasi-elastic neutron scattering to obtain information about the dynamics of the main chains of polymers in the bulk has been widespread in recent years.The quasi-elastic spectra obtained from polymers in the bulk are characterised by a single quasi-elastic component whose width is strongly Q dependent (where Q is the momentum transfer in the scattering process).Such behaviour is indicative of translational motion in the system, and since the melt is the liquid state of a polymer, preliminary investigations involved analysing the data in terms of an effective diffusion

coefficient, by assuming that the scattering law for the system could be described in terms of a single Lorentzian whose full width half maximum (FWHM) should vary as Q^2, in analogy to a simple liquid[4 5 6].However, it was clear that the Q dependence of the FWHM of the spectra was much greater than Q^2, and in addition, the measured data was only poorly fitted by a single Lorentzian, with a marked discrepancy between the observed spectra and fitted Lorentzian in the wings.

In the low Q region, it was proposed that the motion of a polymer might well be described by the Rouse model[7], in which the polymer chain is described in terms of the normal modes of a set of beads connected by Hookean springs. Using the Rouse model as a basis, a scattering law may be calculated[8].The scattering law in this case is predicted to have greater intensity in the wings than a simple Lorentzian, and a FWHM varying as Q^4.Much work in recent years has involved verifying the applicability of the Rouse model to polymers in the melt[9 10] and conclusions reached most recently[11] suggest that in the range $1/R_g<Q<1/\sigma$ (where R_g is the radius of gyration of the chain, and σ the length of one bead-spring segment) the local motion of the polymer backbone may be well described by this model.

A similar situation has arisen for the case of polymers in dilute solution, where it is found that the motion cannot be adequately described in terms of a single Lorentzian (corresponding to Brownian diffusion) in the Q range explored by most neutron scattering experiments.Quasi-elastic results have shown[12 13 14] that the main chain motion of polymers in dilute solution is best described in terms of the Zimm model[15] again applicable in the range $1/R_g< Q<1/\sigma$.In this case, the scattering law calculated by de Gennes[16] predicts a FWHM variation of the quasi-elastic component with Q^3.

Although some small angle scattering measurements have been made on polymer networks[17] , very little quasi-elastic scattering work has been done to study the local motions of the chains in the system.One exception is that of Walsh et al[18] , who investigated the effect of hydrogen bonding on

chain mobility in urethane networks.Little theoretical work has been done in terms of predicting the scattering law for polymer networks, or indeed, to describe the chain motion quantitatively in any way at all. A recent paper[19], however, discusses the relative motion of the crosslink points and chains in a network, and is therefore of some relevance to the work discussed in chapter 4.

On the other hand, a considerable amount of work has been published relating to the sidechain motion in polymers, obtained using not only neutron scattering, but NMR and mechanical and dielectric relaxation techniques as well. With regard to neutron scattering, the motion of the side groups may be investigated using both quasi-elastic techniques to obtain the rotational scattering law, and also inelastic incoherent scattering methods to obtain the frequency distribution function and vibrational frequencies of the molecule, thus leading to calculations of barrier heights to rotation.

With particular reference to PMMA, some interesting neutron scattering measurements regarding the vibrational motion of the two methyl groups have been reported[20 21 22]. It has been found that the torsional frequencies (and thus the barrier height) of the α-methyl group are strongly dependent on the specific stereoregularity of the polymer, and final results quoted[22] give a value of V_3 of 33kJ/mol for syndiotactic PMMA, and 23kJ/mol for isotactic PMMA.A value of 5.0kJ/mol is also quoted[21] for the ester methyl group in an atactic sample of PMMA.This strong dependence of V_3 on tacticity for the α-methyl group has also been observed by other workers using NMR and other relaxation techniques[23 24 25 26 27 28]. Values of E_a[29] obtained are as follows; for syndiotactic PMMA, 23-35 kJ/mol and for isotactic PMMA, 16 kJ/mol. In order to compare the values of E_a obtained using relaxation techniques with the values of V_3 obtained using inelastic neutron scattering, the problem of quantum mechanical tunnelling must be considered.Strong evidence for quantum mechanical tunnelling at low temperatures in the methyl groups in PMMA has been presented by various workers[27 29 30 31].This means that

values of E_a and V_3 are not directly comparable, but if E_a is used to obtain a value of V_3(NMR) as suggested in 22, V_3(NMR) and V_3(neutron scattering) may be compared.Adopting this approach,V_3(NMR) for the α-methyl group in isotactic PMMA is found to be 22.6 kJ/mol and V_3(NMR) for syndiotactic PMMA to be 30 kJ/mol.These revised values are now in excellent agreement with the neutron scattering values of V_3 quoted above.

Somewhat less information is available regarding the rotation of the ester methyl group.The only inelastic neutron scattering value of the barrier height obtained (for atactic PMMA) is that quoted above, of 5.0 kJ/mol.Since this rotation sets in at extremely low temperatures (below 4.2K)[21 27 32] , it is difficult to obtain reliable NMR data, and the only value of E_a quoted is again for atactic PMMA[24] .This is tentatively given as 2.9 kJ/mol, although the result is somewhat uncertain.No values of either V_3 or E_a for the ester methyl group in stereoregular PMMA have been found in the literature.

As indicated earlier,in addition to obtaining values of V_3 for the methyl groups using inelastic scattering techniques, it is also possible to obtain rotational frequencies from quasi-elastic measurements.If this is done over a range of temperatures,an activation energy,E_a, may be obtained for direct comparison with values of E_a given by relaxation techniques.No values of E_a for either of the methyl groups in PMMA using quasi-elastic neutron scattering are reported in the literature to date.

The series of inelastic and quasi-elastic neutron scattering experiments performed on PMMA was intended to provide a detailed and comprehensive set of results relating to the motion of the two methyl sidegroups.For the α-methyl group, values of V_3 obtained on stereoregular samples would be compared to those obtained previously, and, in addition, measurement of the rotational frequency at several temperatures should provide a value of E_a for comparison with relaxation measurements.Since no measurements have been reported in the literature relating the stereoregularity of the polymer to

the motion of the ester methyl group, it was intended that conclusive evidence would be obtained using neutron scattering to establish the effect of tacticity on E_a and V_3.

In addition to providing a value of the rotational frequency, quasi-elastic neutron scattering data from side-groups also gives specific information about the actual geometry of the rotation[33] .Neutron scattering is the only spectroscopic technique which can do this.The parameter obtained from the measurements is the Elastic Incoherent Structure Factor (EISF), which is the time averaged spatial distribution function of the moving protons in the system.Although the EISF has never been measured for the two methyl groups in PMMA, its usefulness has been demonstrated by a number of workers[33 34 35 36 37 38] , who have shown that careful measurement of the EISF allows exact determination of the geometry of the rotation, so that of a number of different possible motions in a system, all may be discounted except one. Thus the measurement of the EISF for the ester methyl group in PMMA should be particularly useful in determining the exact combination of motions involved in the rotation of this group.

In chapters 3 and 4, the results referred to briefly above will be discussed in more detail, in comparing them with results obtained from the set of experiments described in this thesis.

Chapter 2. General Neutron Scattering

This chapter deals with general aspects of neutron scattering.The basic theory is discussed, followed by a description of the instruments used to obtain the results presented in chapters 3 and 4.An outline of the methods used to analyse the raw data concludes the chapter.More detailed theory and methods of data analysis relating specifically to sidechain motion and the dynamics of main chains are given in the appropiate chapters.

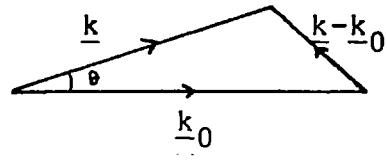
2.1 Basic Principles of Neutron Scattering Theory

In order to describe a scattering event between a neutron and a nucleus, consideration must be given to two processes.The main interaction is via purely nuclear forces - this is known as nuclear scattering.An alternative interaction is possible if there are unpaired electrons present, when the magnetic moment of the neutron may interact with the magnetic moments of the unpaired electrons, leading to magnetic scattering.Magnetic scattering is not encountered in the polymer systems under discussion in this thesis, so future considerations are limited to only nuclear scattering processes by thermal neutrons.

The basic theory described in this section is intended by way of a general outline only, and a more detailed description may be found elsewhere[39 40 41] .

2.1.1 Energy and Momentum Transfer in the Scattering Process

$k_0=2\pi/\lambda_0$



Consider an incident beam of neutrons with initial energy and wavevector E_0 and $\underline{k}_0$ respectively to be scattered by a sample at an angle θ, as shown schematically in the

vector diagram above.If the energy and wavevector after the scattering event are E and $\underline{k}$, then the energy transfer in the process,ΔE, is given by

$$\Delta E = \hbar\omega = E - E_0 \qquad (2.1)$$

and the momentum transfer , $\hbar Q$, by

$$\hbar\underline{Q} = \hbar(\underline{k} - \underline{k}_0) \qquad (2.2)$$

Using (2.1), (2.2) and elementary geometry,

$$Q = (k^2 + k_0^2 - 2kk_0\cos\theta)^{\frac{1}{2}} \qquad (2.3)$$

In a purely elastic process, $k = k_0$ and (2.3) reduces to

$$Q = \frac{4\pi}{\lambda_0}\sin\frac{\theta}{2}$$

2.1.2 Scattering from a Single Nucleus - Relationship Between the Scattering Length,b, and the Cross-Section,σ

The interaction potential between the incoming neutron and the scattering nucleus is very short range- of the order of 1.5×10^{-15}m.Since this is considerably less than the wavelength of the incident neutron (typically $\sim 10^{-10}$m), the neutron-nucleus scattering function will contain only s-wave components[41] and the scattering will be purely isotropic.In addition, for distances very much greater than r_0 (where r_0 defines the range of the interaction) it can be shown[41] that the amplitude of the scattered wave may be defined by only a single parameter, the scattering length,b.b is usually positive, although it may be negative, or even complex, in which case the imaginery component represents absorption (which is small, in most cases).The scattering length varies in a random manner throughout the periodic table, and for any given atomic species, it varies between isotopes.

2.1.3 Scattering from an Array of Nuclei-Coherent and Incoherent Scattering

Since the scattering lengths of different isotopes in a material are not constant, and in addition, can be shown to depend on the relative nuclear spin orientation of the neutron-nucleus system[40 41], the incident neutron does not see a uniform scattering potential. The mean scattering potential gives rise to interference effects between different scattering centres, leading to coherent scattering. This mean scattering is proportional to $\bar{b}$, so the coherent cross-section is given by $4\pi|\bar{b}|^2$.

Incoherent scattering arises because of the deviations from the mean, and the incoherent cross-section is thus given by $4\pi(\overline{|b|^2}-|\bar{b}|^2)$. Clearly, these deviations are random, so no phase relationships will be observed in an experiment designed to measure incoherent scattering.

Thus, measurement of coherent scattering gives information about the collective behaviour of the scattering centres, whereas incoherent scattering gives details about individual atoms.

Table 2.1 lists the scattering cross-sections for some common atoms (from 42).

Table 2.1 Scattering Cross-sections for some Common Atoms

Atom	Spin	$\sigma_{coh}(10^{-24}cm^2)$	$\sigma_{incoh}(10^{-24}cm^2)$
^{16}O	0	4.2	-
^{12}C	0	5.5	-
^{14}N	1	11.6	0.3
D	1	5.6	2.0
H	½	1.76	79.7

Whilst oxygen, carbon and nitrogen are almost purely coherent scatterers, hydrogen is a very strong, almost purely incoherent scatterer.Since deuterium is a relatively weak incoherent scatterer, selective deuteration of polymers has become an important technique for studying specific groups in the molecules.

2.1.4 The Double Differential Cross-section

The quantity measured experimentally in a neutron scattering experiment is the double differential cross-section, $\partial^2\sigma/\partial\Omega\partial E$. This is the probability that neutrons will be scattered by an array of N atoms with cross-section σ into solid angle $\partial\Omega$ with energy change ∂E.

i.e.

$\frac{\partial^2\sigma}{\partial\Omega\partial E}$ = no. neutrons with energy E to E+δE scattered into $\delta\Omega$ per second, divided by the incident flux x$\delta\Omega$ x δE.

It can be shown[39] that $\partial^2\sigma/\partial\Omega\partial E$ may be given by the following expression:

$$\frac{\partial^2\sigma}{\partial\Omega\partial E}=\frac{k}{k_0}\left(\frac{m}{2\pi\hbar^2}\right)^2\sum_{\lambda_0,s_0}p_{\lambda_0}p_{s_0}\sum_{\lambda,s}|\langle\underline{k}s\lambda|\hat{V}|\underline{k}_0s_0\lambda_0\rangle|^2\delta(\hbar\omega+E_{\lambda_0}-E_\lambda) \quad (2.4)$$

This is the first Born approximation to the cross-section, obtained using first order perturbation theory. The terms included in the expression may be identified with the following probabilities:

(1) the probability that a neutron with wavevector $\underline{k}_0$ will be scattered with wavevector $\underline{k}$, where $\hat{V}$ is the interaction potential in the scattering process.

(2) the probability that the nucleus will go from initial state λ_0 to final state λ when it undergoes an inelastic collision with the neutron, in which case, energy must be conserved, i.e.

energy gained by nucleus = $E_\lambda - E_{\lambda_0}$
= energy lost by neutron
= $E_0 - E = \hbar\omega$

This is represented by the δ-function term in the expression.

(3) the probability that if the initial spin state of the neutron is s_0, the final spin state will be s.

The application of first order perturbation theory to obtain this expression is not strictly valid, since although the nuclear forces are very short range, they are also extremely large.However, it is a good approximation well outside the range of these forces (i.e $r \gg r_0$)and so appropiate for the discussion of neutron scattering spectroscopy.

In order to evaluate (2.4) further, it is necessary to find some appropiate form of $\hat{V}(\underline{r})$.The only form of $\hat{V}(\underline{r})$ which gives the correct s-wave scattering in the Born approximation[241] is the Fermi pseudo-potential,

$$\hat{V}(\underline{r}) = \frac{2\pi h^2 b}{m}\,\delta(\underline{r}-\underline{R})$$

where $\underline{r}$ is the position vector of the neutron, and
$\underline{R}$ is the position vector of the nucleus.

Substituting for $\hat{V}(\underline{r})$, the final form of $\partial^2\sigma/\partial\Omega\partial E$ is given by,

$$\frac{\partial^2\sigma}{\partial\Omega\partial E} = \frac{k}{k_0}\sum_{\lambda_0 s_0} p_{\lambda_0} p_{s_0} \sum_{\lambda s} \left| \langle s\,\lambda \left| \sum_l b_l \exp(i\underline{Q}.\underline{R}_l) \right| s_0\lambda_0 \rangle \right|^2 \delta(h\omega + E_{\lambda_0} - E_\lambda) \quad (2.5)$$

This is the equation on which neutron scattering theory is based.

The function may be obtained in a more useful form by expanding the δ-function as a series of exponentials, i.e.

$$\delta(h\omega + E_{\lambda_0} - E_\lambda) = \frac{1}{2\pi\hbar}\int_{-\infty}^{\infty} dt\, \exp\left\{\frac{-it}{\hbar}(\hbar\omega + E_{\lambda_0} - E_\lambda)\right\}$$

Substituting in (2.5) it may be shown[43] that the double differential cross-section may now be written,

$$\frac{\partial^2\sigma}{\partial\Omega\partial E} = \frac{k}{k_0}\,\frac{1}{2\pi\hbar}\int_{-\infty}^{\infty} dt\, \exp(-i\omega t)\sum_{ll'} \overline{b_l^* b_{l'}} \langle \exp(-iQ.\hat{R}_l(0))\, \exp(iQ.\hat{R}_{l'}(t)) \rangle$$

(2.6)

where $\langle\ \rangle$ denotes the thermal average $\sum p_{\lambda_o}\langle\lambda_o|\ |\lambda\rangle$ and where $\overline{b_l^* b_{l'}}$ is an average over random spin orientations and isotope distributions of $b_l^* b_{l'}$

i.e. $$\overline{b_l^* b_{l'}} = \sum_{\lambda_o} p_{\lambda_o}\langle\lambda_o|\ b_l^* b_{l'}\ |\lambda_o\rangle$$

2.1.5 The Scattering Law, $S(Q,\omega)$, and the Van Hove Correlation Functions

In a system where the value of b_l is independent of l, i.e. a system which is composed of a single chemical species only, the average $\overline{b_l^* b_{l'}}$ may be taken outside the sum over l, and equation (2.6) rewritten as[43]

$$\frac{\partial^2\sigma}{\partial\Omega\partial E} = \frac{Nk}{k_0}\,\overline{b_l^* b_{l'}}\,S(\underline{Q},\omega) \qquad (2.7)$$

$S(Q,\omega)$ is the scattering law for the system. It uniquely defines the particular system in terms of energy and momentum transfer, and is independent of experimental conditions. In addition, it may be shown that[39]

$$S(\underline{Q},\omega) = \exp\left(-\frac{\hbar\omega}{kT}\right) S(-\underline{Q},-\omega)$$

This is due to the condition of detailed balance, whereby the number of neutrons gaining a quantum of energy, $\hbar\omega$, from the system must be equal to the number of neutrons losing $\hbar\omega$.

A symmetrical scattering law, $\tilde{S}(Q,\omega)$ may be defined by,

$$\tilde{S}(\underline{Q},\omega) = \exp\left(-\frac{\hbar\omega}{kT}\right) S(\underline{Q},\omega)$$

and this symmetrical form is often found to be of more use for the purposes of data analysis than the asymmetric $S(\underline{Q},\omega)$.

Since there is no correlation between the scattering lengths of the l^{th} and l'^{th} nucleus, then

$$\text{if } l = l' \text{ then } \overline{b_l^* b_l} = \overline{|b_l|^2} = \overline{|b|^2}$$

$$\text{and} \quad \text{if } l \neq l' \text{ then } \overline{b_l^* b_l} = |\bar{b}|^2$$

thus (2.7) may be separated into a coherent and incoherent component,

$$\left(\frac{\partial^2\sigma}{\partial\Omega\partial E}\right)_{coh} = \frac{Nk}{k_0} |\bar{b}|^2 S_{coh}(\underline{Q},\omega)$$

where

$$S_{coh}(\underline{Q},\omega) = \frac{1}{2\pi\hbar N}\int dt\ \exp(-i\omega t)\sum_{ll'} \langle \exp(-i\underline{Q}.\hat{\underline{R}}_l(0))\ \exp(i\underline{Q}.\hat{\underline{R}}_{l'}(t))\rangle$$

and

$$\left(\frac{\partial^2\sigma}{\partial\Omega\partial E}\right)_{inc} = \frac{Nk}{k_0} |b-\bar{b}|^2\ S_{inc}(\underline{Q},\omega)$$

where

$$S_{inc}(\underline{Q},\omega) = \frac{1}{2\pi\hbar N}\int dt\ \exp(-i\omega t)\sum_{l} \langle \exp(-i\underline{Q}.\underline{R}_l(0))\exp(i\underline{Q}.\underline{R}_l(t))\rangle$$

In real terms, the assumption that the scattering is limited to only one chemical species is reasonable for the polymers under investigation in this thesis, since the observed scattering will be largely incoherent scattering from the hydrogen in the system.

For future reference, it is informative to consider the Fourier transforms in both time and space of the coherent and incoherent scattering laws.

The incoherent scattering function is the time Fourier transform of the intermediate scattering function, $I_{inc}(Q,t)$[41], i.e.

$$S_{inc}(\underline{Q},\omega) = \frac{1}{2\pi}\int_{-\infty}^{\infty} \exp(-i\omega t)\ I_{inc}(\underline{Q},t)\, dt$$

where $I_{inc}(\underline{Q},t) = <\exp\{-i\underline{Q}.\underline{r}(0)\}\ \exp\{i\underline{Q}.\underline{r}(t)\}>$ [35]

where $<\ >$ again denotes a thermal average.

The space Fourier transform introduces the self pair correlation function, $G_s(\underline{r},t)$ [35] [39]

$$\text{where}\quad I_{inc}(\underline{Q},t) = \int \exp(i\underline{Q}.\underline{r})\ G_s(\underline{r},t)\, d\underline{r}$$

$$\text{and}\quad G_s(\underline{r},t) = \frac{1}{N}\sum_{l}\int d\underline{r}' <\delta\{\underline{r} - \underline{r}' + \hat{\underline{R}}_l(0)\}\delta\{\underline{r}' - \hat{\underline{R}}_l(t)\}>$$

$$\text{Hence,}\quad S_{inc}(\underline{Q},\omega) = \frac{1}{2\pi}\iint \exp\{i(\underline{Q}.\underline{r} - \omega t)\}\ G_s(\underline{r},t)\, d\underline{r}dt$$

Similar definitions apply for the coherent scattering law, leading to

$$S_{coh}(\underline{Q},\omega) = \frac{1}{2\pi}\iint \exp\{i(\underline{Q}.\underline{r} - \omega t)\}\ G(\underline{r},t)\, d\underline{r}dt$$

where $G(\underline{r},t)$ is the pair correlation function, and

$$G(\underline{r},t) = \frac{1}{N}\sum_{ll'}\int d\underline{r}'\ <\delta\{\underline{r} - \underline{r}' + \hat{\underline{R}}_l(0)\}\delta\{\underline{r}' - \hat{\underline{R}}_{l'}(t)\}>$$

The physical meanings of $G(\underline{r},t)$ and $G_s(\underline{r},t)$ are made clearer if the system is considered in the classical limit, so that all nuclei are equivalent. In this case, the average $\frac{1}{N}\sum_{l}$ may be dropped[43] and

$$G_s^{cl}(\underline{r},t) = <\delta\{\underline{r} - \hat{\underline{R}}_0(t) + \hat{\underline{R}}_0(0)\}>$$

$$\text{and}\quad G^{cl}(\underline{r},t) = <\delta\{\underline{r} - \hat{\underline{R}}_{l'}(t) + \hat{\underline{R}}_0(0)\}>$$

that is, $G_s^{cl}(\underline{r},t)$ is the probability that if a given scattering centre is at R_0 at time $t = 0$, then the same scattering centre will be at $\underline{r}$ at time $t = t$. $G^{cl}(\underline{r},t)$ is the probability that if a nucleus is at R_0 at time $t = 0$, then any scattering centre (including the original one) will be at $\underline{r}$ at time $t = t$.

2.2 Experimental Techniques and Instrumentation

A wide range of spectrometers is available for neutron scattering experiments,covering various energy and momentum transfers, and with very different resolution properties. To obtain the results presented in chapters 3 and 4, five instruments were used. Quasi-elastic experiments to study the rotational motion of the ester methyl group in poly(methyl methacrylate) were performed on the time-of-flight spectrometer, IN5, at the Institut Laue-Langevin (ILL), Grenoble, France, and the new time-focussing time-of-flight spectrometer, IN6, also at the ILL. Observation of the slower rotational motion of the α-methyl group required an instrument with considerably better resolution, and these experiments were performed on the high resolution back-scattering spectrometer, IN10, at the ILL, France. IN10 was also used for studying the dynamics of the polymer networks. Inelastic measurements to obtain the hydrogen-amplitude-weighted density of states function for various partially deuterated samples of PMMA were made on 4H5 , AERE, Harwell, and additional inelastic data relating to the effect of stereoregularity on the motion of the two sidegroups made on the time-of-flight spectrometer, IN6. In addition, supplementary experiments to measure the coherent scattering from PMMA were made on the powder diffractometer, 10H, also at Harwell.

A brief description of each instrument now follows. More detailed information may be found elsewhere (44-51).

2.2.1 Use of a Cold Source

Neutrons from a reactor pile have a thermal neutron wavelength distribution which peaks at about 1 Å. However, the most useful incident wavelength in many experiments (particularly time-of-flight) is likely to be greater than 4 Å, where the neutron flux is far removed from its peak value. The problem of low flux at longer wavelengths may be overcome by suitable adjustment of the moderator temperature, and this is achieved in practice by the use of so-called 'cold sources' which shift the peak of the Maxwellian wavelength distribution to longer wavelengths. The cold source usually takes the form of a small volume of liquid hydrogen.

All the time-of-flight spectrometers described below, and IN10, are located on a cold source, giving a peak flux at greater than 4 Å.

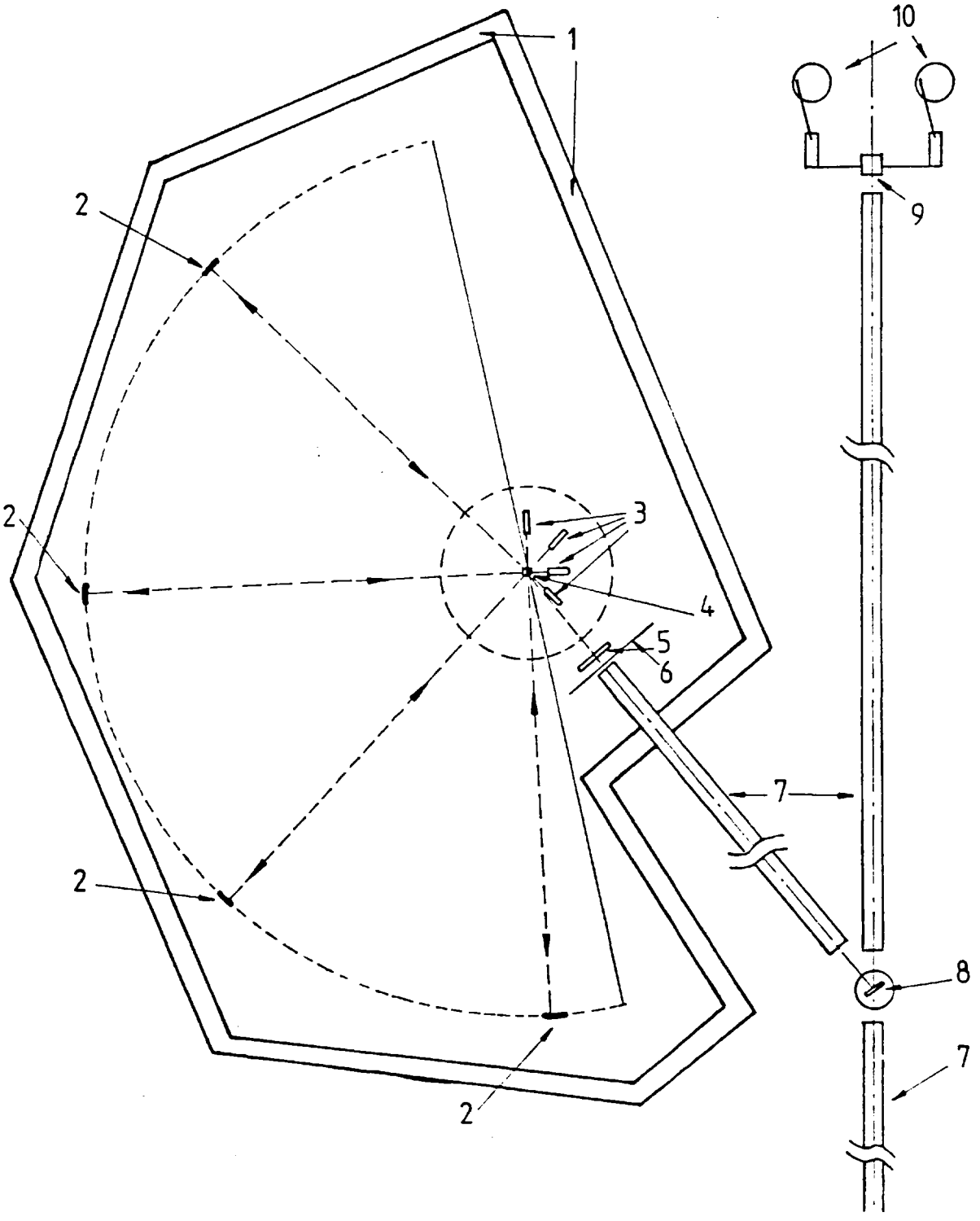
2.2.2 The Backscattering Spectrometer, IN10

IN10 is intended for the measurement of very small energy transfers in the range ±10μeV. It is a high resolution instrument, having a typical full width half maximum (FWHM) elastic resolution of the order of 1μeV.

The instrument is shown schematically in figure 2.1. Cold neutrons, with a flux $\sim 2 \times 10^9$ neutrons/s/cm^2 and incident wavelength peaked around 7 Å travel along the main guide tube to the monochromator crystal, where they are back-scattered along their incident path. On returning, they strike a (0 0 1) oriented graphite crystal, positioned slightly higher than the incident beam, from which about 40% of the back-scattered beam is reflected along the guide to the sample. After passing through a chopper (to pulse the beam and ensure that neutrons scattered directly into the detectors are not counted) and monitor, the neutrons are scattered by the sample onto one of several curved analyser plates arranged around the wall of the helium container. These back-reflect the scattered beam into ^{3}He detectors

Fig. 2,1 Back Scattering Spectrometer IN 10

1 Shielding
2 Analyzer Crystals
3 ^{3}He Detectors
4 Sample
5 Monitor
6 Auxiliary Chopper
7 Neutron Guide
8 Graphite Crystal
9 Monochromator Crystal
10 Doppler Drive



positioned around the sample. Since this arrangement will detect only elastically scattered neutrons, to measure quasi-elastic scattering the monochromator crystal is driven backwards and forwards in the direction of the beam by a Doppler drive, thus slightly varying the incident energy of the neutrons striking the sample. Only those neutrons which receive equal and opposite energy transfer in the scattering process will be reflected by the analysers into the detectors.

Polished and unpolished analysers and monochromators are available, the former giving better resolution, and the latter, increased flux. The analyser plates are supported on rails and can be moved around the wall of the helium box to be set in various positions corresponding to different Q values, between 0.6 and 2.0 Å^{-1}.Typically, measurements will be made at six or seven angles. In addition, for relatively small angle scattering experiments ($Q<0.31\text{Å}^{-1}$) a system of seven concentric analyser circles may be used.

The Q resolution is ± 0.017 Å^{-1} for $Q<0.31$ Å^{-1}, and of the order of 0.05 Å^{-1} for $Q>0.57$ Å^{-1}.

Perfect Back-scattering to Achieve High Resolution[51]

High resolution on IN10 is achieved by using Bragg reflection through 180^0 (i.e. perfect back-scattering) as a method of monochromation.

$$G = 2k\sin\theta \qquad \text{where } G = 2\pi/d_{hkl} \text{ and } k = 2\pi/\lambda$$

The spread in energy of the reflected beam is thus given by

$$\frac{\Delta E}{E} = \frac{2\Delta k}{k} \simeq \frac{2\Delta G}{G} + 2\cot\theta\Delta\theta$$

The spread, $\Delta\theta$, is due to the mosaic spread of the crystal and divergence of the beam. The term ΔG originates because only a finite number of lattice planes are cont-

ributing to the Bragg reflection, leading to a broadening of the reciprocal lattice points. High resolution may be achieved by reducing the divergence of the beam, or alternatively, by minimising the $\cot\theta$ term by making $\theta=\pi/2$, in which case $\Delta\theta$ may be relatively large without affecting the energy resolution. In this case the resolution is determined only by the term $\Delta G/G$, which is of the order of 10^{-4} for a good monochromator crystal.

The resolution function is well approximated by a Lorentzian.

Data Acquisition

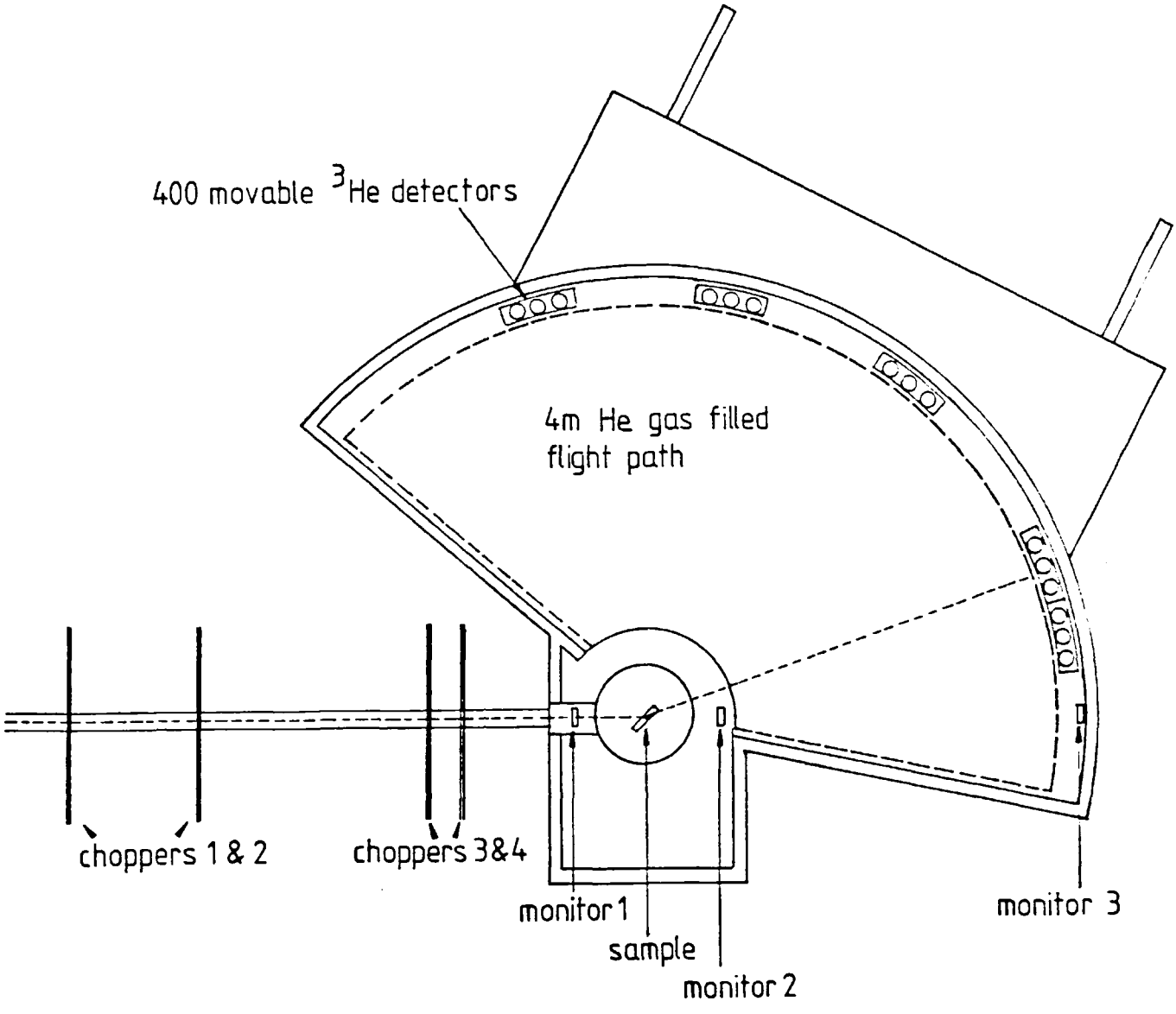
The instrument is controlled by a PDP11 computer. During each run, data is updated from core to disk at preset intervals (typically every two hours). At the end of each run, data is transferred from the disk to the IN10 area on the main DEC10 computer.

2.2.3 The Time-of-Flight Spectrometer, IN5

IN5 is a high resolution time-of-flight spectrometer capable of achieving its best energy resolution of about 24 μeV (FWHM) at an incident wavelength of 10 Å with the chopper frequency at 165 Hz. Figure 2.2 shows schematically the mode of operation of the instrument. Four disc choppers rotate in a vertical plane about a common horizontal axis. The overall frequency of rotation is variable between 100 and 165 Hz. The relative phase of chopper 1 and chopper 4 defines the incident wavelength, which is variable between 1 Å and 10 Å. Peak flux of 1×10^5 n/s/cm^2 at the sample position is achieved at about 4.5 Å. Chopper 2 eliminates higher orders, and chopper 3 is rotated at a multiple of the overall period to reduce pulse rate and eliminate frame overlap when this is a problem (i.e at long wavelength). Neutrons leaving the fourth chopper are monitored, and then strike the sample. Some will be scattered, the rest will pass directly through the sample to the second monitor.

Fig 2.2

Time-of-Flight Spectrometer IN5



The scattered neutrons are detected at various angles between 5^0 and 135^0 by a large number of ^3He detectors arranged in groups. The detectors can be grouped vertically along Debye-Scherrer rings, or horizontally to detect the scattered neutrons over a range of Q values (the Q range available is defined by the incident wavelength and sample orientation to the beam). The sample box and flight path are filled with helium to prevent air scattering.

The resolution function is well fitted by a Gaussian- in fact, it is very nearly triangular, with only very small wings, a feature which is very useful in quasi-elastic analysis.

Data Acquisition

IN5 is controlled by a PDP11 computer. During an experiment, data is continuously updated, and on completion of the run, written to disk. Transfer is then made to the DEC10.

2.2.4 The Time-of-Flight Spectrometer, IN6

IN6 is a new, time-focussing, time-of-flight spectrometer designed for quasi-elastic and inelastic scattering for incident wavelengths in the range 4-6 Å. The elastic resolution is similar to that of IN5 in this wavelength range (FWHM of 170 μeV at 4.16 Å and 60 μeV at 5.9 Å), but with a three-fold increase in flux at the sample position. This is achieved by the use of three curved, vertically focussing monochromator crystals, which enable the full height of the guide beam (20cm) to be focussed to a height of 5cm at the sample position.However, this method of increasing the flux implies a large increase in the energy spread, ΔE_0, of the primary beam. This problem is resolved by combining the spatially focussing monochromator system with the principle of time focussing. This is achieved by pulsing the beam with a Fermi chopper. By spinning

this chopper in the right sense, one allows the slow neutrons of the primary beam to depart earlier than the faster ones. The detector is placed at the distance where the fast neutrons are on the point of overtaking the slow ones. As a result, a fairly short pulse of neutrons is obtained, with a resolution $\delta(\hbar\omega)$ which can be considerably better than the energy spread ΔE_0. However, perfect time-focussing can only be achieved for one energy transfer, and this loss of generality is the price paid for increased intensity.

The sample to detector distance is 2m, and the detector bank houses 369 ^{3}He detectors, giving a useful detector area of $3.3m^2$. The incident wavelength used in the experiments described in chapter 3 was 4.1 Å, giving a Q range of 0.4 to 2.6 $Å^{-1}$.

Data Acquisition

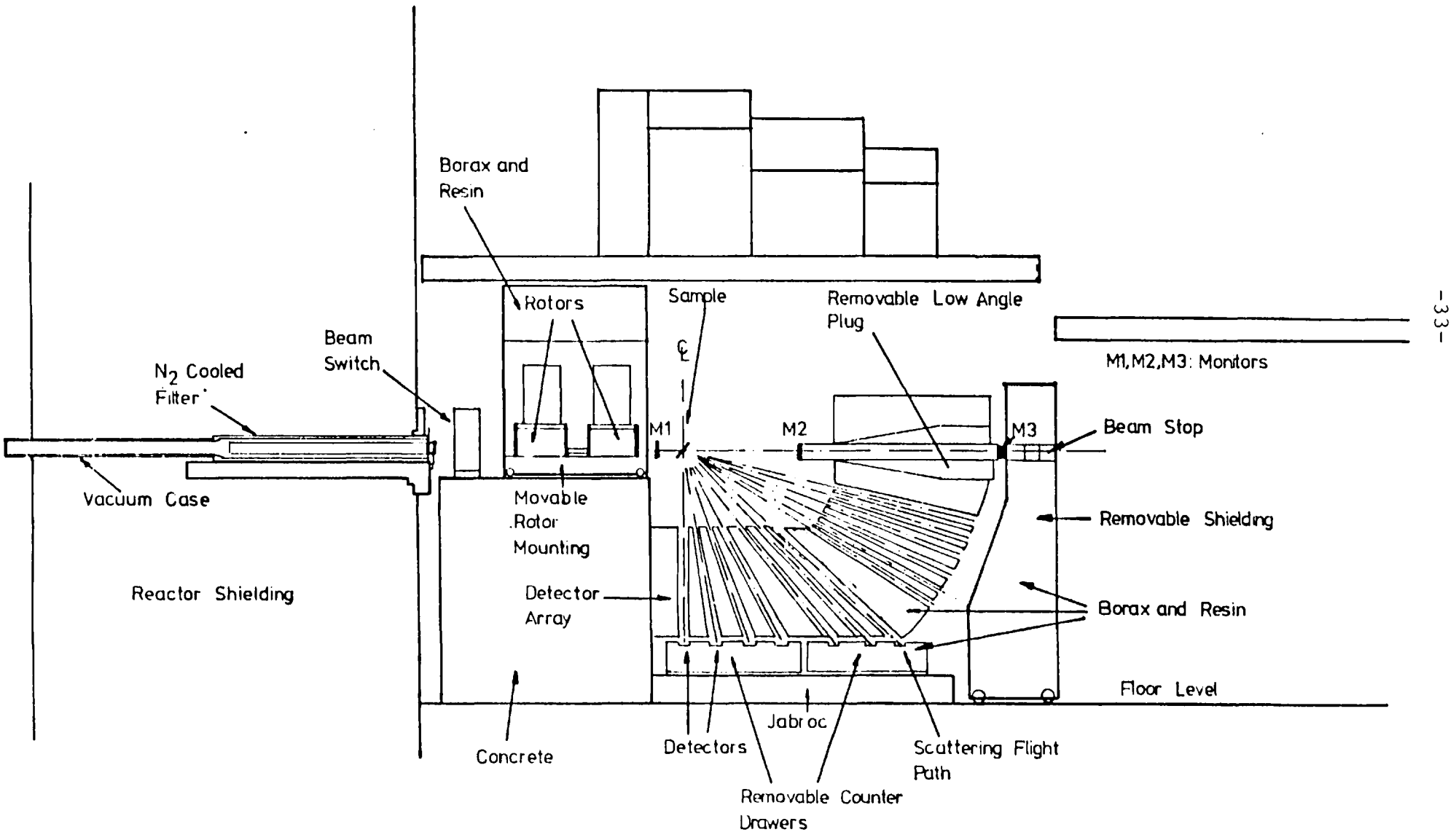
Due to increased flux, statistically good data may be collected in a very short time.The data is recorded by a PDP11 computer in exactly the same way as IN5.

2.2.5 The Time-of-Flight Spectrometer, 4H5

4H5 is a time-of-flight spectrometer which is, in principle, very similar to IN5. However, one major difference lies in the method used to produce the pulsed,monochromated neutrons. Instead of a series of rotating discs, 4H5 employs two rotors of helical slot design to pulse and monochromate the beam simultaneously. The required wavelength is achieved by adjusting the speed and phase of these two rotors. Six and twelve slot rotors are available, and best resolution is achieved with 2 x 12 slot. However, the flux is reduced by a factor of 12 by changing from a 2 x 6 slot system to a 2 x 12 slot arrangement,so again, resolution can only be achieved at the cost of intensity. The resolution, $\Delta\lambda/\lambda$ is typically 1-5%.

The use of a cold source means that good counting

Fig 2.3 Cold Neutron Spectrometer 4H5



rates can be obtained at incident wavelengths 4-10 Å, with peak flux at 5.3 Å. Detectors are arranged in fixed positions between 13^0 and 90^0. The length of the flight path varies from 1.2m at 90^0 to 1.9m at low angles. The instrument is shown schematically in figure 2.3.

Sample Changer

Use of the sample changer on 4H5 is standard practice. Samples are mounted in the sample changer which periodically cycles up to three samples into and out of the beam. One of the three available positions is permanently occupied by a plate of vanadium for calibration purposes.The aim of this cycling process is to allow for fluctuations in instrument characteristics, especially variation in incident flux and background.

Samples are arranged in a holder along a central axis, usually oriented at 45^0 to the beam, in transmission. The samples are moved along the axis into position in the beam using an electric motor;preset micro-switches regulate the exact positioning. Cycling is controlled by the PDP8 computer via an interface control unit.

Data Collection

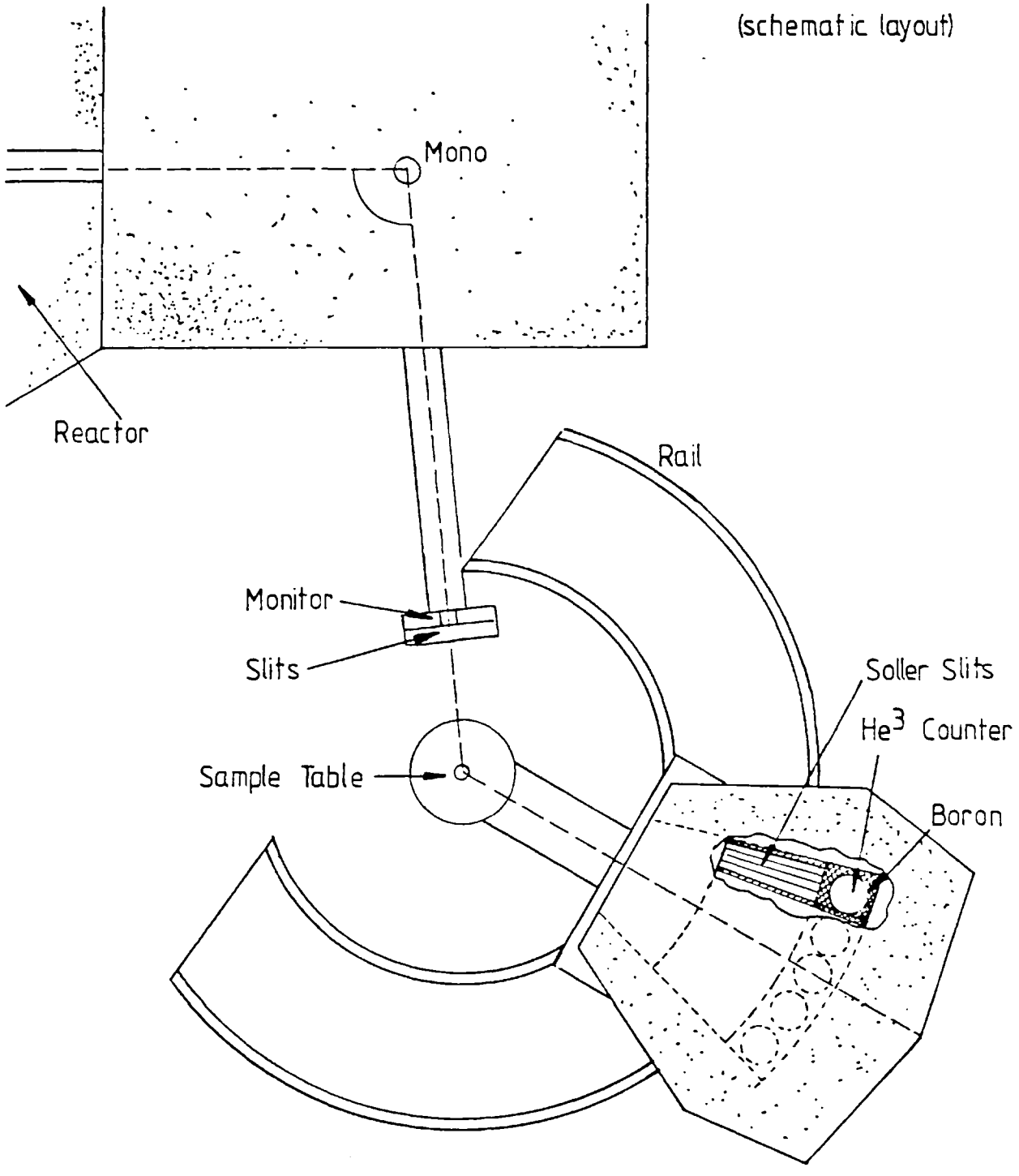
The Cassandra system, based on the PDP8 data processing unit is used to control 4H5 and collect the data. During an experiment,every scattering event is recorded on a magnetic drum, sorted according to sample changer position, detector number (scattering angle) and time of flight (channel number). At the end of a run, the data is transferred via a core buffer unit to a DEC tape for subsequent analysis.

2.2.6 The Powder Diffractometer, 10H

This instrument is designed for structure studies of powders and amorphous solids. The incident wavelength is 1.0 Å, and the available angular range 8^0 to 130^0,giving

Fig 24

10H Powder Diffractometer
(schematic layout)



a Q range of 0.8 to 11.4 $\AA^{-1}$. The diffractometer has good angular resolution ($\sim 0.5^0$) over all angles. Data acquisition is by punched tape and teletype. 10H is shown in figure 2.4.

2.2.7 Use of Vanadium as a Standard

Since vanadium is an almost pure incoherent elastic scatterer, it is used as a standard for measuring the resolution function of an instrument.A vanadium run is recorded under exactly the same conditions as the sample run (i.e same orientation to the beam, same sample container and so on). For quasi-elastic experiments it is particularly important to obtain good statistics in the vanadium calibration, since this often plays a vital part in convolution programs in subsequent data analysis.

2.2.8 Sample Heating During Experiments

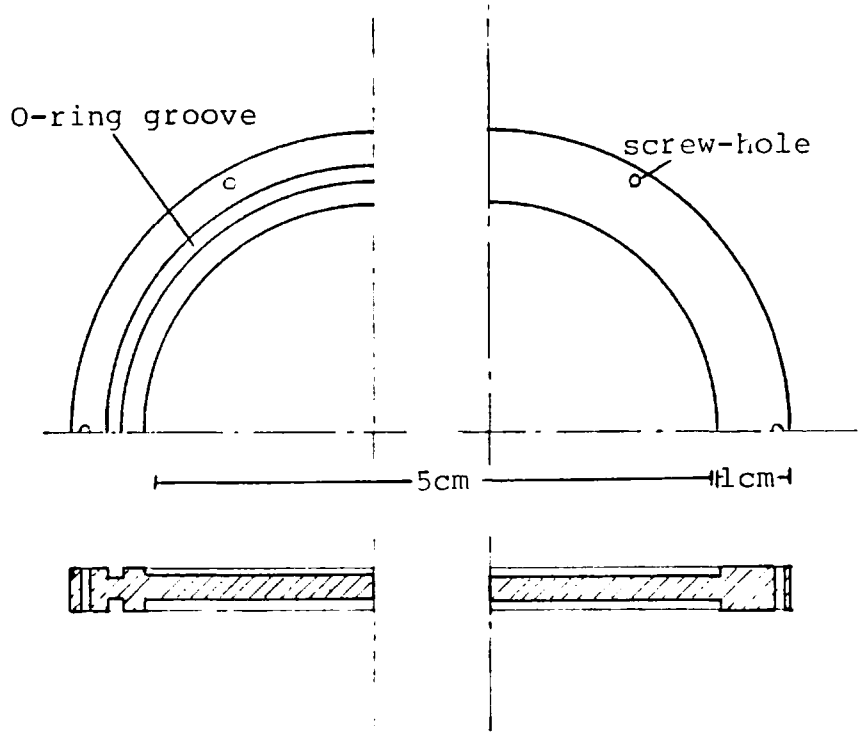
In all cases when it was required to heat the samples during the neutron scattering experiment, the standard furnace on the instrument was used. Details of these may be found in the appropiate User's Guide.

2.2.9 Sample Containers

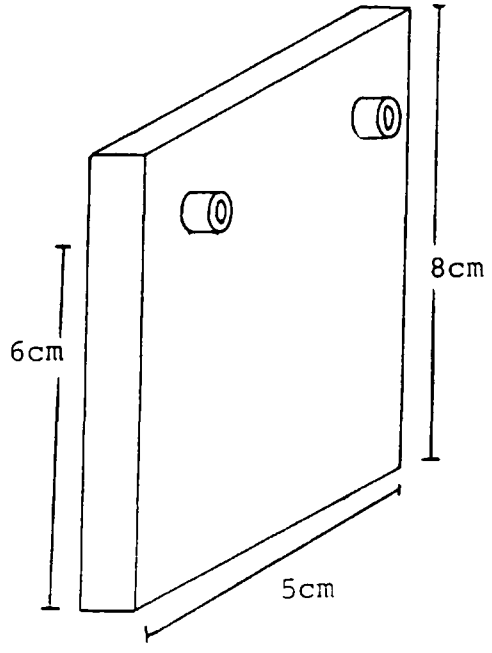
(A) IN10

During the experiments performed on poly(methyl methacrylate) it was necessary to heat the sample. The sample cans used in this case are composed of two halves which screw together. Essentially, they comprise two aluminium discs,each of the order of 5mm thick, and 7cm in diameter. The centre of each is milled out to provide a circular recess 5cm in diameter, and 2mm deep, in which to place the sample. The two halves are screwed together with aluminium screws, using Teflon washers. The use of an

O-ring to provide a leak-proof seal means that these sample cans are also suitable containers for viscous fluids. The cans are shown schematically below.



The network films were also held in these cans. The rubber solutions were contained in cells designed specifically for polymer solutions. These are shown below.



These cans are also made of aluminium, and are rectangular, with dimensions approximately 8cm x 5cm. Cans of differing thicknesses are available,the appropiate thickness required depending on the percentage of hydrogen in the sample. The cans are filled through the screwholes at the top, using a small syringe. After filling, they are securely sealed using screws and Teflon washers. During an experiment, the can is mounted on a candle-stick, ensuring that the height is correctly adjusted so that the screwholes are above the beam. These cans are not suitable for use in the IN10 furnace.

(B) IN5

The PMMA samples investigated on IN5 were held in standard IN5 sample holders.These consist of two round aluminium halves, which screw together. These cans are approximately 5cm in diameter and 1cm thick, and are designed for use in the IN5 furnace.

(C) IN6

Room temperature measurements only were made on the PMMA.Since the pressed film is self-supporting under these conditions,no sample can was required.The sample was supported on a candlestick, aligned to be central in the beam.

(D) 4H5

The PMMA samples were held between sheets of aluminium foil in the standard 4H5 sample changer.

(E) 10H

Since measurements were made at room temperature, again a can was not required, and the PMMA simply supported

on a candlestick during the experiment.

2.3 Data Analysis

2.3.1 Analysis of Quasi-elastic Data from IN10

With reference to section 2.2.2, it can be seen that the scattering angle between the incident and scattered neutrons with regard to the detector are kept fixed, so that the analyser reflects only neutrons of a fixed energy, which satisfy the condition[51]

$$E_M \pm \Delta E_D \mp \Delta E_S = E_A$$

where $E_M = E_A$ = energy of Bragg reflected neutrons from the fixed monochromator or analyser crystal

ΔE_S = energy change by scattering from sample

and ΔE_D = energy change by Doppler shifting

Thus, $$\Delta E_D = \Delta E_S$$

and so direct energy analysis of the scattered neutrons is performed.

From 2.1.4, the double differential cross-section is defined by the ratio of the number of neutrons with energy between E and E + δE scattered into solid angle δΩ per second, to the incident flux x δΩ x δE. On IN10, this is measured directly, allowing the scattering law $S(\underline{Q},\omega)$, to be simply obtained via the relationship

$$\frac{\partial^2\sigma}{\partial\Omega\partial E} = \frac{Nk}{k_0} |b-\bar{b}|^2 S(\underline{Q},\omega)$$

This measured scattering law $S_M(\underline{Q},\omega)$ is the convolution of the true scattering law with the instrument resolution function, and subsequent data analysis involves extracting $S_{TRUE}(\underline{Q},\omega)$.

Initial Profile Fitting

Before running the programs designed to make detailed convolution analysis, it is necessary to run the program FIRST[52] to obtain starting parameters, such as position, height and width of the measured spectra. FIRST calculates these variables by simply fitting a single Lorentzian through the data, after subtracting a flat background. The observed spectrum is a convolution of the resolution function with the true sample scattering law, but an approximation of the true width of $S_{TRUE}(\underline{Q},\omega)$ may be made in the following way.

Since $$S_{OBS}(\underline{Q},\omega) = S_{TRUE}(\underline{Q},\omega) * R(Q)$$

where $R(Q)$ is the resolution function, then if both $S_{TRUE}(\underline{Q},\omega)$ and $R(Q)$ are single Lorentzians, the convoluted result $S_{OBS}(\underline{Q},\omega)$ will also be a single Lorentzian and

$$FWHM_{TRUE} = FWHM_{OBS} - FWHM_{RESOL}$$

Although it is likely that the measured resolution function and scattering law are not true Lorentzians, so that strictly speaking the above relationship is not true, the widths obtained using this expression will be quite adequate as starting parameters.

Convolution Analysis

As indicated above, the measured spectrum is a convolution of the true scattering law with the resolution function of the instrument. Since deconvolution to obtain $S_{TRUE}(\underline{Q},\omega)$ is, in general,a difficult and inaccurate process, an alternative approach is used, in which the experimental resolution function (measured using a vanadium standard) is convoluted with a theoretical model of the sample scattering law, and the resulting curve then fitted to the measured data, until an acceptable fit is obtained.

Two programs were used to analyse the results from experiments performed on PMMA to study the rotational motion of the α-methyl group - program SAND[52] , in which a δ-function plus a single Lorentzian is fitted to the data, and program SUPER[52] , in which two Lorentzians of different widths, but centred at the same origin are fitted to the data. The width of the first component is assumed to very small, corresponding to the elastic δ-function, whilst the second Lorentzian is fitted to the broadened quasi-elastic component associated with the rotational motion. (The form of the rotational scattering law is discussed in chapter3)

Results from the polymer networks were analysed using a fitting program POLLY[52] . In this program, a model scattering law is again convoluted with the resolution function and then fitted to the experimental data. It is not clear exactly what form the model scattering law should take for the polymer networks (see 4.1), but following the same analysis procedure as used for melt samples, two different forms of $S_{inc}(\underline{Q},\omega)$ were fitted to the data.

(1) a single Lorentzian, corresponding to Brownian diffusion, for which, ΔE, the FWHM of the scattering law is expected to vary as Q^2.

(2) a model scattering law $S_{inc}(\underline{Q},\omega)$, based on the Rouse model (see 4.1), which predicts a FWHM variation of Q^4.

Output from POLLY takes the form of a line-printer listing, giving both the observed and fitted values obtained.

Extraction of the EISF from $S(Q,\omega)$

Output from SUPER and SAND takes the form of a line-printer listing, giving both the observed and fitted $S(\underline{Q},\omega)$, as well as the final parameters used in obtaining an acceptable fit. In addition, areas and integrated intensities of the elastic and quasi-elastic components are given, so that the EISF may be calculated directly, using,

$$EISF = \frac{I_{el}}{I_{el} + I_{qel}} \qquad \text{(see chapter 3)}$$

An alternative approach may be made using the program FURY[53], which has recently been written and which calculates the Fourier Transform of the scattering law, i.e $S(Q,t)$. This may be used to give the EISF directly, in the following way.

For a random molecular motion, such as rotation, the incoherent scattering law is given by (see chapter 3),

$$S_{rot}(\underline{Q},\omega) = A_0(\underline{Q})\,\delta(\omega) + \sum_{n=1}^{\infty} A_n(\underline{Q})\; L(\tau_n^{-1})$$

so that $$S(\underline{Q},t) = A_0(\underline{Q}) + \sum_{n=1}^{\infty} A_n(\underline{Q})\; \exp(-\tau_n t)$$

Thus the EISF may be extracted directly.

Output from FURY is in the form of a line-printer listing, giving the Fourier deconvoluted coefficients and their logarithm, together with error tables.

2.3.2 Analysis of Quasi-elastic Data from IN5

Data reduction in this case is slightly more complex, since it is first necessary to obtain the scattering law $S(\underline{Q},\omega)$ from the measured time-of-flight spectrum, $\partial^2\sigma/\partial\Omega\partial\tau$, as outlined below.

Correction and Conversion of Time-of-Flight Data to $S(Q,\omega)$

This is achieved using two programs, PRIME and CROSSX[54]. The purpose of PRIME is to perform monitor peak analysis and vanadium peak evaluation to calculate various experimental parameters, such as the incident time-of-flight, position of the elastic peak and so on. The results are stored on disk in binary to be referred to later when running CROSSX.

CROSSX is used to obtain an absolute value of the scattering law, $S(\underline{Q},\omega)$ from the experimental measurements by comparison with the results obtained from the vanadium standard.

The counts, S , in a given channel at a given scattering angle are given by[54]

$$S = n \frac{\partial^2\sigma}{\partial\Omega\partial\tau}.\Delta\tau.\Omega_0.N_s.\varepsilon_\tau$$

where $\Delta\tau$ = channel width in μsec^{-1}

Ω_0 = solid angle subtended by the detector at the sample

n = no. of incident neutrons

N_s = no. of atoms in unit area of the beam

ε_τ = efficiency of detector to neutrons with time-of-flight, τ.

Similarly, for vanadium, if the total counts in the elastic peak are denoted by V, then,

$$V = n' \frac{\partial\sigma}{\partial\Omega}(\text{elastic}).\Omega_0.N_{VAN}.\varepsilon_{\tau_0}$$

Strictly, this is only true for the limiting case of an infinitely thin plane; corrections for scattering and absorption by a sample of finite thickness will be discussed later.

If the monitor 1 efficiency is α_{τ_0} *and the observed* monitor counts for vanadium and the sample are M_v and M_s respectively, then

$$M_s = \alpha_{\tau_0} n \qquad \text{and} \qquad M_v = \alpha_{\tau_0} n'$$

The scattering by the vanadium is dependent only on the Debye-Waller factor, i.e

$$\left(\frac{\partial\sigma}{\partial\Omega}\right)_{VAN} = \left(\frac{\sigma}{4\pi}\right)_{VAN} \exp(-2W)$$

where W is the Debye-Waller factor.

It is now possible to compare the flux of neutrons detected from the sample after normalisation to that detected from the vanadium at the same angle, to eliminate instrumental corrections, to give,

$$\frac{S/M_S}{V/M_V} = \left[\left(\frac{\partial^2\sigma}{\partial\Omega\partial\tau}\right)_{SAM} \Big/ \left(\frac{\partial\sigma}{\partial\Omega}\right)_{VAN}\right] \Delta\tau . \frac{N_S}{N_V} . \frac{\varepsilon_\tau}{\varepsilon_{\tau_0}}$$

CROSSX then obtains the corrected time-of-flight cross-section, YC, given by

$$YC = \frac{\partial^2\sigma}{\partial\Omega\partial\tau} . \frac{4\pi}{\sigma_{SAM}}$$

so

$$YC = \left[\frac{A1(S-B_S)}{V_S} - \frac{A2(B-B_B)}{V_B}\right] \frac{1}{\Delta\tau} . \frac{1}{A3} . \frac{N_V}{N_S} . \frac{\sigma_{VAN}}{\sigma_{SAM}} \frac{\varepsilon_{\tau_0}}{\varepsilon_\tau}$$

where S = sample counts (gouped for better statistics, if required)

B_S, B_B = flat backgound

V_S, V_B = vanadium elastic peak counts for sample and background runs.

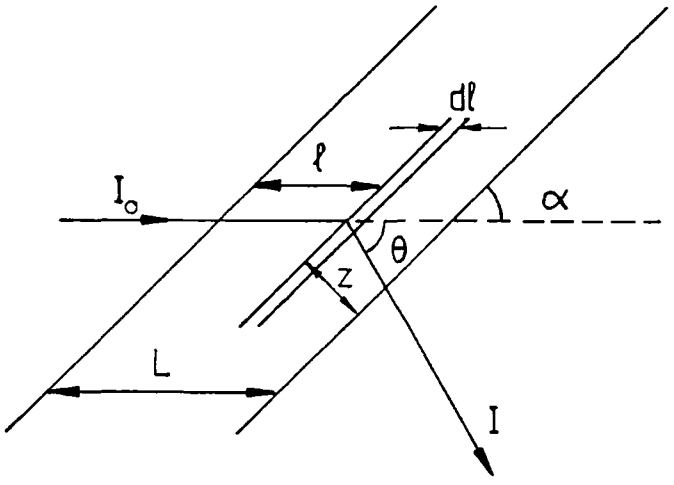
B = empty container counts

A1, A2 = normalisation factors

A3 = correction factor calculated to account for sample (or vanadium) scattering and absorption of the incident beam

Calculation of Correction Factor, A3[47]

The following diagram shows a beam of neutrons with initial intensity I_0 incident upon a plane sample of uniform finite thickness L. α defines the relative orientation of the incident neutrons and the sample. The incident beam is scattered through an angle θ to emerge with final intensity I. A3 is a factor to correct for loss of intensity due to scattering and absorption by a sample of finite thickness.



This method of calculating A3 assumes that the scattering of more-than-once scattered neutrons should be ignored.

$$\frac{I}{I_0} = \exp(-\rho\sigma_T \ell) \cdot \rho \cdot \int_0^L \frac{\partial\sigma}{\partial\Omega} \cdot \exp(-\rho\sigma_A z)\, d\ell$$

where σ_T = total(absorption + scattering) cross-section
ρ = no. of atoms per cm^3
and other variables are as indicated in the diagram.

Now $$\frac{z}{\sin\alpha} = \frac{L-l}{\sin(\pi-(\alpha+\theta))} = \frac{L-l}{\sin(\alpha+\theta)}$$

so $$z = (L-l)\frac{\sin\alpha}{\sin(\alpha+\theta)} = (L-l)S \quad \text{where } S = \frac{\sin\alpha}{\sin(\alpha+\theta)}$$

Then $$\frac{I}{I_0} = \rho\left(\frac{\partial\sigma}{\partial\Omega}\right)\exp(-\rho\sigma_A(L-l)S)\int_0^L \exp(-\rho\sigma_T \ell)\, d\ell$$

giving $$\frac{I}{I_0} = \rho\left(\frac{\partial\sigma}{\partial\Omega}\right)L \left[\frac{\exp(-x_A S) - \exp(-x_T)}{x_T - x_A S}\right]$$

where $x_A = \rho\sigma_A L$ and $x_T = \rho\sigma_T L$

The term outside the brackets gives the intensity obtained when loss from the incident beam, and loss from the scattered beam by absorption or second scattering is ignored. Thus

$$A3 = \left[\frac{x_T - x_A S}{\exp(-x_A S) - \exp(-x_T)}\right]$$

Having obtained YC, the corrected counts, the double differential cross-section with respect to energy is easily obtained, using the expression[55]

$$\frac{\partial^2\sigma}{\partial\Omega\partial E} = \frac{\tau^3}{\hbar m}\left(\frac{\partial^2\sigma}{\partial\Omega\partial\tau}\right)$$

and thence the scattering law, $S(\underline{Q},\omega)$, via

$$S(\underline{Q},\omega) = \frac{k_0}{Nk|b-\bar{b}|^2}\left(\frac{\partial^2\sigma}{\partial\Omega\partial E}\right)$$

A line-printer listing and plots of the scattering law, $S(\underline{Q},\omega)$, or the symmetrised scattering law, $\tilde{S}(\underline{Q},\omega)$ are available as required.

Treatment of CROSSX Data to obtain the EISF

CROSSX data is subsequently analysed using the program WONDERPROG[56] .This program is available both at the ILL and at the Rutherford Laboratory. CROSSX data to be analysed in England is written to a magnetic tape at the ILL, using the program TENIBM[52] which converts it into acceptable format for the IBM 360 computer at the Rutherford Laboratory.

Two stages are involved in using WONDERPROG. The

first stage is to create an input file for the fitting program by taking the required resolution and sample data and writing them onto a separate disk file.

The second stage involves fitting a model to the experimental data. As in SUPER and SAND, the fitting program convolutes the resolution function with a model scattering law and fits to the measured sample scattering data. Various model scattering laws are available - these include simple jump models (e.g the Barnes model[57] for N-fold jump rotational motion) which are designed for extracting the EISF and rotational time constants from the quasi-elastic data (see chapter 3), and also more general models, which are able to fit a sum of δ-functions, Lorentzians and Gaussians to the data, as required.

Various starting parameters are used to define the approximate quasi-elastic width, position of the elastic peak etc.,and in addition, for reorientational models, the number of sites and radius of gyration of the rotating group are also required for calculation of the model $S(\underline{Q},\omega)$.

Output is in the form of a line-printer listing which gives final fitted parameters including the quasi-elastic width and the experimental value of the EISF.

2.3.3 Analysis of Inelastic Data from 4H5[47]

Since 4H5 is also a time-of-flight spectrometer,much of the initial analysis is similar to that described previously for IN5.Again, a preliminary program is run for monitor and vanadium peak analysis to calculate run parameters to be used subsequently. This program at Harwell is known as PRESCAT[47] and is exactly analogous to PRIME. The corrected time-of-flight cross-section, YC, and the symmetrised scattering law $\tilde{S}(\underline{Q},\omega)$ are calculated exactly as in CROSSX, using the Harwell form of the program called CIRCA[47] .

A most useful function obtained from inelastic neutron scattering data is the hydrogen-amplitude-weighted frequency distribution function, $\rho(\omega)$ (or $\rho(\beta)$, since $\beta=h\omega/kT$) (see chapter 3), and this calculated using the program FLORENCE[58].

$\tilde{S}(\underline{Q},\omega)$ is related to $\tilde{S}(\alpha,\beta)$ via the relationships[58]

$$\alpha = \frac{\hbar^2 Q^2}{2MkT} \qquad \text{and} \qquad \beta = \frac{\hbar\omega}{kT}$$

(where all symbols have their usual meanings)

and $$\rho(\beta) = \lim_{\alpha \to 0} \left(\frac{\ln S(\alpha,\beta)}{\alpha} \right) \times 2\beta\sinh\beta/2$$

Since the flight path is different for every scattering angle, the energy transfer (or β) for a given channel number varies with different angles. The experimental values of $\tilde{S}(\alpha,\beta)$ and α are sorted into sets with similar values of β. (The deviation of β values in each set is limited to less than 1% from the mean and less than the instrument resolution). This results in three arrays- one containing the average values of β, $\bar{\beta}$, and the other two dimensional arrays defining α and $\tilde{S}(\alpha,\beta)$ for each angle and each value of $\bar{\beta}$. A least squares straight line fit is made for each value of $\bar{\beta}$ to give

$$\ln \frac{\tilde{S}(\alpha,\beta)}{\alpha} \quad \text{against } \alpha$$

to allow the extrapolation to zero α (i.e zero Q) to be made.

Output takes the form of a line-printer listing with plots as required. Values of $\rho(\beta)$ are printed, along with $2\beta\sinh\beta/2$, and $\tilde{S}(\alpha,\beta)/\alpha$.

2.3.4 Analysis of IN6 Data

Raw data obtained from IN6 is initially analysed using PRIME and CROSSX[54], exactly as for IN5 and 4H5. Subsequent analysis of the inelastic spectra to obtain the hydrogen-amplitude-weighted frequency distribution function is identical to that performed on 4H5 inelastic data, using FLORENCE. Quasi-elastic analysis is identical to that performed on IN5 data, using the program WONDERPROG.

2.3.5 Analysis of 10H Data

Output of the data from an experiment on 10H takes the form of a teletype listing of the number of neutrons detected at each angle of scatter. Preliminary analysis simply involves subtracting a background recorded over the same Q range as the sample run. The corrected intensity as a function of Q now gives the structure factor, S(Q), directly.

Chapter 3 Application of Neutron Scattering to the Study of Sidechain Motion in Poly(methyl methacrylate)

In this chapter the rotational and vibrational motions of the two methyl groups in poly(methyl methacrylate) (PMMA) will be discussed. It will be shown that detailed information about torsional frequencies and barrier heights to rotation for the two sidegroups may be obtained from inelastic neutron scattering measurements. A function, the hydrogen-amplitude-weighted density of states at zero momentum transfer, $\rho(\omega)$, is introduced, which allows direct comparison between neutron and optical data. Later, it will be shown that the geometry of the rotational motion of the sidegroups may be defined by a single function, the elastic incoherent structure factor (EISF) which is a direct measure of the spatial distribution of the protons. In addition, measurements relating rotational correlation times to temperature in order to calculate activation energies are presented, and compared to barrier heights obtained from the inelastic measurements.

Since the systems under study contain a large percentage of hydrogen, the scattering is expected to be almost totally incoherent,due to the large incoherent scattering cross-section of hydrogen. Any coherent scattering arising will be from elastic (Bragg) reflections, and the problems associated with accounting for coherent scattering are discussed in section 3.3.6

3.1 Theoretical Considerations

3.1.1 Theory of Incoherent Scattering from a Polymer Molecule

As shown in chapter 2, the incoherent scattering law, $S(\underline{Q},\omega)$ is directly related to the space-time distribution function of the moving proton, via

$$S_{inc}(\underline{Q},\omega) = \int_{-\infty}^{\infty} G_s(\underline{r},t) \exp i(\underline{Q}.\underline{r} - \omega t) d\underline{r} dt$$

$$\text{with} \quad \int_{-\infty}^{\infty} S_{inc}(\underline{Q},\omega)\,d\omega = I_{inc}(\underline{Q},t=0) = 1$$

so that in principle, at least, a neutron scattering experment should give very direct dynamical information about the system.

On the other hand, however, because the neutron does follow the motion of the moving protons so closely, all possible kinds of motion (torsion, rotation, diffusion etc.) undergone by the protons are reflected together in the observed spectra, and separation of the individual components is an almost impossible task without making some simplifying assumptions.

The motions in a molecular system are generally divided into two categories - short-time motions, to include vibration and libration, and long-time motions, to include translational and rotational motions. This separation into different components on different time-scales will be important in the following section, where the overall scattering law for a polymer molecule is established.

Consider the position vector, $\underline{R}_L$, of a proton in a molecule. This may be expanded into the following form:

$$\underline{R}_L = \underline{c}_L + \underline{b}_L + \underline{u}_L$$

where $\underline{c}_L$ is the position vector of the centre of mass
$\underline{b}_L$ the mean position vector of the proton relative to the centre of mass
and $\underline{u}_L$ is its displacement from the mean

$\underline{c}_L$, $\underline{b}_L$ and $\underline{u}_L$ are time-varying functions, where $\underline{u}_L$ depends on the internal molecular vibrations, $\underline{b}_L$ varies with overall molecular rotations and $\underline{c}_L$ with translational motions.

If each is expressed as an independent Heisenberg operator, then the overall scattering law, to include terms for all three types of motion is given by[43]

$$S_{inc}(\underline{Q},\omega) = \frac{1}{2\pi\hbar N}\int dt\ \exp(-i\omega t)\sum_{n} p_n \langle\psi_n|\exp\{-i\underline{Q}.(\hat{\underline{c}}_L(0)+\hat{\underline{b}}_L(0)+\hat{\underline{u}}_L(0))\}$$

$$\times\ \exp\{-i\underline{Q}.(\hat{\underline{c}}_{L'}(t)+\hat{\underline{b}}_{L'}(t)+\hat{\underline{u}}_{L'}(t))\}\psi_n^*\rangle$$

At this point the first major assumption for simplifying $S(\underline{Q},\omega)$ is made. The three motions - translation, rotation and vibration - are assumed to be dynamically uncoupled, so that the total wave function ψ_n can be expressed as a product of three separate terms i.e

$$\psi_n = \psi_n(trans)\psi_n(rot)\psi_n(vib)$$

and $$S_{inc}(\underline{Q},\omega) = \frac{1}{2\pi\hbar N}\int dt\ \exp(-i\omega t)\sum_{ll'}\langle\exp(-i\underline{Q}.\hat{\underline{c}}_L(0))\ \exp(i\underline{Q}.\hat{\underline{c}}_{L'}(t))\rangle$$

$$\times\ \langle\exp(-i\underline{Q}.\hat{\underline{b}}_L(o))\exp(i\underline{Q}.\hat{\underline{b}}_{L'}(t))\rangle$$

$$\times\ \langle\exp(-i\underline{Q}.\hat{\underline{u}}_L(0))\exp(i\underline{Q}.\hat{\underline{u}}_{L'}(t))\rangle$$ [43]

Since the Fourier transform of a product is a convolution,

$$S_{inc}(\underline{Q},\omega) = \frac{1}{2\pi\hbar N}\ S_{inc}^{trans}(\underline{Q},\omega) * S_{inc}^{rot}(\underline{Q},\omega) * S_{inc}^{vib}(\underline{Q},\omega)$$

Clearly the assumption that the three motions are uncoupled may not be true. The separation of the vibrational motion is probably reasonable, since vibrations occur on a much shorter timescale than the other two motions. However, the validity of separating the rotational and translational motion is not obvious, and in some cases, particularly in liquids, these two motions probably are coupled. However, in the system under study, the methyl groups are highly symmetric, so the coupling is expected to be small[42]. In addition, since the rotational motion is being observed at temperatures below the glass transition, no translational contribution to the overall scattering law is expected.

The independent contributions to the overall scattering law will now be considered in greater detail. As mentioned previously, translational motion of the protons

in the methyl groups will not be encountered for PMMA under the given experimental conditions, so $S_{inc}^{trans}(\underline{Q},\omega)$ will not be discussed.

3.1.2 The Scattering Law for Molecular Vibrations, $S_{inc}^{vib}(\underline{Q},\omega)$, and the Hydrogen-Amplitude-Weighted Density of States

The study of molecular vibrations has traditionally been performed using infra-red and Raman spectroscopy techniques. These provide a great deal of information about a system,but for highly symmetrised molecules neither technique alone is sufficient to reveal all of the vibrational frequencies, because of optical selection rules, and it is necessary to use the two techniques in conjunction. Furthermore, there are even some normal modes (e.g methyl torsions) where the electric dipole moment change and polarisability change of the molecule are so small that the mode is inaccessible with either technique. Neutron spectroscopy is not limited by such selection rules, and it will be shown that modes such as methyl torsions are expected to appear strongly in the inelastic neutron spectrum. In addition, data at appreciable momentum transfers are measured in an inelastic neutron scattering experiment, thus allowing the whole density of states for both intra- and intermolecular modes of vibration to be measured, in contrast to optical spectroscopy in which only modes close to zero momentum transfer may be observed.

It can be shown that the double differential cross-section for incoherent inelastic scattering may be given by[59]

$$\frac{\partial^2\sigma}{\partial\Omega\partial E} = \sum_{\lambda,k}\frac{k}{k_0}\,\delta(\hbar\omega\pm\hbar\omega_\lambda(k))\,\frac{\hbar(n_\lambda+\frac{1}{2}\pm\frac{1}{2})}{2\omega_\lambda(k)}\;x\;\sum_\rho\frac{b^2}{M}\,|\underline{Q}.\underline{U}_\rho(k)|^2\exp(-2W_\rho)$$

where the first sum (over wave vectors $\underline{k}$ and normal modes λ) is over all internal and external modes of the molecule, and the second sum is over all atoms of mass M_ρ within the molecule.

$$n_\lambda = \{\exp(\hbar\omega/kT - 1\}^{-1} \quad \text{(i.e the Bose-Einstein distribution)}$$

As defined previously, $\underline{Q}$ is the momentum transfer, and $\hbar\omega$ the energy transfer on scattering. $\underline{U}_\rho$ is the mass-weighted displacement vector of the atom, and $\exp(-2W_\rho)$ the Debye-Waller factor.

It is possible to transform the summation over $\underline{k}$ and λ to an integration over a density of states, $g(\omega)$[59] so that,

$$\left(\frac{\partial^2\sigma}{\partial\Omega\partial E}\right) = \frac{k}{k_0} \sum_\nu (b^\nu_{inc})^2 Q^2 \ (n_\lambda + \tfrac{1}{2} \pm \tfrac{1}{2}) \exp(-2W_\nu) \ \frac{N g(\omega)}{\omega} \qquad (3.1)$$

where $$g(\omega) = \sum_{\underline{k},\lambda} |C_\rho(k)|^2 \ \delta\{\hbar\omega - \hbar\omega_\lambda(k)\}$$

and $C_\rho(k)$ are the normalised position vectors ($\sum_\rho (C^\lambda_\rho(k))^2 = 1$) for each atom of type ρ in the normal mode λ.

$C_\rho(k)$ is directly related to $u_\rho(k)$ via

$$|u_\rho(k)| = \left[\frac{\hbar}{2m_\rho\omega_\lambda(k)} \coth\left(\frac{\hbar\omega_\lambda(k)}{2kT}\right)\right]^{\frac{1}{2}} |C_\rho(k)|$$

In equation (3.1) the upper sign in $\pm\frac{1}{2}$ refers to neutron energy loss - so-called 'down scattering' and the lower sign to neutron energy gain, corresponding to 'up scattering'.

ν now represents the sum over those atoms having a large incoherent scattering cross-section, b_{inc}, since $g(\omega)$ is heavily weighted by these[59]. Since the incoherent scattering cross-section for hydrogen is an order of magnitude greater than that of any other common element, and in addition, because of its small mass, $\langle u_\nu^2 \rangle$, the amplitude of displacement is expected to be large ($\langle u_\nu^2 \rangle$ is inversely related to mass). Thus for hydrogenous materials, such as the poly(methyl methacrylate) under investigation in this thesis, the incoherent scattering cross-section is

dominated by the hydrogenous contribution. It is therefore possible to remove the $\sum_{\nu}$ in equation (3.1) and consider the incoherent inelastic scattering to be solely due to hydrogen. The incoherent scattering law for molecular vibrations may then be obtained from

$$S_{inc}^{vib}(\underline{Q},\omega) = \frac{\hbar}{Nb_H^{inc}} \frac{k}{k_0} \left(\frac{\partial^2\sigma}{\partial\Omega\partial E}\right)_{inc}$$

where $\left(\frac{\partial^2\sigma}{\partial\Omega\partial E}\right)_{inc}$ is now given by

$$\left(\frac{\partial^2\sigma}{\partial\Omega\partial E}\right)_{inc} = \frac{k}{k_0} (b_H^{inc})^2 \; Q^2 \; (n_\lambda + \tfrac{1}{2} \pm \tfrac{1}{2}) \exp(-2W) \frac{N\, g(\omega)}{\omega} \qquad (3.2)$$

Combination of these last two expressions allows $g(\omega)$ to be obtained directly. However, since neutron scattering experiments are normally performed by detecting neutrons which have <u>either</u> gained <u>or</u> lost energy, it is often useful to consider the symmetrised scattering law $\tilde{S}(\underline{Q},\omega)$, in which case it can be shown[43 55] that $g(\omega)$, the hydrogen-amplitude-weighted density of states, is given by

$$g(\omega) = \sinh(\hbar\omega/2kT) \exp(2W) \frac{\tilde{S}(\underline{Q},\omega)}{Q^2}$$

The question now arises of relating the spectra observed using inelastic neutron scattering techniques to those obtained from optical measurements. Three types of behaviour are possible. Firstly, the optical and neutron spectra may show the same number of vibrational features (although with different intensities). Secondly, since neutron scattering is not subject to optical selection rules, it might be expected that the neutron spectra should reveal more information than the optical spectra. Thirdly, because the neutron spectrum is heavily dominated by the hydrogen in the system, it could be expected that it might contain

fewer vibrational features than the optical spectrum, due to lack of information about atoms other than hydrogen. As pointed out earlier, an inelastic neutron scattering experiment measures the intensity of the scattered neutrons both as a function of energy transfer and momentum transfer (i.e the neutron spectrum represents a cut through energy-transfer and momentum transfer space), so that it is not suitable for direct comparison with optical data, measured at close to zero momentum transfer. A function found to be more suitable than the inelastic scattering law for direct comparison with optical measurements is the hydrogen-amplitude-weighted density of states function at zero Q, $\rho(\omega)$ (also known as the hydrogen-amplitude-weighted frequency distribution function at zero Q). This is obtained from the experimental data by extrapolation over all scattering angles to zero momentum transfer, and is given by[59],

$$\rho(\omega) = \lim_{Q\to 0}\left[\frac{\tilde{S}(Q,\omega)}{Q^2}\right] \sinh(\hbar\omega/2kT)\ \exp(2W)$$

Clearly $\rho(\omega)$ is directly related to $g(\omega)$, the difference between the two lying in the extrapolation to zero Q.

It has been shown[59] by direct comparison that the features observed in $\rho(\omega)$ are essentially identical to those obtained from Raman and infra-red measurements, although optical intensities are proportional to transition probabilities, whereas neutron scattering is only intense where there is a large amplitude of motion of hydrogen. It is worth mentioning briefly the use of isotopic substitution as an aid to making vibrational assignments. In optical spectroscopy the method depends upon selective substitution of, for example, hydrogen by deuterium, and noting the subsequent shifts in the IR or Raman spectrum. In neutron scattering, however, not only do these shifts occur, but furthermore, because of the large difference in cross-section of hydrogen and deuterium, very large changes in band intensity also occur, and so the modes with large hydrogen amplitudes can be made to disappear almost completely, with suitable substitution.

For the PMMA investigated in this work, it might be expected that substitution of the hydrogen by deuterium should lead to large shifts in the bands observed in the frequency distribution function, since the peak position is determined by the mean amplitude of displacement of the atom, which is inversely related to mass. Thus replacement of hydrogen by deuterium should lead to a change in peak position given by a factor of $\sqrt{2}$. However, the vibrational motion being studied is not that of single hydrogen atoms, but of the entire methyl group - whose atomic weight is 15. The corresponding atomic weight with deuterium substitution is 18, thus the change of peak position is predicted to be only of the order of $\sqrt{18/15}$, a much smaller change than expected at first sight.

For the band assignments made later in the chapter, use is made both of the difference in intensities of diif-erent peaks due to the differing hydrogen content of the sample,using selective deuteration, and also direct comparison between $\rho(\omega)$ and optical measurements.

3.1.3 Calculation of Barrier Heights from Inelastic Data

For poly(methyl methacrylate), the inelastic peaks in $\rho(\omega)$ may be identified with vibrational frequencies of the methyl groups in the molecule, and in certain circumstances it is possible to calculate a barrier to rotation. The conditions to be satisfied are, firstly, that the group should be symmetric, so that the potential function $V(\phi)$ can be reasonably assumed to be a function of only barrier height (V_3) and torsional angle ϕ, and secondly that the observed inelastic peak is due mainly to the $1 \rightarrow 0$ transition. Clearly, for PMMA, the first condition is satis-fied, and the second is reasonably assumed, based on comparison with the simple harmonic oscillator[34] - a simple calculation of the scattering law for this case shows that more than 88% of the inelastic intensity is due to the $1 \rightarrow 0$ transition at 373K.

The rotation of a methyl group hindered by a potential barrier $V(\phi)$ may be well approximated by the first term in a Fourier series

$$V(\phi) = \frac{V_3}{2}(1 - \cos 3\phi)$$

Since the methyl groups are attached to relatively heavy main chains, coupling between methyl torsional oscillations and other normal modes may be ignored.

For a CH_3 group undergoing rotation about the C - C bond, the Schrödinger wave equation is [60]

$$\left[-F\frac{\partial^2}{\partial\phi^2} + V(\phi)\right]\psi_{\nu\sigma}(\phi) = E_{\nu\sigma}\,\psi_{\nu\sigma}(\phi)$$

where ν is the torsional quantum number, F is a geometrical factor representing the reduced rotational constant of the group and σ specifies the periodicity of the wave functions, ψ. E is the torsional eigenvalue.

This equation may be transformed into Mathieu's differential equation[61]

$$\frac{\partial^2 y}{\partial x^2} + (b - s\cos^2 x)y = 0 \qquad (3.3)$$

by substituting $\quad 2x = 3\alpha + \pi \qquad y_{\nu\sigma}(x) \equiv \psi_{\nu\sigma}(\phi)$

It can then be shown[60 61]

$$V_3 = \frac{9Fs}{4} \qquad E_{\nu\sigma} = \frac{9F}{4}\,b_{\nu\sigma} \qquad (3.4)$$

In equation (3.3) s and b are dimensionless parameters corresponding to barrier height and torsional energy levels. For each value of s, there is a set of eigenvalues b_ν, further specified by the parameter σ, which identifies the periodicity of the wave function.

For a three-fold symmetric top, the allowed values of σ are 0 and ± 1[60 61] and the eigenfunctions have A or E symmetry character respectively. When V_3 is not too low (> 1 kcal/mol) the energy difference between the two states is small for the ground level, and may be considered negligible, so the subcript may be omitted.

$$\text{Thus,} \quad E_1 - E_0 = \hbar\omega_0$$

where $\hbar\omega_0$ is the observed position of the peak in the neutron spectrum, and from (3.4)

$$b_0 - b_1 = \frac{4\omega_0}{9F}$$

If the geometry of the molecule is known, F, and hence $b_0 - b_1$ may be calculated. The value of s corresponding to Δb can be obtained from tables listing values of b as functions of s, and finally V_3 may be found, using

$$V_3 = \frac{9\,Fs}{4}$$

3.1.4 The Rotational Scattering Law, $S^{rot}_{inc}(\underline{Q},\omega)$

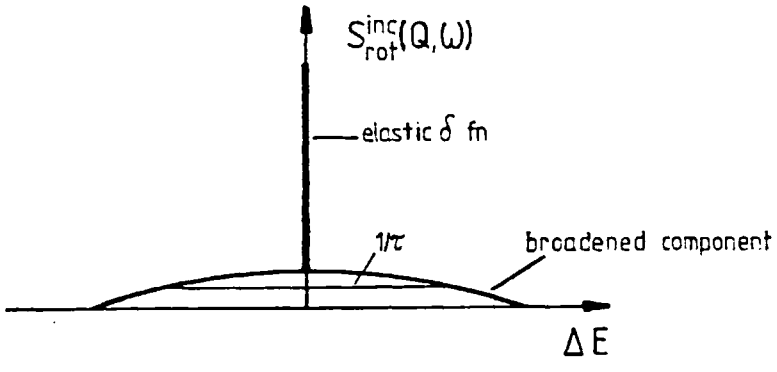
In a polymer system containing rotating sidegroups, but with no translational motion of the backbone (i.e below T_g, the glass transition temperature) it can be shown[33] that the incoherent quasi-elastic scattering law is expected to take the form of a δ-function, attributed to fixed centre of mass motion of the group, superimposed on a broad quasi-elastic component whose width characterises the frequency of rotation i.e in the most general case,

$$S^{rot}_{inc}(\underline{Q},\omega) = A_o(\underline{Q})\,\delta(\omega) + S^{qel}_{inc}(\underline{Q},\omega)$$

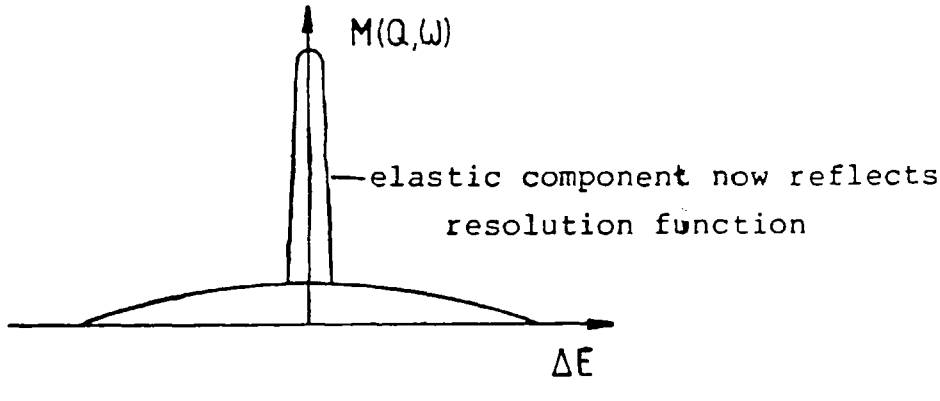
(Later in the chapter, specific models of rotation applicable to the methyl group motion in PMMA will be

considered, and it will be seen that in all cases the rotational scattering law is of this general form.)

Schematically, $S^{rot}_{inc}(\underline{Q},\omega)$ may be represented in the following way



However, due to the finite resolution of any spectrometer, the measured spectrum usually has an appearance similar to that shown below.



Thus the measured scattering law comprises a convolution of the resolution function with the true scattering law, i.e

$$M^{rot}_{inc}(\underline{Q},\omega) = S^{rot}_{inc}(\underline{Q},\omega) * R(\underline{Q})$$

where $R(\underline{Q})$ represents the resolution function.

The methods of deconvolution to obtain $S^{rot}_{inc}(\underline{Q},\omega)$

the true rotational scattering law have been discussed in chapter 2.

Furthermore, although the problem of translational motion may be overcome by working below the glass transition temperature, the contribution of vibrational motions to the observed spectrum must be considered. If the vibrational frequencies are sufficiently high, the scattering law for molecular vibrations may be expanded in terms of $\hbar\omega$[33 36 42] and it can be shown[42] that the only vibrational contribution to the quasi-elastic scattering law is expected to be through the Debye-Waller factor, $\exp(-Q^2\langle u^2\rangle)$, where $\langle u^2\rangle$ is the mean square amplitude of vibration.
Thus,

$$S_{obs}(\underline{Q},\omega) = \exp(-Q^2\langle u^2\rangle)\ S^{rot}_{inc}(\underline{Q},\omega)$$

where $S^{rot}_{inc}(\underline{Q},\omega)$ is the scattering law which would be observed if the molecules in the sample were undergoing purely random reorientational motion.

Finally, $$M^{rot}_{inc}(\underline{Q},\omega) = S_{obs}(\underline{Q},\omega) * R(\underline{Q})$$

If $\langle u^2\rangle$ is small in the region covered by the quasi-elastic scattering measurements, the exponential may be expanded, and a flat background fitted to the data during analysis. However, it may be that $\langle u^2\rangle$ is not sufficiently small for this approximation to be valid, in which case the full exponential form of the Debye-Waller factor must be considered.

As mentioned, in the most general case, the final rotational scattering law obtained, $S^{rot}_{inc}(\underline{Q},\omega)$ is predicted to be of the form[33 42]

$$S^{rot}_{inc}(\underline{Q},\omega) = A_0(\underline{Q})\,\delta(\omega) + S^{qel}_{inc}(\underline{Q},\omega)$$

$A_0(\underline{Q})$, which defines the intensity of the purely elastic

component (provided the scattering law is normalised, so that $\int S^{rot}_{inc}(\underline{Q},\omega)d\omega = 1$) is known as the elastic incoherent structure factor (EISF) and gives the time averaged spatial distribution of the protons, thus describing completely the geometry of the rotational motion. The time evolution of the proton position is contained in the quasi-elastic term.

An experimental value of the EISF may be obtained provided the experiment is performed at sufficiently high resolution to separate the two components of the scattering law, in which case the experimental EISF is given by,

$$EISF = \frac{I_{el}}{I_{el} + I_{qel}}$$

In some cases the separation of the purely elastic component from the quasi-elastic contribution may be made by natural extrapolation, after the subtraction of a flat inelastic background. The uncertainty in the separation and in the relative intensity and separation of the inelastic background gives the accuracy in the experimentally determined $A_0(\underline{Q})$.

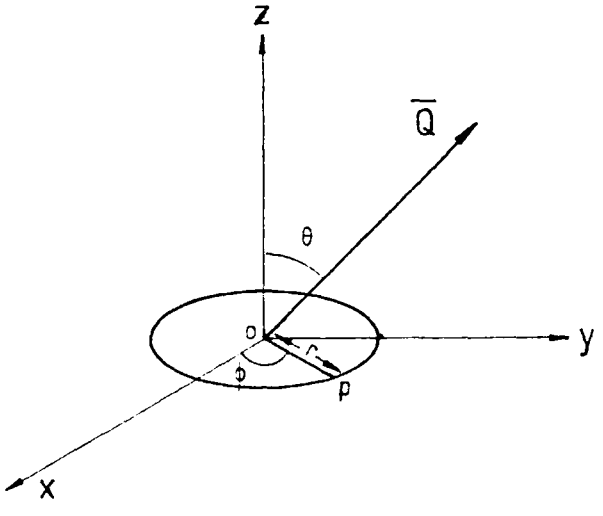
It may be that the two components are not sufficiently well defined to separate them in this way. In this case, the relative intensities, and hence the EISF may be obtained using computer fitting programs, as outlined in chapter 2, whereby a model scattering law is folded with the resolution function and fitted to the experimental data.

The following sections show the calculation of $A_0(\underline{Q})$ for various models of rotation, with a view to comparison between the calculated $A_0(\underline{Q})$ and the experimental EISF obtained for the rotation of the α-methyl and ester methyl groups in poly(methyl methacrylate).

3.1.5 Rotational Motion Between N Equivalent Sites on a Circle of Radius r

Calculation of the rotational scattering law may be approached in a number of ways. The method outlined here follows that of Dianoux and Volino[35] .

It is assumed that the motion consists of a number of instantaneous jumps between N equivalent sites on a circle of radius r. The motion is characterised by a mean jump time, τ.



ϕ_0 and ϕ are the angular positions of the scattering nucleus on a circle of radius r, at times t=0 and t=t, respectively.

It is first necessary to obtain an expression for the motion in terms of a distribution function describing the possible positions, ϕ. This distribution function is given by the Fokker-Planck equation[35] .

$$\frac{\partial P_{rot}(\phi,\phi_0;t)}{\partial t} = -\frac{1}{\tau} P_{rot}(\phi,\phi_0;t) + \frac{1}{2\tau} \{P_{rot}(\phi-\alpha,\phi_0;t) + P_{rot}(\phi+\alpha,\phi_0;t)\} \qquad (3.5)$$

where α is the jump angle and τ the time between sites.

The most general solution to (3.5) is

$$P_{rot}(\phi,\phi_0;t) = \frac{1}{2\pi}\sum_{n=-\infty}^{\infty}\exp\{in(\phi-\phi_0)\}\exp\left[-\frac{(1-\cos n\alpha)|t|}{\tau}\right] \qquad (3.6)$$

For a random walk among N equivalent sites, $\alpha = 2\pi/N$. Substituting for α, and letting

$$\tau_n = \frac{\tau}{1-\cos n\alpha} \qquad \tau_{n+pn} \equiv \tau_n \quad (p=\text{integer})$$

(3.6) becomes

$$P_{rot}(\phi,\phi_0;t) = \frac{1}{N}\sum_{n=0}^{N-1}\exp\left[-\frac{|t|}{\tau_n}\exp\{in(\phi-\phi_0)\} \times \sum_{p=-\infty}^{\infty}\delta(\phi-\phi_0-2\pi p/N)\right]$$

The intermediate scattering law, $I^{rot}_{inc}(\underline{Q},t)$ is then given by[35]

$$I^{rot}_{inc}(\underline{Q},t) = \int_0\int^{2\pi}\exp\{-i\underline{Q}.\underline{r}(0)\}\exp\{i\underline{Q}.\underline{r}(t)\}\ P_{rot}(\phi,\phi_0;t)\,d\phi\,d\phi_0$$

Substituting for $P_{rot}(\phi,\phi_0;t)$ and performing the integral,

$$I^{rot}_{inc}(\underline{Q},t) = \sum_{n=0}^{N-1} a_n(Q\sin\theta)\exp(-|t|/\tau_n)$$

where $$a_n(Q\sin\theta) = \frac{1}{N}\sum_{p=1}^{N} J_0\{2Q\sin\theta\sin(\pi p/N)\}\cos(n2\pi p/N)$$

and the rotational scattering law is given by,

$$S^{rot}_{inc}(\underline{Q},\omega) = a_0(Q\sin\theta)\delta(\omega) + \frac{1}{\pi}\sum_{n=1}^{N-1} a_n(Q\sin\theta)\ \frac{\tau_n}{1+(\omega\tau_n)^2} \qquad (3.7)$$

where $\tau_n = \dfrac{\tau_1 \sin^2\pi/N}{\sin^2 n\pi/N}$ and $\tau_1 = \dfrac{\tau}{1-(\cos 2\pi/N)}$

This result has been obtained by Barnes[57].

Equation (3.7) is for a single crystal, and for an amorphous material it is necessary to perform an isotropic average

over θ, to give,

$$\overline{S_{inc}^{rot}(\underline{Q},\omega)} = A_0(\underline{Q})\,\delta(\omega) + \frac{1}{\pi}\sum_{n=1}^{N-1} A_n(\underline{Q})\,\frac{\tau_n}{1+(\omega\tau_n)^2}$$

where $$A_n(\underline{Q}) = \frac{1}{N}\sum_{p=1}^{N} j_0\{2Qr\sin(\pi p/N)\}\cos(n2\pi p/N)$$

$j_0(x)$ is the zero order spherical Bessel function.

Figures 3.1 and 3.2 show the behaviour of $A_0(\underline{Q})$ for some specific cases. Comparison of the curves leads to some general conclusions regarding the shape of $A_0(\underline{Q})$, applicable to all values of N and r for a powder sample.

For a given value of N, increasing r moves the minimum of the curve in, towards Q=0, in direct proportion to the increase in r (i.e if r is doubled, then the Q value at the position of the minimum is halved), although the actual value of the EISF at the minimum is constant. A clear difference between curves with the same N, but different r exists even at low values of Q.

For a given r, but with the possibility of varying N, the position of the minimum is not much changed, but the value of the EISF at its minimum point is no longer constant. In addition, the curves appear very similar until much higher Q values.

3.1.6 Calculation of the EISF for a More Complex Rotation

On considering the application of the measurement of the EISF to the specific case of the rotation of the methyl groups in PMMA, it is useful to investigate the types of motion which the sidegroups could conceivably be undergoing.

The case of the α-methyl group is quite simple. Almost

Fig 3.1 Random jump between 3 sites

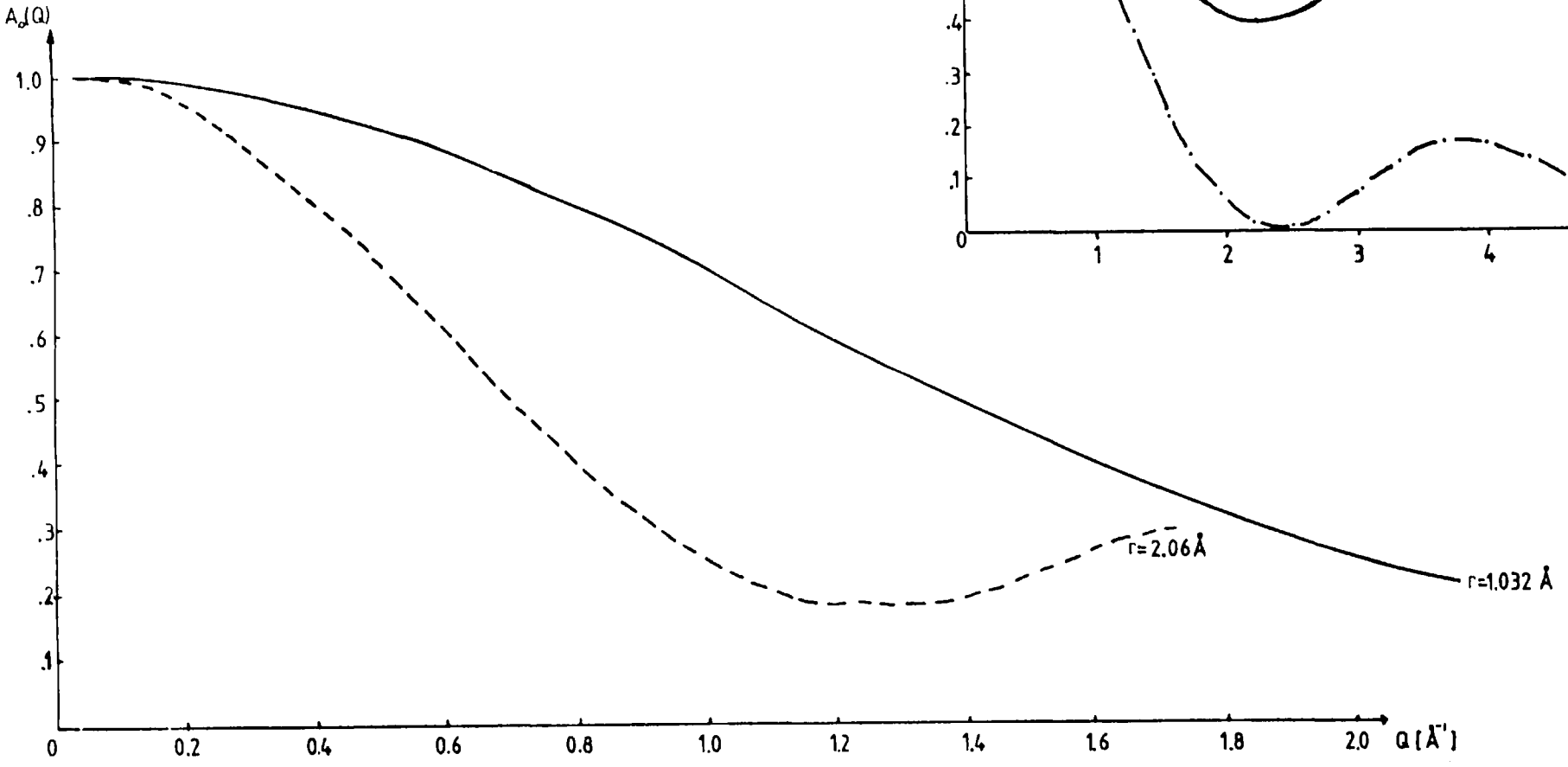
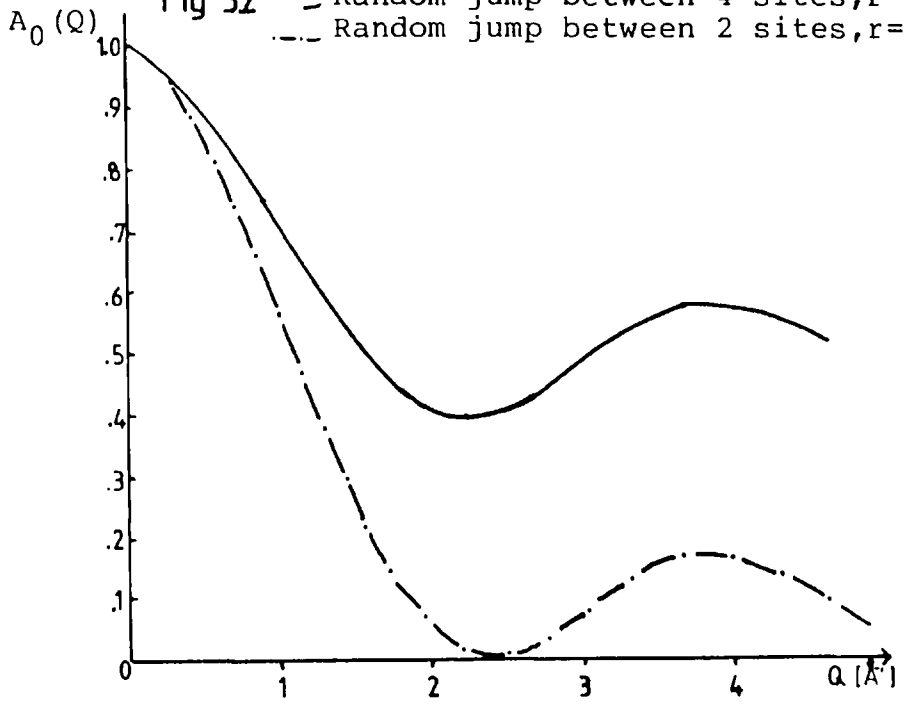


Fig 32 — Random jump between 4 sites, r=1Å
-.-.- Random jump between 2 sites, r=1Å



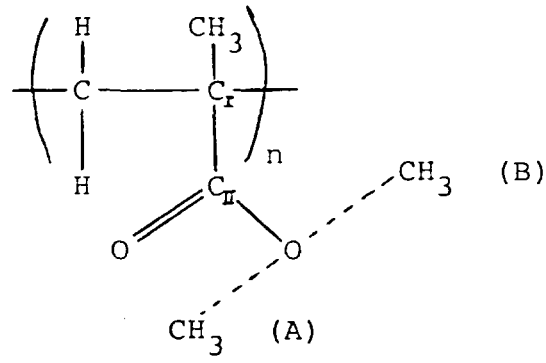
undoubtedly the motion comprises either a simple jump motion between three equivalent sites, or possibly continuous rotational diffusion on a circle. In either case, a theoretical value of the expected EISF can be calculated using equation (3.7), with r=1.032 Å and N=3 in the first case, or r=1.032 Å and N→∞ in the second, i.e for the first case,

$$A_0(\underline{Q}) = \frac{1}{3}\{1+2j_0(Qr)\} \qquad (3.8)$$

and for the second case,

$$A_0(\underline{Q}) = j_0^2(Qr)$$

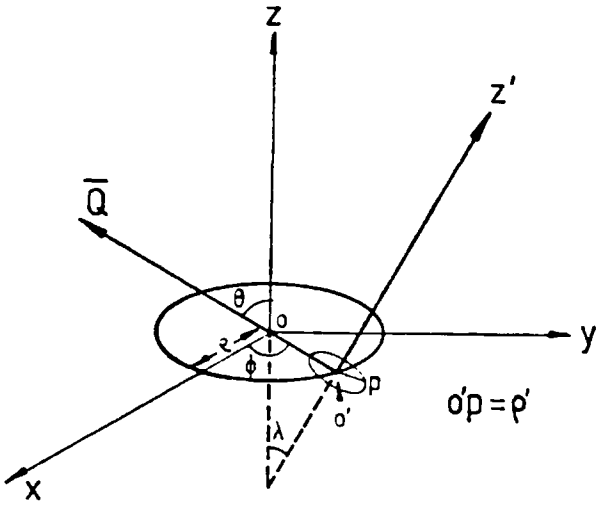
Calculation of the EISF for the ester methyl group does not appear to be so straightforward, since, in principle, at least, various combinations of motions about several different axes could be possible. However, after consideration of the most likely configuration of the PMMA chain[62 63], it is clear that only one possibility really exists. The ester group in PMMA adopts a planar configuration, as shown below, with the ester methyl group positioned at either (A) or (B).



Consideration of heats of formation[64] has shown position (A) to be more energetically favourable.

In view of this, the ester methyl group is expected to be undergoing a combination of only two motions - the first is the simple three-fold jump about the O-C axis (as in the case of the α-methyl group) and the second, a 180° jump corresponding to the whole ester plane flipping about the C_r-C_{II} bond.

Again, there is more than one method to calculate the EISF for a complex rotation, but the one described here follows Dianoux and Volino[35]



The scattering centre P (equivalent to a proton in the ester methyl group) moves on a circle of radius ρ' whose normal O'Z' is making an angle λ with the director OZ. The centre of the circle O' itself moves on a circle of radius ρ around OZ (to correspond with the 180° planar flipping motion)

α and θ are the polar angles of $\underline{Q}$ with respect to the laboratory frame Oxyz. ($\underline{Q}$ is the momentum transfer, as before).

At time t, OO' makes an angle φ with Ox and O'P makes an angle φ' with the normal to the plane OO'Z.

Assuming the two motions are uncorrelated, it can be shown[35] that the distribution functions in this case are given by

$$P_{rot}(\phi,\phi_0;t) = \frac{1}{N}\sum_{n=0}^{N-1}\exp(-|t|/\tau_n^{\rho})\exp\{in(\phi-\phi_0)\}\times\sum_{p=-\infty}^{\infty}\delta\{\phi-\phi_0-(2\pi p/N)\}$$

$$P'_{rot}(\phi',\phi'_0;t) = \frac{1}{N'}\sum_{n'=0}^{N'-1}\exp(-|t|/\tau_{n'}^{\rho'})\exp\{in'(\phi'-\phi'_0)\}\times\sum_{p'=-\infty}^{\infty}\delta\{\phi'-\phi'_0-(2\pi p'/N')\}$$

Performing the integrals over ϕ, ϕ' and ϕ_0, ϕ_0' to obtain the intermediate scattering law,

$$I_{inc}^{rot}(\underline{Q},t) = \sum_{n=0}^{N-1} \sum_{n'=0}^{N'-1} \exp\{-|t|\,(1/\tau_n^{\rho} + 1/\tau_{n'}^{\rho'})\}\, A_{nn'}(\underline{Q}) \qquad (3.9)$$

where the coefficients $A_{nn'}(\underline{Q})$ are given by

$$A_{nn'}(\underline{Q}) = \frac{1}{NN'} \sum_{p=1}^{N} \sum_{p'=1}^{N'} J_0\{Q \sin\theta\, (R^2 + S^2)^{\frac{1}{2}}\} \cos(TQ)\, \cos\theta \cos\{\frac{2\pi}{NN'}(np+n'p')\}$$

where

$$R = \rho'\cos(2\pi p/N)\cos\{\phi_0' + (2\pi p'/N')\} - \rho'\cos\phi_0' - \rho\sin(2\pi p/N)$$

$$- \rho'\cos\lambda\, \sin(2\pi p/N)\sin\{\phi_0' + (2\pi p'/N')\}$$

$$S = \rho'\sin(2\pi p/N)\cos\{\phi_0' + (2\pi p'/N')\} - \rho'\cos\lambda\sin\phi_0' - 2\rho\sin^2(\pi p/N)$$

$$+ \rho'\cos\lambda\cos(2\pi p/N)\, \sin\{\phi_0' + (2\pi p'/N')\}$$

$$T = 2\rho'\sin\lambda\, \sin(\pi p'/N')\, \cos\{\phi_0' + (\pi p'/N')\}$$

The isotropic average over the initial position ϕ_0' must be done numerically for the actual values of $\rho, \rho', \lambda, \theta$ and Q. In addition, for a powder sample, it is also necessary to average over θ, in which case,

$$\overline{A_{nn'}(\underline{Q})} = \frac{1}{NN'} \sum_{p=1}^{N} \sum_{p'=1}^{N'} j_0\{Q(R^2 + S^2 + T^2)^{\frac{1}{2}}\} \cos\{\frac{2\pi}{NN'}(np + n'p')\}$$

The rotational scattering law for the combined rotation is now given by the Fourier transform of (3.9) with $A_{nn'}(\underline{Q})$ replaced by $\overline{A_{nn'}(\underline{Q})}$. The EISF is given by $\overline{A_{00}(\underline{Q})}$, i.e

$$EISF = \overline{A_{00}(\underline{Q})} = \frac{1}{NN'} \sum_{p=1}^{N} \sum_{p'=1}^{N'} j_0\{Q(R^2 + S^2 + T^2)^{\frac{1}{2}}\} \qquad (3.10)$$

where R,S and T retain their original definitions.

A simple program to calculate the EISF for the ester methyl group in PMMA was written, assuming a combination of the motions mentioned earlier. The numerical integration was performed using Simpson's rule, with the option of varying the step size as required. In addition, provision was also made for varying the two radii of gyration, and their relative angle, λ. The final parameters used were based on bond angles and bond lengths taken from 62 and 63, with ρ=1.16 Å, ρ'=1.032 Å and $\lambda=4^0$. Figure 3.3 shows the EISF obtained in this case, for complex rotation, compared to a simple three-fold jump motion.

Experimental Determination of the EISF for a Complex Rotation

Equation (3.10) predicts the EISF for a complex rotation, such as that undergone by the ester methyl group in PMMA. However, the true EISF will only be obtained experimentally if the timescale of both kinds of motion are comparable, and only if this is less than $1/\Delta\omega_{\frac{1}{2}}$, where $1/\Delta\omega_{\frac{1}{2}}$ is the full width half maximum (FWHM) of the resolution function of the spectrometer used for making the measurement.

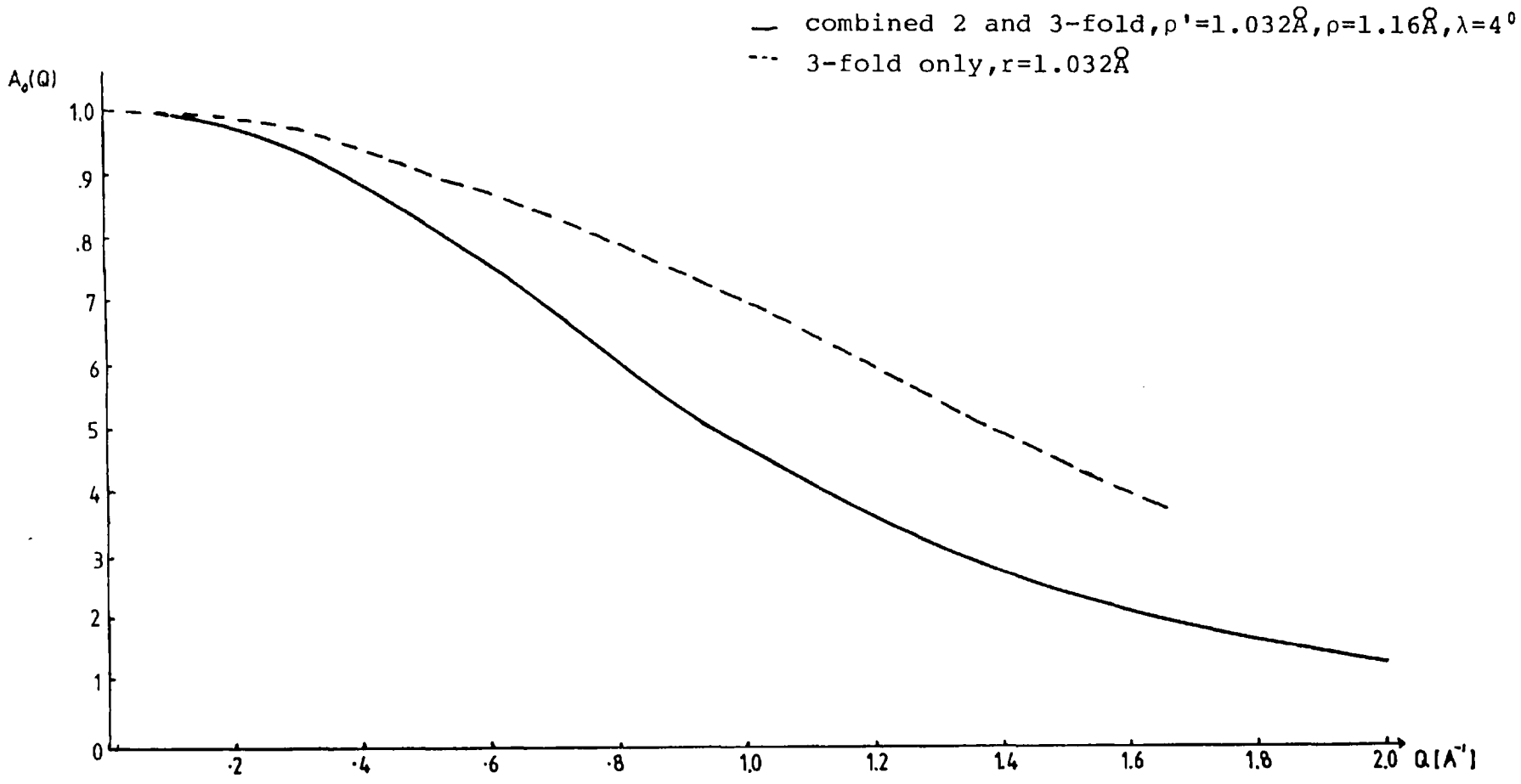
If, in the particular case of PMMA, the correlation time of the two fold jump is very much shorter (or longer) than that of the rotating ester methyl group, the experimental EISF will reflect only one of the two possible motions (which one depends on the instrumental resolution).

3.1.7 Temperature Dependence of the Mean Jump Time and Calculation of the Activation Energy

The mean jump time, τ, is given by the FWHM of the quasi-elastic component of the rotational scattering law. For a simple jump model, the broad component is predicted to be a single Lorentzian, characterised by the FWHM, τ. For this model, τ is not expected to vary with Q.

Assuming an Arrhenius law to describe the variation

Fig 3.3 EISF for Complex Rotation



of τ with temperature[34]

$$\tau = \tau_0 \exp(-E_a/kT)$$

Thus measurement of τ over a range of temperatures will allow an activation energy to be extracted directly.

3.1.8 Relationship Between E_a and V_3[34]

In deriving this relationship, it is assumed that the jump probability τ^{-1} is proportional to the probability that the system is in an activated energy state $E = V_3$.

For a thermally activated process[34] ,

$$\tau^{-1} = \frac{kT}{h} Z^{-1} \exp\{-(V_3 - E_0)/kT\} \qquad (3.11)$$

where $$Z = \sum_{\nu=0}^{\infty} \exp\{-(E_\nu - E_0)/kT\}$$

and is the vibrational partition function of the activated state.

Thus, $$\tau_0^{-1} = \frac{kT}{h} Z^{-1}$$

In principle, the right hand side of equation (3.11) can be calculated if V_3 is known. If the model chosen to calculate V_3 from inelastic data is correct, the variation of (3.11) with temperature should reproduce that of τ^{-1} deduced from the variation of quasi-elastic widths.

3.1.9 The Question of Quantum Mechanical Tunnelling

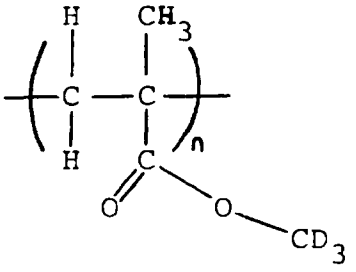
Various workers[21 27 30 31] have proposed that quantum mechanical tunnelling may be an important relaxation process at low temperatures for both the methyl groups in PMMA.

The evidence supporting this proposal will be discussed in section 3.3.11. If, however, tunnelling is a major relaxation process, the activation energy, E_a, cannot be estimated from simple Arrhenius plots as outlined in 3.1.7, because the frequency - temperature^{-1} plots are no longer linear at low temperatures. Stejskal and Gutowsky[17] have calculated the average tunnelling frequency as a function of temperature for a series of barrier heights. A regular set of curves is obtained, as shown in figure 3.4, and it is on the basis of these calculations that values of V_3(tunnelling) should be obtained from quasi-elastic neutron scattering data and NMR T_1 measurements for comparison with the values of V_3 found using inelastic neutron scattering techniques.

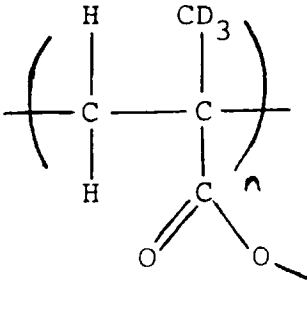
3.2 Sample Preparation

Various selectively deuterated forms of atactic poly(methyl methacrylate) were prepared by Dr.R.H.Hall of Imperial College. The three samples used in the neutron scattering experiments were as follows.

(1) Deuteration of the ester methyl group, to allow observation of the α-methyl group only.

PMMA1  MW~520,000

(2) Deuteration of the α-methyl group to allow independent study of the ester methyl group.

PMMA2  MW~450,000

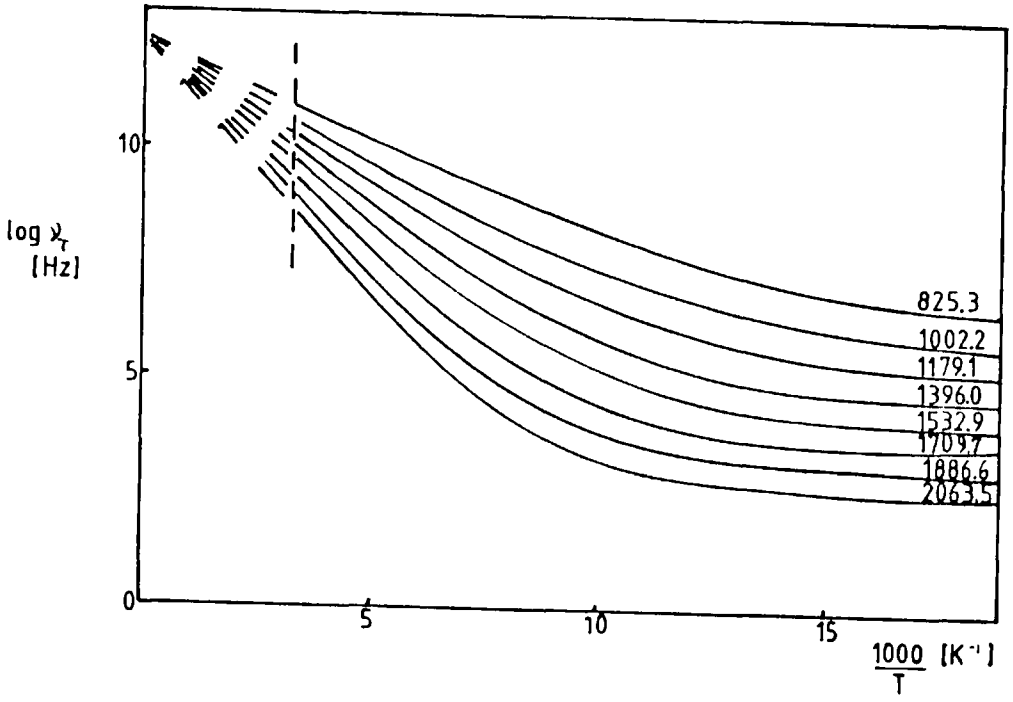
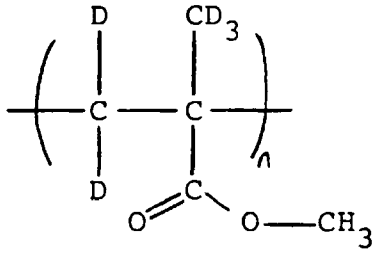


Fig 3.4 Variation of ν_t with T for different V_3

(3) Replacement of hydrogen by deuterium in both the α-methyl group, and the backbone, again to allow study of the ester methyl group only, but also considerably reducing the incoherent elastic scattering from the backbone hydrogen.

PMMA3  MW~250,000

NMR measurements made on the samples (in dilute $CDCl_3$ solution) showed the percentage of deuteration to be ~97% for PMMA3 and close to 100% for PMMA1 and PMMA2. In addition, analysis of tacticity splitting[65] of the α-methyl peak showed PMMA1 to approximately 50% syndiotactic, 40% atactic and 10% isotactic. It is more difficult to estimate the percentage of different tacticity triads for the other two samples, PMMA2 and PMMA3, from investigation of the ester methyl peak, since the tacticity splitting is much less clear. However, since the samples were prepared in the same way as PMMA1, the relative percentages will probably be much the same. The NMR spectrum for PMMA2 is shown in figure 3.5 (sweep frequency 100MHz).

A small quantity of poly(methyl methacrylate) catalogued as being purely isotactic was purchased from Polysciences Inc., Warrington, and some pure syndiotactic PMMA from Polymer Laboratories Ltd., Church Stretton, Shrewsbury, for use in the investigation of the effect of tacticity on the methyl group rotation. These are subsequently referred to as ISOT1 and SYNDIO1.

NMR measurements were made to check the stereoregularity of the commercial samples. Figure 3.6 shows the relevant section of the spectrum for ISOT1 (sweep frquency 250MHz). The intense peak at 1.2 ppm is associated with the isotactic resonance of the α-methyl group. The almost imperceptible humps at 0.9 and 1.06 ppm are associated with the syndiotactic and atactic resonances respectively. Comparison of the integrated intensities indicates that the sample is better

Fig 3.5

NMR spectrum for PMMA2

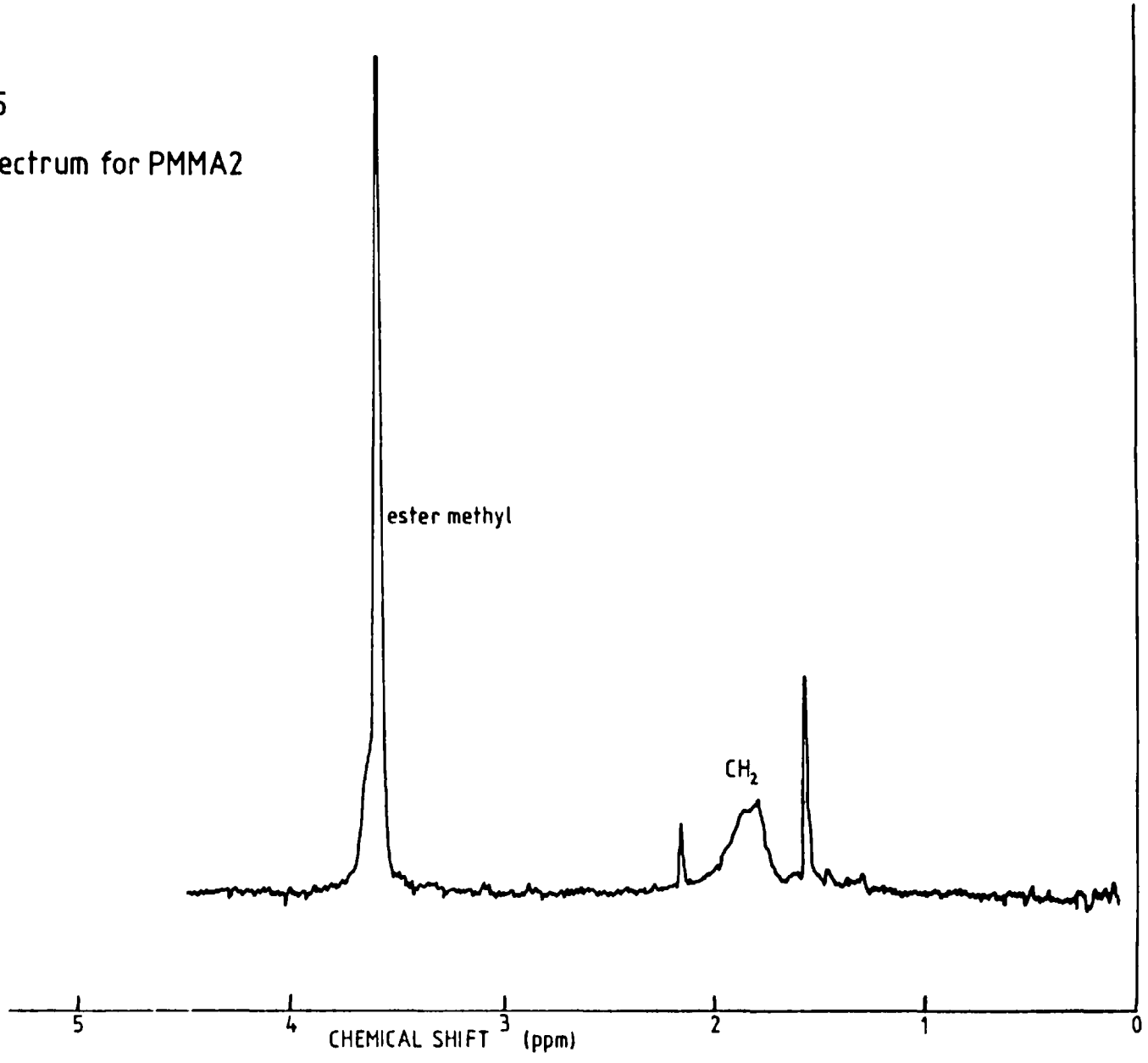
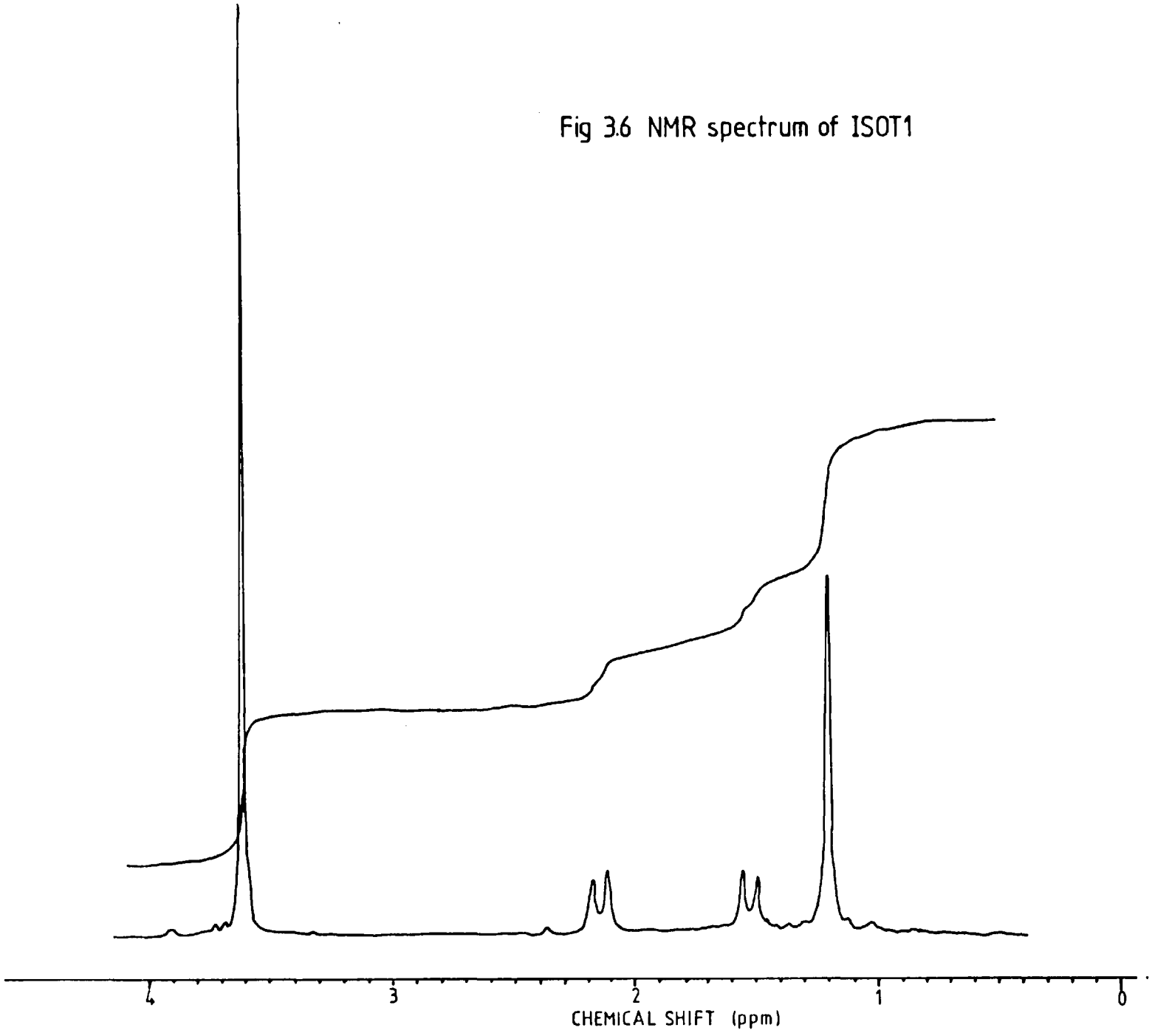


Fig 3.6 NMR spectrum of ISOT1

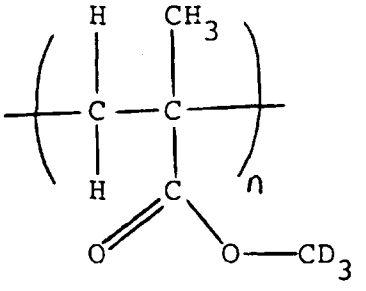


than 95% isotactic. The peaks positioned between 1.4 and 2.4 ppm are methylene resonances, and the peak at 3.6 ppm is attributed to the ester methyl group.

Figure 3.7 shows the NMR spectrum for SYNDIO1 (sweep frequency 250 MHz). This sample is predominantly syndiotactic, but not as stereoregular as ISOT1. Calculation of integrated intensities shows that it contains 76% syndiotactic sequences, 21% atactic and 3% isotactic triads. The sharp peak at 1.6 ppm is attributed to either trace impurities, or, a more likely explanation, to water in the sample.

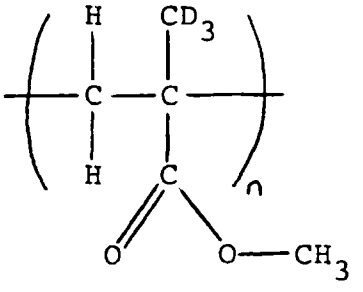
All samples of poly(methyl methacrylate) used in the neutron scattering experiments are summarised below, showing their chemical composition, and name by which they are referred to later in the thesis.

PMMA1



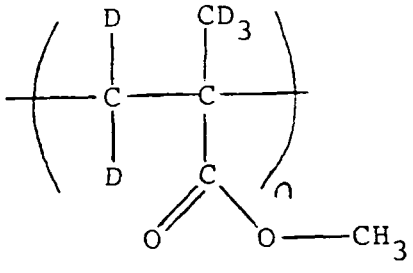
50% syndiotactic
40% atactic
10% isotactic

PMMA2



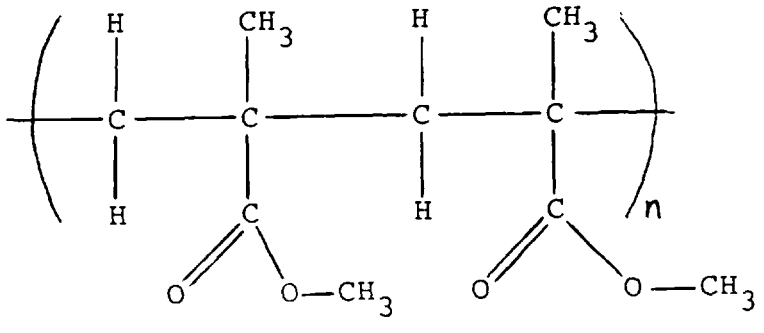
50% syndiotactic
40% atactic
10% isotactic

PMMA3



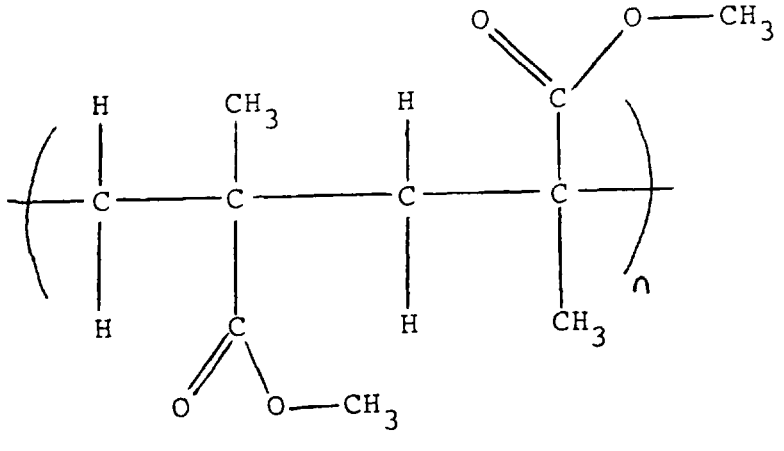
50% syndiotactic
40% atactic
10% isotactic

ISOT1



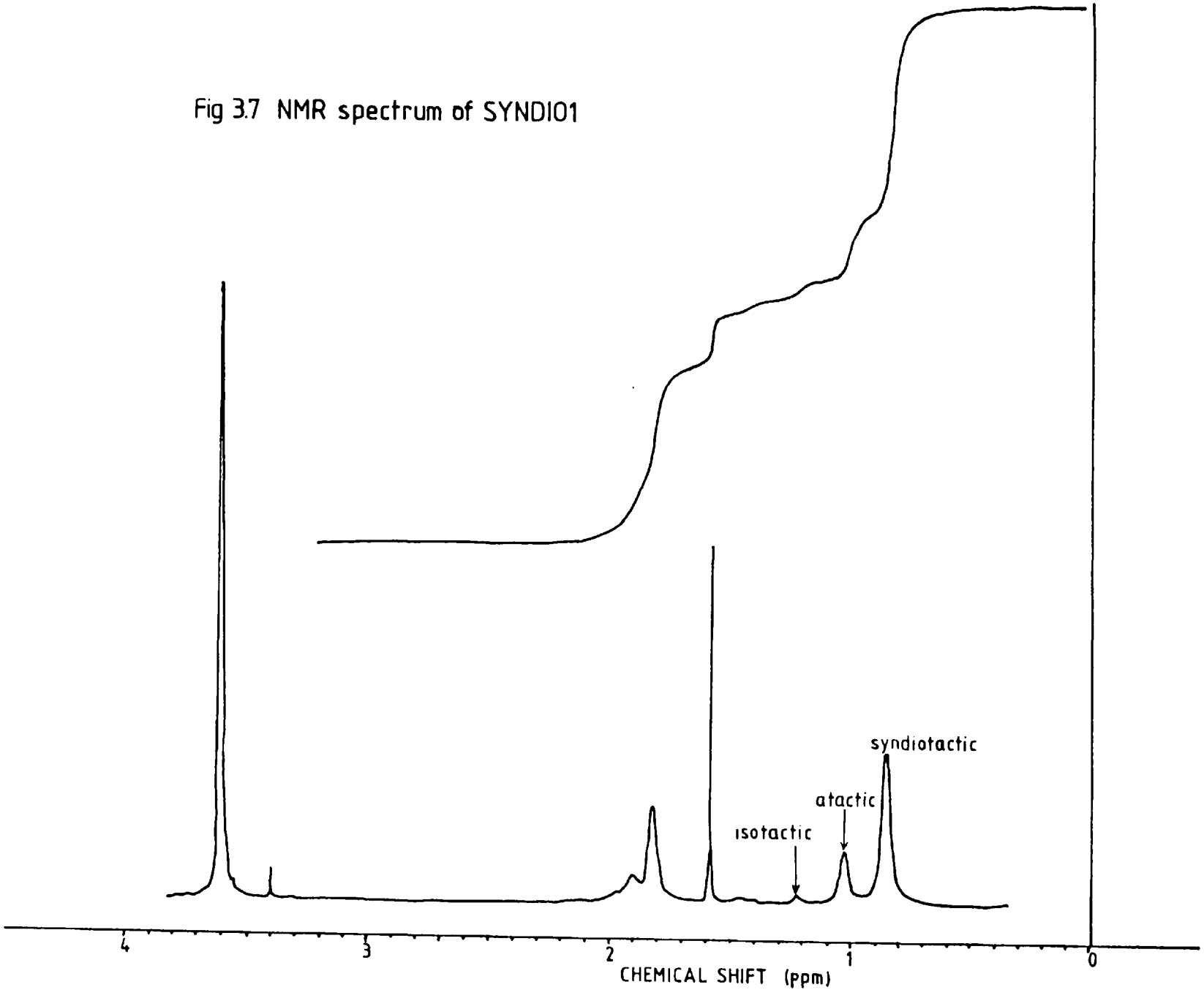
> 95% isotactic

SYNDIO1



76% syndiotactic
21% atactic
3% isotactic

Fig 3.7 NMR spectrum of SYNDI01



In all cases the samples were hot pressed (at approx. 120°C) for neutron scattering experiments, the thickness of each sample being calculated to give 10% scatter. (This is a compromise between reducing multiple scattering as far as possible, but retaining sufficient intensity to obtain good statistics in reasonable counting times). The required thickness is calculated using the Beer-Lambert law,

$$N = N_0 \exp(-st)$$

where N and N_0 are the final and incident neutron flux (in the calculation N/N_0 is set to 0.9) and t is the sample thickness

s is the macroscopic cross-section, and is given by

$$s = \sigma_{total} \cdot A \cdot \rho \cdot M$$

where σ_{total} = sum of scattering cross-sections over all species in a single monomer

A = Avogadro's number

ρ = sample density

M = molecular weight of one repeat unit.

so for a polymer composed of different atomic species, i,

$$s = A\ \rho \sum_i m_i \sum_i \sigma_i$$

where i denotes the sum over one monomer.

3.3 Experimental Results and Interpretation

3.3.1 Inelastic Neutron Scattering Results

Inelastic measurements were made on the three partially deuterated samples, PMMA1, PMMA2 and PMMA3. For these experiments, the time-of-flight spectrometer, 4H5, was used, with a 6+12 slot rotor configuration, and an incident wave-

length of 4.8 Å. This gave a FWHM elastic resolution of the order of 400 μeV. All data were recorded at ambient temperature.

The position of the inelastic peaks in the raw time-of-flight data was noted for each angle of scatter. Since the peak position did not change appreciably with angle, it was concluded that dispersion effects in the system were small, and therefore it would be possible to sum data taken over all angles. The raw data were therefore analysed as indicated in section 2.3, to obtain, firstly, $\Sigma g(\omega)$, i.e the density of states function, $g(\omega)$, summed over all angles, to improve statistics, and secondly, $\rho(\omega)$, the hydrogen-amplitude-weighted density of states function, extrapolated to zero Q. In general, provided that dispersion effects are small, $\rho(\omega)$ and $\Sigma g(\omega)$ will be very similar, although the extrapolation to zero momentum transfer may sharpen some of the more indistinct peaks.

Both $\Sigma g(\omega)$ and $\rho(\omega)$ for each of the three samples are shown in figures 3.8 to 3.13, as a function of energy transfer.

Further inelastic data from PMMA3 were recorded using IN6, and, in addition, measurements were also made on the stereoregular samples ISOT1 and SYNDIO1. An incident wavelength of 4.1 Å was used, giving a FWHM elastic resolution of the order of 250 μeV (i.e identical to that of IN5 at the same incident wavelength).

Figures 3.14, 3.15 and 3.16 show the final frequency distribution functions extrapolated to zero Q, for ISOT1, SYNDIO1 and PMMA3.

3.3.2 Consideration of Errors in Extracting $\rho(\omega)$

The magnitude of the error bars in the plots of $\rho(\omega)$ indicates the standard deviations of the data points from the calculated line of best fit on the intermediate logarithmic

Fig 3.8 $\rho(\omega)$ for PMMA1

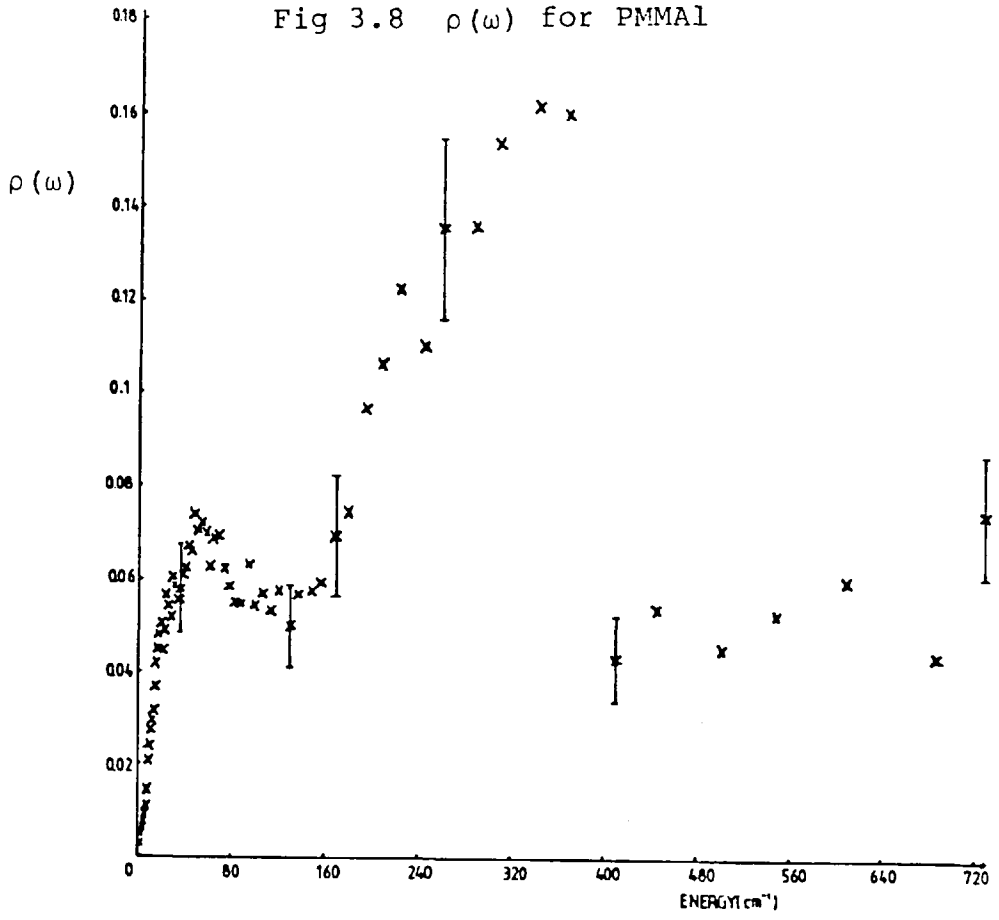


Fig 3.9 Sum of $g(\omega)$ for PMMA1

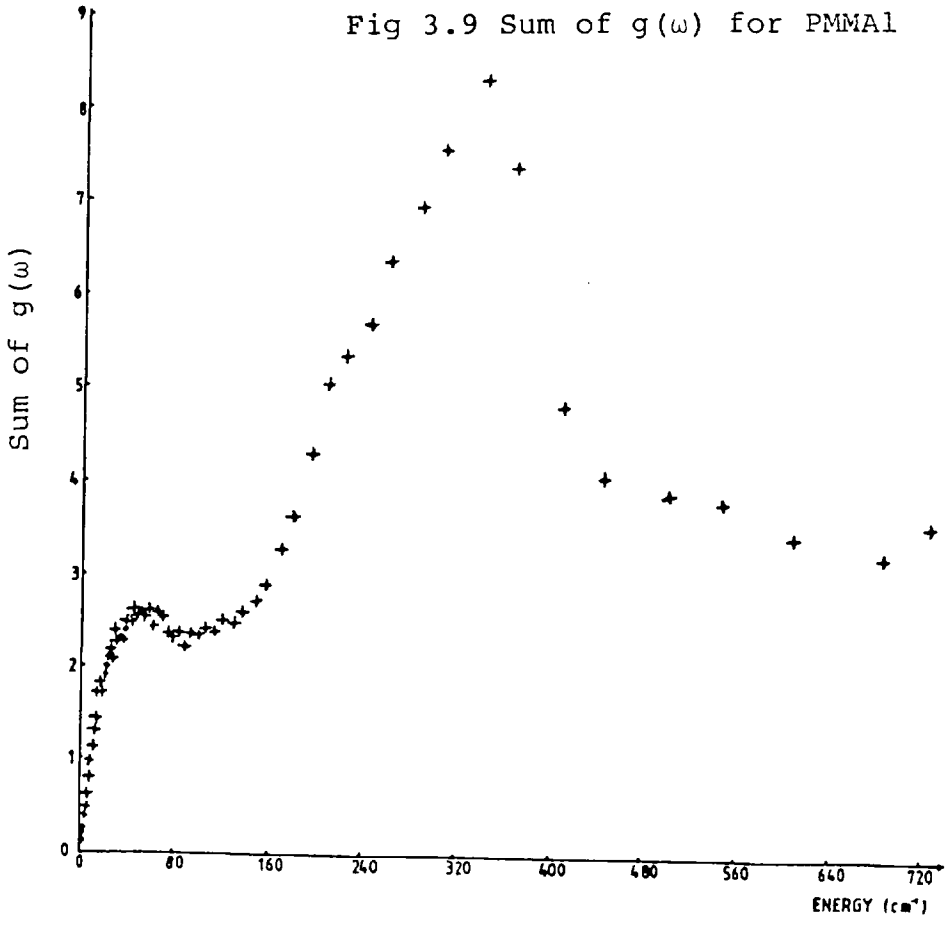


Fig 3.10 ρ(ω) for PMMA2

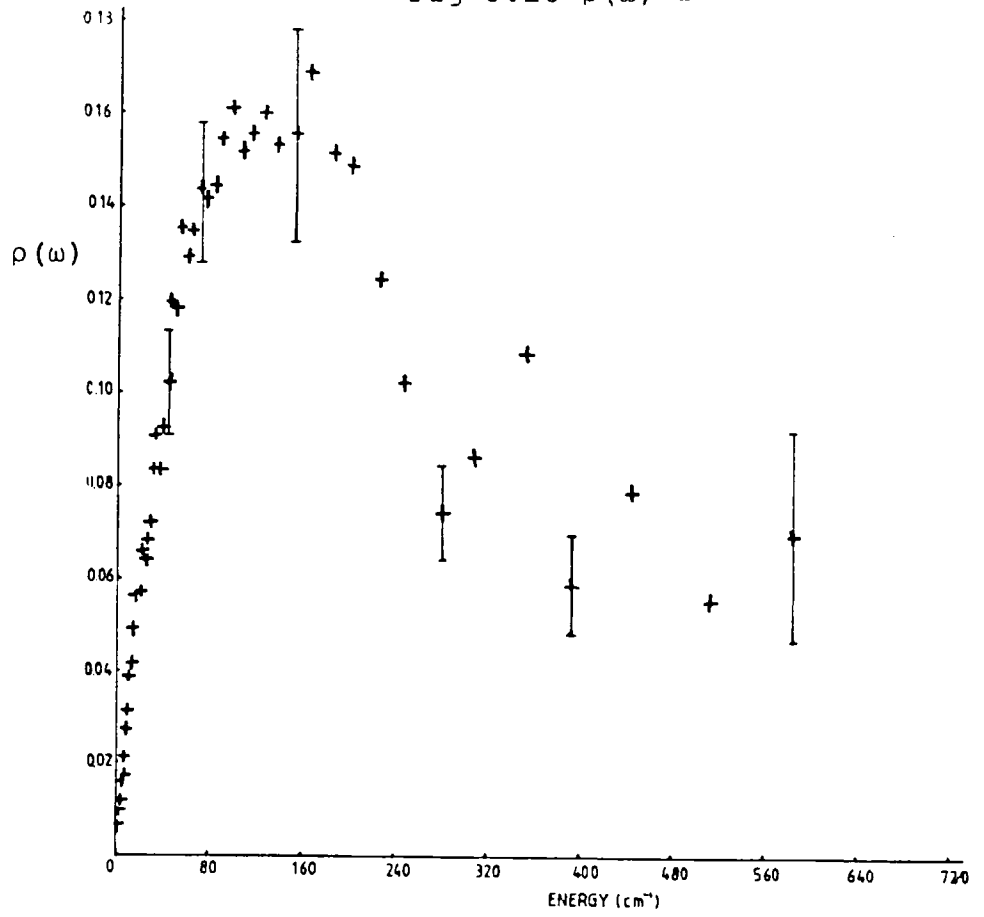


Fig 3.11 Sum of g(ω) for PMMA2

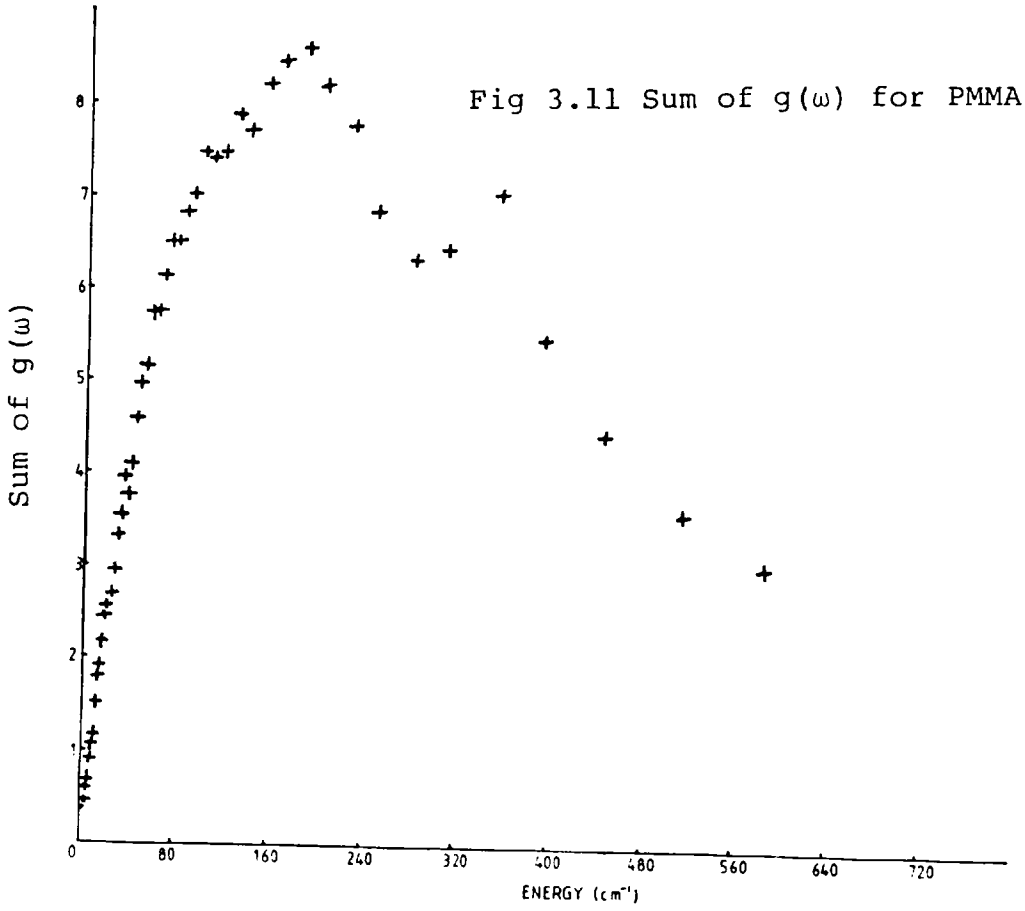


Fig 3.12 ρ(ω) for PMMA3

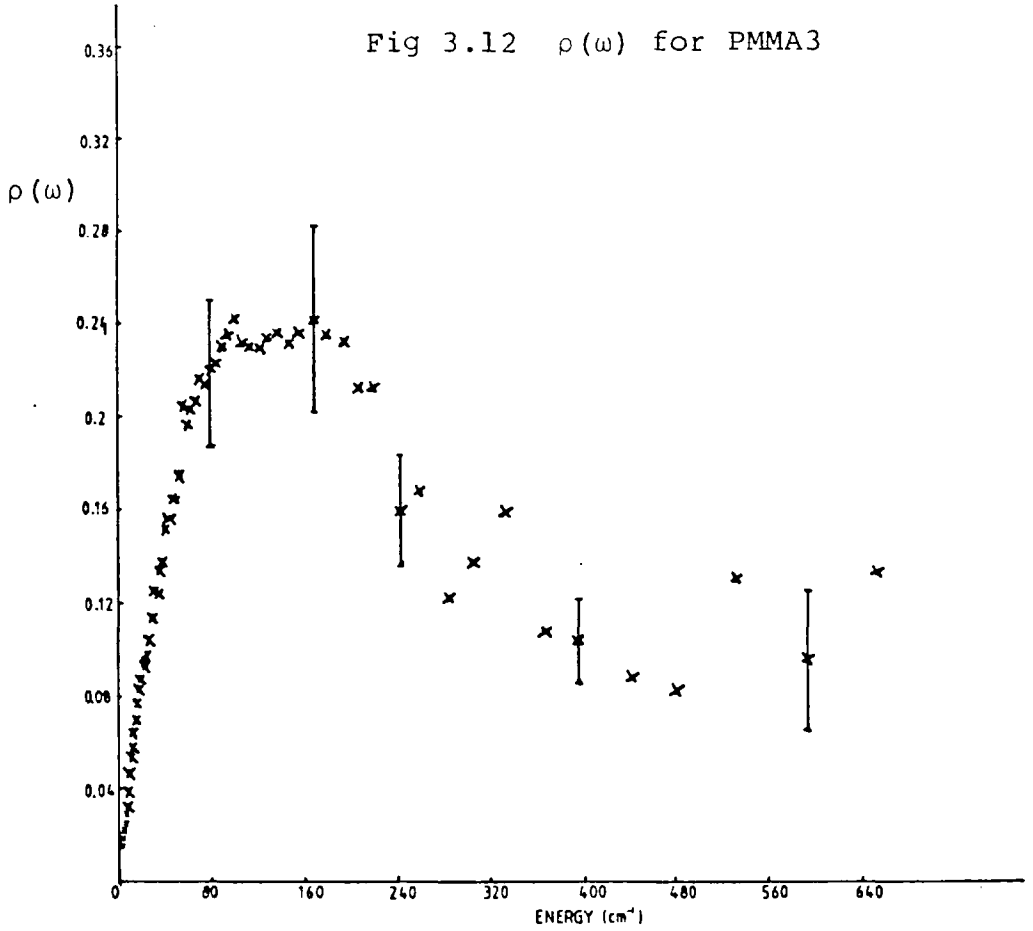


Fig 3.13 Sum of g(ω) for PMMA3

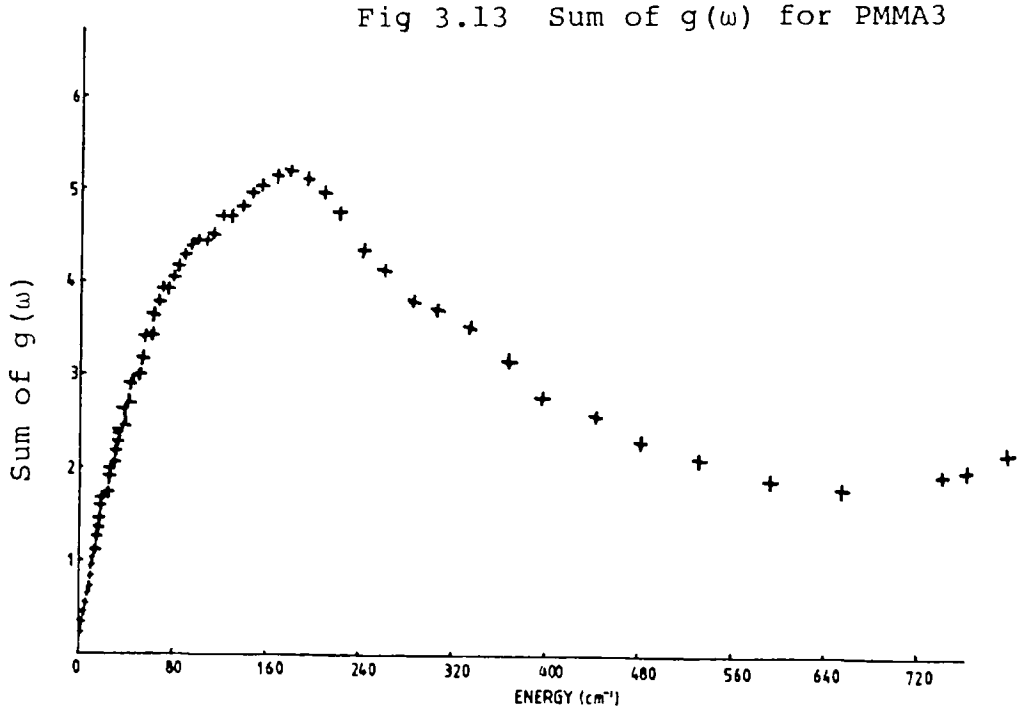


Fig 3.14 $\rho(\omega)$ for ISOT1

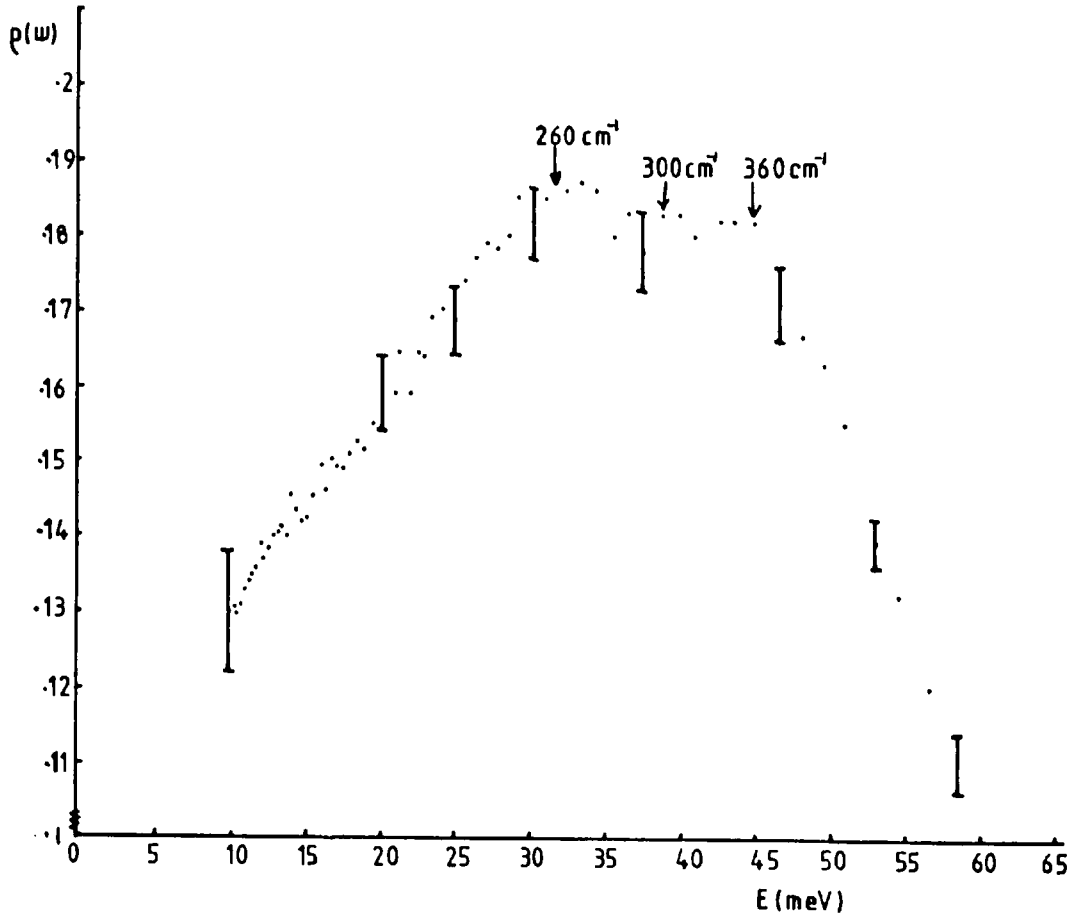


Fig 3.15 $\rho(\omega)$ for PMMA3

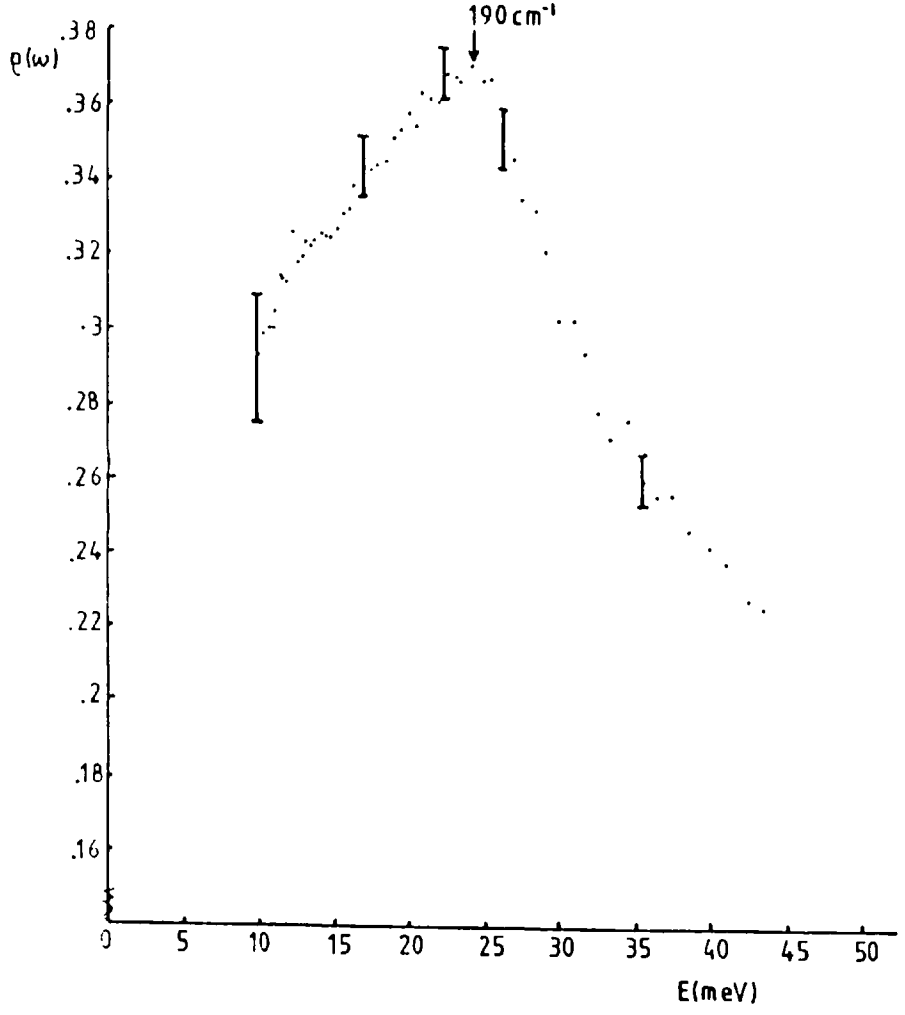
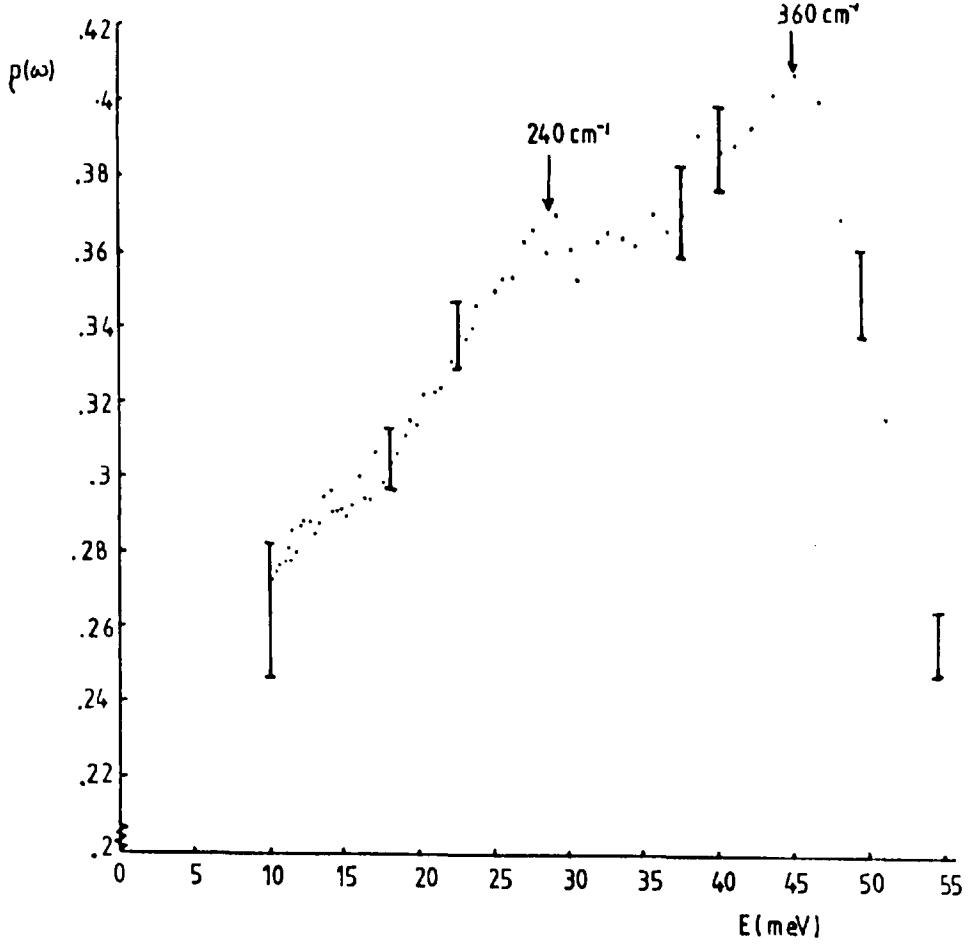


Fig 3.16 $\rho(\omega)$ for SYNDIO1



plots. The size of these errors may be considerably reduced by the elimination of one or two bad angles, and so, to some extent, the purpose of these error bars on $\rho(\omega)$ is for relative comparison of adjacent points, and also as an aid in deciding which (if any) of the data should be discarded in the extrapolation to zero Q. The error in deciding at exactly which frequency a peak in $\rho(\omega)$ is positioned is rather difficult to quantify. This difficulty arises because of two factors. The first of these is the inherent broadness of the peaks being studied in poly(methyl methacrylate), and the second is in resolving peaks falling rather close together, which tend to appear merely as 'shoulders' in the frequency distribution function. For example, the dominant α-methyl peak at 350 cm^{-1} (see figure 3.8) is probably located reliably to ±10 cm^{-1}, whereas the precise position of the shoulders nominally quoted as being at 280 cm^{-1} and 220 cm^{-1} are probably only accurate to ±20 cm^{-1}, at best.

3.3.3 Interpretation of Inelastic Measurements, and Assignment of Peaks in $\rho(\omega)$

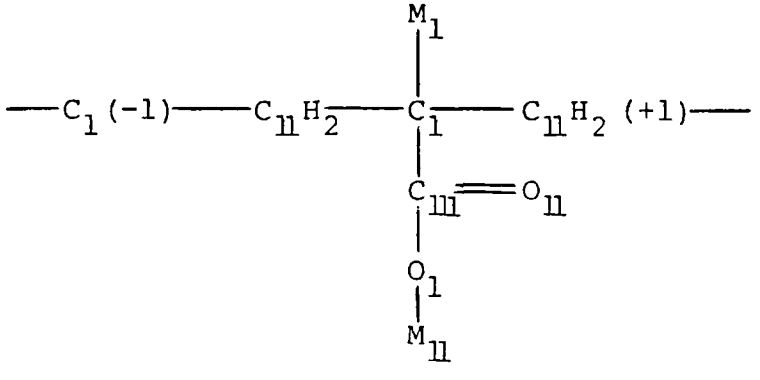
Assignment of peaks in $\rho(\omega)$ is made easier by comparison of the inelastic neutron scattering data with far infra-red measurements, as suggested in section 3.1.2. Although the relative intensities of specific peaks measured using the two methods are likely to be rather different, since the frequency distribution function obtained from inelastic neutron scattering is hydrogen-amplitude weighted, whereas the peak intensities in the IR spectra are not related to the motion of the hydrogen in the sample,the peak positions in both cases are expected to be identical, provided there are no dispersion effects.

Far infra-red studies on syndiotactic PMMA have been made by Mandley[66], who observed transition bands at 35 cm^{-1}, 58 cm^{-1}, 95 cm^{-1}, 225 cm^{-1}, 320 cm^{-1} and 400 cm^{-1}. He was able to assign some of these bands to skeletal motion of the PMMA, by comparison of the observed frequencies with normal co-ordinate calculations of predicted frequencies based on

a simple model. Bands associated with sidegroup motion were assigned by comparison with IR data on PMMA from other sources, and by comparison with methyl group motion observed in other polymers. The final results obtained are summarised below. (δ = bending)

Position of Observed Band (cm^{-1})	Identification
400	$\delta(\overset{\|\|}{C}\text{-O-C})$ out-of-plane
320 (shoulder)	δ(C-C-C) in-plane
225	δ(C-C-C) out-of-plane
190	$\delta(\overset{\|\|}{C}\text{-O-C})$ in-plane
95	δ(C-C-C) out-of-plane
58, 34	hindered rotation

Far infra-red investigations have also been made by Tadohoro et al[67] on isotactic PMMA. Peak assignments in this case were made by comparison of observed bands with those predicted by full normal co-ordinate analysis of a model, including predictions of sidegroup motions. They established that the totally symmetric A species gave rise to 19 fundamental modes with transition moments parallel to the molecular axis (i.e equivalent to in-plane motion in the above nomenclature) and that the doubly degenerate E_1 species gave rise to transition moments perpendicular to the molecular axis (i.e out-of-plane). Adopting the following notation for labelling the atoms in PMMA,



their results may be summarised as follows:
(δ = bending, w = wagging, τ = torsion)

Species A

Observed Frequency (cm^{-1})			Assignment
391	($\|\|$)	weak (sh)	$w(C_1M_1) + \delta(C_{II}\,C_1\,C_{II}\,(+1))$
365	($\|\|$)	very strong	$\delta(C_{III}O_1M_{II})$
314	($\|\|$)	medium	$\tau(C_{III}O_1) + w(C_1C_{III})$
217	($\|\|$)	strong	$\delta(C_1C_{III}O_1) + \delta(C_1M_1)$
165	($\|\|$)	very weak	$\tau(C_{III}O_1)$
109	($\|\|$)	medium	$\tau(C_1C_{III})$

Species E_1

Observed Frequency (cm^{-1})			Assignment
406	($\perp$)	medium	$\delta(C_{III}{=}O_{II})$
368	($\perp$)	very strong	$\delta(C_{III}O_1M_{II}) + \delta(C_1M_1)$
338	($\perp$)	medium (sh)	$w(C_1M_1) + \delta(C_1C_{III}O_{II})$
232	($\perp$)	strong	$\delta(C_1C_{III}) + \delta(C_1C_{III}O_1)$
188	($\perp$)	very weak	$\delta(C_1C_{III}) + \delta(C_{II}\,C_1C_{II}(+1))$
140	($\perp$)	very weak	$\tau(C_{III}O_1)$
113	($\perp$)	weak	$\tau(C_1C_{III})$

It is now possible to assign the peaks in $\rho(\omega)$ observed in figures 3.8, 3.10, 3.12, 3.14, 3.15 and 3.16.

Figure 3.14 shows the frequency distribution function extrapolated to zero Q for isotactic PMMA. Three dominant peaks may be observed at 260 cm^{-1}, 300 cm^{-1} and 360 cm^{-1}. Comparison with the results quoted above suggests that the band at 360 cm^{-1} may be assigned to ester methyl group bending, and that at 260 cm^{-1} corresponds (within experimental error) to the band observed at 232 cm^{-1} in the infra-red spectrum, involving bending of the ester group. Tadohoro assigns the peak at 314 cm^{-1} to torsional motion within the ester group about the $C_{III}O_1$ bond, combined with C_1C_{III} wagging. However, Allen et al[22] have previously observed an intense peak positioned at 300 cm^{-1} in the inelastic neutron scattering spectrum from a pure isotactic sample of PMMA, which had been partially deuterated to effectively remove any effects associated with the motion of the ester methyl group from the spectrum - thus the peak at 300cm^{-1}could confidently be assigned to α-methyl motion. In view of this result, and also because Tadohoro et al have neither observed nor calculated any other frequency associated with the α-methyl torsion, the peak at 300 cm^{-1} in figure 3.14 is assigned to α-methyl torsion in an isotactic sample (although it is possible that this is combined with the motions mentioned by Tadohoro et al).

Comparison of figure 3.16, the frequency distribution function of pure syndiotactic PMMA with the results of Mandley allows the following assignments to be made. The peak at 240 cm^{-1} may be assigned to out-of-plane main chain bending, and the shoulder at 320 cm^{-1} to in-plane main chain bending. No peak in the region of 360 cm^{-1} was observed by Mandley, and so this peak is assigned to α-methyl torsion, for two reasons. Firstly, of all motions observed in the neutron scattering spectrum, the torsional peaks associated with the two methyl groups are likely to have the greatest intensity, since they involve the hydrogen motion with the greatest amplitude. As discussed later, the ester methyl torsional peak is expected to appear at much lower frequencies, suggesting that this peak at 360 cm^{-1} be assigned to α-methyl motion. Furthermore, this is in good agreement with Higgins et al [21 22], who established the position of the α-methyl

torsion in syndiotactic PMMA to be at 360 cm^{-1}.

Figures 3.12 and 3.15 both show $\rho(\omega)$ for PMMA3 (the former obtained using 4H5, and the latter, IN6) and so are expected to be identical. Both show a peak at approximately 190 cm^{-1}, although at lower frequencies, the relative intensity of the spectrum appears to be lower in figure 3.15 than in figure 3.12. To some extent, this is not surprising, since the frequency distribution function in this frequency range is very dependent on instrumental parameters (in particular, the inelastic resolution) and, as yet, the exact behaviour of IN6 is not known.

Figure 3.10 shows $\rho(\omega)$ for PMMA2. This is expected to be very similar to 3.12, since the only difference between the two samples is that PMMA3 is more fully deuterated. In both cases the α-methyl group is deuterated, so the dominant features of the spectrum are expected to be due to ester methyl group motion. The two functions are almost identical, and with reference to the IR measurements, the following peak assignments can be made. The peak at 320 cm^{-1} in both cases is assigned to in-plane main chain bending. It should be noted that this peak is rather more intense for PMMA2. This is a direct result of the hydrogen-amplitude weighting of the spectrum - in PMMA3 the backbone hydrogen is deuterated, in PMMA2 it is not, thus the peak reflecting backbone motion is more intense for PMMA2. The shoulder at 240 cm^{-1} is assigned to out-of-plane backbone bending. The region between 50 and 200 cm^{-1} is associated with the ester methyl group motion and crystalline lattice modes. The region may be further specified by comparison with figure 3.8, which shows $\rho(\omega)$ for PMMA1, and is therefore expected to be dominated by motion of the α-methyl group. A relatively intense peak is observed in the region 20-90 cm^{-1}. Since the ester methyl group motion has effectively been removed by deuteration, this peak is assigned to crystalline lattice modes. Referring back to figure 3.12, it is now possible to separate the broad band between 50 and 200 cm^{-1} into two specific regions. Crystalline backbone modes dominate in the region 50-90 cm^{-1}, and the higher frequency region 90-200 cm^{-1}

is associated with ester group motion. Mandley's results suggest that a peak at 190 cm^{-1} be attributed to ester group bending motion. It is further expected that the ester methyl torsional frequency should lie between 90 and 200 cm^{-1} - Tadohoro predicts peaks due to torsional motion of the ester group as a whole, and internal motion within the group in this frequency region for isotactic PMMA. Although it is not yet known whether tacticity affects the position of the torsional peak for the ester methyl group (as it clearly does for the α-methyl group, these results showing the torsional peak for isotactic PMMA to be at 300 cm^{-1}, and for syndiotactic PMMA at 360 cm^{-1}, in excellent agreement with Higgins et al[21 22]), it is unlikely to shift it entirely out of this frequency range. Furthermore, Higgins et al[21] report the position of the ester methyl torsional peak in predominantly syndiotactic PMMA to be at about 100 cm^{-1}.

As already mentioned, figure 3.8 shows the frequency distribution function for PMMA1 (a sample prepared to be atactic, but, in fact, ∿50% syndiotactic) which is expected to be dominated by the motion of the α-methyl group, since the ester methyl group is deuterated. The region between 20 and 90 cm^{-1} is associated with crystalline backbone modes. The shoulder at 240 cm^{-1} is assigned to out-of-plane backbone bending, and that at 300 cm^{-1} to either in-plane backbone bending (expected to be relatively intense, since the backbone of this sample is hydrogenous) or torsional motion of the α-methyl group within isotactic sequences in the sample, which would also lead to a relatively intense peak, due to the large scale amplitude of the motion, although the percentage of isotactic sequences in PMMA1 is quite small. The peak at 360 cm^{-1} is assigned to α-methyl torsion in either atactic or syndiotactic sequences. This assignment is made on the basis that this peak is the most intense in the spectrum, and by comparison with other inelastic neutron scattering data[21 22]. Although this data is not fully conclusive at higher frequencies, the appearance of a peak at 400 cm^{-1} is predicted by Mandley, and is assigned to out-of-plane ester group bending.

The following table, 3.1, summarises the assignment of bands observed in the inelastic neutron scattering spectra.

Table 3.1 Assignment of Peaks in $\rho(\omega)$

Sample	Band Position (cm^{-1})	Assignment
ISOT1	260	ester group bending
(Fig 3.14)	300	α-methyl torsion
	360	ester methyl bending
SYNDIO1	240	out-of-plane main chain bending
(Fig 3.16)	320	in-plane main chain bending
	360	α-methyl torsion
PMMA1	20-90	crystalline lattice modes
(Fig 3.8)	240	out-of-plane backbone bending
	300	either in-plane bending,or α-methyl torsion in isotactic sequences
	360	α-methyl torsion (atactic or syndiotactic sequences)
	400	out-of-plane ester bending
PMMA2 and	20-90	crystalline backbone modes
PMMA3	90-200	ester methyl torsion
(Figs. 3.10,	240	out-of-plane backbone bending
3.12 & 3.15	320	in-plane backbone bending

Having assigned all the peaks occurring in the frequency distribution function obtained using inelastic neutron scattering, it is possible to specify the bands associated with torsional motion of the methyl groups, and using equation (3.4) to calculate the barriers to rotation.

The following table summarises the values of the torsional frequency, ν_τ, and barrier height, V_3, obtained for all samples.

Table 3.2 Torsional Frequencies and Barrier Heights Obtained from Inelastic Measurements

Sample	ν_τ (cm^{-1})	V_3 (kJ/mol)
Isotactic PMMA, α-methyl torsion	300	23
Syndiotactic PMMA α-methyl torsion	360	33
Predominantly syndiotactic PMMA ester methyl torsion	90-200	3.2-10.5

The possibility of more specific assignment of ν_τ for the ester methyl group is discussed later in the chapter.

3.3.4 Quasi-elastic Neutron Scattering Results Relating to the Rotational Motion of the Ester methyl Group in Poly(methyl methacrylate)

Quasi-elastic spectra were obtained from PMMA3, using the time-of-flight spectrometer, IN5. An incident wavelength of 4.7 Å, combined with a chopper speed of 10,000 rpm gave a FWHM elastic resolution of the order of 200 μeV. Data were recorded at 25°C, 47°C, 60°C, 88°C and 118°C over the Q range 0.3 to 2.3 $Å^{-1}$. In addition, a single run at room temperature (25°C) was recorded for the pure isotactic sample, ISOT1.

Figures 3.17 to 3.20 show the scattering law obtained for PMMA3 at 47°C for several Q values. Spectra recorded at

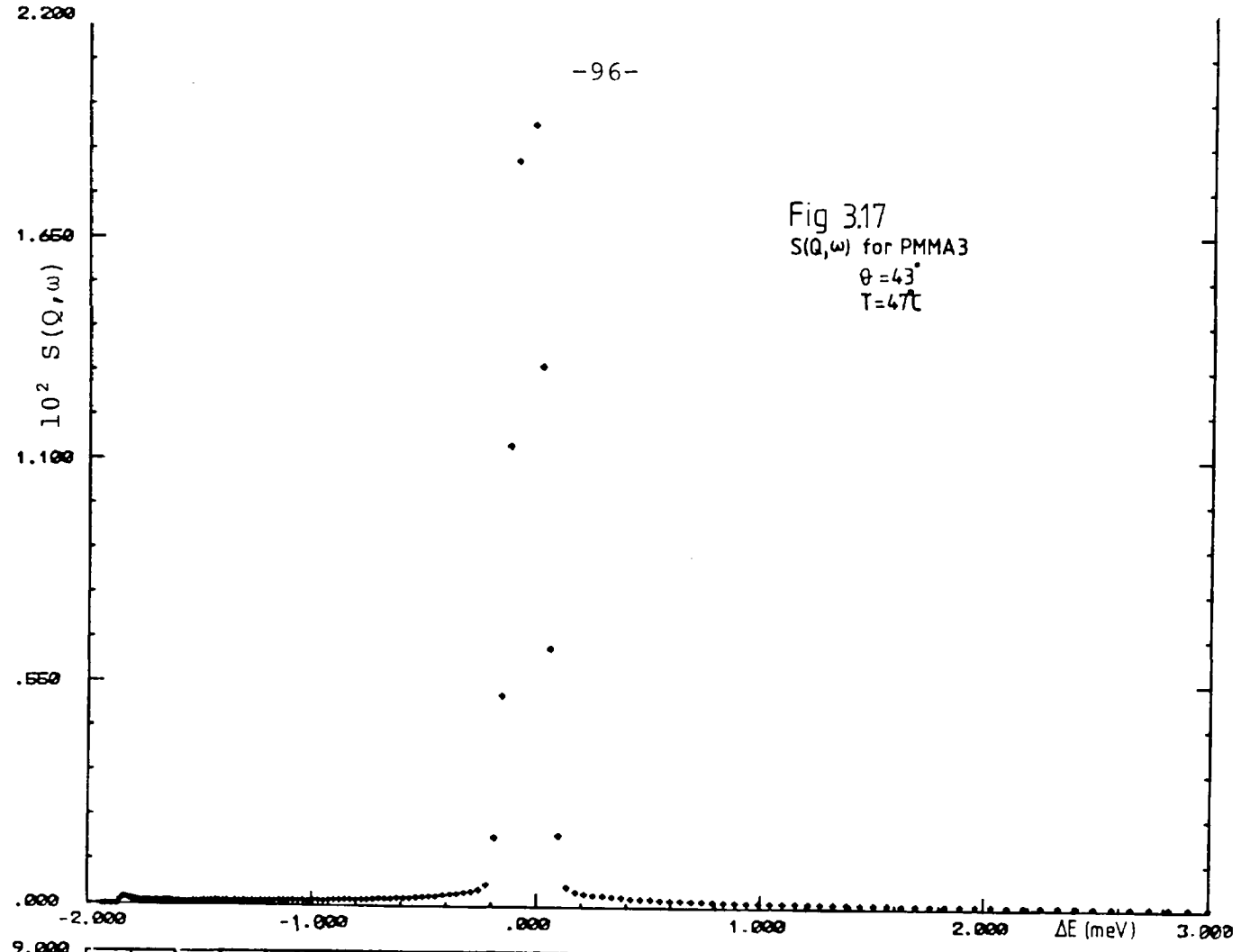


Fig 3.17
S(Q,ω) for PMMA3
θ = 43°
T = 47°C

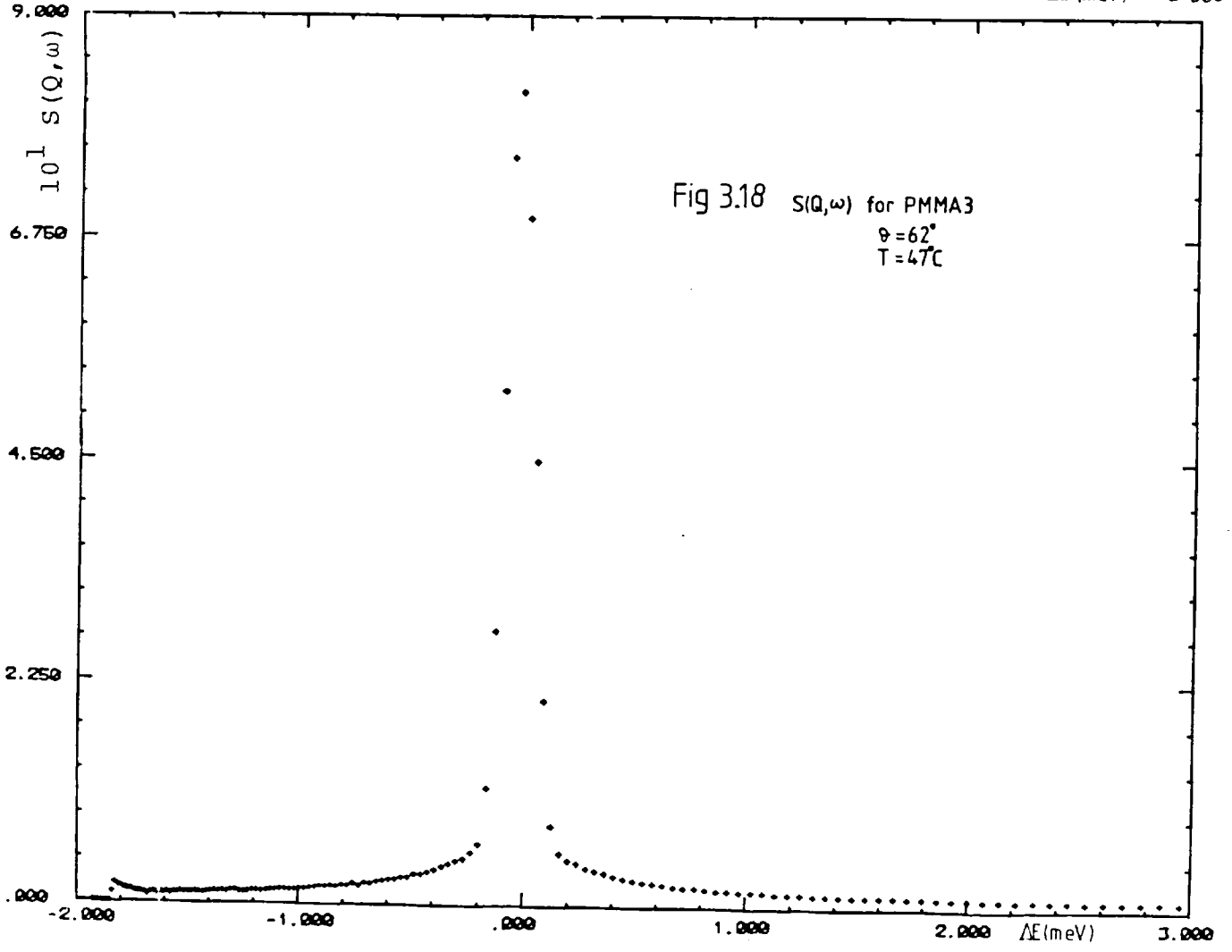


Fig 3.18 S(Q,ω) for PMMA3
θ = 62°
T = 47°C

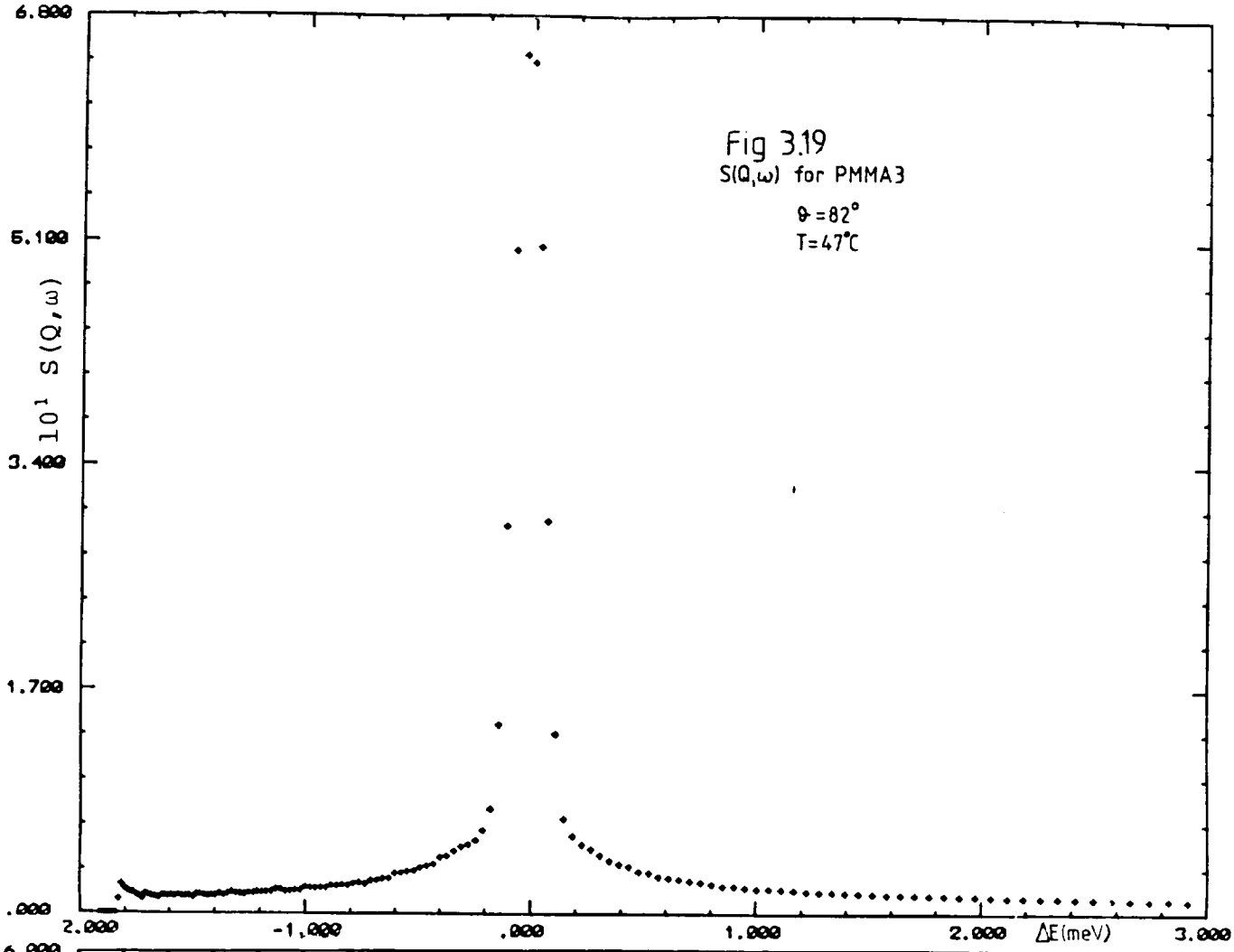


Fig 3.19
S(Q,ω) for PMMA3
θ = 82°
T = 47°C

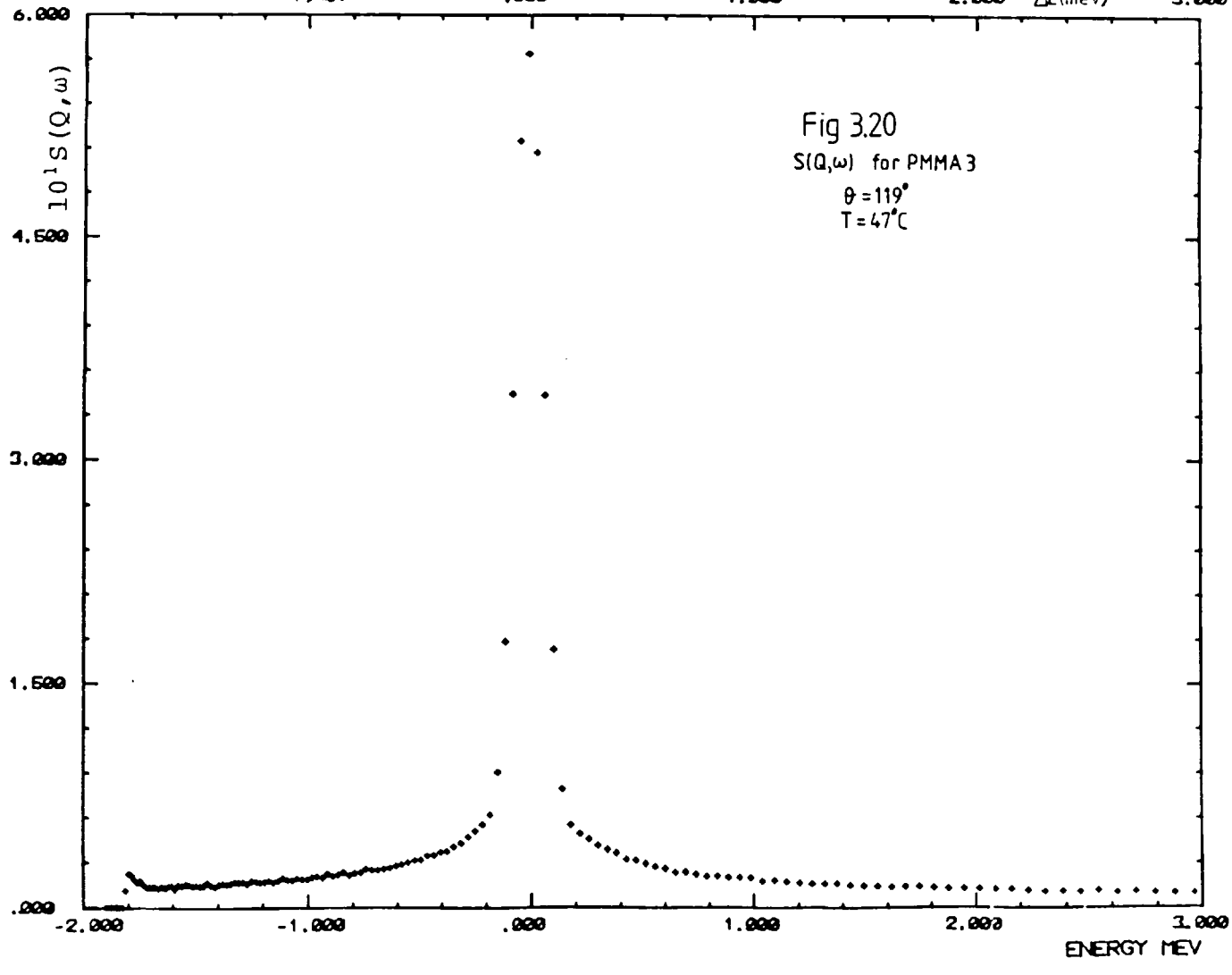


Fig 3.20
S(Q,ω) for PMMA3
θ = 119°
T = 47°C

other temperatures appear almost identical to these. Figures 3.21 and 3.22 show the spectra obtained from ISOT1 at two angles of scatter. The greatly increased elastic intensity in this case is mainly due to incoherent scattering from the hydrogen in the backbone and α-methyl group (since the FWHM of the quasi-elastic component associated with the rotational motion of the α-methyl group is less than 8 μeV at room temperature, its contribution to the quasi-elastic width observed in these spectra (FWHM ∿800 μeV) is negligible, and may be considered purely elastic.)

In addition to these experiments performed on IN5, room temperature measurements were made on PMMA3, ISOT1 and SYNDIO1 using IN6. An incident wavelength of 4.1 Å was used, giving a FWHM elastic resolution of the order of 250 μeV, and a Q range 0.4 to 2.6 $Å^{-1}$.

It should be emphasised that all quasi-elastic scattering measurements were made below the glass transition temperature of the samples, in order to eliminate problems in analysis associated with translational motion.

3.3.5 Corrections to the Calculated EISF for Comparison with Experimental Values

The EISF calculated according to equation (3.8) or (3.10) assumes that all the elastic intensity measured in the observed spectrum is due to centre of mass motion of the rotating group. However, for the PMMA samples used in this series of experiments, this assumption is not true, and before comparing the EISF calculated for a specific model to the EISF obtained experimentally, it is necessary to correct the theoretical values to take account of extra hydrogen in the sample which will increase the observed elastic intensity. For PMMA3, this will be a relatively small correction, due only to incomplete deuteration of the α-methyl and backbone hydrogen. However, for the pure stereo-isomers, and PMMA1, the calculated EISF will be considerably different after applying the correction, since these samples contain

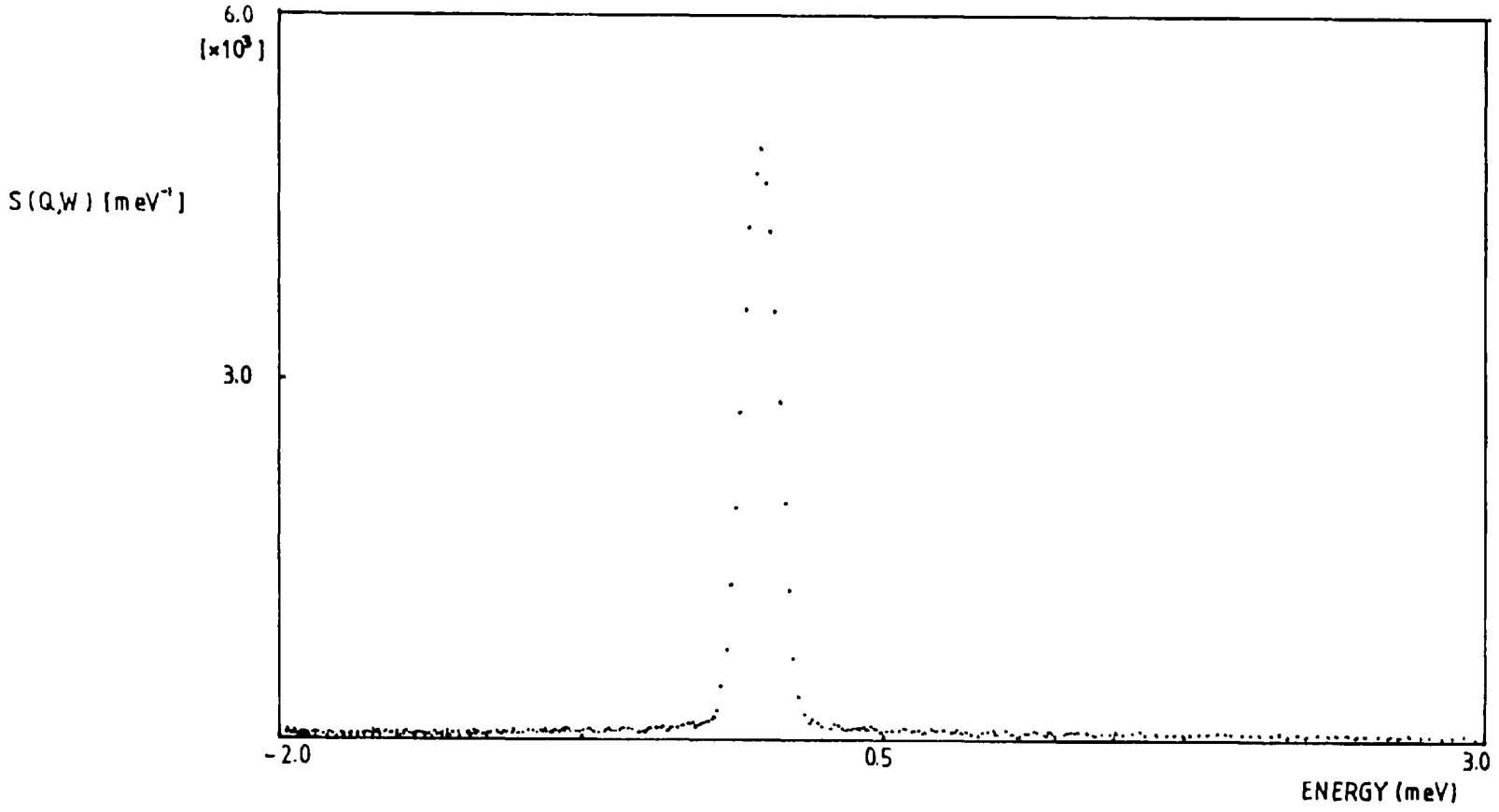
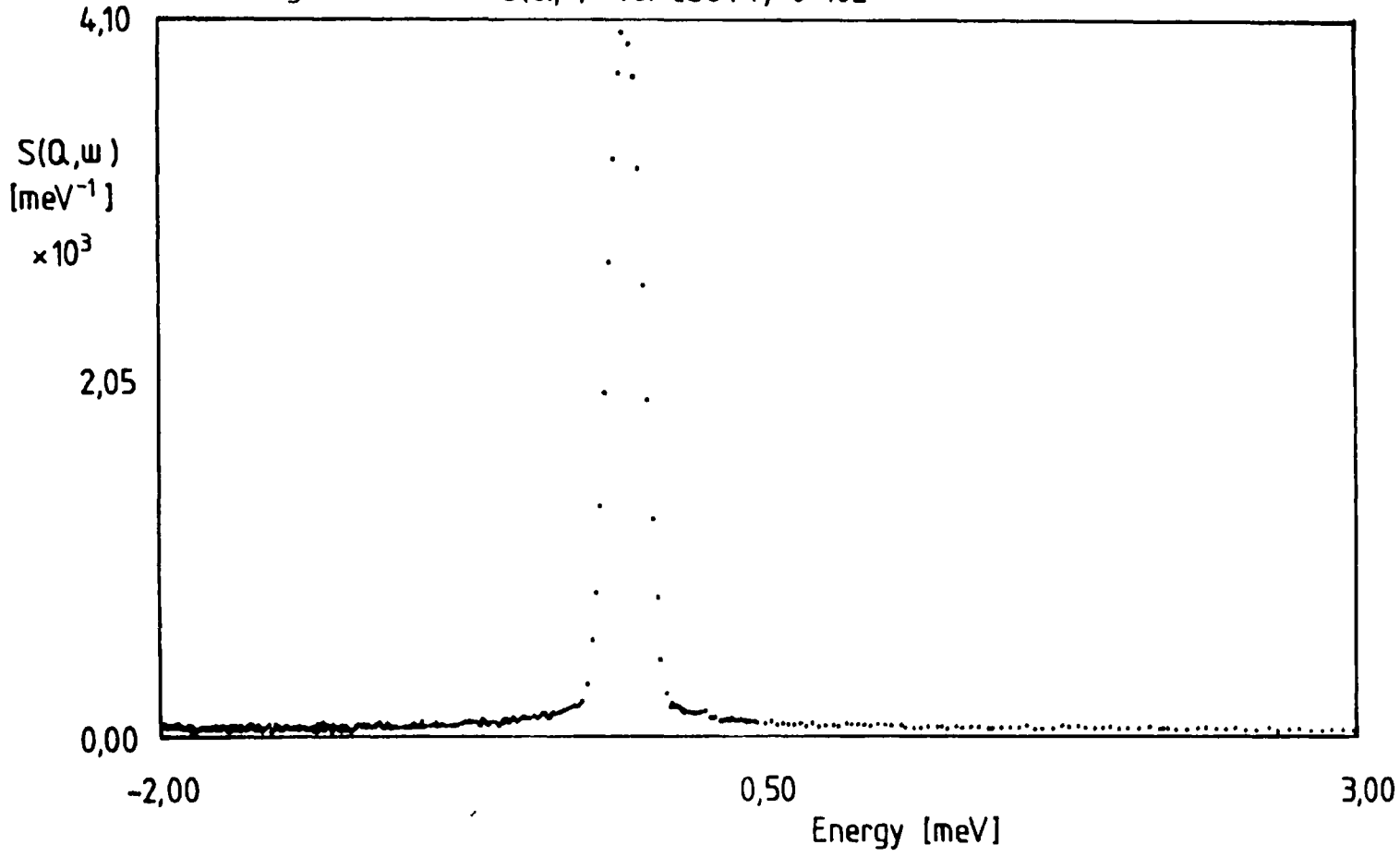


Fig 3.21 S(Q,W) for ISOT1, θ=62°

Fig 3.22 S(Q,ω) for ISOT1, θ=102°



such a high percentage of hydrogen.

The method used to calculate the corrected EISF follows Dianoux[34], and is outlined below for the specific case of PMMA3.

In deriving the corrected EISF, the incoherent contribution of the α-methyl and backbone deuterium (σ_{inc} = 2.26 b for deuterium) and the small percentage, z, of hydrogen (σ_{inc}(hydrogen) = 79.7 b) which has not been replaced by deuterium only is considered, since the incoherent cross-sections of the other nuclei (oxygen and carbon) are considered negligible. Since only the ester methyl group is considered to be rotating (because, as pointed out earlier, the rotation of the α-methyl group is much too slow to be observed on the timescale of this experiment), the contribution to the scattering law by the deuterium and unsubstituted backbone and α-methyl hydrogen will be purely elastic and affect only the δ-function component of the rotational scattering law. Thus the scattered intensity for the sample will be proportional to

$$\{5\sigma_H z + 5\sigma_D(1 - z)\}\ \delta(\omega) + 3\sigma_H\ S^{rot}_{inc}(\underline{Q},\omega)$$

where $$S^{rot}_{inc}(\underline{Q},\omega) = A_0(\underline{Q})\,\delta(\omega) + \frac{1}{\pi}\{1 - A_0(\underline{Q})\}\frac{2\tau/3}{1 + \omega^2(2\tau/3)^2}$$

with $$A_0(\underline{Q}) = \frac{1}{3}\{1 + 2j_0(Qr)\}$$

(In fact, this correction is calculated for the case of a simple three-fold jump motion - the applicability of this model to the ester methyl group is considered later in the chapter. Of course, the method is equally applicable to complex rotations, with suitable forms of $A_0(\underline{Q})$ and $S^{rot}_{inc}(\underline{Q},\omega)$ inserted in the above expressions).

In order to obtain a normalised scattering law, $\int_{-\infty}^{\infty} S(\underline{Q},\omega)d\omega = 1$, $S(\underline{Q},\omega)$ is defined by

$$S(\underline{Q},\omega) = \frac{\underline{P}_f}{P_t}\,\delta(\omega) + \frac{\underline{P}_m}{P_t}\,S^{rot}_{inc}(\underline{Q},\omega)$$

with $$\frac{\underline{P}_f}{P_t} = \frac{(5/3)z + (5/3)(\sigma_D/\sigma_H)(1-z)}{1 + (5/3)z + (5/3)(\sigma_D/\sigma_H)(1-z)}$$

and $$P_f + P_m = P_t$$

P_f and P_m represent the total number of fixed and rotating scattering sites, expressed in units of σ_H. Since the extra hydrogen and deuterium contribute additional intensity to the elastic component of the scattering law, the coefficient $A_0'(\underline{Q})$ of the $\delta(\omega)$ peak is no longer the true EISF, but may be considered as an apparent EISF, related to the true value, $A_0(\underline{Q})$, by

$$A_0'(\underline{Q}) = \frac{\underline{P}_f}{P_t} + \frac{\underline{P}_m}{P_t}\,A_0(\underline{Q})$$

For PMMA3, z=0.03, giving $P_f/P_t = 0.0864$ and $P_m/P_t = 0.9136$.

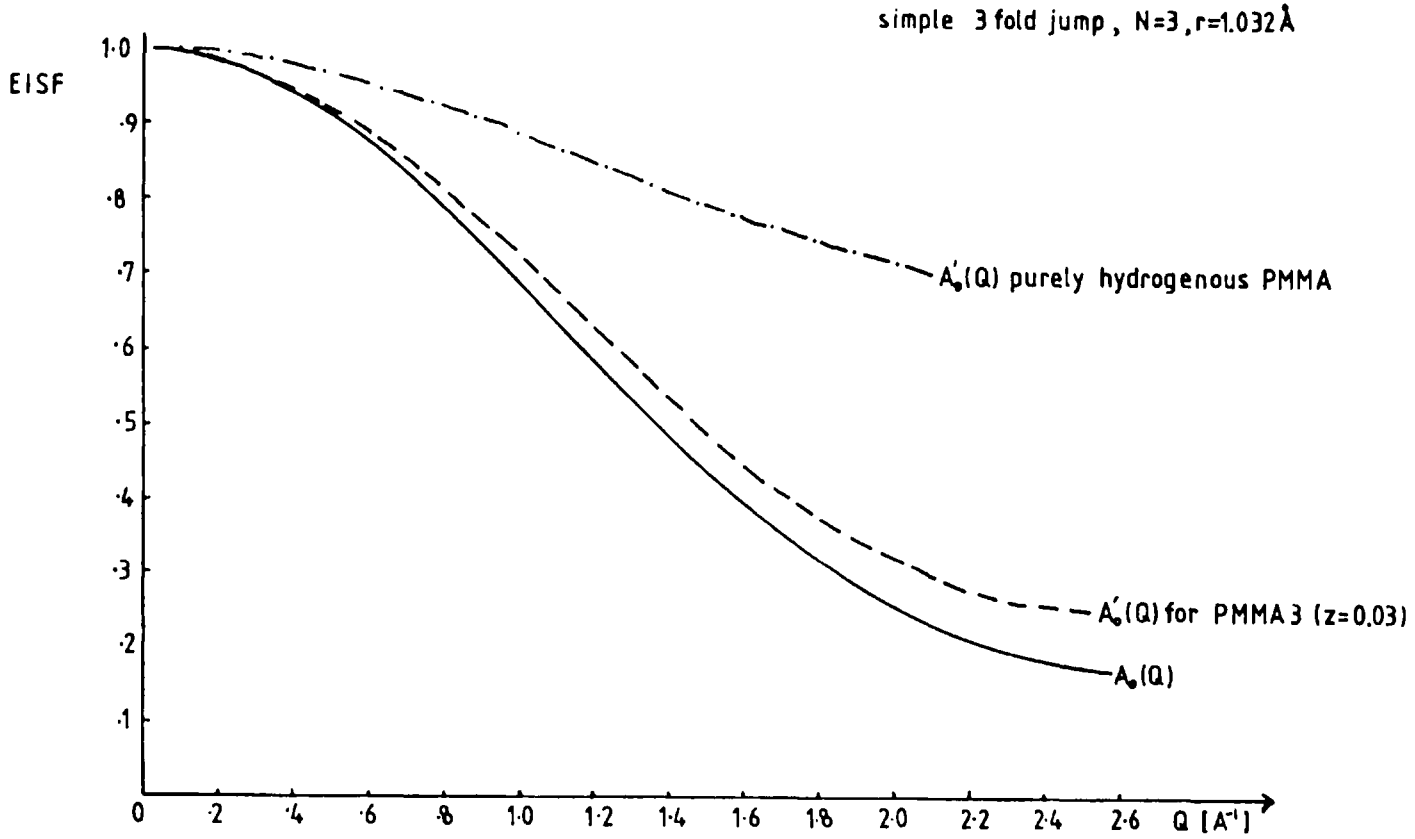
These correction factors may be calculated in exactly the same way for PMMA1 and the pure stereo-isomers, ISOT1 and SYNDIO1.

Figure 3.23 shows $A_0(\underline{Q})$ and $A_0'(\underline{Q})$ for PMMA3, and also for a purely hydrogenous sample of PMMA.

3.3.8 Experimental Values of the EISF and the Problem of Coherent Scattering

For data recorded on IN5, experimental values of the EISF for PMMA3 were obtained using the fitting program WONDERPROG (see section 2.3.1 for a description of this program), assuming a simple three-fold jump model, with

Fig 3.23 EISF for rotation of ester methyl group in PMMA



r = 1.032 Å. Plots showing the scattering law obtained using this model (referred to as W3 on the figures) compared with the actual data are shown for a range of Q values and temperatures in figures 3.24 to 3.27. The elastic and quasi-elastic components are indicated by a dashed line in each fit. If the ester methyl group is undergoing only a simple three-fold jump, the quasi-elastic component is predicted to be a single Lorentzian, whose width is characterised only by temperature, and is independent of Q. Thus a model comprising a single Lorentzian plus an elastic δ-function should fit the experimental data to give exactly the same values of the EISF as those obtained using the Barnes' three-fold jump model. Fits based on a single Lorentzian plus a δ-function are shown in figure 3.28 for PMMA3 at room temperature. The components comprising the scattering law are again separated by a dashed line.

Figure 3.29 shows the scattering law fitted at two angles of scatter for the isotactic sample, ISOT1, obtained using the three-fold jump model fitting program, W3.

The quasi-elastic data recorded on IN6 for PMMA3, ISOT1 and SYNDIO1 were also analysed using WONDERPROG, fitting a simple three-fold jump model to the data. However, due to its slightly greater energy range, an appreciable inelastic component due to the density of states function was found to contribute to the observed rotational scattering law, and it is no longer adequate to assume a flat inelastic background (as suggested in 3.1.4) when fitting to the data. Instead, to obtain an accurate fit, it is necessary to estimate a value of $\langle u^2 \rangle$ and calculate the Debye-Waller factor across the quasi-elastic spectrum. An alternative approach is to limit the energy range of the fitting routine, so that within these new limits the inelastic background appears flat. Results obtained in this way are essentially identical to those obtained applying the full exponential form of the Debye-Waller factor, $\exp(-Q^2\langle u^2 \rangle)$.

It will become clear later in the chapter that due to the timescale of the neutron scattering experiments, only the three-fold jump component of the ester methyl group

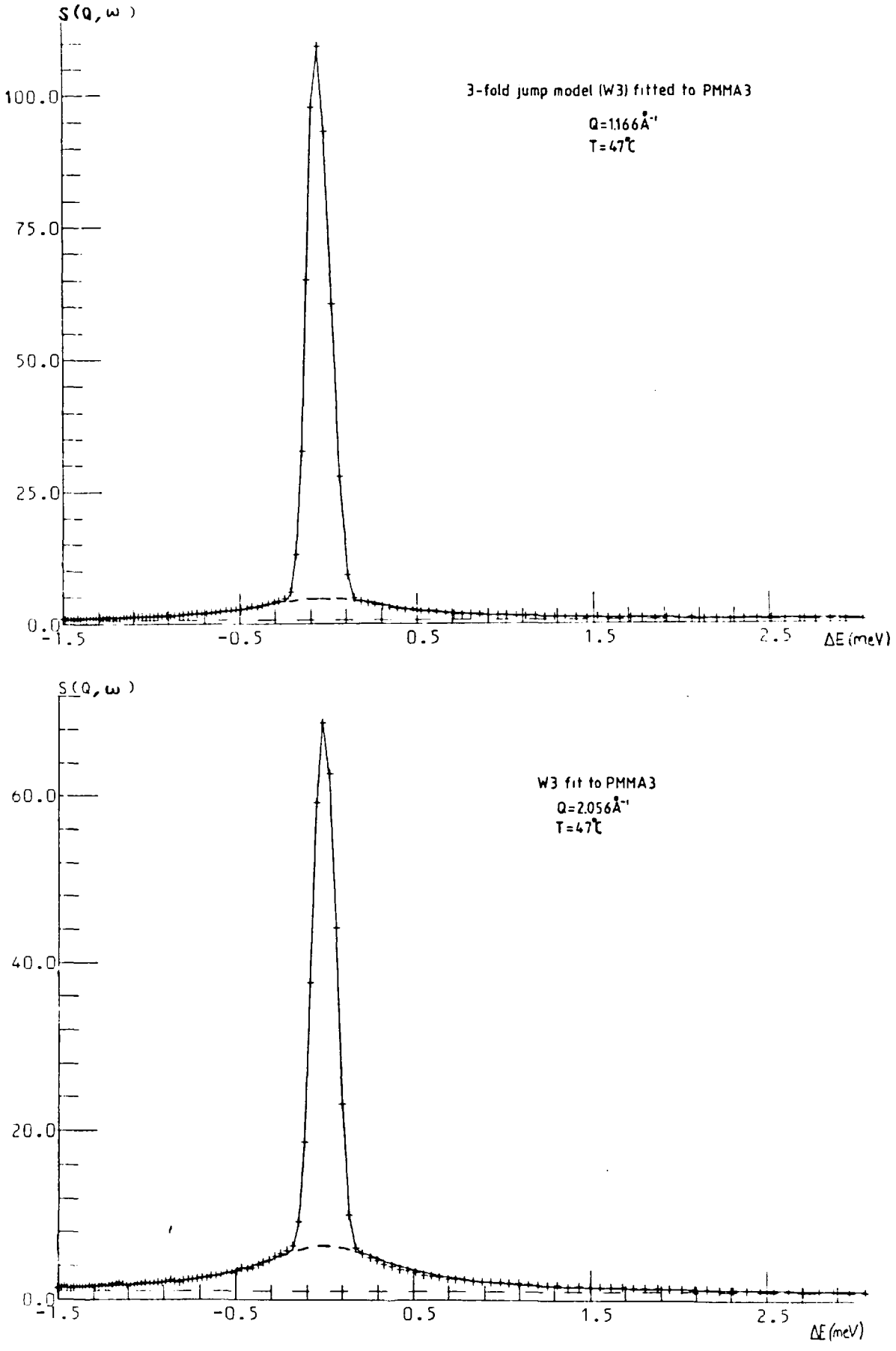
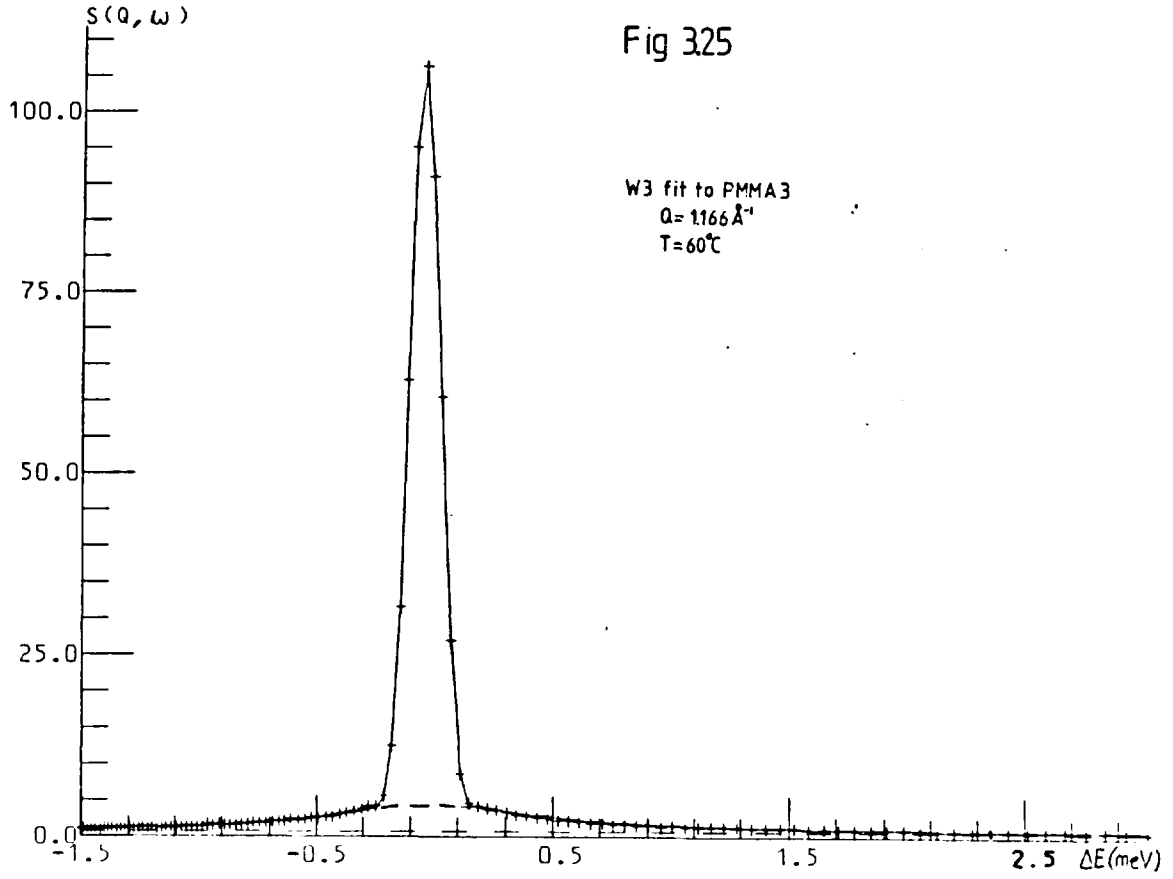
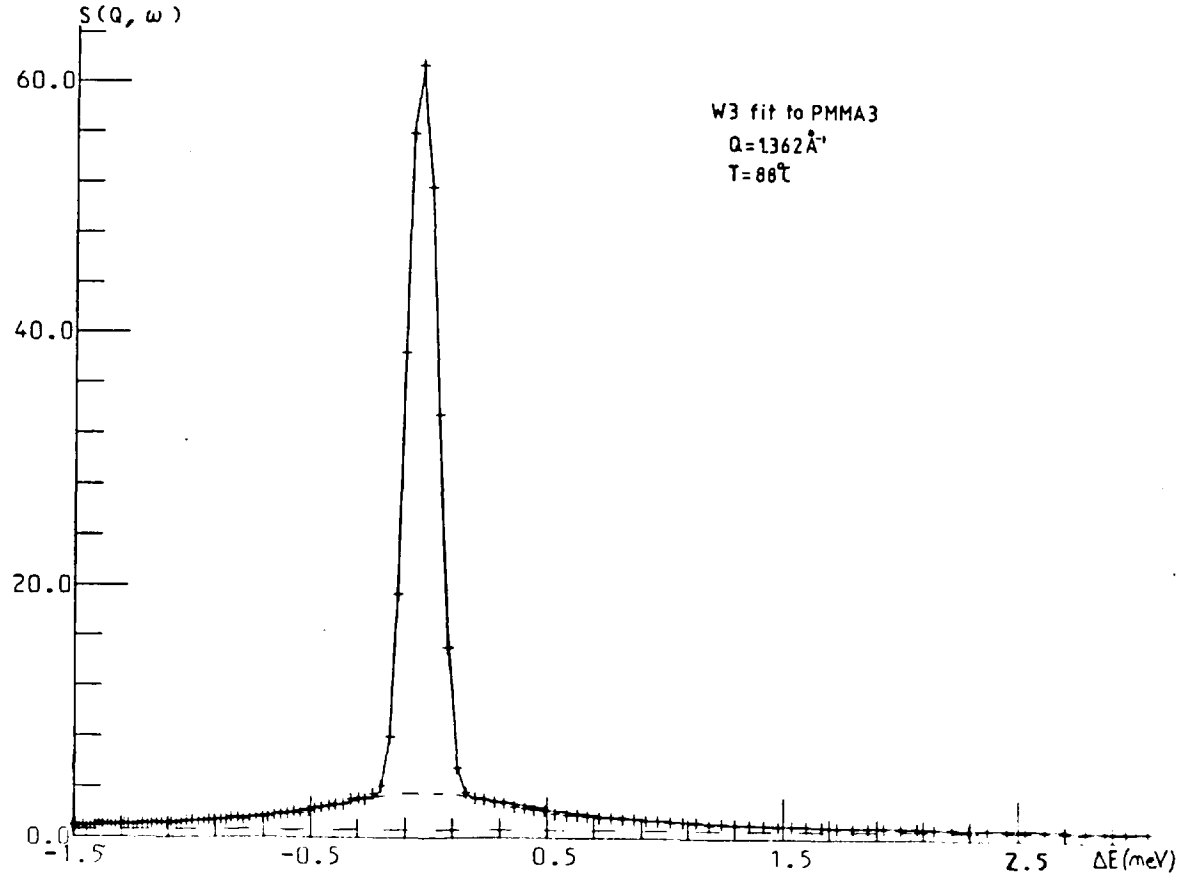

S(Q, ω)
100.0
75.0
50.0
25.0
0.0
-1.5
-0.5
0.5
1.5
2.5
ΔE (meV)
3-fold jump model (W3) fitted to PMMA3
Q=1.166Å⁻¹
T=47°C
S(Q, ω)
60.0
40.0
20.0
0.0
-1.5
-0.5
0.5
1.5
2.5
ΔE (meV)
W3 fit to PMMA3
Q=2.056Å⁻¹
T=47°C

Fig 3.24

Fig 3.25


S(Q, ω)
100.0
75.0
50.0
25.0
0.0
-1.5
-0.5
0.5
1.5
2.5
ΔE(meV)
W3 fit to PMMA3
Q= 1.166 Å⁻¹
T=60°C


S(Q, ω)
60.0
40.0
20.0
0.0
-1.5
-0.5
0.5
1.5
2.5
ΔE(meV)
W3 fit to PMMA3
Q=1.362 Å⁻¹
T=88°C

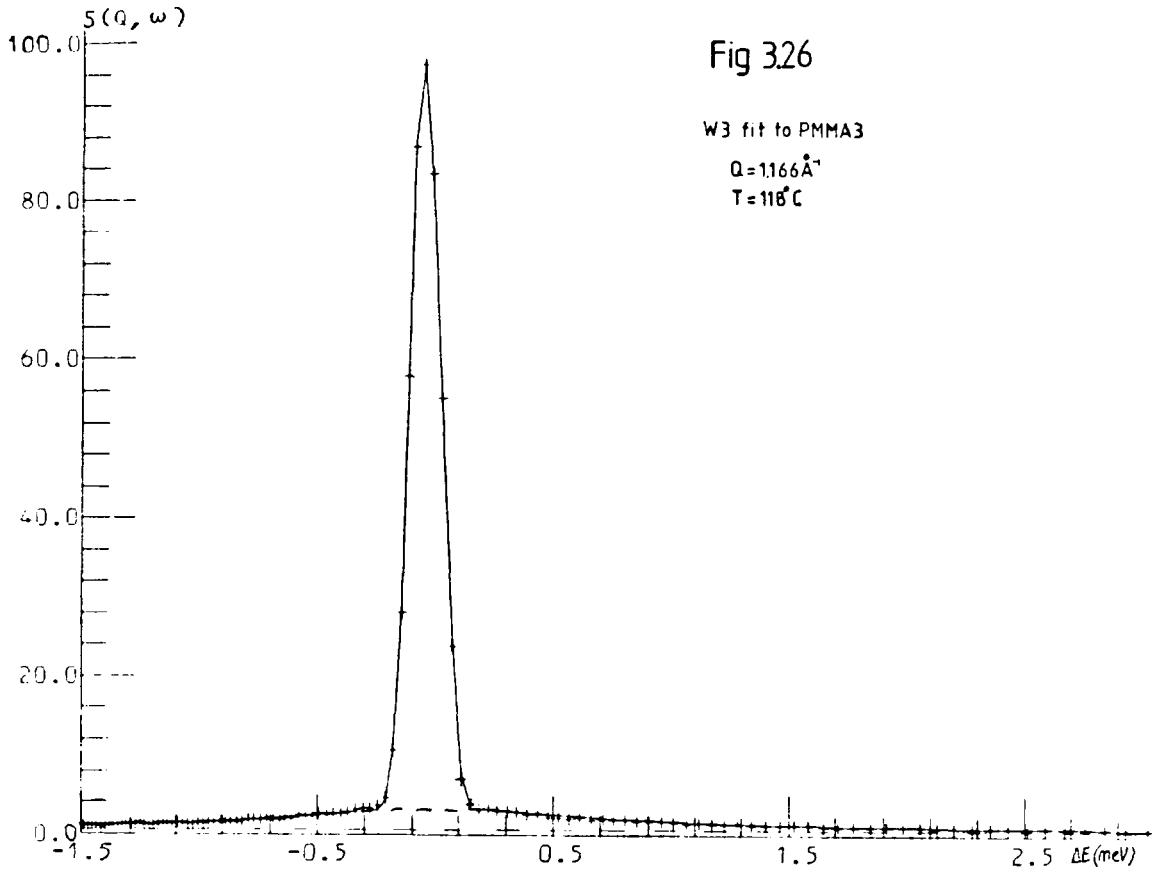
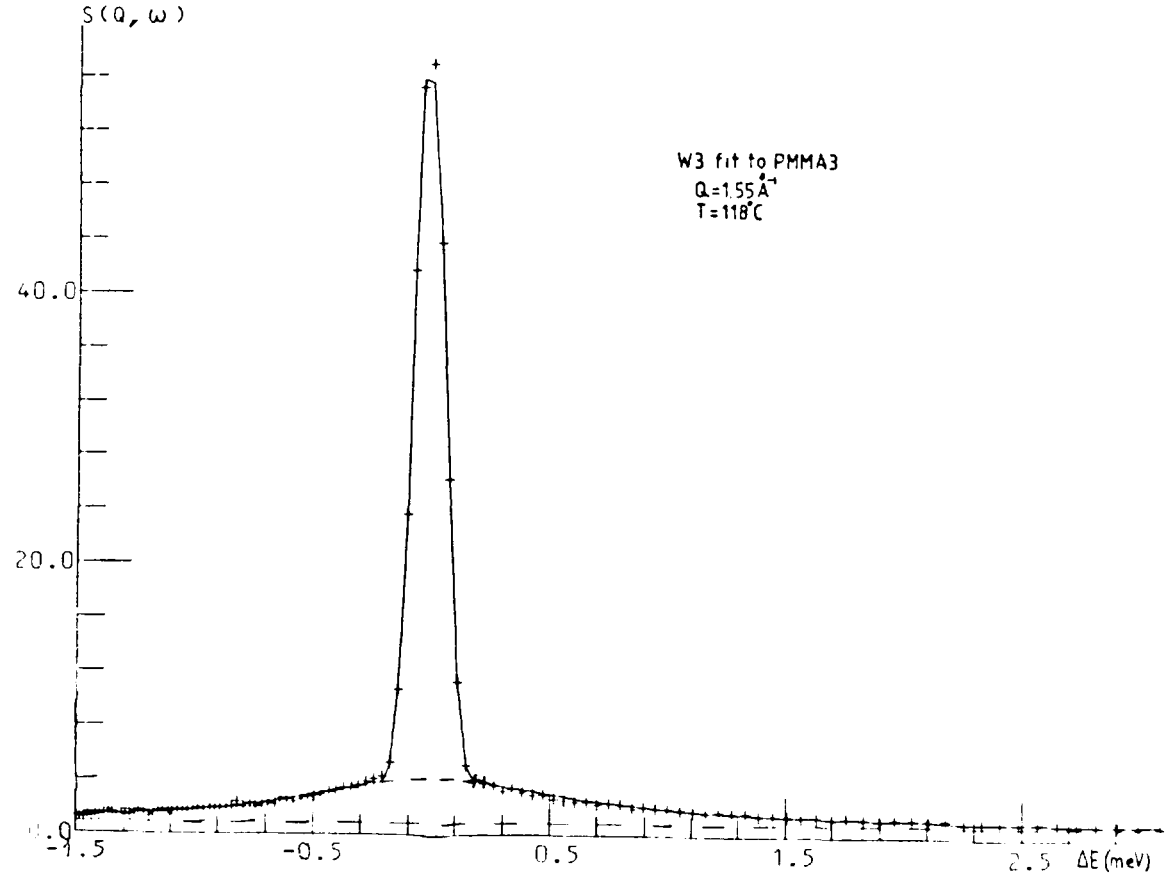

S(Q, ω)
100.0
80.0
60.0
40.0
20.0
0.0
-1.5
-0.5
0.5
1.5
2.5
ΔE(meV)
W3 fit to PMMA3
Q=1.166Å⁻¹
T=118°C

Fig 3.26


S(Q, ω)
40.0
20.0
0.0
-1.5
-0.5
0.5
1.5
2.5
ΔE (meV)
W3 fit to PMMA3
Q=1.55Å⁻¹
T=118°C

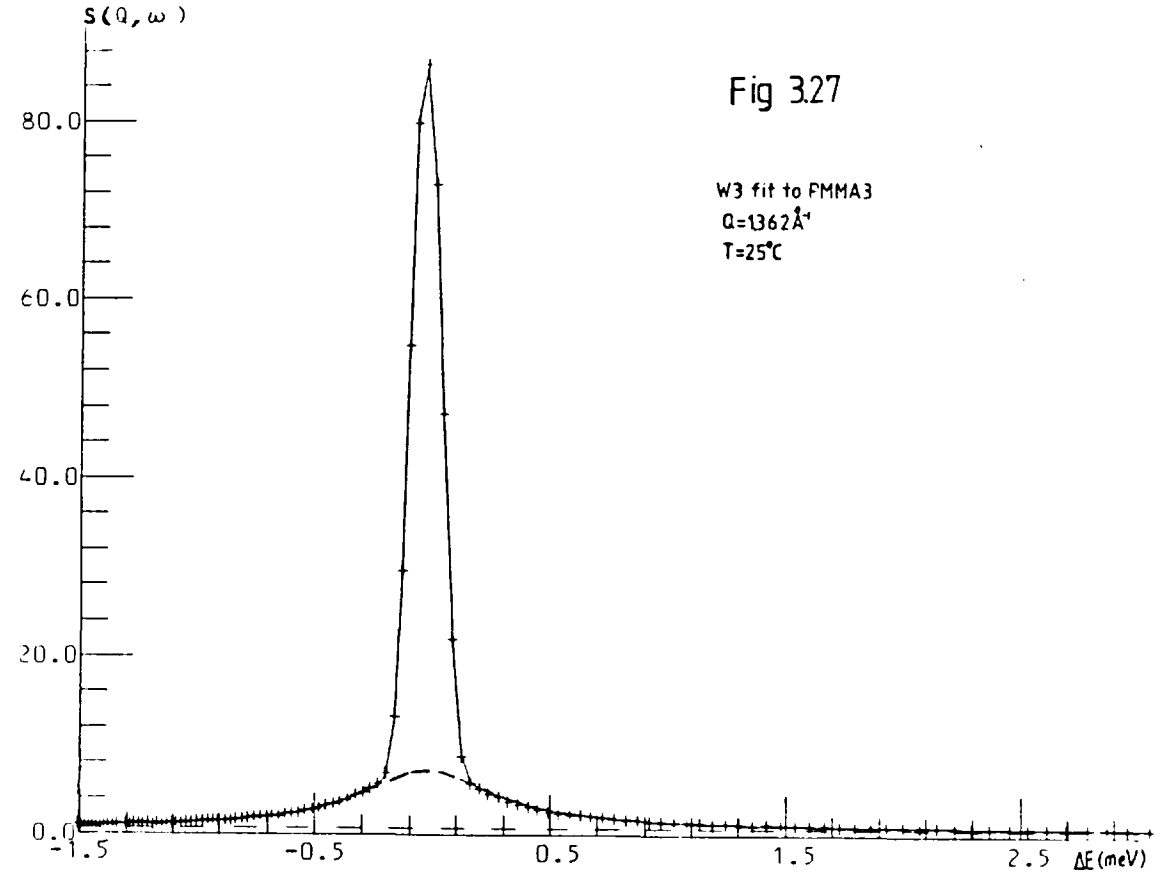
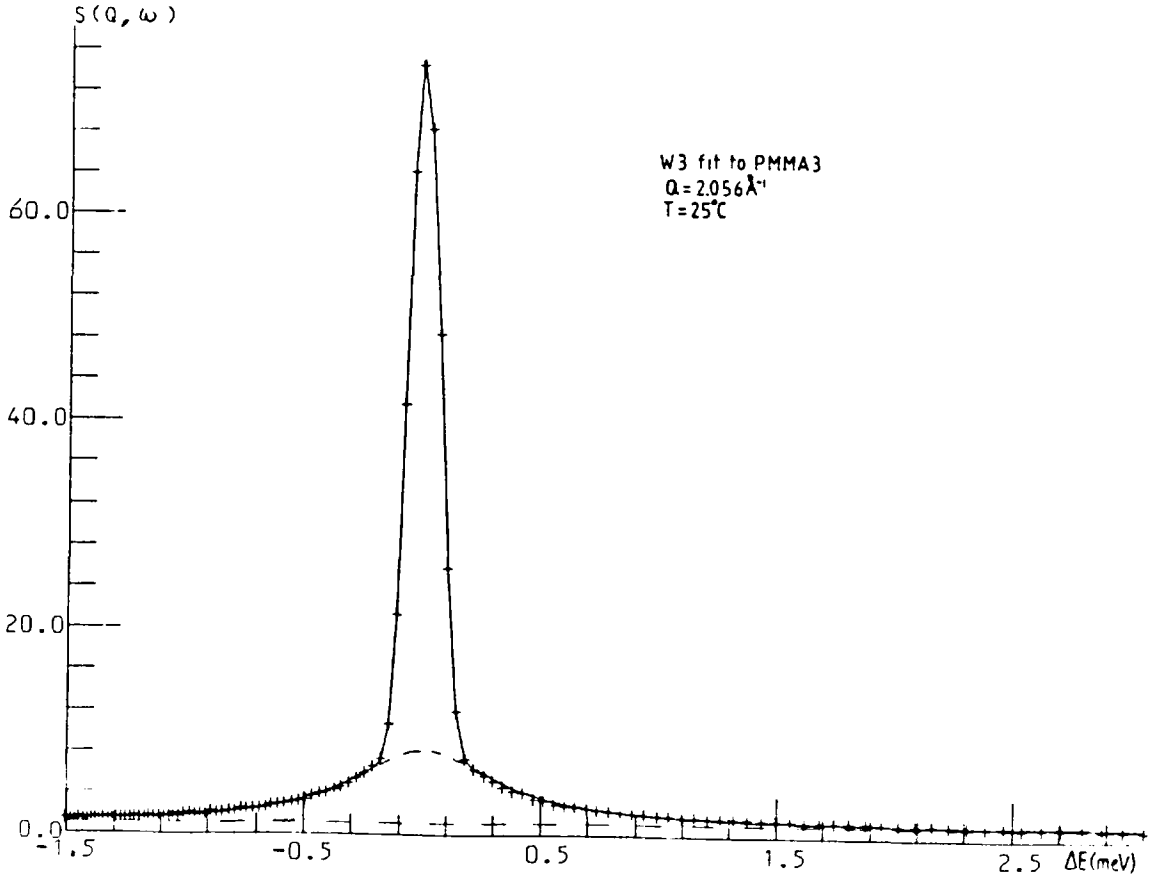

S(Q, ω)
80.0
60.0
40.0
20.0
0.0
-1.5
-0.5
0.5
1.5
2.5
ΔE(meV)
W3 fit to PMMA3
Q=1.362Å⁻¹
T=25°C

Fig 3.27


S(Q, ω)
60.0
40.0
20.0
0.0
-1.5
-0.5
0.5
1.5
2.5
ΔE(meV)
W3 fit to PMMA3
Q=2.056Å⁻¹
T=25°C

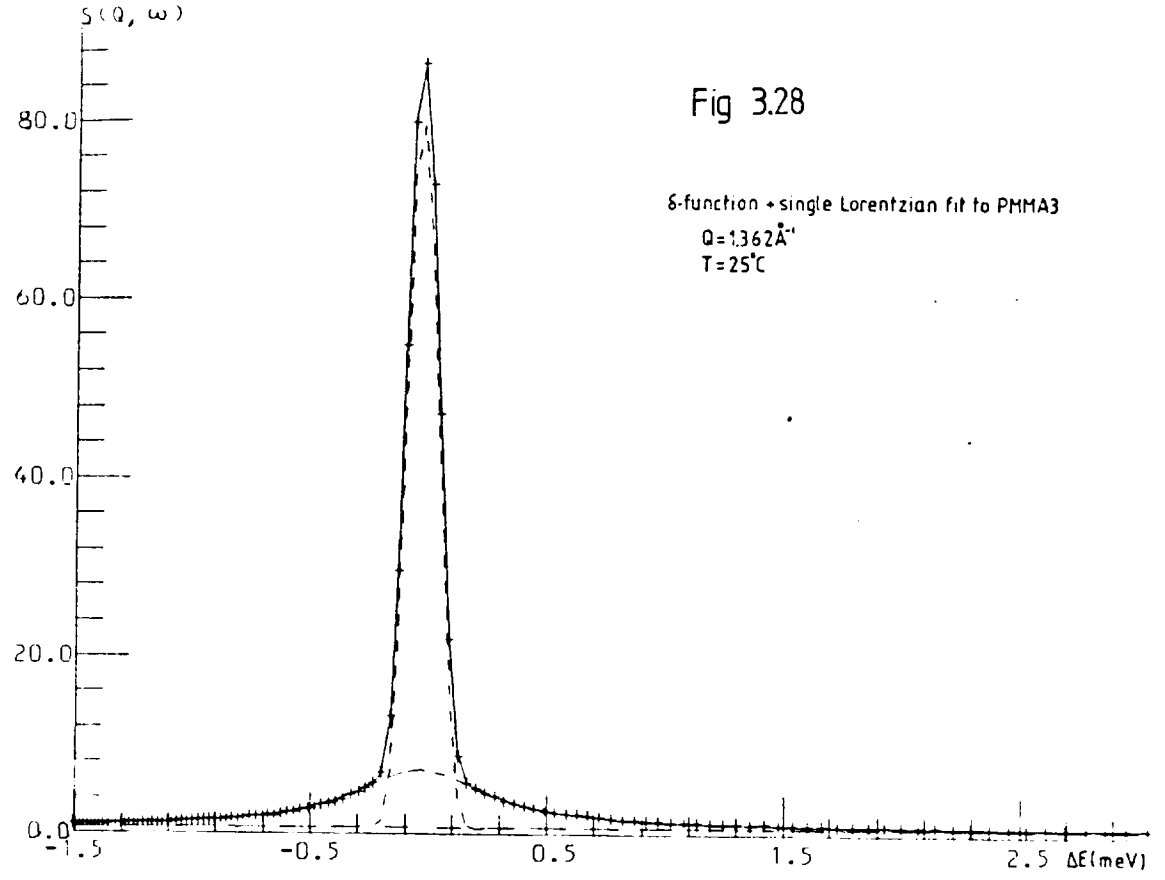
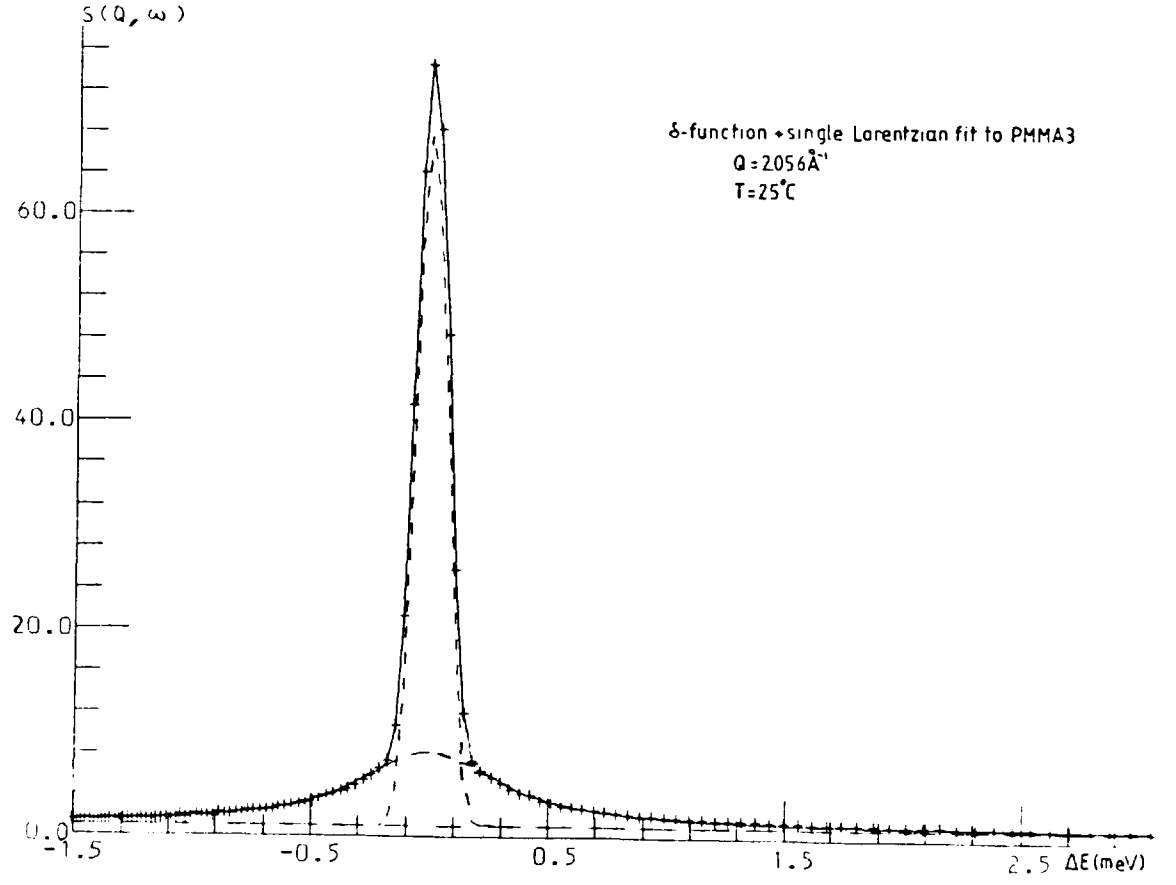


Fig 3.28

δ-function + single Lorentzian fit to PMMA3
Q = 1.362Å⁻¹
T = 25°C



δ-function + single Lorentzian fit to PMMA3
Q = 2.056Å⁻¹
T = 25°C

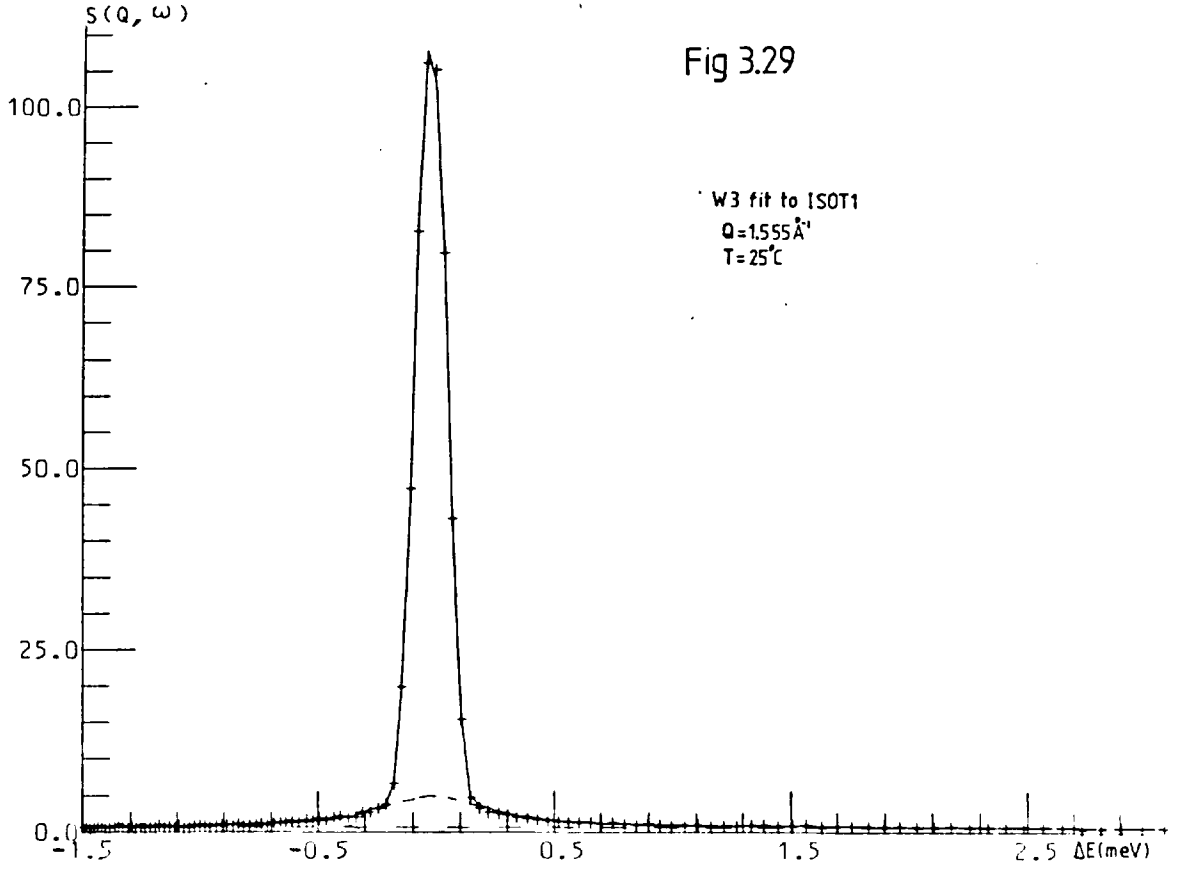
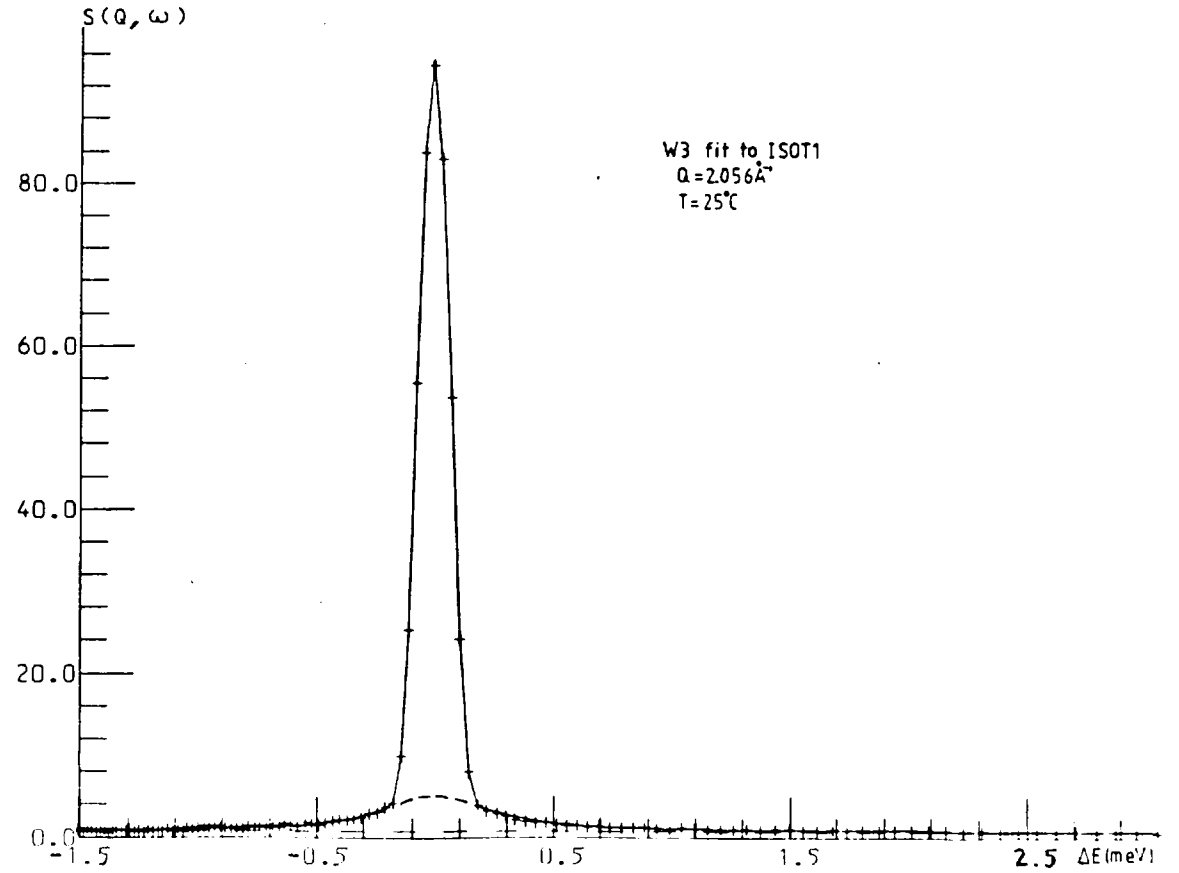

S(Q, ω)
100.0
75.0
50.0
25.0
0.0
-1.5
-0.5
0.5
1.5
2.5 ΔE(meV)
W3 fit to ISOT1
Q=1.555Å⁻¹
T=25°C

Fig 3.29


S(Q, ω)
80.0
60.0
40.0
20.0
0.0
-1.5
-0.5
0.5
1.5
2.5 ΔE(meV)
W3 fit to ISOT1
Q=2.056Å⁻¹
T=25°C

motion is being observed, with no contribution of the two-fold flipping motion associated with the rotational motion of the whole ester group. For this reason, further analysis concentrates mainly in terms of the Barnes' three-fold jump model to describe the observed motion.

Figure 3.30 shows the experimental values of the EISF obtained from PMMA3 from IN5 for the ester methyl group measured at various temperatures, using a three-fold jump model fit to the data, compared with $A_0'(\underline{Q})$, the corrected calculated EISF for a three-fold jump. Clearly there is a large discrepancy between the observed and predicted EISF (although it should be noted that the alternative model of a combined two and three fold motion would show an even larger discrepancy, since the EISF for this model drops off even more quickly with Q). Figure 3.31 shows the EISF obtained by fitting a single Lorentzian plus a δ-function to the experimental scattering law for the IN5 data. The values obtained using this fitting routine are identical to those obtained using the three-fold jump model fitting program, W3. In addition, in both cases, the width of the quasi-elastic component is found to be independent of Q, as predicted by the Barnes' model. Also shown in figure 3.31 is the experimental EISF obtained from PMMA3 from data measured using IN6. These values were obtained using the three-fold jump model fitting program, W3, with a value of $\langle u^2 \rangle$ of 0.5 used to calculate the Debye-Waller factor, $\exp(-Q^2\langle u^2 \rangle)$. (As indicated earlier in the chapter, due to the slightly greater energy transfer range covered by IN6, the experimental scattering law obtained is not the pure rotational scattering law, $S_{inc}^{rot}(\underline{Q},\omega)$, but instead $S_{inc}^{rot}(\underline{Q},\omega)$ combined with a significant inelastic contribution from the density of states function (which appears in the spectrum at higher energies). Unless due account is taken to correct for this extra inelastic intensity, the values of the EISF obtained will no longer be correct, since the calculation to obtain the EISF will no longer be solely defined by the ratio of the areas of the elastic component of the rotational scattering law to the quasi-elastic component, but instead by the ratio of the

Fig 3.30 Experimental values of the EISF for PMMA3 (IN5)

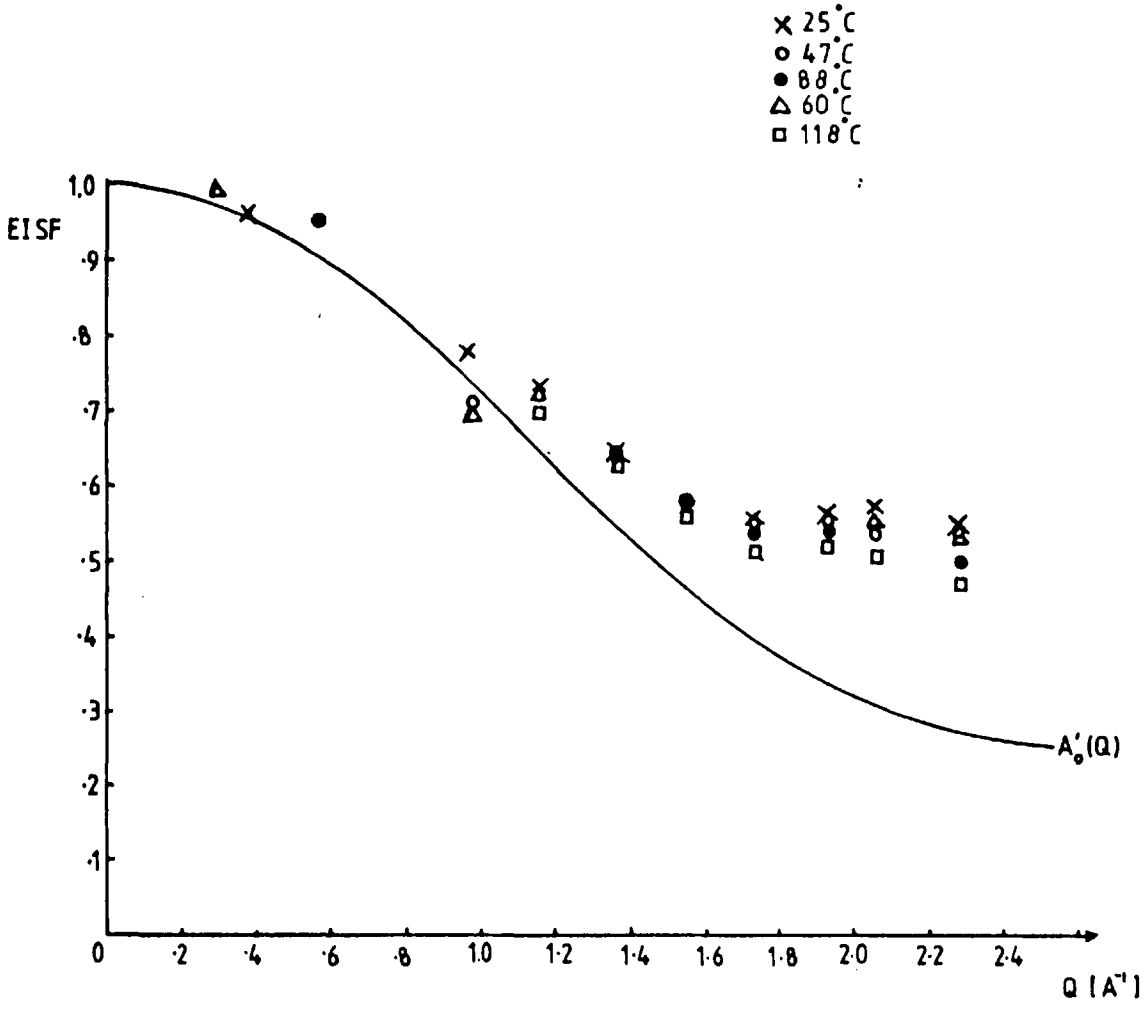
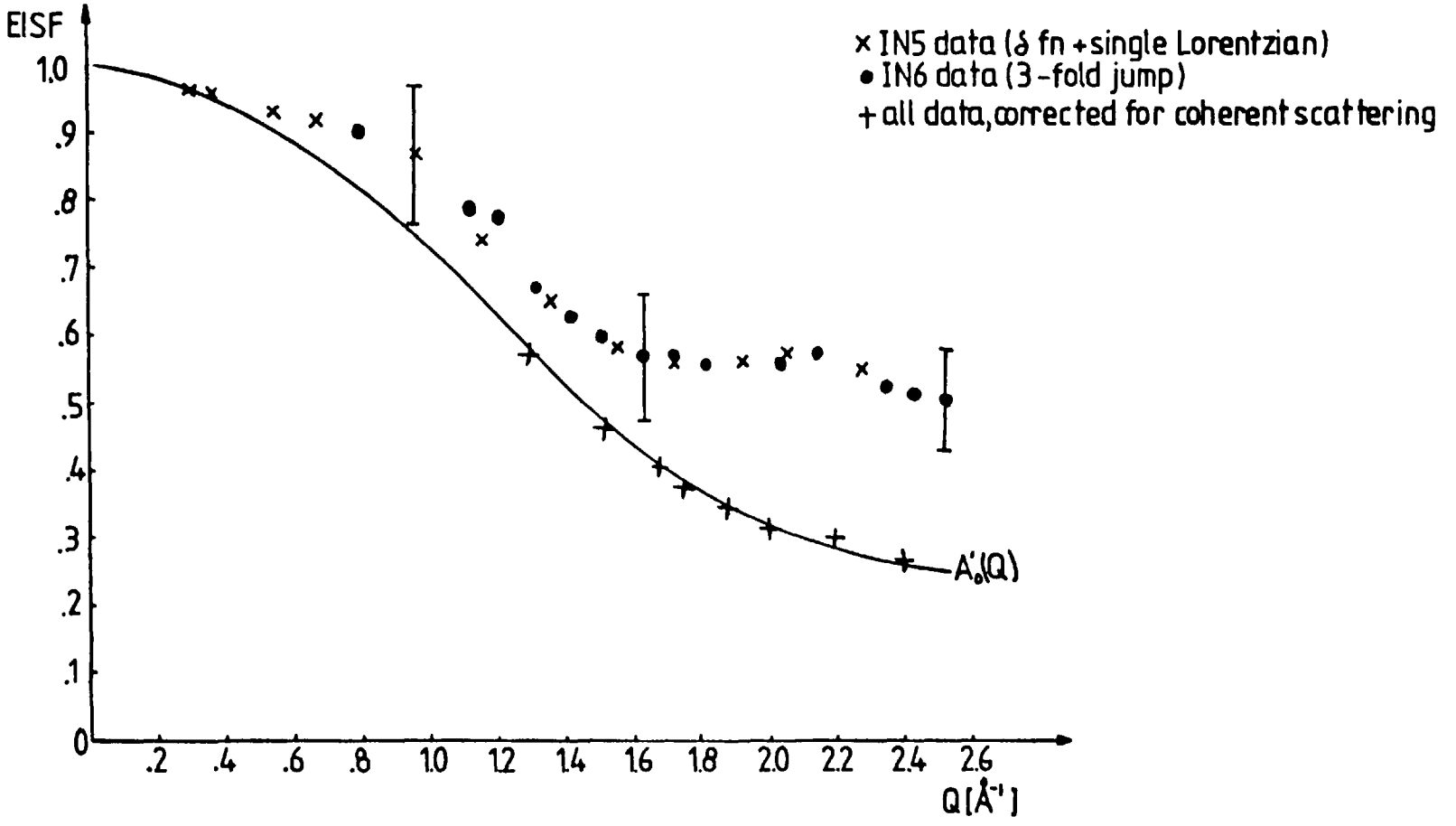


Fig 3.31 EISF for PMMA3 - Comparison of IN5 and IN6 data



area of the elastic component of $S^{rot}_{inc}(\underline{Q},\omega)$ to the area of the quasi-elastic component of $S^{rot}_{inc}(\underline{Q},\omega)$ plus extra area due to the contribution of the density of states function. This will therefore give values of the EISF which are smaller than the true values.

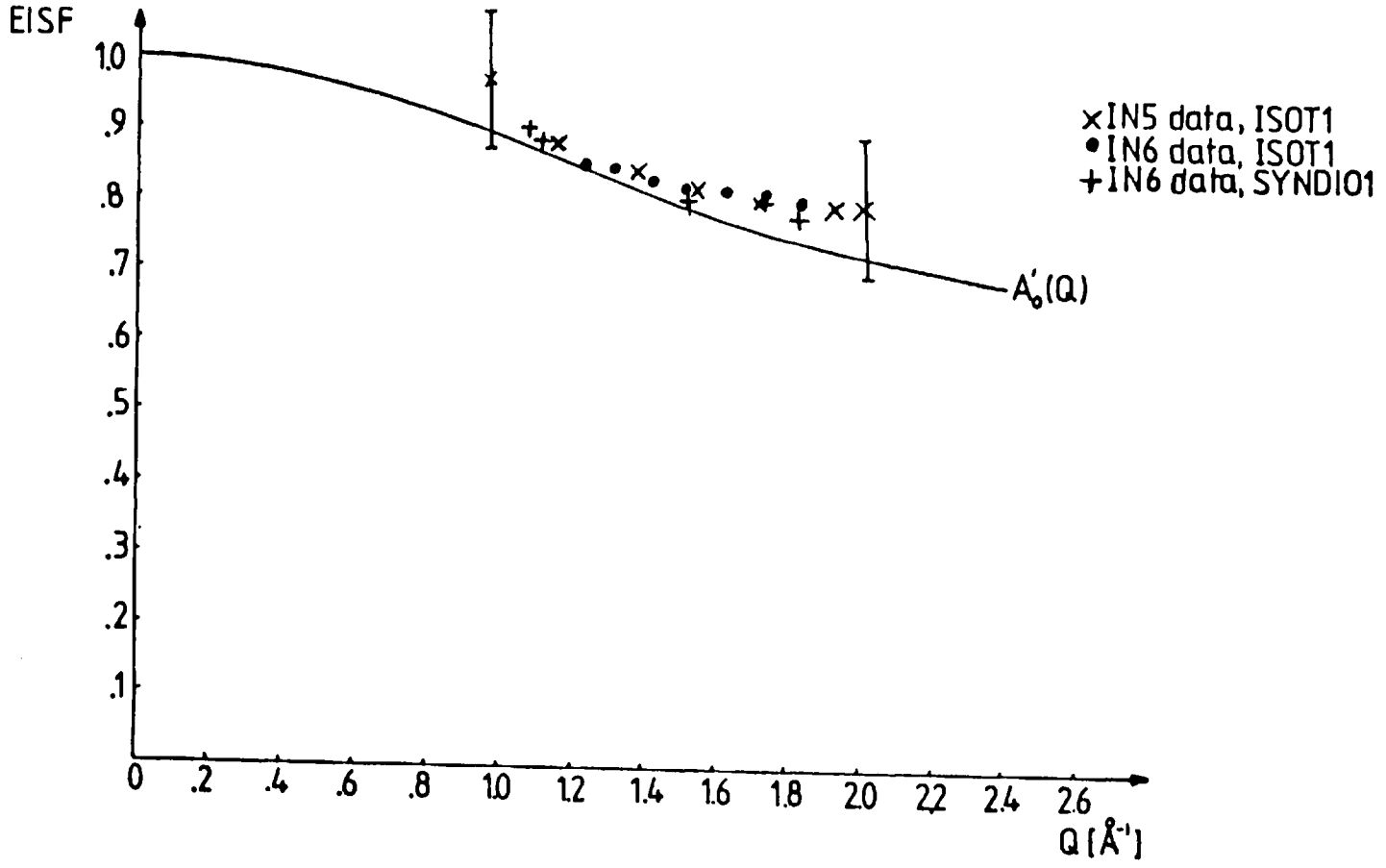
The inelastic contribution is thus corrected for by either estimating a value of $\langle u^2 \rangle$ and calculating the Debye-Waller factor across the spectrum, or by analysing the data across a narrower energy transfer range, thus effectively eliminating the contribution due to inelastic scattering)

The EISF calculated assuming the scattering law to comprise a δ-function plus a single Lorentzian, but fitted across a narrower energy range than for W3, was found to give identical results to those obtained using W3 with a value of $\langle u^2 \rangle$ of 0.5, and fitting across the entire spectrum.

The excellent agreement of the experimental values of the EISF obtained from two different fitting routines, and furthermore, from two different instruments, would suggest that the three-fold jump model is appropiate for describing the observed motion on the timescale of a neutron scattering event, and the apparent discrepancy must be attributed to some other factor.

Figure 3.32 shows the EISF obtained for ISOT1, from IN5 measurements, and that obtained for both ISOT1 and SYNDIO1 from IN6 measurements. Again, for IN6 measurements, due account was taken of the Debye-Waller factor in the data analysis. It should be pointed out that analysis for these purely hydrogenous samples is rather more difficult than for the partially deuterated PMMA3, due to the enormous amount of extra elastic scattering from the extra hydrogen in the samples. However, there is again found to be excellent agreement between IN5 and IN6 data, and in addition, the EISF is found to be identical for the two stereoregular forms of the polymer. This is as expected, since the EISF

Fig 3.32 EISF for stereoregular PMMA



reflects only the geometrical motion of the rotating methyl group, which is probably independent of tacticity.Comparison of figures 3.31 and 3.32 show that the values of the EISF for the pure stereo-isomers, ISOT1 and SYNDIO1 cover a rather more limited Q range than the values obtained for the partially deuterated sample PMMA3. This is due to problems in obtaining an acceptable fit at the extreme Q values for the purely hydrogenous samples. Also shown in figure 3.32 is the calculated EISF, $A_0'(\underline{Q})$, corrected for a purely hydrogenous sample. Again, a large discrepancy is observed between the predicted and observed data.

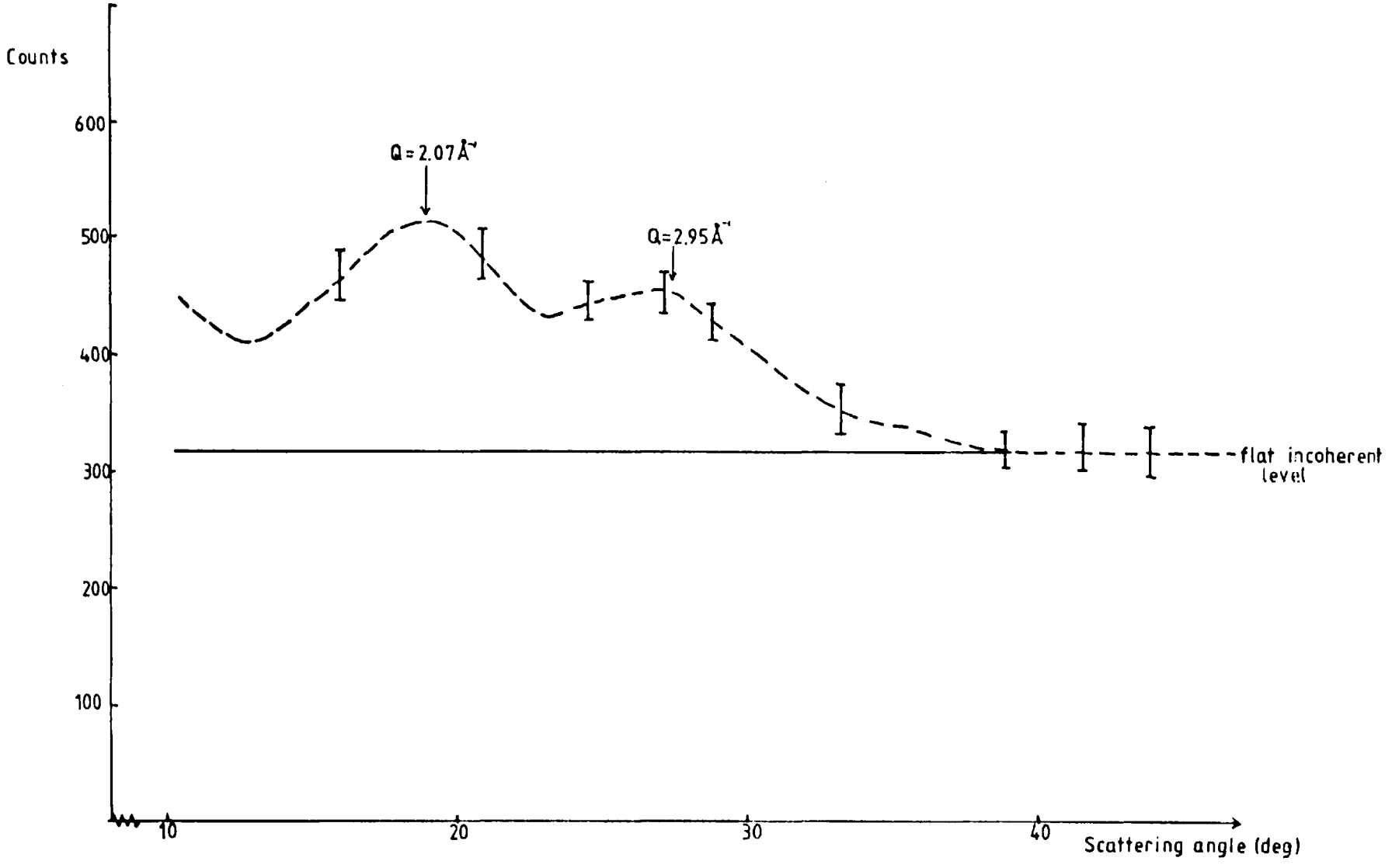
This large difference between the predicted theoretical EISF and the experimental values for all the PMMA samples is attributed to elastic coherent scattering from the sample. Supplementary measurements were made to obtain the coherent structure factor, $S(\underline{Q})$, for PMMA3, using the powder diffractometer, 10H. The results obtained are shown in figure 3.33. Clearly there is a significant coherent contribution across the whole Q range covered by the IN5 and IN6 experiments. Figure 3.34 shows the wide angle X-ray diffraction pattern for commercial PMMA[63] . Although it was not possible to measure the primary diffraction peak positioned at about 1 Å^{-1} on 10H, due to experimental limitations, in all other respects the structure factor, $S(\underline{Q})$, measured using neutron diffraction techniques is identical to that obtained using X-ray scattering.

Since it seems most likely that the differences between the predicted and observed EISF, $M(\underline{Q})$, are due principally to coherent scattering, it is possible to correct $M(\underline{Q})$ in the following way.

$$M(\underline{Q}) = \frac{\text{El.Coh.} + \text{El.Inc}}{\text{El.Coh} + \text{El.Inc} + \text{Q.El.Inc}}$$

The diffraction pattern for PMMA3 shown in figure 3.33 reflects the total scattering from the sample i.e both the coherent and incoherent contributions. It is reasonable to assume that with increasing Q (corresponding

Fig 3.33 Coherent scattering from PMMA3



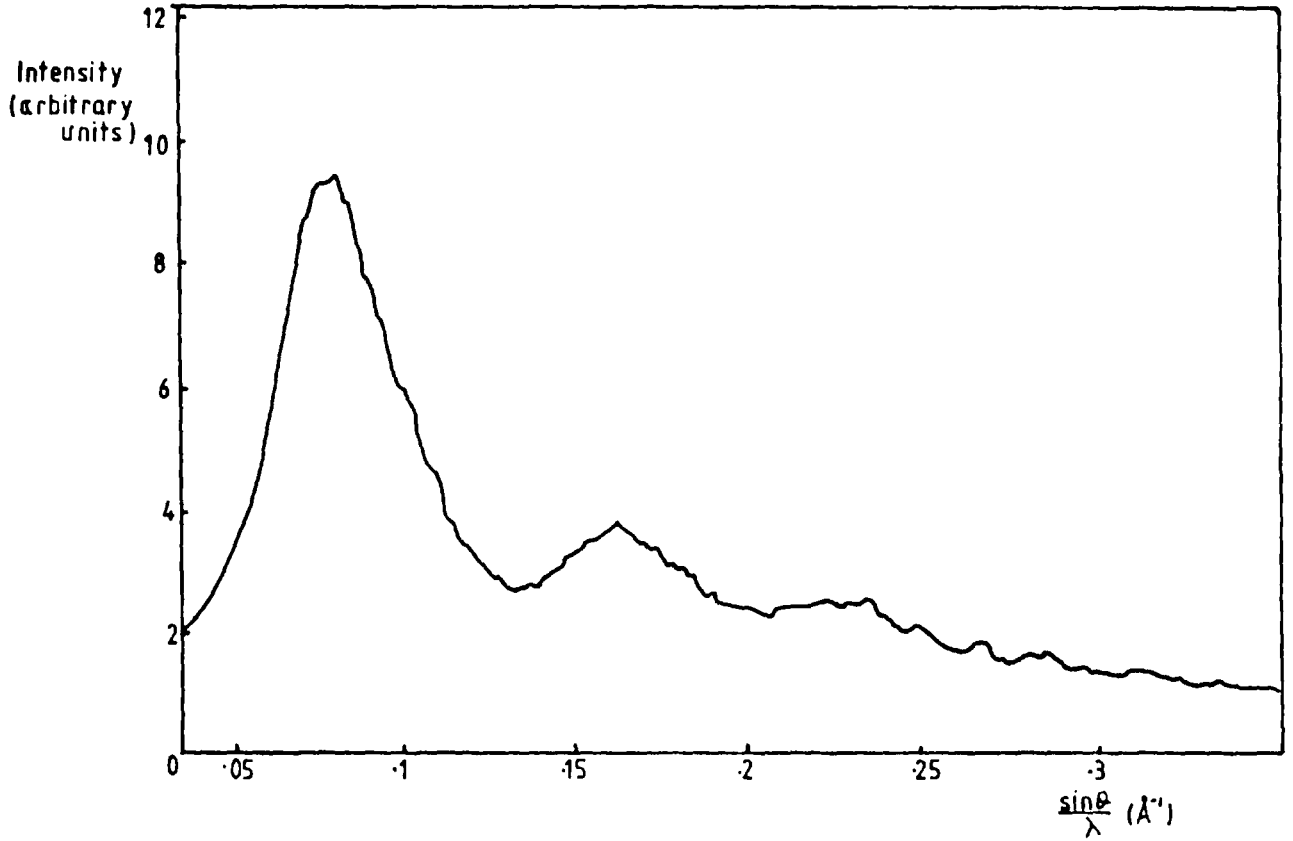


Fig 3.34 Wide angle X-ray scattering pattern from PMMA (from 19)

to shorter distances being explored in the polymer chain) coherent effects in the sample will be lost, and at high Q values, an almost constant, flat incoherent scattering level will be reached. In fact, the incoherent level will not be exactly flat across the spectrum, but decrease slightly with Q. This arises because the static approximation (i.e $k = k_0$) is not strictly true. Calculations to correct for the effect of inelasticity (so-called Plazcek corrections, since the problem was first considered by Plazcek[95]) are complex, and not well understood. However, it is believed[68] that for neutrons of high incident energy and heavy scattering centres the correction will be only a few percent. The scattering centres in PMMA may be considered as heavy, since they are all attached to a long polymer chain, thus recoil (inelastic) effects from the scattering event will be small. For the purposes of this analysis, the incoherent level is assumed to be constant across the entire Q range, and the static approximation to be valid, so that the coherent scattering is assumed to be purely elastic. This assumption has been made by other workers involved in analysing coherent scattering data, principally to overcome the difficulties in making inelastic corrections[68], and is shown to be a valid approximation at low Q values. The problem of contamination of the incoherent quasi-elastic spectrum by coherent scattering has also been encountered by Richardson et al[69] in the measurement of the EISF for liquid crystals. In their treatment of the data to correct the observed EISF, the coherent scattering was again assumed to be purely elastic.

Thus the ratio,

$$x = \frac{\text{El Coh}}{\text{Inc. Total}}$$

at any Q value may be found from the measured $S(\underline{Q})$.
Also,

$$\text{El.Inc.} = A_0'(\underline{Q}) \times \text{Inc.Total}$$

$$\text{Thus,} \qquad M(\underline{Q}) = \frac{x + A_0'(\underline{Q})}{1 + x}$$

This result has also been used by Richardson et al[69].

Knowing x, $M(\underline{Q})$ and $A_0'(\underline{Q})$ for all Q values, it is possible to obtain an experimental value of the EISF, $A_0'(\text{exp})$, for all Q values for comparison with the calculated $A_0'(\underline{Q})$. $A_0'(\text{exp})$ for PMMA3 is shown in figure 3.31 (denoted by (+)). Having accounted for the coherent contribution, as well as incomplete deuteration, it is now clear that the motion being observed in the ester methyl group is that of the three-fold jump component only.

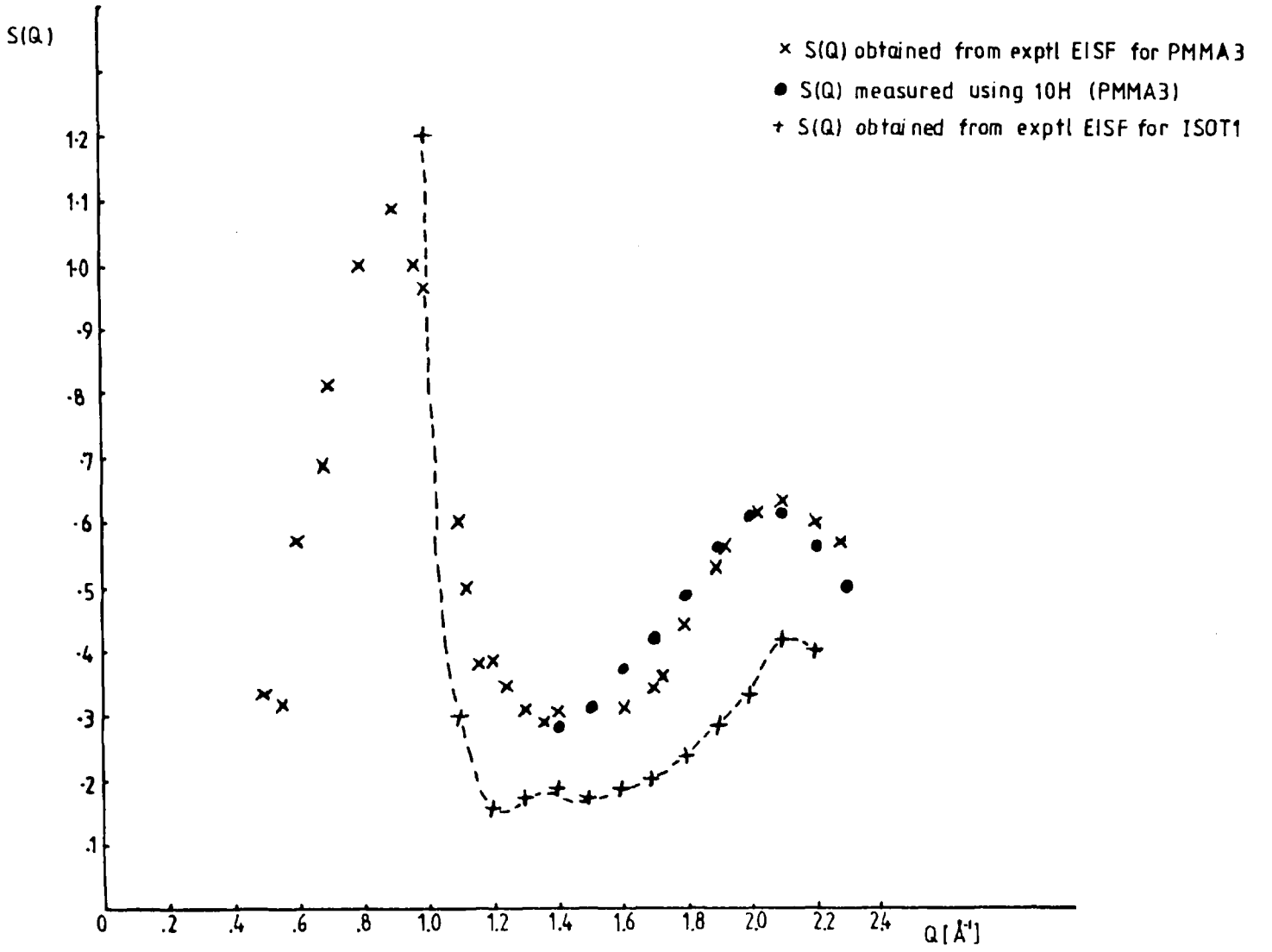
Due to experimental limitations on 10H, it was not possible to measure $S(\underline{Q})$ below $Q=1.2\ \text{Å}^{-1}$, and consequently it is not possible to correct the experimental values of the EISF below this Q value. However, having established the validity of the three-fold jump model to describe the observed scattering law, it is possible to perform the reverse operation to that described above, and extract $S(\underline{Q})$ from the deviation of the measured EISF from $A_0'(\underline{Q})$, for comparison with $S(\underline{Q})_{10H}$ and $S(\underline{Q})_{x\text{-ray}}$, since

$$S(\underline{Q}) = \frac{\text{El.Coh}}{\text{Inc. Total}} = \frac{M(\underline{Q}) - A_0'(\underline{Q})}{1 - M(\underline{Q})}$$

The comparison between $S(\underline{Q})$ measured directly on 10H for PMMA3 and that obtained using the above expression is shown in figure 3.35. Within experimental error, the two curves are identical.

It was not possible to measure $S(\underline{Q})_{10H}$ for the isotactic or syndiotactic samples of PMMA, thus it is not possible to correct the measured EISF and obtain $A_0'(\text{exp})$. However, also shown in figure 3.35 is the structure factor $S(\underline{Q})_{ISOT}$ calculated using the above expression. Although the

Fig 3.35 Structure factor, S(Q), for PMMA



relative intensities of the two curves, $S(\underline{Q})_{ISOT1}$ and $S(\underline{Q})_{PMMA3}$ are different, primarily because of difference in sample thickness, in essence, the shape of the structure factor is identical in both cases.

The contamination of the quasi-elastic spectrum by elastic coherent scattering also presents another problem. It was indicated earlier in the chapter that the extensive energy range of IN6 led to inclusion of part of the density of states function in the measured quasi-elastic spectrum, and in order to subtract this contribution, a Q-varying background, $\exp(-Q^2\langle u^2\rangle)$ was introduced. The most convenient way[36] of establishing the value of $\langle u^2\rangle$ is from the slope of a logarithmic plot of the total integrated intensity of the spectrum against Q^2. This method is clearly valid if the spectrum is composed only of incoherent scattering. However, this is obviously not the case for the PMMA samples under study, and indeed, the effect of coherent scattering could be easily observed by an enormous increase in the value of the integrated intensities at about 1 $\mathring{A}^{-1}$ and 1.6 $\mathring{A}^{-1}$, reflecting the dominant peaks in $S(\underline{Q})$. Since it was not possible to verify the value of $\langle u^2\rangle$ in the usual way, it was necessary to make an estimate in order to fit the inelastic contribution to the spectrum.

On considering the variation of the integrated intensity with Q, an interesting point arises. The integrated intensity (area) of the observed spectrum is given by $\int_{-\infty}^{\infty} S(\underline{Q},\omega)d\omega$, and since this includes both coherent and incoherent contributions, is expected to be identical to $S(\underline{Q})$, the structure factor, thus providing yet another method of obtaining $S(\underline{Q})$. However, due to insufficient data points, it is not really possible to extract $S(\underline{Q})$ in this way with the present quasi-elastic data, although as mentioned above, the dominant features in $S(\underline{Q})$ are apparent as sharp variations in the integrated intensity.

3.3.7 Experimental Values of Rotational Frequencies and Activation Energies for the Ester methyl Group

Table 3.3 lists the average value of the FWHM of the quasi-elastic component of the rotational scattering law for PMMA3 for various temperatures. These values were all found to conform to the Q independence predicted by the three-fold jump model. The rotational frequency corresponding to each width is also given.

Table 3.3 Variation of Quasi-elastic Width with Temperature for PMMA3

T (^{0}C)	FWHM (meV)	ν_{rot} x 10^{11} (Hz)
25 (IN6)	0.84 ± 0.1	2.04 ± 0.15
25 (IN5)	0.7 ± 0.07	1.7 ± 0.17
47 "	0.88 ± 0.06	2.13 ± 0.15
60 "	0.99 ± 0.08	2.4 ± 0.2
88 "	1.16 ± 0.1	2.81 ± 0.2
118 "	1.57 ± 0.16	3.8 ± 0.3

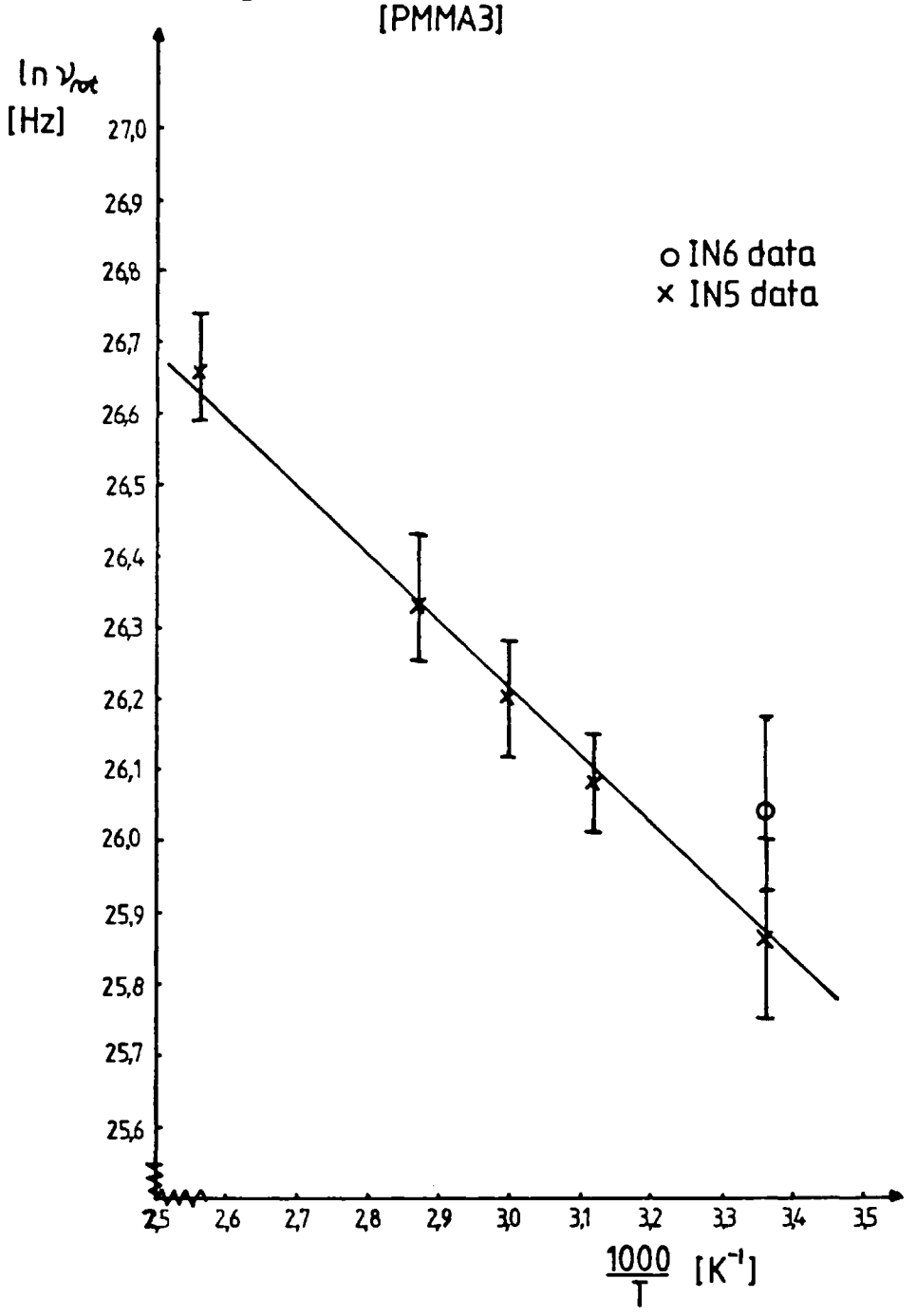
Table 3.4 lists the values obtained for ISOT1 and SYNDIO1

Table 3.4 Variation of the Quasi-elastic Width for the Pure Stereo-isomers

Sample	T (^{0}C)	FWHM (meV)	ν_{rot} x 10^{11} (Hz)
ISOT1 (IN5)	25	0.52 ± 0.1	1.26 ± 0.2
ISOT1 (IN6)	25	1.6 ± 0.44	3.88 ± 1.1
SYNDIO1 (IN6)	25	2.07 ± 0.6	5.0 ± 1.6

Figure 3.36 shows an Arrhenius plot for PMMA3. A linear regression to obtain the line of best fit through the IN5

Fig 3.36 Arrhenius plot for ester methyl group [PMMA3]



data gives a value of ν_0 of 3.78×10^{11} Hz and a value of E_a of 7.62 kJ/mol.

3.3.8 Results Obtained Using Quasi-elastic Neutron Scattering Relating to the Rotational Motion of the α-methyl Group in Poly(methyl methacrylate)

Since the rotational frequency of the α-methyl group is much lower than that of the ester methyl group, an instrument with considerably better resolution than IN5 or IN6 is required to observe the motion, and consequently, experiments were performed on IN10. A standard Si(111) unpolished monochromator was used, and unpolished analysers positioned at Q=0.29 (combination of two outer circles at $\theta=15.5^0$ and $\theta=17.8^0$), 0.586, 0.815, 1.15, 1.65 and 1.91 $\AA^{-1}$. The fast Doppler drive was used (11.57 Hz) giving an energy window of the order of ±14 μeV.

The quasi-elastic spectra for the α-methyl group rotation were recorded at temperatures of 80^0C, 100^0C and 120^0C. The experimental EISF at each temperature was obtained using the fitting programs SAND, QUASI and FURY (see section 2.3.1). Figure 3.37 shows the values of the EISF obtained using SAND, the error bars indicating the purely statistical errors calculated within the fitting program. Also shown in this figure is the variation of the values of the EISF obtained by using the three different fitting programs.

Figure 3.38 shows the results obtained for the α-methyl rotation at the three different temperatures, calculated using QUASI. At each temperature, the FWHM of the quasi-elastic component was fixed at the value given using SAND, in order to obtain a fit.

In addition, figure 3.38 shows a combination of the data recorded at 80^0C on IN10 with some measurements made some years ago on IN5 (also at 80^0C)to observe the α-methyl rotation. In themselves, the IN5 data were not found to be

SAND fits to PMMA1 - data measured at 80°C

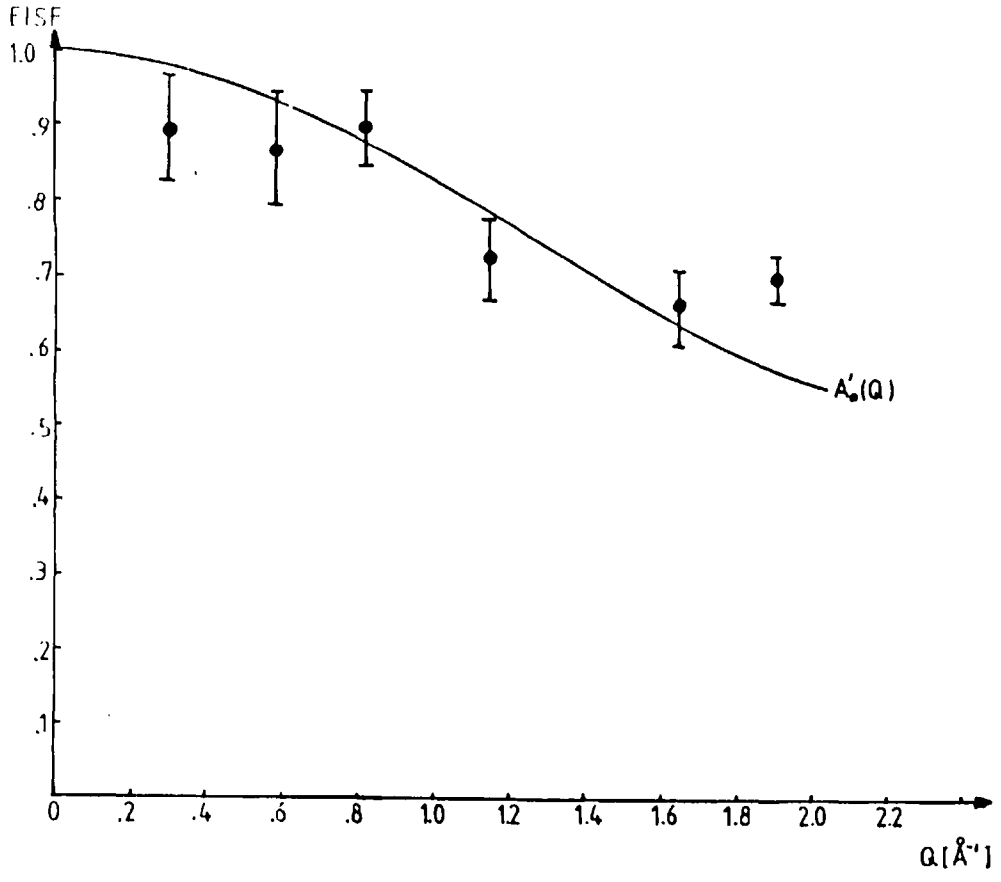
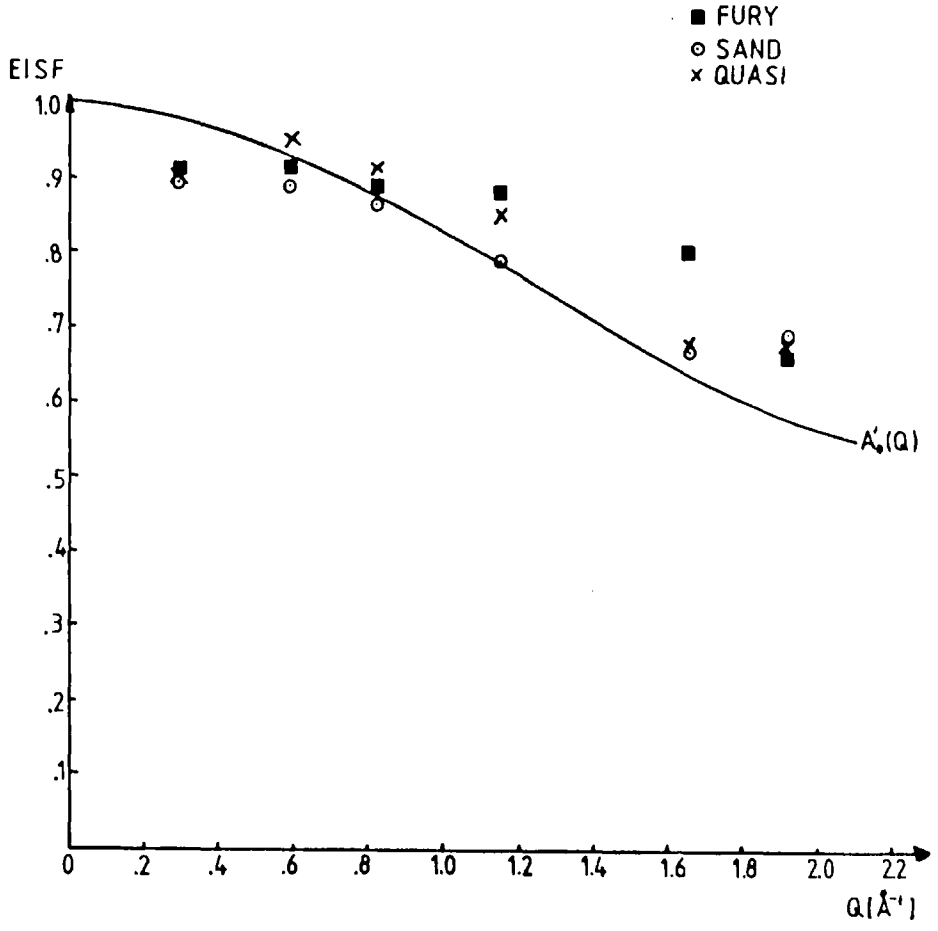
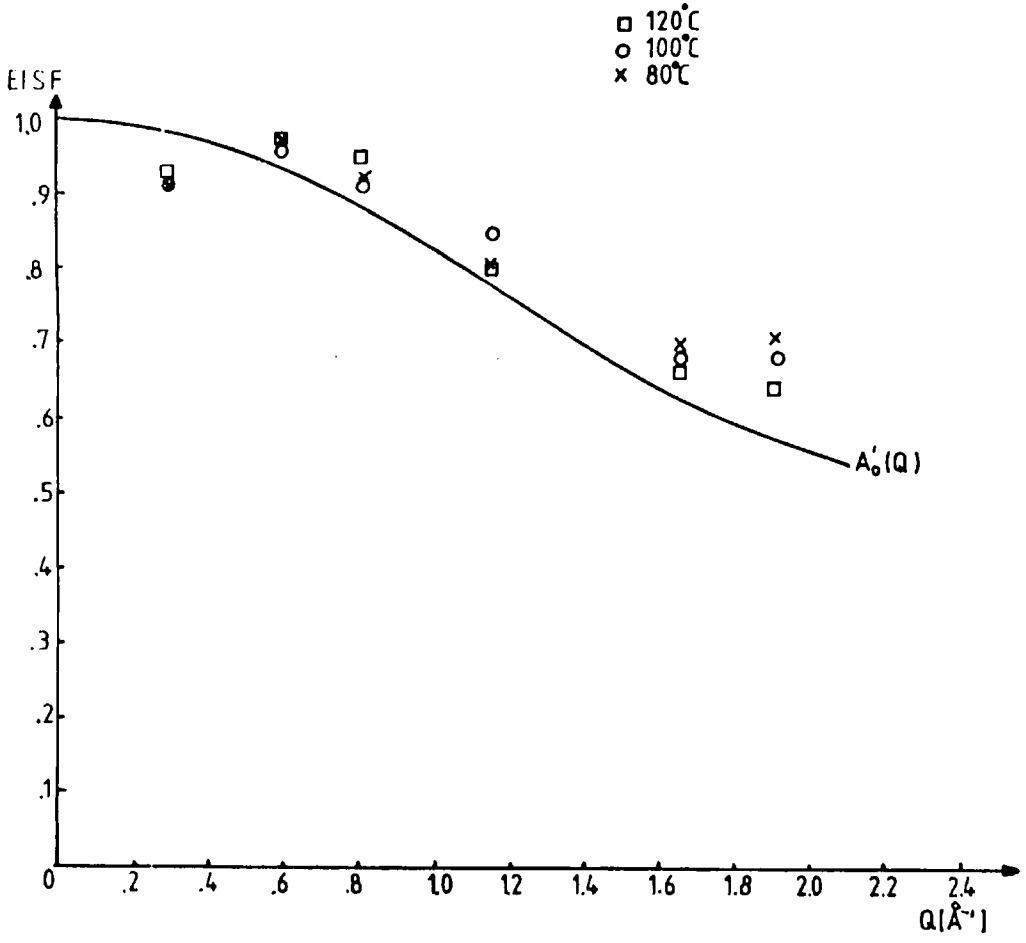


Fig 3.37

Results obtained from PMMA1 at 100°C



QUASI fits at different temperatures for PMMA1



Comparison of IN5 and IN10 data from PMMA1

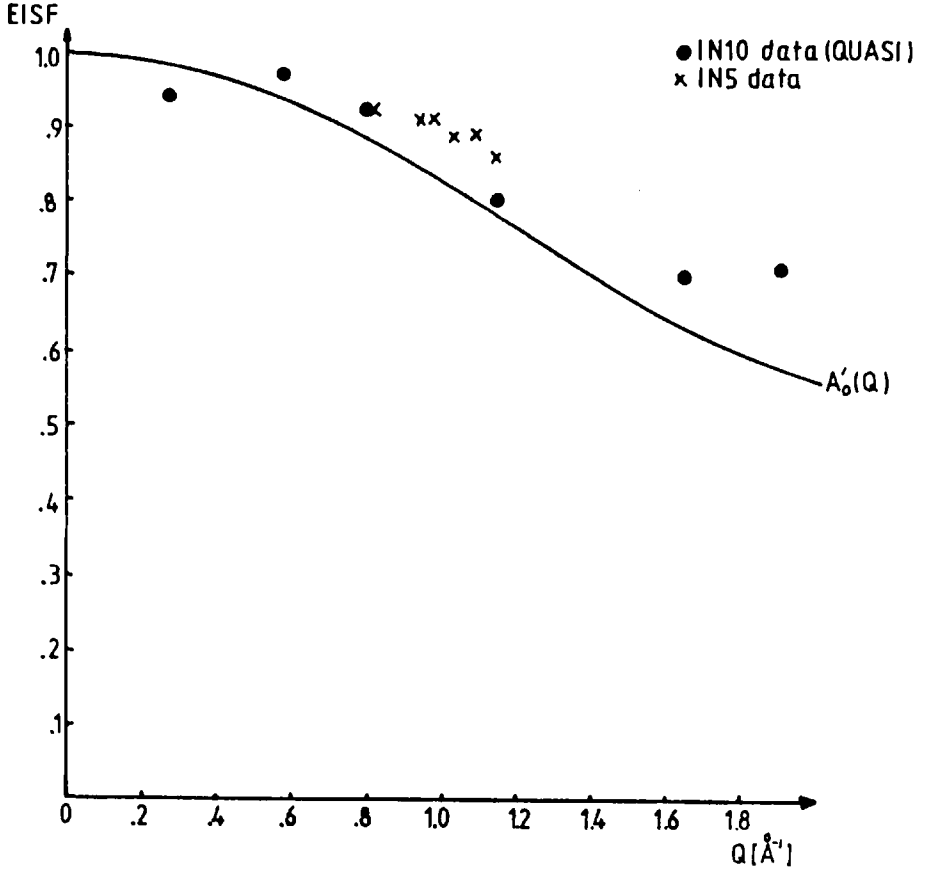


Fig 3.38

very informative, but taken in conjunction with the IN10 data, and also knowing now that there is a considerable amount of elastic coherent scattering at $Q=1.\mathring{A}^{-1}$, it can be seen that the IN5 data lie exactly as expected with respect to the calculated EISF.

The mean values of the widths of the quasi-elastic component obtained using SAND, and corresponding rotational frequencies are given below.

Table 3.5 Variation of Quasi-elastic Width with Temperature for PMMA1

Width (μeV)	Rotational Frequency (Hz)	T (K)
8.72 ± 0.4	2.11×10^9	353
11.36 ± 1.4	2.74×10^9	373
14.69 ± 0.8	3.55×10^9	393

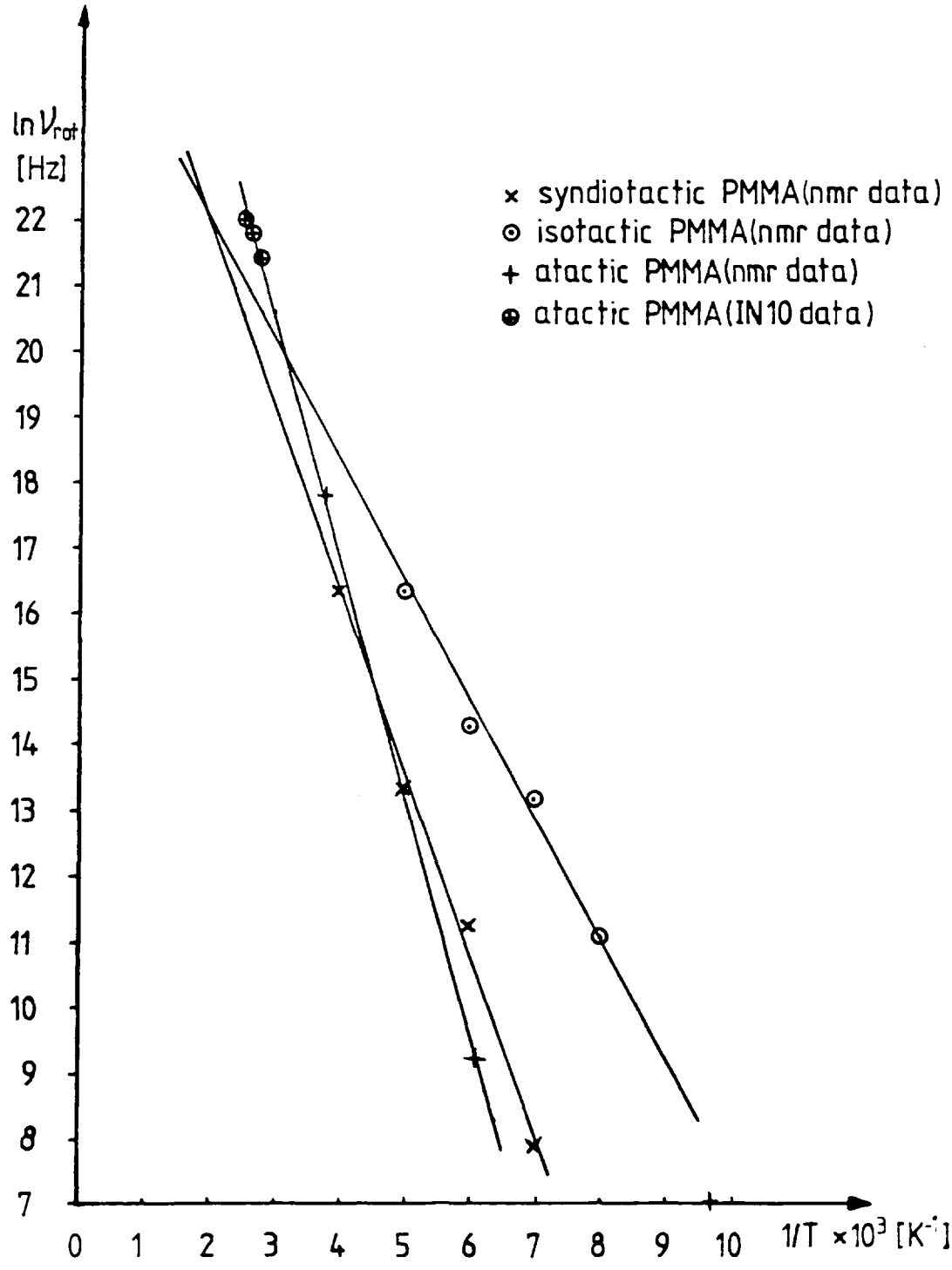
Figure 3.39 shows an Arrhenius plot of the frequency of rotation of the α-methyl group against temperature. The values of ν_{rot} obtained from the neutron scattering experiment have been combined with NMR measurements for atactic PMMA (taken from 24). The slope of the line gives an activation energy of 29.1 kJ/mol. For comparison, NMR data[25 26] on pure stereo-isomers is also shown, giving activation energies of 23.3 kJ/mol for syndiotactic PMMA and 15.8 kJ/mol for isotactic PMMA. Corresponding values of ν_0 are 2.9×10^{13} Hz, 9.7×10^{11} Hz and 1.45×10^{11} Hz for atactic, syndiotactic and isotactic PMMA respectively.

3.3.9 Consideration of Errors for Quasi-elastic Data

Statistical errors on the final parameters obtained (i.e the final value of the EISF or FWHM of the quasi-elastic

Fig 3.39

Arrhenius plots for α-methyl rotation



component, for example) using the fitting programs are largely determined by the quality of the raw data. These errors may be reduced by counting for as long as is practically possible on each sample. In general, for results obtained from PMMA, these statistical errors were found to be typically 5-10% of the value of the parameter obtained.

Apart from the inherent quality of the raw data,the other main source of error to be considered is multiple scattering. This is reduced by using as thin a sample as possible, within the constraint of obtaining good statistics in reasonable counting times, but some error from multiple scattering effects will still be introduced.

The effect of multiple scattering on the EISF has been considered in some detail by various workers[36 69 70] . To actually calculate the corrections needed to account for multiple scattering is a tedious process, involving a Monte-Carlo simulation, requiring a great deal of computer time. However, Hervet et al[70] estimate the effect on the value of the EISF due to multiple scattering to be only a few percent, whilst Richardson et al [69] suggest an error on the EISF of the order of 10%. In addition, Gardner et al[36] have observed that accounting for multiple scattering always tends to increase the observed value of the EISF, and suggest an upper limit of 15%.

If multiple scattering and statistical errors are taken into account, it is expected that an average error of ±15% may be reasonably attributed to the values of the EISF obtained. All errors indicated on the experimental values of the EISF are calculated on this basis, unless specified otherwise .

3.3.10 Interpretation of the Structure Factor, S(Q)

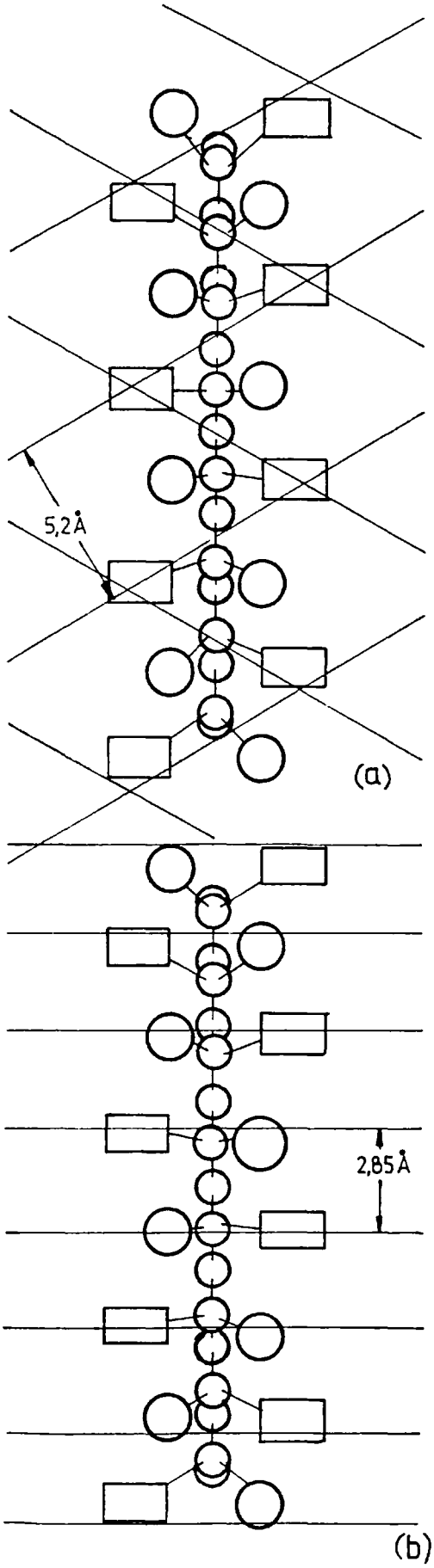
Figure 3.35 shows the structure factor obtained for PMMA3 and ISOT1 at room temperature, calculated by the subtraction of the calculated EISF, $A_0'(\underline{Q})$ from the measured

EISF, M(Q), as outlined in section 3.3.6. Also shown in this figure is S(Q) for PMMA3, measured directly using 10H. As pointed out in section 3.3.6, the structure factor obtained from M(Q) is identical to that measured directly using a powder diffractometer, and both are identical to S(Q) obtained from wide angle X-ray scattering measurements made on commercial PMMA[63] .

The main features of the scattering pattern may be accounted for in a model proposed by Lovell and Windle[63] . This model is shown schematically in figure 3.40. Each of the three diffraction maxima may be related to important periodicities in the molecule. Figure 3.40(a) represents a segment of syndiotactic molecule in the proposed conformation, looking at the outside edge of the curved chain. The first intramolecular peak at $Q=1.2$ $\mathring{A}^{-1}$ corresponds to a periodicity of 5.2 $\mathring{A}$. Figure 3.40(a) indicates the probable origins of this peak. Figure 3.40(b) shows that the periodicity of the second intramolecular peak (2.85 $\mathring{A}$) corresponds to the repeat distance between ester groups as projected onto the segment axis (i.e tangent to the midpoint of the molecular segment). Lovell and Windle[63] point out that this repeat is longer than the 2.5 $\mathring{A}$ axial repeat distance typical of a molecule in the all-trans conformation, and suggest that this is a direct result of curvature of the chain. Figure 3.40(c), which is a schematic representation of the proposed conformation viewed normal to the plane of curvature demonstrates this effect. It also shows that the repeat distance of 2.15 $\mathring{A}$ corresponding to the third halo at $Q=2.95$ $\mathring{A}^{-1}$ can be accounted for by the carbon-second carbon distance along the backbone, again projected onto the segment axis. It is clear that the fore-shortening which occurs in the projection of a curved molecule onto the axis is primarily responsible for the average carbon-second carbon distance being less than 2.5 $\mathring{A}$.

Figure 3.35 shows that the structure factor is identical for isotactic and predominantly syndiotactic forms of PMMA. This has also been observed by Lovell and Windle[63] , who

Proposed Model of PMMA



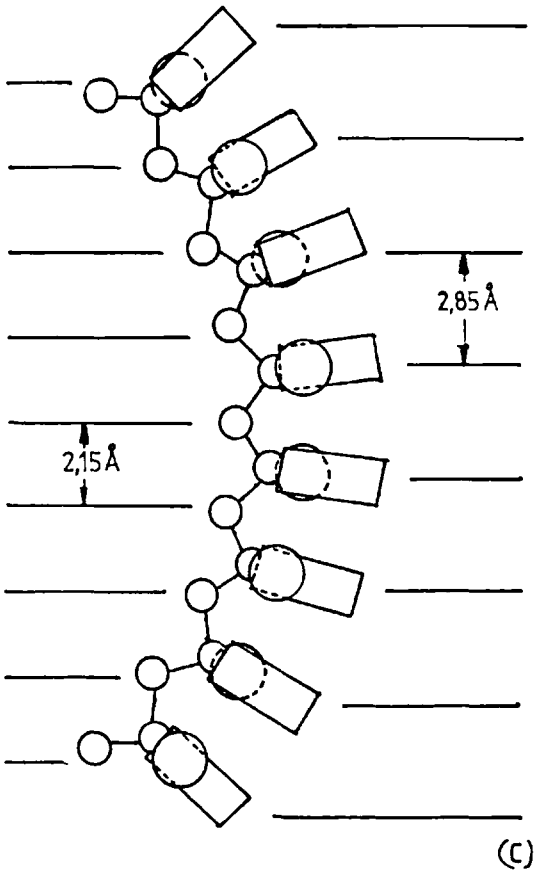


Fig 3.40

interpret it as an indication that the conformation of PMMA remains close to all-trans, irrespective of tacticity.

3.3.11 Discussion and Comparison of V_3 and E_a

Under some circumstances, it is possible to compare directly the values of V_3 obtained from inelastic measurements with the values of E_a obtained from an Arrhenius plot. For the two methyl sidegroups in PMMA, however, this is not possible, because of the effect of quantum mechanical tunnelling. Strong evidence indicating the probability of tunnelling at low temperatures has been presented by various workers[27 29 30 31], using proton NMR methods such as spin-lattice relaxation, line width and second moment studies. As the temperature is lowered, minima in the spin-lattice relaxation time and increases in line width occur, corresponding to a freezing in of the methyl motion. In each type of experiment, a frequency ν may be associated with the motion[71] and correlated with the temperature. Hence frequency-temperature relationships can be established for particular methyl group motions.

The temperature dependence of group motions such as barrier hopping is often expressed by an Arrhenius equation, as quoted in section 3.1.7. This predicts a linear relationship between $\ln\nu$ and $1/T$, with a slope proportional to the activation energy E_a.

Low temperature NMR studies on methyl-containing materials have not, however, shown this predicted Arrhenius behaviour[72 73], and the frequency-temperature plot is observed to be curvilinear. Such deviations from an Arrhenius behaviour are attributed to low temperature quantum mechanical tunnelling. Rotational quantum mechanical tunnelling has been treated from a theoretical point of view by various workers[29 72 74 75 76 77 78]. The theory most relevant to this work, presented by Stejskal and Gutowsky, has been used to calculate the average tunnelling frequency as a function of

temperature for barrier heights V_3 over the range 2.36 to 7.92 kcal/mol. (these results are presented in section 3.1.9). The theoretical curves predict that, at high temperatures, i.e in the absence of tunnelling, the frequency obeys an Arrhenius temperature dependence, whilst at lower temperatures, in the presence of QM tunnelling, it flattens out, ultimately becoming independent of temperature. A wide range of NMR experimental results are in agreement with this hypothesis[72 79 80]. In particular, the line width results of Odajima[79] and Kosfeld[80] are of particular relevance, since they demonstrate the levelling off of the correlation frequency of methyl motion in PMMA.

Further evidence for quantum mechanical tunnelling of methyl groups has emerged from other types of experiment, including ESR studies[82 83 84 85] and nuclear double resonance[86].

Having established the presence of QM tunnelling, it is clear that the direct comparison between E_a and V_3 suggested in section 3.1.8 is not possible. Instead, Gutowsky's theory must be followed to extract a value of V_3(tunnelling) from the E_a value, and a comparison between V_3(tunnelling) and V_3(inelastic neutron scattering) may then be made.

Table 3.6 compares the barrier heights obtained using inelastic neutron scattering with E_a and V_3(tunnelling) from other sources for the α-methyl group in PMMA. The sample used for obtaining the value of V_3 quoted is given in brackets, and, for data presented from results in this thesis, the instrument used for making the neutron scattering measurements.

Table 3.7 compares values of V_3 obtained from different sources for the ester methyl group in poly(methyl methacrylate).

Table 3.6 Comparison of V_3 and E_a from Various Sources for the α-methyl Group

V_3 (kJ/mol) (this work)	E_a (kJ/mol) (this work)	V_3 (tunnel) from E_a	E_a (NMR)	V_3 (tunnel) from NMR[25 26]	V_3 (other IENS)[21 22]
33 (PMMA1, 4H5)	29.1 (PMMA1, IN10 with NMR)	31.1			
33 (SYNDIO1, IN6)			23.3 (synd)	30 (synd)	33 (pred. synd)
23 (ISOT1, IN6)			15.5 (isot)	22.6 (isot)	23 (isot)

Table 3.7 Comparison of V_3 and E_a from Various Sources for the Ester methyl Group

V_3 (kJ/mol) (this work)	E_a (kJ/mol) (this work)	V_3 (tunnel) from E_a	V_3 (tunnel) (from NMR)[22]	V_3 (other IENS)[22]
3.2 - 10.5 (PMMA3 4H5, IN6)	7.6 (PMMA3, IN5)	8.82	10.1*	5.04

* from one datum only.

These results show that the values of V_3 for the α-methyl group for syndiotactic and isotactic PMMA (33 and 23 kJ/mol, respectively) obtained from inelastic neutron scattering data presented in this thesis are in excellent agreement with those obtained by other workers also using inelastic neutron scattering [21] [22] (it should perhaps be pointed out that these earlier measurements were not made on PMMA samples which had been partially deuterated, since at this time this was not possible, but instead on samples of poly(α-chloro methacrylate) in which the hydrogen in the ester methyl group had been replaced by chlorine. Since the exact effect of this substitution on the inelastic neutron scattering spectrum could not really be predicted, these earlier results were not fully conclusive. As the results presented in this thesis (performed on somewhat better samples) are in such good agreement with this earlier work, it would suggest that the chlorine substitution had little effect in influencing interactions relating to the values of the barrier height etc.) and with values of V_3(tunnelling) obtained from E_a measured using NMR techniques.

The value of E_a obtained for PMMA1 (29.1 kJ/mol) using quasi-elastic neutron scattering techniques combined with data measured using NMR gives a value of V_3(tunnelling) of 31.1 kJ/mol. This compares well with the value of V_3 of 33 kJ/mol observed using inelastic neutron scattering. However, although the values of E_a from NMR measurements would suggest a difference between atactic and syndiotactic PMMA, because the value of V_3 for the two cases are almost identical, it is not possible to resolve the two peaks in the inelastic spectrum falling so close together.

Due to the influence of crystalline lattice modes at low frequencies, the inelastic data relating to the torsional motion of the ester methyl group in PMMA were not fully conclusive, giving a value of V_3 in the range 3.2 - 10.5 kJ/mol. However, this is in good agreement with the value of V_3(tunnelling) of 8.82 kJ/mol obtained from measurements of E_a using quasi-elastic neutron scattering, and that of 10.1 kJ/mol obtained from NMR data. Unfortunately, it

was only possible to obtain the value of E_a for PMMA3. However, if some consideration is given to the value of the pre-exponential prefix, ν_0, in the Arrhenius relationship it is possible to comment on predicted values of E_a for the ester methyl group rotation in stereoregular forms of PMMA.

An approximate value of ν_0 may be obtained in the following way. Equation (3.11) suggests that ν_0 is given by the following expression

$$\tau_0^{-1} = \nu_0 = \frac{kT}{h} Z^{-1}$$

where Z is the vibrational partition function of the system. In the classical limit, it can be shown[96] that Z for a one-dimensional simple harmonic oscillator is given by $h\nu_{vib}/kT$ where ν_{vib} is the fundamental frequency of the oscillator, which has been measured directly using inelastic incoherent neutron scattering for PMMA, thus $\nu_0 = \nu_{vib}$. If the validity of the application of classical thermodynamics to the system is defined by the condition $h\nu \sim kT$, then its usage in this case for PMMA is expected to be acceptable, since $h\nu \sim 300\ cm^{-1}$ and for T = 300K, $kT = 207\ cm^{-1}$, thus $h\nu \sim kT$. For the NMR measurements made at rather lower temperatures, kT is rather less, leading to perhaps a factor of two or three in the comparison of ν_{vib} with ν_0. Further evidence for a direct relationship between ν_{vib}, the fundamental frequency of the harmonic oscillator, and ν_0, the pre-exponential factor is given by Brot[97], who suggests that for a plane rotator (i.e one in which the rotational motion is about only a single axis, such as the methyl groups in PMMA) the frequency factor ν_0 should be approximately equal to the vibrational frequency.

Thus the values of ν_{vib} obtained using inelastic scattering, of 1.1×10^{13} Hz and 9×10^{12} Hz for the α-methyl group in syndiotactic and isotactic forms of PMMA respectively, may be compared to the values of ν_0 obtained from the extrapolation of the Arrhenius plot, which are 2.9×10^{13} Hz

9.7×10^{11} Hz and 1.45×10^{11} Hz respectively, for atactic, syndiotactic and isotactic PMMA.

Although the values are not in total agreement, presumably because of the effect of anharmonicity and the long extrapolation range of the Arrhenius plot, they are certainly within an order of magnitude.

The value of ν_0 obtained for the ester methyl group in PMMA using this method of comparion with ν_{vib} is predicted to be between 3.0 and 6.0×10^{12} Hz, and the actual value obtained from the Arrhenius plot to be 3.8×10^{11} Hz.

Theoretical prediction would suggest that the value of ν_0 is much less sensitive to tacticity than found experimentally, but both methods of extracting ν_0 demonstrate that it varies with tacticity in exactly the same way as E_a, i.e

$$E_a(\text{atact}) > E_a(\text{synd}) > E_a(\text{isot})$$

and

$$\nu_0(\text{atact}) > \nu_0(\text{synd}) > \nu_0(\text{isot})$$

for the α-methyl group. (This is, in fact, an obvious result, since ν_0 depends only on the fundamental frequency of the potential well, which is defined by E_a).

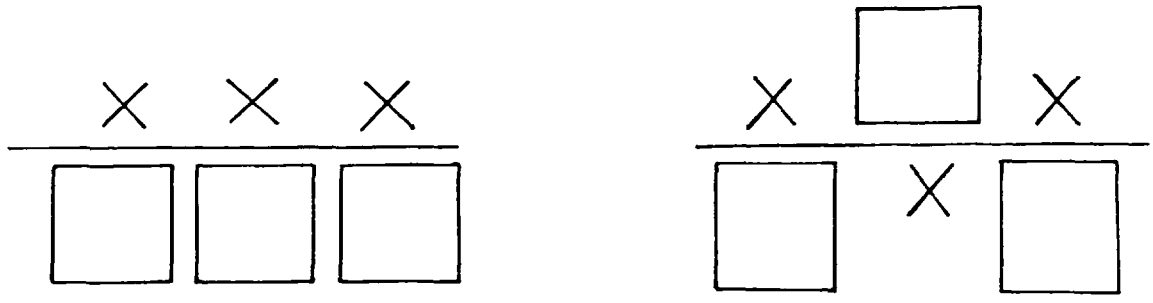
If ν_0 for the ester methyl group is assumed to behave in the same way, so that it is of the same order of magnitude for pure stereoregular forms as it is for PMMA3, and that any increase in E_a leads to a corresponding increase in ν_0, it is possible to comment on the expected values of the activation energies for the ester methyl group in stereoregular PMMA, knowing the frequency of rotation at only one temperature.

The results presented in Table 3.4 suggest that the ester methyl group is rotating faster in syndiotactic PMMA than in isotactic PMMA (at room temperature), thus suggesting that the barrier to rotation is lower for the syndiotactic

isomer than the isotactic form. Unfortunately, there is a rather large discrepancy between the actual values of ν_{rot} obtained for isotactic PMMA from IN5 and IN6. In some respects, this large discrepancy is surprising, because the values of ν_{rot} obtained for PMMA3 from data recorded from the two instruments were in reasonable agreement, and furthermore, the EISF obtained for isotactic PMMA using IN5 was found to be identical to that obtained using IN6. However, it has been pointed out that data analysis for the purely hydrogenous samples is rather more difficult than for the partially deuterated ones, simply because the elastic contribution comprises such a large percentage of the total area of the spectrum. This means that although a change in width of the quasi-elastic component will obviously lead to a change in the quasi-elastic integrated intensity, because the EISF is so heavily dominated by the elastic contribution, it will appear to be reasonably similar for quite a wide range of quasi-elastic widths, and moreover, still a good fit to the data. This is not true for the partially deuterated samples, where the relative elastic intensity is much lower, due to the absence of extra incoherent elastic scattering from hydrogen. An alternative suggestion to account for the differences in values of ν_{rot} obtained for ISOT1 from IN5 and IN6 is some kind of instrumental effect. Comparison of the values of ν_{rot} obtained from IN5 and IN6 (see tables 3.3 and 3.4) show that for both PMMA3 and ISOT1, ν_{rot} is greater for IN6 than for IN5, although the difference is much more considerable for the isotactic sample. It is difficult to propose an instrumental effect that could account for the observed differences in ν_{rot}, but as mentioned earlier, because IN6 is such a new instrument, its characteristics are not well understood, so the possibility of a systematic instrumental effect should be considered.

Due to the uncertainty in the data, this discussion of barrier heights for the ester methyl group rotation is clearly of a rather speculative nature, but it is not unreasonable to suggest $E_a(\text{isot}) > E_a(\text{syndio})$. For the α-methyl group it has also been found conclusively that $E_a(\text{syndio}) > E_a(\text{isot})$.

These differences in activation energy for different stereoregular forms of the polymer may be explained in simple terms with the aid of a schematic diagram.



(a) (b)

Figure (a) represents purely isotactic PMMA, and (b) purely syndiotactic PMMA, assumed to be in the close to all-trans conformation suggested by Windle [63] . The cross denotes the position of the α-methyl group, and the square, the much bulkier ester group. For the α-methyl group, there is clearly much more freedom for rotation in the isotactic form of the polymer, thus E_a(isot) < E_a(syndio). However, for the ester methyl group, the converse would appear to be true, so E_a(syndio) < E_a(isot). This dependence of barrier height upon the stereoregularity of the polymer has also been discussed by Allen et al[22] , who consider in some detail the different values of V_3 obtained for the α-methyl group in syndiotactic and isotactic PMMA. It is suggested that the observed different values of V_3 may be accounted for in terms of non-bonded repulsions which influence the barriers to internal rotation of the methyl groups, and a calculation of V_3 made including a term to account for these repulsions revealed that the value of V_3 for isotactic PMMA would be predicted to be less than that for syndiotactic PMMA, in good agreement with experiment.

Unfortunately a problem arises in explaining the values of E_a for the atactic form of PMMA, using the simple model presented above. Experimental results for the α-methyl group show that E_a(atactic) is slightly higher than E_a(syndio).

The problem is intensified for the case of the ester methyl group, where experimental results suggest that E_a(atactic) is greater than E_a(syndio), but may be more or less than E_a(isot), depending on whether the IN5 or IN6 data for ISOT1 are more reliable. In any event, the simple model proposed above allows no suggestions to be made about the expected behaviour of E_a(atactic).

The actual values of V_3 obtained for the ester methyl group might, at first sight, seem rather low, considering how closely packed these groups must be in the bulk. However, this problem has been considered by Heatley[92], who suggests the following explanation. The motion of a single methyl group is dominated by firstly, a three-fold potential well in which it moves, and secondly, by the potential due to the proximity of other methyl groups, all of which are also moving in their own individual potential wells. Consideration of the situation shows that it would not be unreasonable for many of these interactions to be out-of-phase, thus effectively cancelling each other out, and leading to a barrier height which could conceivably be quite low, as observed in this case for the ester methyl group in PMMA. For different stereoregular forms of the polymer, this interaction potential could be quite different, thus further complicating the relationship between E_a and tacticity.

NMR studies of PMMA in dilute solution[93] have further revealed that for the α-methyl group, a range of correlation frequencies is observed at a single temperature. Since these measurements were made in solution, this distribution of frequencies is reasonably interpreted in terms of intramolecular effects, although the exact origins are uncertain. These results would suggest that the quasi-elastic component of the rotational scattering law observed using neutron scattering techniques is either not a single Lorentzian, but a sum of Lorentzians over all possible rotational frequencies, or alternatively, a single Lorentzian giving the average rotational frequency $\bar{\nu}_{rot}$ for a given temperature. Since no evidence of deviation from a single Lorentzian was found, either in $S^{rot}_{inc}(\underline{Q},\omega)$, or in the Fourier transform

$S(\underline{Q},t)$ (which should show clearly any deviations from a single Lorentzian), this second explanation seems more reasonable.

3.4 Final Discussion of Results and the Application of Neutron Scattering to the Investigation of Sidegroup Motion in Poly(methyl methacrylate)

The results presented in this chapter have shown that inelastic neutron scattering can provide valuable information about torsional frequencies and barrier heights to rotation in PMMA. Values obtained for the barrier height for the α-methyl group were found to be in good agreement with those obtained by other workers, using inelastic neutron scattering and NMR techniques[21 21].

The use of inelastic neutron scattering as a method of obtaining the frequency distribution function offers some advantages over more conventional techniques for certain bands. The major advantage lies in the method of partial deuteration to effectively remove some of the contributions to the inelastic spectrum, and thus make peak assignment easier. Indeed, since the vibrational peaks associated with purely hydrogenous polymers tend to be rather broad, a featureless and ill-defined inelastic spectrum may result without partial deuteration. However, even after eliminating some of the possible vibrations, the hydrogen-amplitude-weighted frequency distribution function will still reflect all kinds of motion involving the hydrogen remaining in the sample, including bending, wagging etc., and so, as for infra-red analysis, for accurate peak assignment it is necessary to use some kind of normal co-ordinate analysis based on a model to predict peak position, for comparison with observed bands.

For the particular case of poly(methyl methacrylate) (and, indeed, most other polymers), a difficulty arises in assigning peaks below 200 cm^{-1}, because of the problem of crystalline lattice modes. This leads to uncertainty in

accurate determination of torsional peaks associated with the ester methyl group. However, within the experimental uncertainty, the value of V_3 obtained for predominantly syndiotactic PMMA was in good agreement with that proposed by other workers using neutron and NMR techniques [21]. Inelastic measurements made on pure stereo-isomers using IN6 showed clearly the dependence of the α-methyl torsion on tacticity, but the weaker vibrations of the ester methyl group were totally lost. This problem could be overcome, in principle, by the use of partially deuterated pure stereo-isomers, but the appearance of crystalline backbone modes mentioned above would probably still make definitive peak assignment in this low frequency region difficult, and the dependence of the ester methyl group motion on tacticity is more easily studied using quasi-elastic measurements over a range of temperatures to obtain an activation energy, as in the case of PMMA3. The measurement of E_a for the ester methyl group for PMMA3 is seen as an important step, since to date, NMR measurements and neutron scattering data relating to the motion of this sidegroup have been rather inconclusive. The value of E_a obtained is believed to be reliable, and since it is difficult to obtain values of V_3 from inelastic measurements for this group, it is believed that further quasi-elastic measurements to obtain E_a for the ester methyl group in syndiotactic and isotactic PMMA would be extremely informative.

As mentioned, the values of E_a obtained for the α-methyl group are in good agreement with the inelastic scattering measurements of V_3, and furthermore, reveal a difference in barrier height between syndiotactic and atactic PMMA. This difference is only of the order of 1 kJ/mol, and as such, is not expected to be detectable in the inelastic spectrum, since the resolution is not sufficient to resolve two peaks lying so close together.

The good agreement of values of V_3 obtained directly using inelastic scattering measurements and V_3(tunnelling) calculated from E_a confirm conclusively the presence of quantum mechanical tunnelling at low temperatures in these

samples.

It was shown that neutron diffraction measurements of the structure factor, $S(\underline{Q})$, are identical to those obtained from wide angle X-ray scattering. Furthermore, it is seen that the deviation of $M(\underline{Q})$, the measured elastic incoherent structure factor, from $A_0'(\underline{Q})$, that predicted theoretically, also provides a novel method of measuring $S(\underline{Q})$, provided that the geometry of the motion is well established. The main features of the coherent scattering pattern are found to be well described by the model for PMMA suggested by Lovell and Windle[63] .

The timescale of the neutron scattering experiment is important. After due consideration of coherent scattering and incomplete deuteration, the rotational motion of both methyl groups in PMMA was observed to be well described in terms of a simple jump motion between three equivalent sites on a circle of radius 1.032 Å. This is as expected for the simpler case of the α-methyl group, but a question arises regarding the two-fold flip expected to be observed for the ester methyl group. This component of the motion is simply not observed, since its rotational frequency (estimated to be about 1 Hz at room temperature[23]) is considerably outside the time limits of the neutron scattering experiment. This underlines the necessity of choosing an instrument with appropiate resolution for observing the particular motion of interest - determined by the FWHM elastic resolution being of the same order as the rotational frequency. Thus the 200 μeV resolution of IN5 was appropiate for observing the fast three-fold jump component of the ester methyl group, but clearly not suitable for observing the very slow 1 Hz two-fold flip (indeed, no neutron spectrometer would be able to measure this). A further factor of interest regarding the resolution function is its shape. The almost triangular resolution function of IN5 allows separation of the elastic and quasi-elastic components of the scattering law much more easily than the Lorentzian resolution function on IN10. It should be further pointed out that in order to obtain

definitive values of the EISF and rotational frequencies, it is necessary to obtain extremely good counting statistics, particularly in the wings of the spectrum.

Comparison of IN5 and IN6 data have shown the values of the EISF obtained from the two instruments to be in good agreement, and for the partially deuterated sample, identical values of the rotational frequency were obtained. The difference in the values of ν_{rot} obtained for the isotactic sample are believed to be associated with a difficulty in analysing the data totally satisfactorily for a purely hydrogenous sample, where the elastic component contributes such a large percentage of the total area.

Values of the EISF for the α-methyl group obtained using IN10 were found to be in good agreement with those obtained some years ago using IN5 - since, in section 3.3.8, it was suggested that the resolution of IN5 would be insufficient to measure the quasi-elastic scattering law for the α-methyl group, it might seem incongruous to have actually obtained values of the EISF for this group using IN5 data. It is true that since the best resolution of IN5 (24 μeV at an incident wavelength of 10 Å) is really insufficient to make reliable measurements of a FWHM quasi-elastic component of 8 μeV, IN5 is not really the best instrument to use to make these measurements. However, at the time these experiments were performed, the width of the quasi-elastic component was not known, and was expected to be somewhat greater than 10 μeV. In fact, analysis of the data to extract the EISF was extremely difficult.

Inelastic neutron scattering measurements giving torsional frequencies and barrier heights were found to be identical for IN6 and 4H5.

It is concluded that since both quasi-elastic and inelastic measurements were found to be almost totally reproducible on different instruments, and also in good agreement with results presented by other workers, the values of the parameters obtained are considered definitive.

Chapter 4 Application of Quasi-elastic Neutron Scattering to the Observation of the Dynamics of Polymer Chains

This chapter will show how the use of quasi-elastic neutron scattering can give detailed information about the motion of polymer networks.

The first topic discussed is the effectiveness of hydrogen bonding in forming 'virtual' crosslink points, and thus a totally hydrogen-bonded network. Results from natural rubber samples in the bulk containing differing proportions of modifying sidegroups known to hydrogen bond are first presented. It is found that the samples containing the modifying groups move considerably more slowly than the unmodified natural rubber, thus confirming the formation of a hydrogen-bonded network. In order to show conclusively that the observed effect is genuinely due to interchain bonding, measurements in dilute solution are presented, since under these conditions the polymer chains are so widely separated that any intermolecular interactions are removed. Both modified and unmodified samples are observed to be moving at the same rate in solution, confirming that the slowing down effect in the bulk is truely intermolecular in origin, and thus showing conclusively the existence of intermolecular virtual hydrogen-bond crosslink points.

The second subject discussed deals with networks containing permanent chemical crosslink points. The experiments on these networks show that the crosslink points in the network are moving at about half the rate of the chains between crosslink points. Furthermore, the chains themselves are moving exactly at the same rate as free chains in the melt. In addition, evidence is presented for the presence of virtual hydrogen bond crosslink points in these networks, as well as the permanent chemical crosslinks, and the rôle of these temporary crosslinks in the system is discussed in some detail.

4.1 Theoretical Considerations

Theories to describe the main chain dynamics of polymers have generally been developed in terms of bead-and-spring models[7,15], in which the polymer chain is imagined to be composed of a series of beads, connected by Hookean springs. Before proposing a form of the incoherent scattering law to describe either the motion of polymer chains in dilute solution, or that of chains in the melt, it is informative to consider the relative distances typically explored in a neutron scattering experiment, characterised by $1/Q$. In most experiments, the range $Q\sigma \sim 1$ is explored, where σ is the length of one bead-spring segment.

For a bulk polymer, distances corresponding to $1/Q \gg \sigma$ can well be described in terms of the Rouse model[7], in which the velocity of each segment depends only on the forces applied to it, and all hydrodynamic coupling effects between distant segments are ignored. In this region, internal segmental motion of the chains about the backbone (i.e motions of sections of the polymer chain relative to each other) is being observed. De Gennes[8] has developed the Rouse model for specific application to neutron scattering, and has shown that, in the limit $1/Q \gg \sigma$, an incoherent quasi-elastic scattering law whose FWHM, ΔE, varies as Q^4 is predicted[10]. This is given by the following expression.

$$S_{inc}(\underline{Q},\omega) = \frac{1}{2\pi} \int I(\underline{Q},t) \exp(-i\omega t)dt$$

where $$I_{inc}(\underline{Q},t) = \exp\{-Q^2\frac{\sigma^2}{3}\left(\frac{W}{\pi}|t|\right)^{\frac{1}{2}}\}$$

and $$\Delta E \sim 10^{-2} W \sigma^4 Q^4$$

Again, σ is a step length, and W^{-1} a correlation time, of the order of 10^{-14} s[8].

The Q^4 dependence of the FWHM arises because, although,

in a time t, a signal travels d ($\sim\sqrt{t}$) along the chain, the corresponding distance in space is only of the order of $d^{\frac{1}{2}}$ for a randomly coiled polymer chain.

For distances $1/Q < \sigma$, local Brownian motion of the beads is observed, leading to Q^2 dependence of the FWHM of the quasi-elastic scattering law[11 12]. Typical values of σ range from 3 Å for poly(dimethyl siloxane) to 24 Å for poly(tetrahydrofuran) and 37 Å for polystyrene[13].

Since the neutron scattering experiment measures distances corresponding to $1/Q \sim \sigma$, a scattering law intermediate between Q^2 and Q^4 could be expected, and this has been observed[11 87].

Although the work on bulk polymers described in this chapter concerns networks, and not free chains, it is expected that the Rouse model should still be applicable, since although the Rouse backbone modes might be modified, this will only be observed experimentally if the distance between crosslinks is comparable with the distance scale of the experiments.

A similar situation arises when polymers in dilute solution are considered. Again, for the region $1/Q < \sigma$, local Brownian motion of the individual beads will be observed, leading to a Q^2 dependence of the FWHM of the scattering law. However, mobile solvent molecules in the dilute solution introduce hydrodynamic effects, which modify the Q^4 dependence of the scattering law to a Q^3 dependence in the region $1/Q > \sigma$ [12 13 16].

The incoherent scattering law is now given by[16]

$$S_{inc}(\underline{Q},\omega) = \frac{1}{\pi\tilde{w}\varepsilon^{3/2}} \int_{-\infty}^{\infty} d\theta \, \exp(-\sigma\theta^{2/3}) \cos(\tilde{\omega}\theta)$$

where $\varepsilon = Q^2\sigma^2/6$, $\theta = \varepsilon^{3/2}\tilde{w}|t|$ and $\tilde{\omega} = \omega/\tilde{w}\varepsilon^{3/2}$

$$\tilde{w} = \sqrt{\frac{3}{\pi}} \frac{kT}{\eta_0\sigma^3} \qquad (\eta_0 \text{ is the solvent viscosity})$$

$\tilde{\omega}$ can be considered as the microscopic jump frequency of a single monomer moving in the solvent, and is expected to be of the order of 10^{10} - 10^{13} Hz.

Thus the FWHM of the incoherent scattering law for a polymer in dilute solution will be given by[13]

$$\Delta E_{inc} = \frac{(2.2)\sqrt{3}}{6^{3/2}\pi} \frac{kT}{\eta_0} Q^3 \qquad (4.1)$$

In conclusion, it is clear that since the neutron scattering measurements are made in an intermediate distance scale, it is difficult to predict the exact form of the incoherent quasi-elastic scattering law. However, past measurements on bulk polymers have shown[10 11 87] that the data is best described in terms of the Rouse model, although the power dependence of the FWHM on Q is generally found to be rather less than 4. Similarly, the results obtained from dilute solution are expected to be best described by the Zimm model[12 13 14], with some deviation from Q^3 behaviour at higher Q, dependent on the value of σ for the molecule.

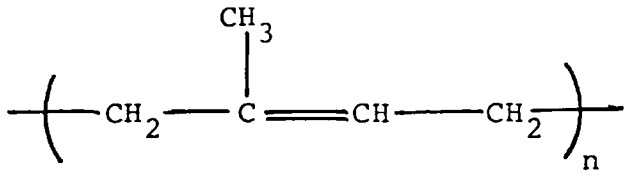
4.2 Sample Preparation

4.2.1 Preparation of Modified Natural Rubber Samples

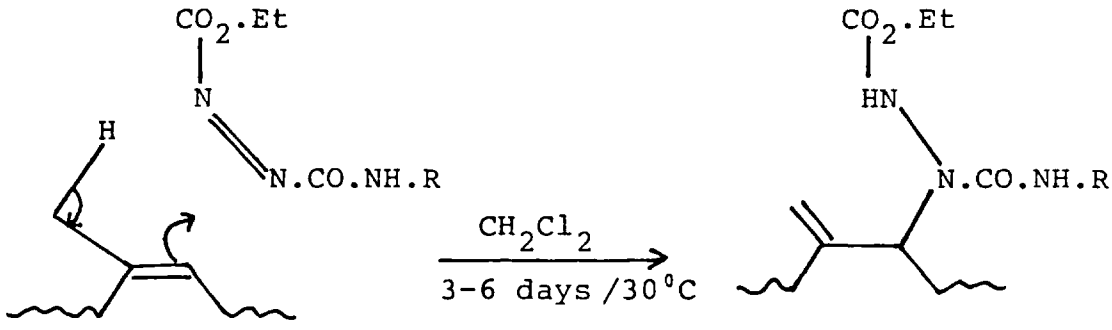
The modified natural rubber samples were prepared by workers at the Malaysian Rubber Producers' Research Association (MRPRA).

Ethyl N-phenyl-carbamoylazoformate (ENPCAF)[88] is incorporated into natural rubber to produce hydrazo-ester pendant groups which are highly polar, and thus readily undergo hydrogen bonding with each other.

The ENPCAF modification is shown schematically below.



Natural Rubber



Three samples were prepared for neutron scattering experiments:

R1 an unmodified natural rubber sample

R5 5 mole % concentration of ENPCAF, equivalent to about one modifying group every 20 isoprene units

R7 7 mole % modification, equivalent to about one modifying group every 14 isoprene units.

In each case the sample took the form of a thin film, pressed between aluminium foil sheets, of thickness calculated to give 10% scatter.

4.2.2 Preparation of Polyester Networks

Polyester network samples were prepared by Dr.R.H.Hall. A detailed account of the preparation may be found elsewhere[89], and a general description of the samples now follows.

Two samples were used in the neutron scattering experiments. Sample N1, which was purely hydrogenous, allowed motion of the entire network to be observed, whereas the partial deuteration of N2 allowed independent study of the motion of the crosslink points only, due to the large difference in the incoherent scattering cross-section of

hydrogen and deuterium. The two samples are shown in figure 4.1. Each sample was moulded into a thin film, with thickness calculated to give 10% scatter.

4.2.3 Measurement of the Shear Modulus, G_0, of the Polyester Networks

Young's modulus, E_0, obtained from the initial slope of a stress-strain curve may be related to the shear modulus, G_0 , using $G_0 = E_0/3$, if the Poisson's ratio of the material is assumed to be 0.5. The shear modulus gives an indication of the degree of crosslinking in the network[18] . E_0 was determined experimentally for N1 and N2 by measuring the shear deformation of a strip of material upon loading with weights up to 20 g. Values of the shear modulus obtained from the two samples were compared to those obtained from a trifunctional polymer network of the same molecular weight with 99% crosslink efficiency[18] .

The following results were obtained:

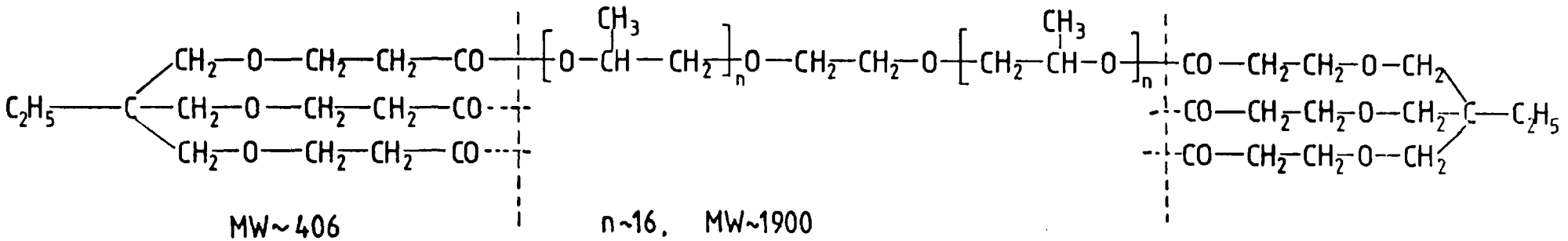
Hydrogenous network N1	$G_0 \sim 867$ g/cm^2	($\equiv$ 73% crosslink efficiency)
Deuterated network N2	$G_0 \sim 533$ g/cm^2	($\equiv$ 71% crosslink efficiency)

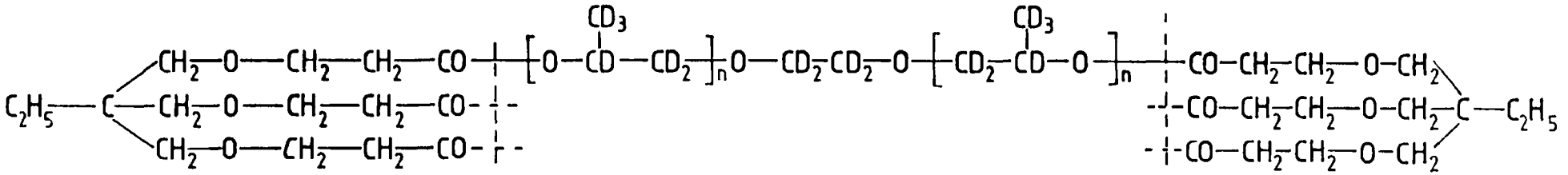
This implies that the deuterated sample, N2, had approximately 2% fewer crosslink points than the hydrogenous sample N1.

In addition, the shear modulus of two more samples were measured, and the crosslink efficiency calculated. For sample N1', a purely hydrogenous sample, this was found to be $\sim$ 71% . For sample N2', a partially deuterated sample, an identical value of the shear modulus was obtained, also giving a value of the crosslink efficiency of 71%.

The low value of the crosslink efficiency obtained

Sample N1: Fully hydrogenous

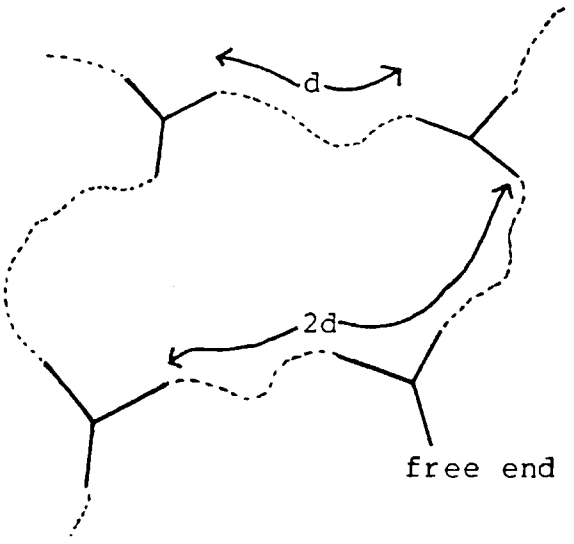




Sample N2: Partially deuterated

Fig 4.1 POLYESTER NETWORKS

in all cases indicates that a trifunctional bridgehead is not always formed, resulting in longer distances between crosslink points, and a free end, as shown schematically below.



Problems introduced by the presence of a large number of free ends in the network are discussed in section 4.5.2.

4.2.4 Preparation of Polypropylene Oxide Chains

Some low molecular weight polypropylene oxide chains were also prepared by Dr.R.H.Hall, using standard methods. These chains were used for supplementary experiments to investigate hydrogen bonding, and as such, were prepared with rather specialised end groups.

PPO1 Bis(hydrogen succinate) of polypropylene oxide diol i.e polypropylene oxide with COOH end groups. (MW $\sim$ 2000). This was prepared by boiling a pyridine solution of a mixture of diol and excess succinic anhydride under reflux for 5h, and then removing the excess of the anhydride.

PPO2 Dimethyl ether of the polypropylene oxide diol i.e polypropylene with methyl end groups. (MW $\sim$2000). This was prepared by the method of Cooper and Booth[18] .

4.3 Quasi-elastic Scattering Results from Polymer Networks

4.3.1 Results obtained from Modified Natural Rubber Samples in the Bulk

The backscattering spectrometer, IN10, was used to measure the quasi-elastic spectra of the three samples, R1, R5 and R7. A standard Si(111) unpolished monochromator was used, and unpolished analyser crystals positioned at angles corresponding to Q values of 0.17, 0.29, 0.6, 0.97, 1.35 and 1.63 $\mathring{A}^{-1}$. An additional polished analyser was placed at Q=1.94 $\mathring{A}^{-1}$. In all three cases data were recorded at 70°C (±1°C).

The un-normalised raw data for the unmodified natural rubber sample (R1) and the 7% modified sample (R7) after counting for 18 hours is shown in figures 4.2 and 4.3, clearly showing the strong Q dependence of the width of the quasi-elastic scattering law. Subsequent data analysis involved obtaining FWHM values (i.e ΔE) using the fitting program POLLY. As expected, the fitting routine based on the Rouse model, giving a width dependent on Q^4 was found to give the best fit to the data. (The goodness of a fit is determined by the value of the residual, defined by the sum of the squares of the deviation of the model scattering law from the actual data points, weighted to the actual number of points).

Double logarithmic plots of the FWHM values obtained using the Q^4 model versus Q for the three samples are shown in figure 4.4. Clearly the two modified samples are moving more slowly than the unmodified sample, although no difference between R5 and R7 can be observed. Error bars are calculated according to the discussion in section 4.4.

4.3.2 Results Obtained from Dilute Solutions of the Modified Rubber Samples

Dilute solutions (∿2% wt/vol) of each of the three

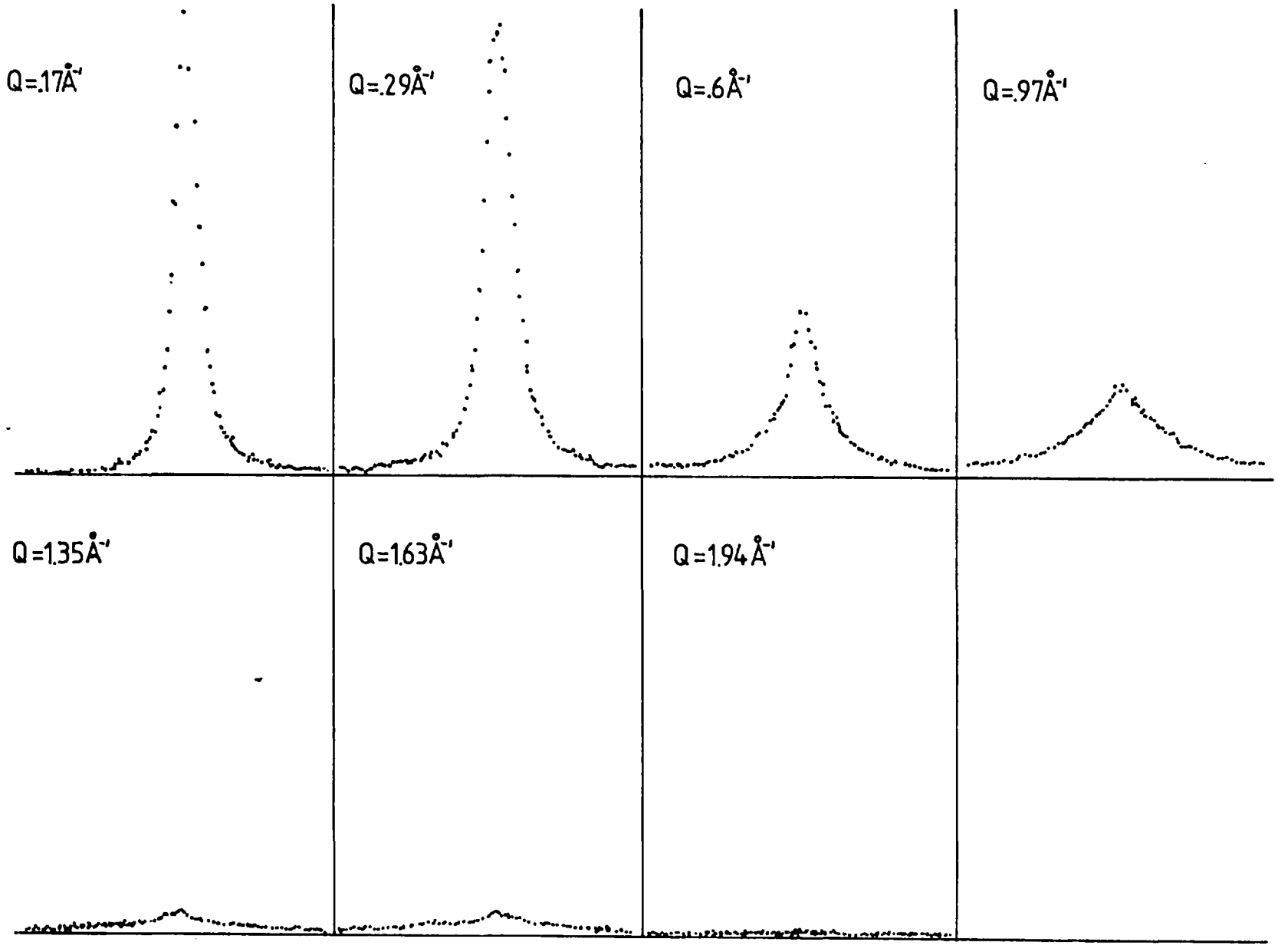


Fig 4.2 Raw data from R1

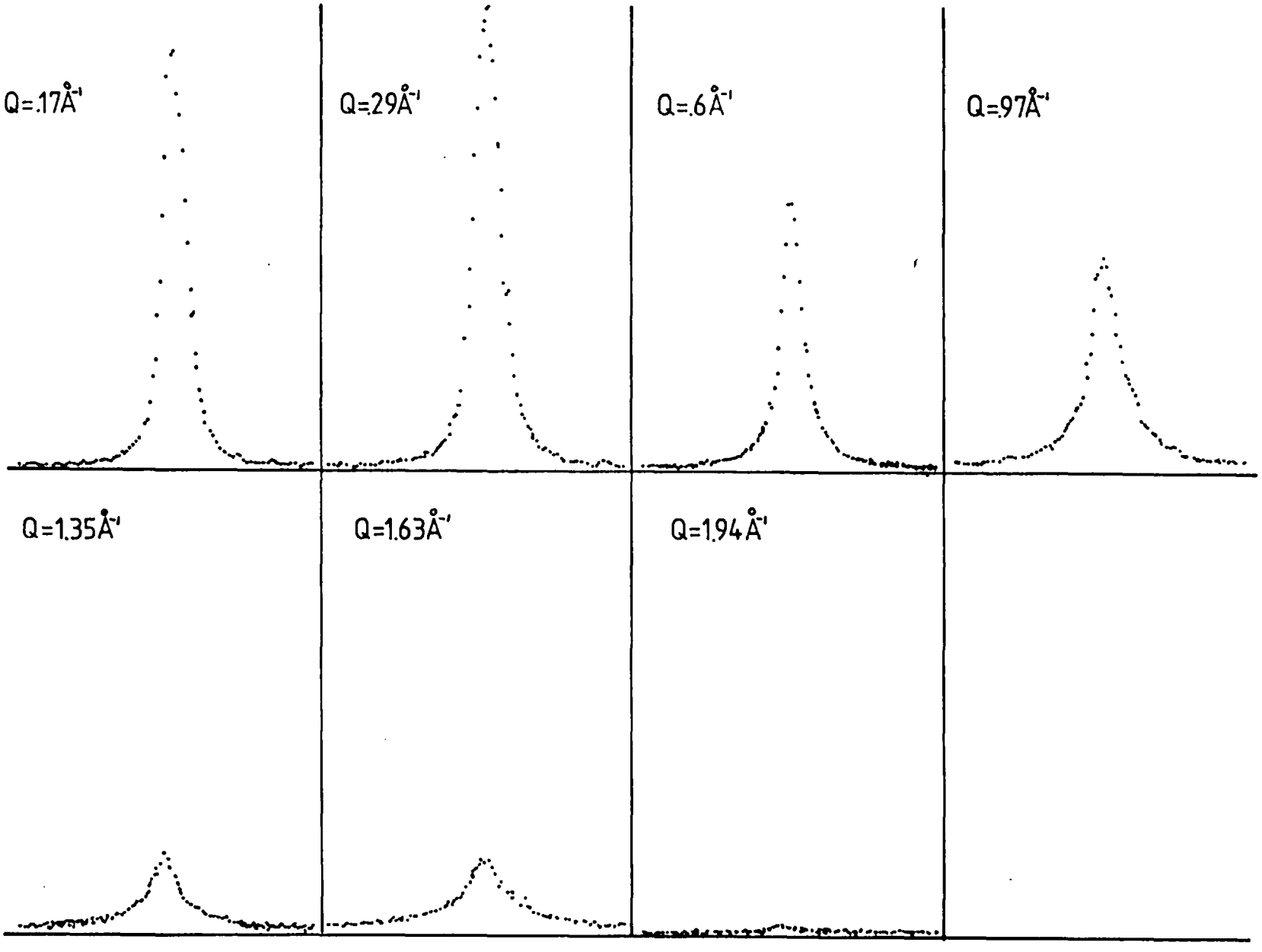
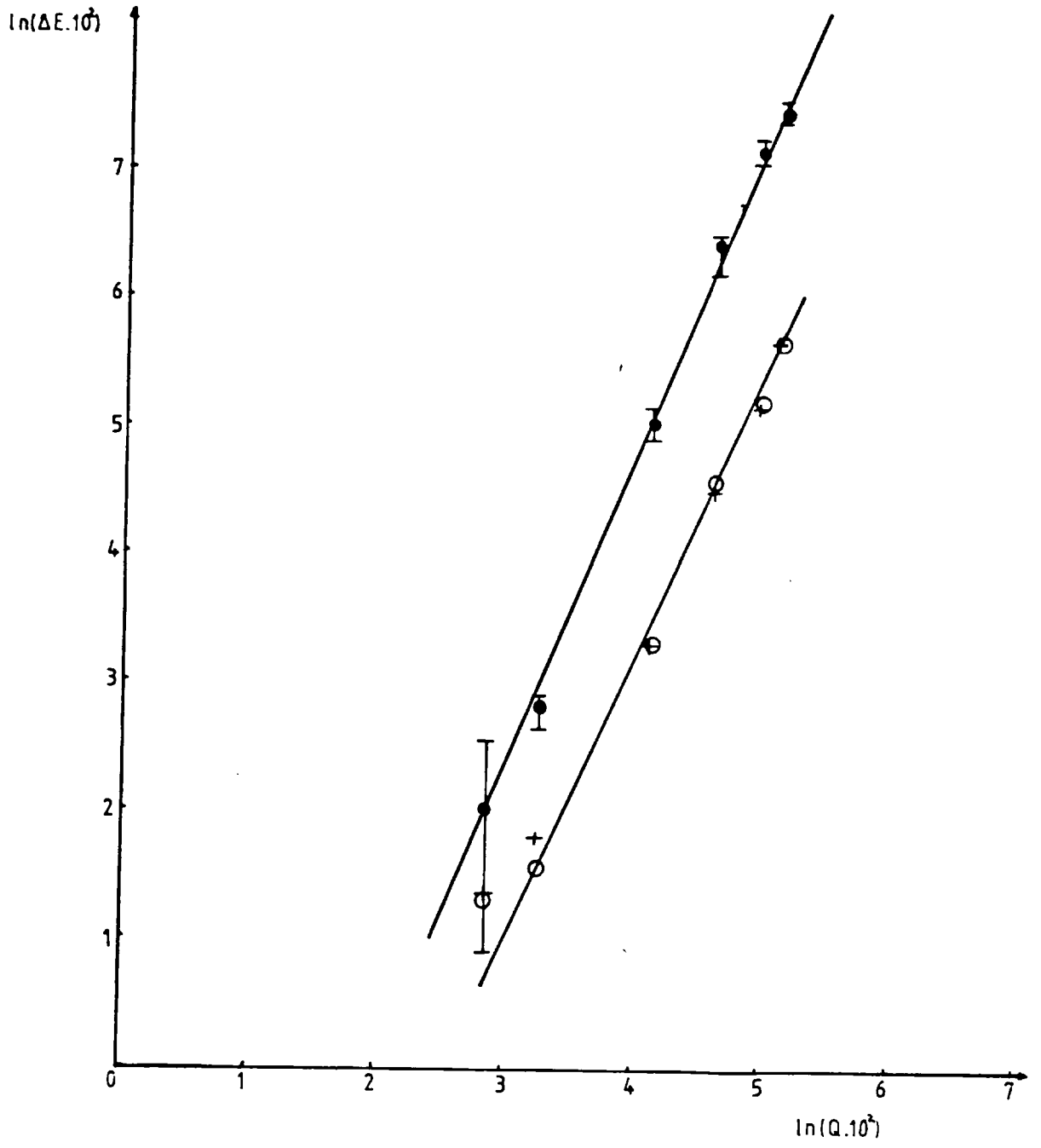


Fig 4.3 Raw data from R7

Fig 4.4 Results from R1, R5 & R7



samples were made up in CS_2.

Quasi-elastic spectra for each solution were recorded at Q values of 0.11, 0.15, 0.19, 0.23, 0.27 and 0.31 $\AA^{-1}$, at a temperature of 25°C.

Data were again analysed using POLLY, and in this case, the best fit was obtained using the Q^3 model scattering law, based on the Zimm model, as predicted for a dilute solution. The FWHM values obtained are plotted against Q in figure 4.5. Also shown is the theoretical dependence of the quasi-elastic width, calculated using equation (4.1) (denoted by the solid line).

4.3.3 Results Obtained from Polyester Networks

Quasi-elastic data for these networks were again recorded using IN10, and also at a temperature of 70°C. Measurements were made in the Q range 0.19 $\AA^{-1}$ to 1.23 $\AA^{-1}$ for the samples N1 and N2, and over a slightly lower Q range for N1' and N2'. Within experimental error, N1' was found to give identical results to N1, implying that although both networks are rather poor, having a crosslink efficiency of only of the order of 70%, the 2% difference between N1 and N1' is negligible.

Figures 4.6 and 4.7 show the measured scattering law for the deuterated sample N2 at various angles of scatter.

FWHM values of the scattering law were obtained using POLLY, and the results of the Q^4 fit are shown in figure 4.8. In addition to simply fitting to the data measured for each of the samples, a Q^4 model scattering law was fitted to data obtained by subtracting the spectra of N2 from those of N1. It is believed that this gives a measure of the rate of motion of the chains between crosslink points, and these results are also shown in figure 4.8. (The solid lines are intended as guides to the

Fig 4.5 Results from R1, R5 & R7 in dilute solution

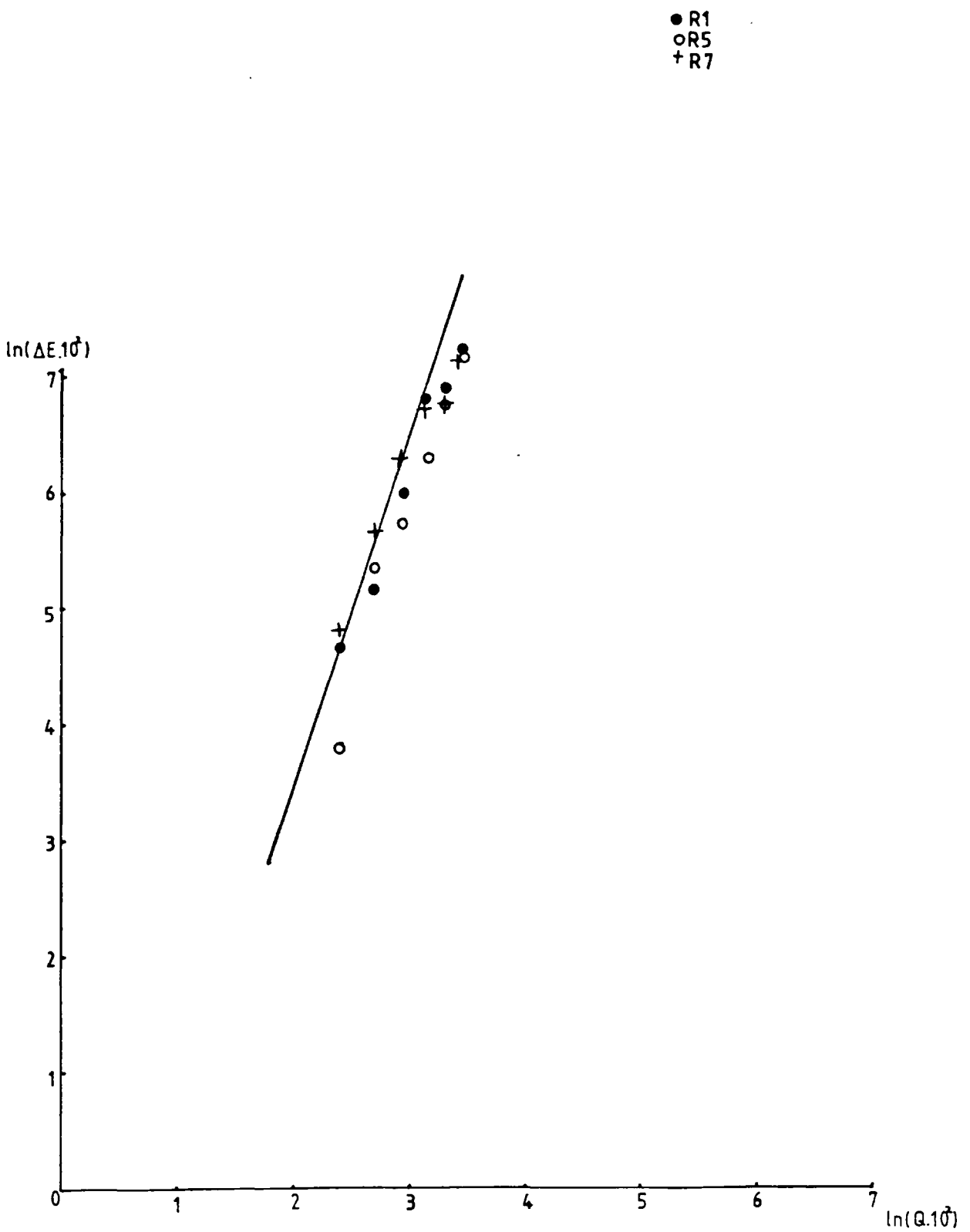


Fig 4.6 S(Q,ω) for N2

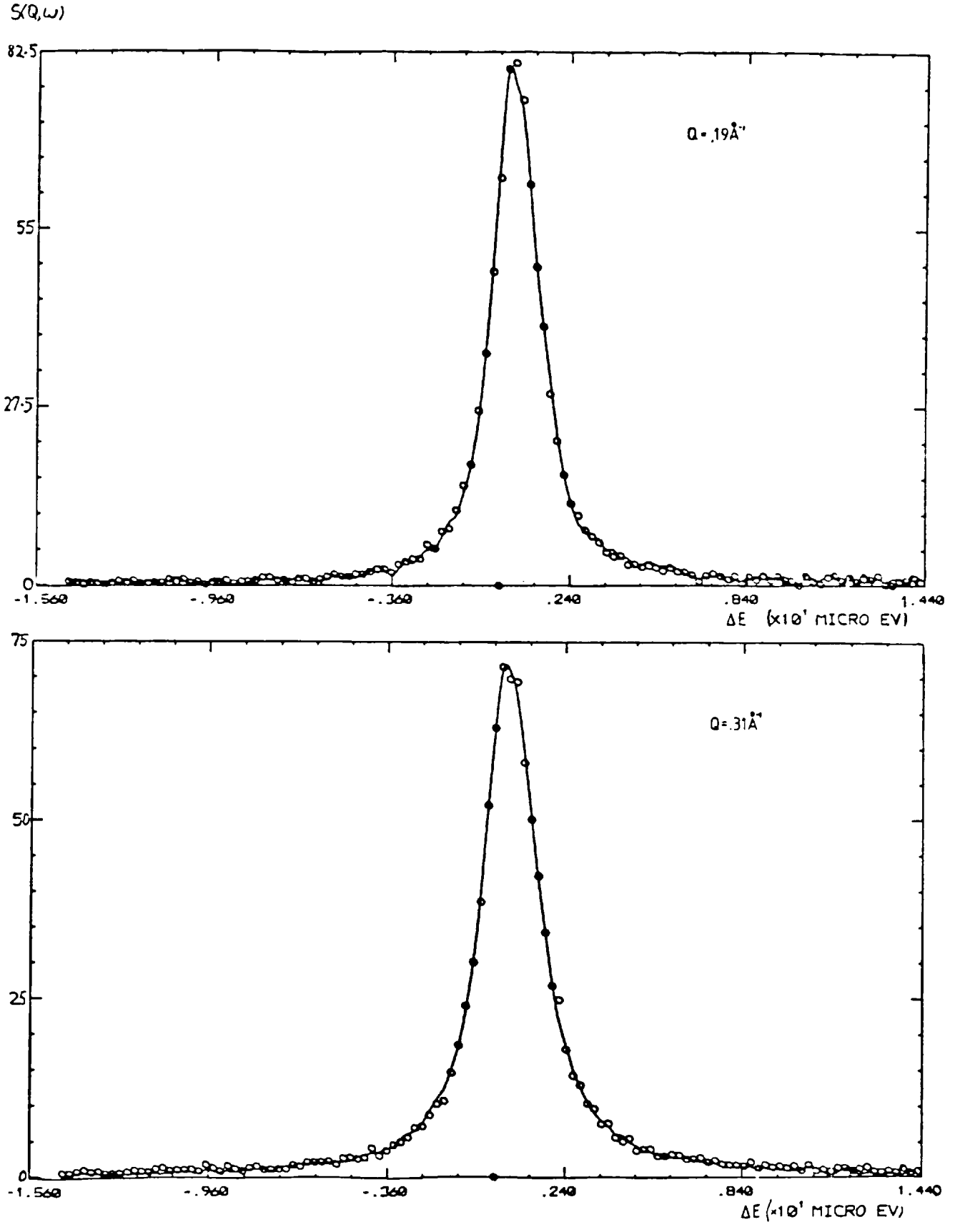


Fig 4.7 $S(Q,\omega)$ for N2

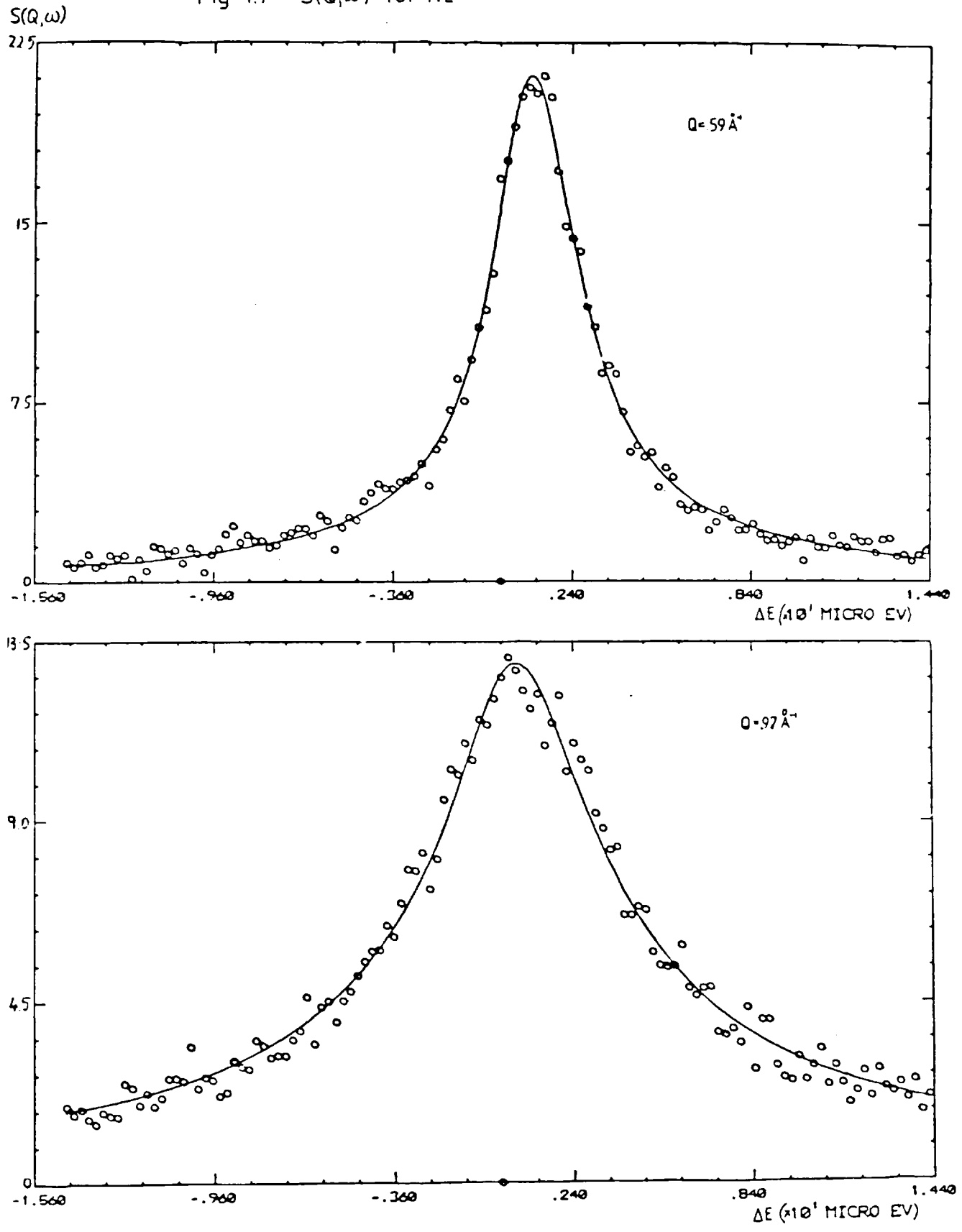
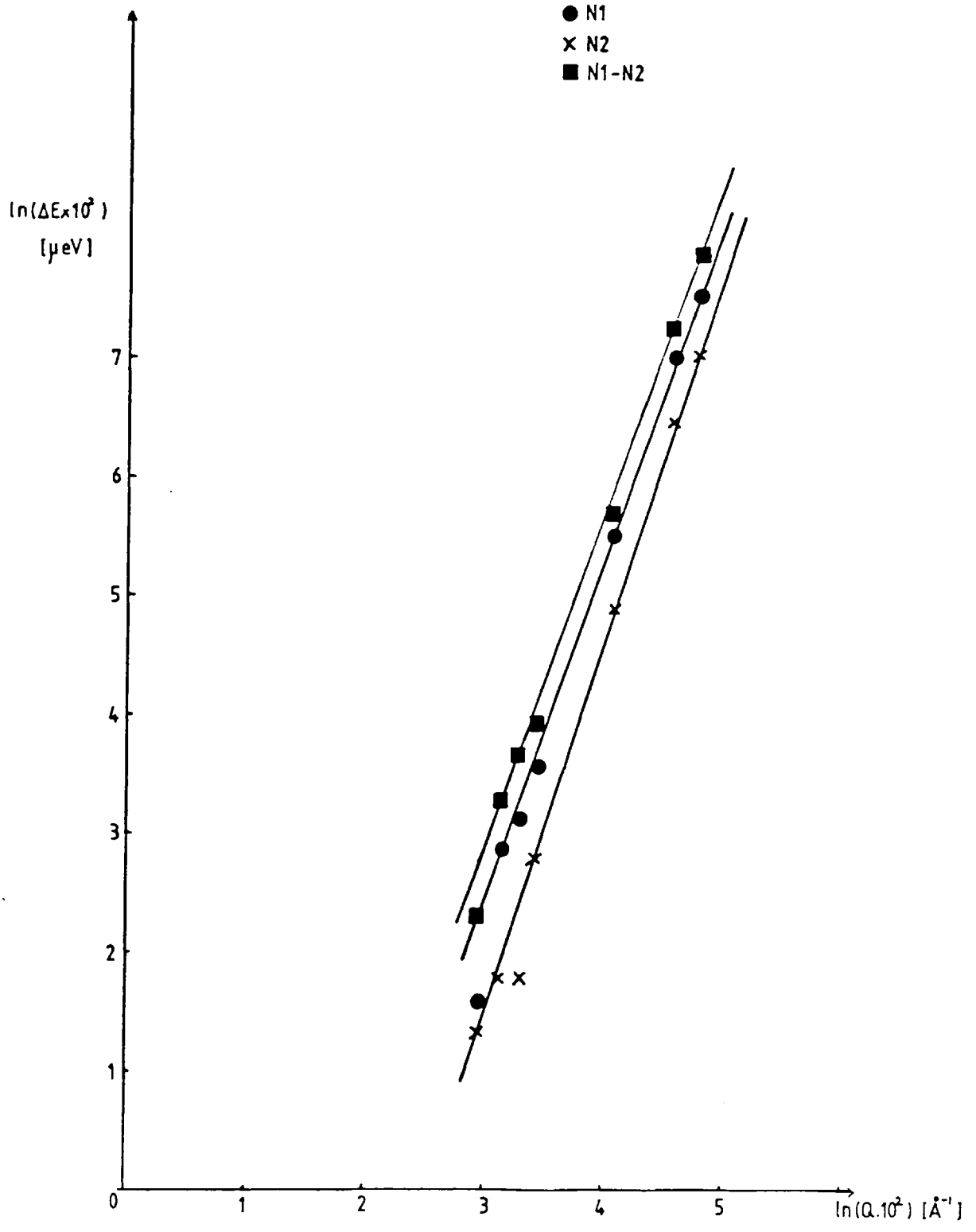


Fig 4.8

Logarithmic plot of FWHM against Q for polyester networks



eye only, and are of no physical significance). Figure 4.9 shows exactly the same data, but plotted differently, to remove the fast Q dependence, and this shows more clearly the differences between the three sets of results. The data plotted in figure 4.10 compares the rate of motion of chains between crosslink points in the network (i.e values obtained from(N1-N2)) with that of a free chain of high molecular weight polypropylene oxide in the bulk (data taken from 9).

4.3.4 Results Obtained from Low Molecular Weight Polypropylene Oxide Chains

Quasi-elastic spectra were recorded for PPO1 and PPO2 under exactly the same experimental conditions as the polyester networks. The data were analysed in the same way, using POLLY, and again the Q^4 model scattering law was found to give the best fit to the data.

Double logarithmic plots of the widths obtained using the Q^4 model against Q are shown in figure 4.11. Figure 4.12 shows plots of $\Delta E/Q^2$ against Q for comparison with figure 4.9.

4.4 Consideration of Errors

Apart from differences introduced into ΔE by the choice of model for $S(\underline{Q},\omega)$, there are two major sources of error to be considered. The least squares fit to the model scattering law fitted to the data generally gives an error of the order of 10% of the value of ΔE. This is a purely statistical error, and it is felt to be a reasonable estimate of the error at high values of Q. However, at low Q values, where the values of ΔE obtained are likely to be considerably less than the resolution function, this 10% error is probably an underestimate. Whilst examination of the measured $S(\underline{Q},\omega)$ shows clear evidence of broadening (especially in the wings of the spectra) even at lowest Q values (see figure 4.13, which compares the resolution

Fig 4.9 Variation of FWHM with Q

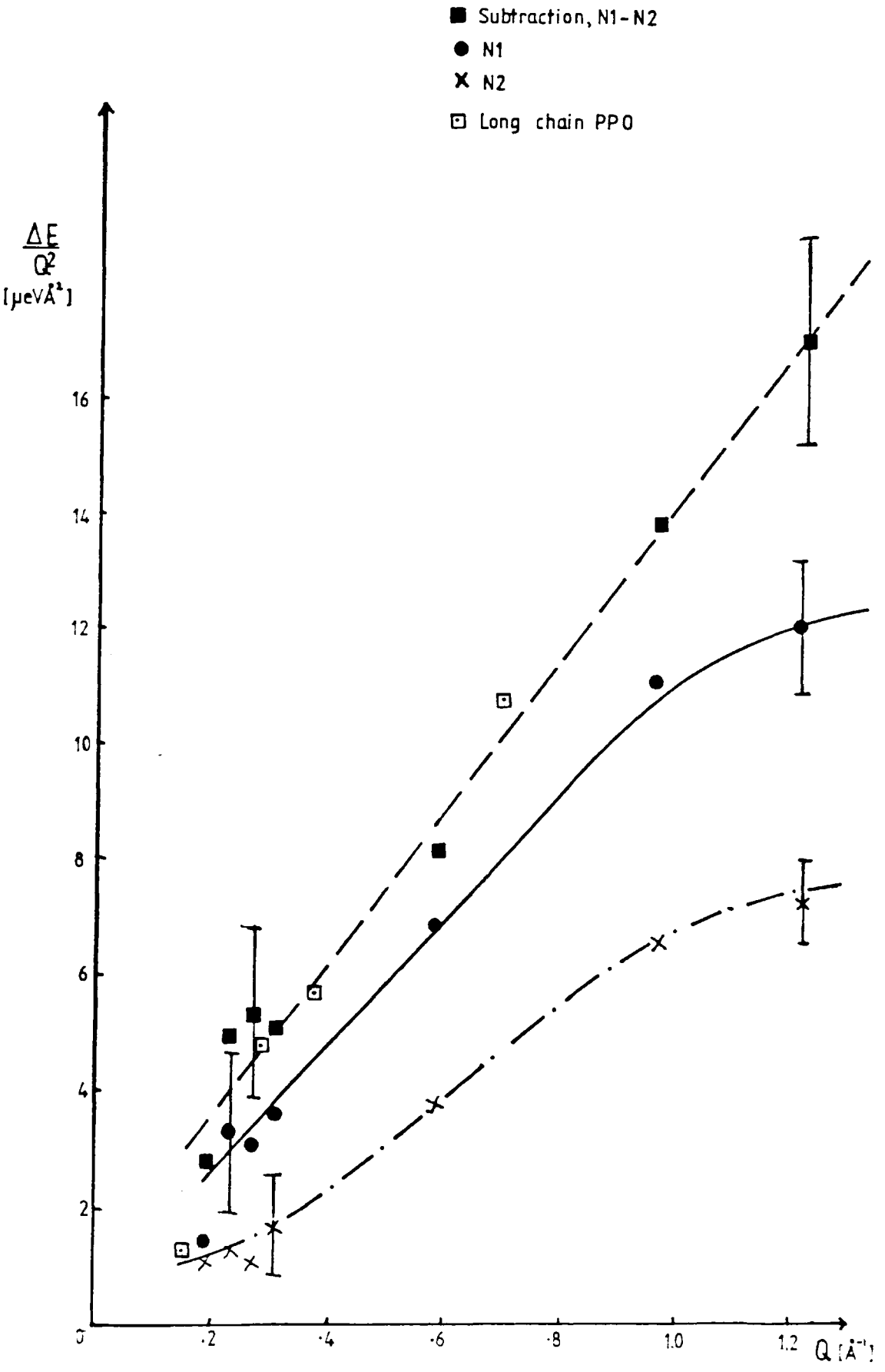


Fig 4.10

Double logarithmic plot of ΔE against Q, for N1-N2(■) and a high molecular weight sample of pure PPO (●)

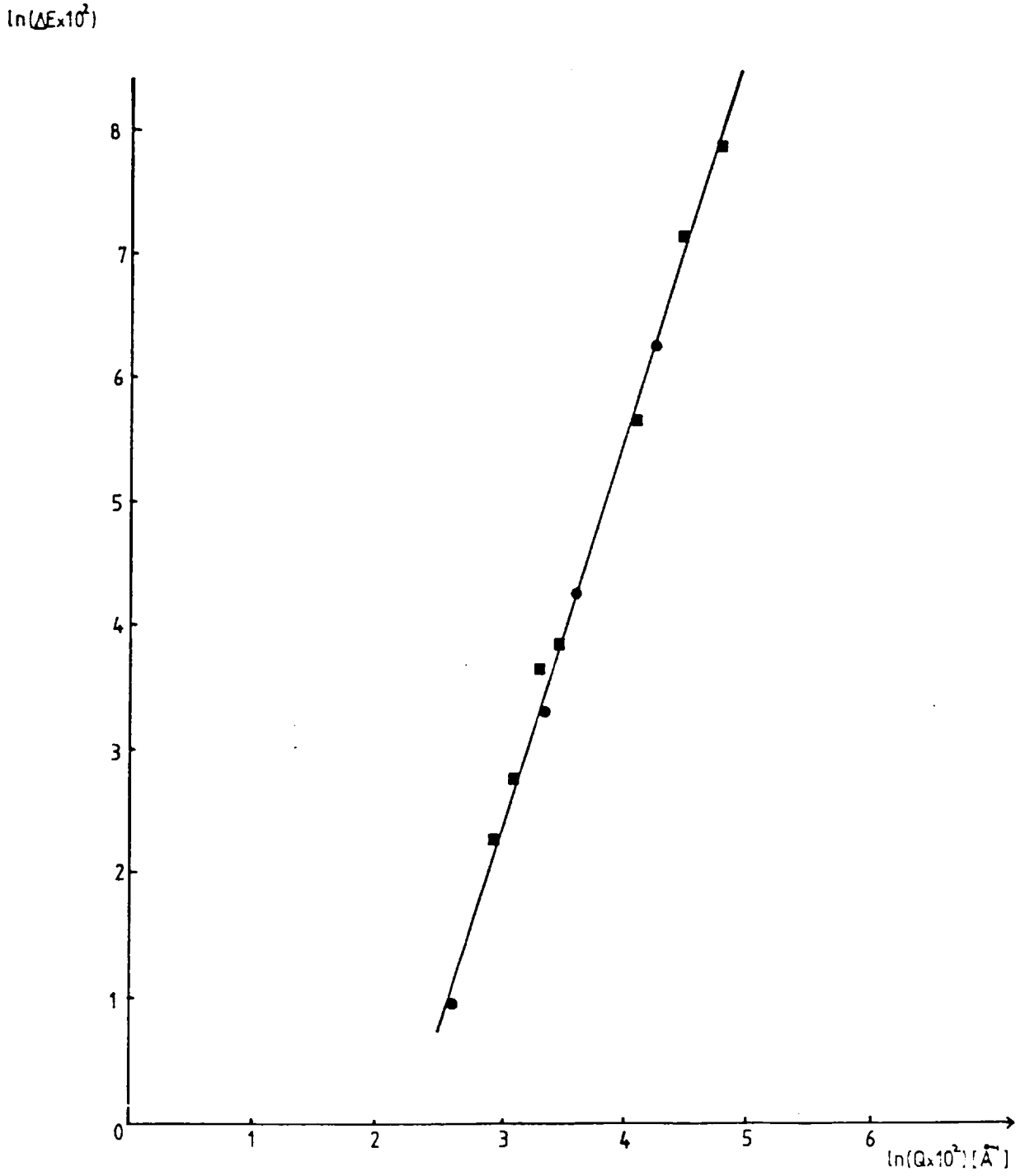


Fig 4.11

Comparison of variation of ΔE with Q for PP01 and PP02

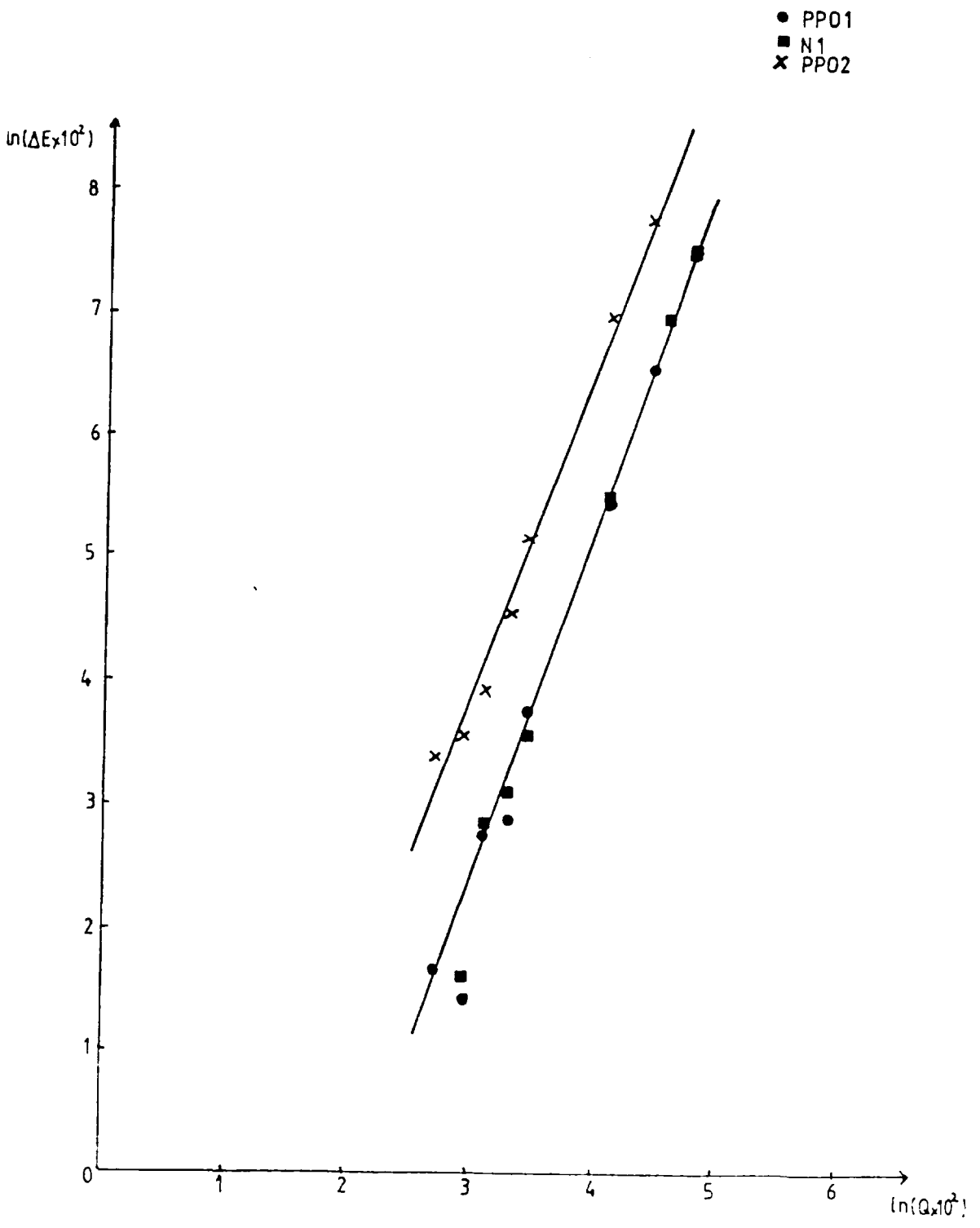


Fig 4.12

Variation of FWHM with Q for PPO chains

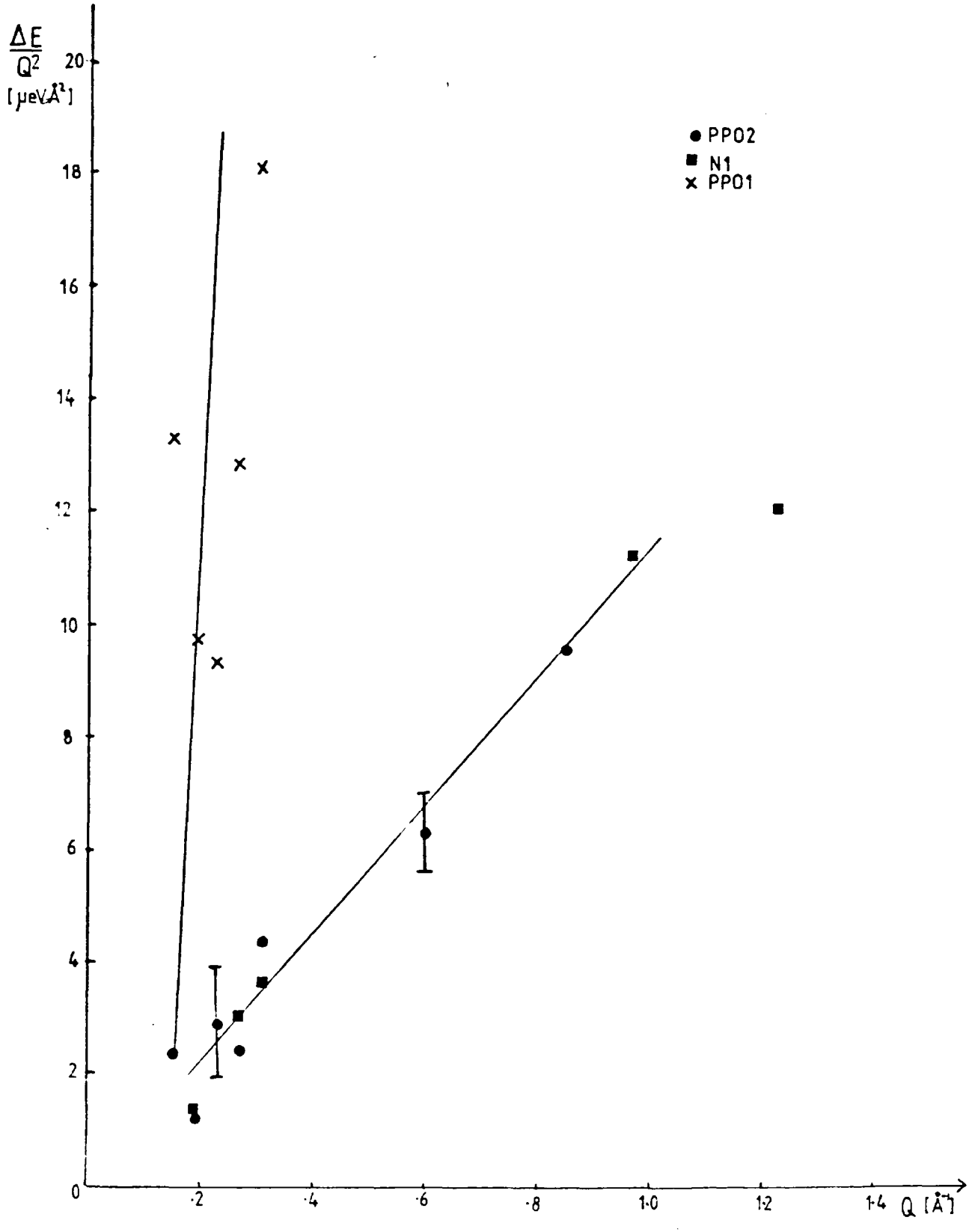
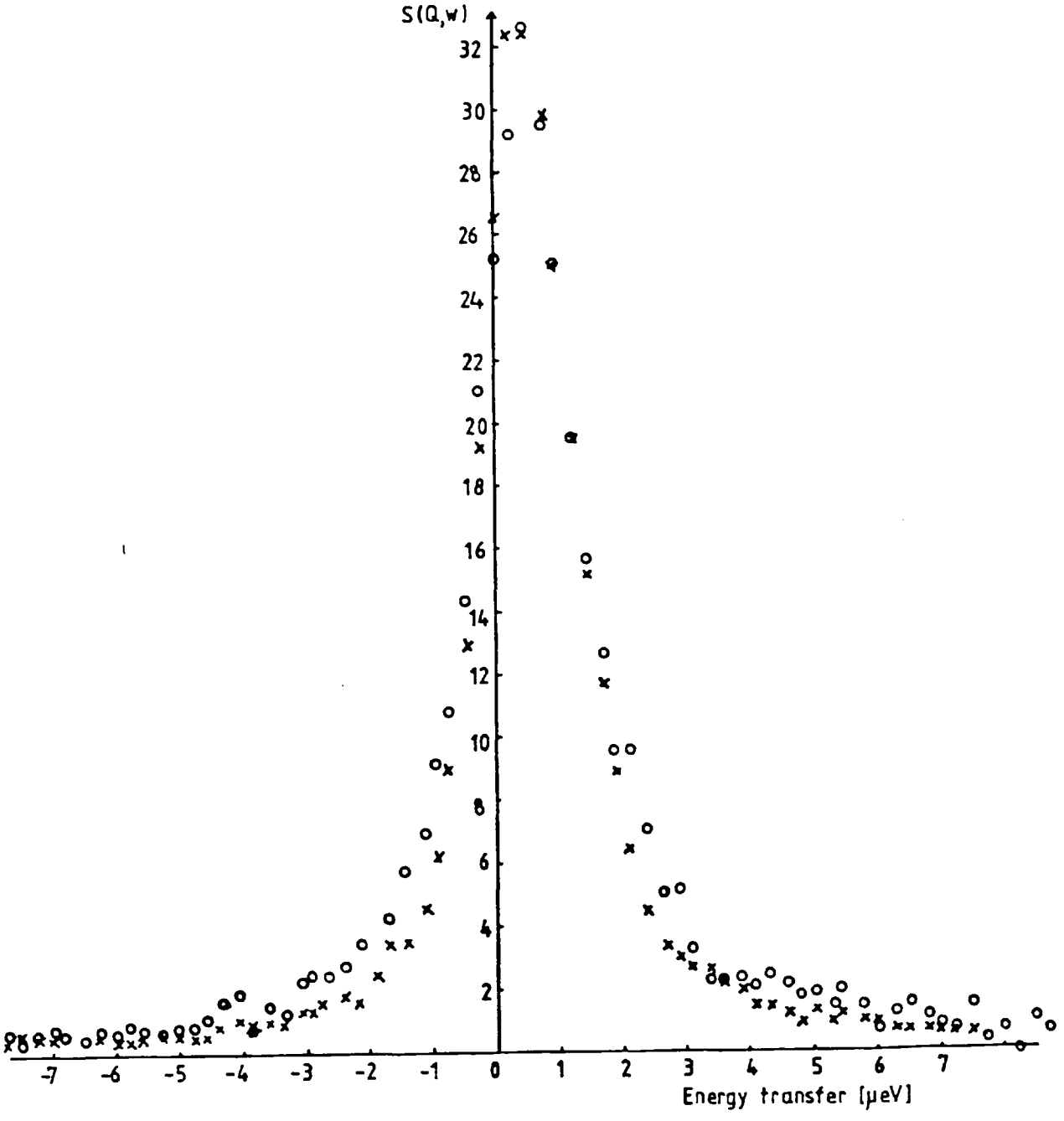


Fig 4.13

Comparison of spectrum obtained from N1-N2 with vanadium [Q=.19Å^{-1}]



function with (N1-N2) at Q=0.19 $\AA^{-1}$) where $\Delta E \sim 0.1$ μeV, it is believed that the precision in the data points themselves can be no better than about 5% of the resolution width, i.e ~ 0.05 μeV. Error bars calculated on these assumptions are shown in figures 4.4 and 4.9, but have been omitted from some of the other figures for the sake of clarity.

4.5 Discussion of Results

4.5.1 Discussion of Results Obtained from Modified Natural Rubber Samples

Figure 4.4 shows the values of ΔE obtained for the natural rubber samples R1, R5 and R7, using a Q^4 dependent model scattering law. As predicted, this model gave the best fit to all three sets of data, although, since the slope of the best line through the data is always less than 4, it is clear that the model is not really ideal for describing the motion in this intermediate distance scale region ($Q\sigma \sim 1$). However, the actual choice of model chosen to fit the data and its true applicability in the experimental Q range is not critical in this case, since whatever choice of model scattering law is used, a clear difference is observed between the modified and unmodified samples. The introduction of highly polar groups into R5 and R7 has obviously produced a slowing down of the main chain motion of the rubber, although it is interesting to note that apparently no difference can be observed between R5 and R7. This is not altogether surprising, however, since it is conceivable that the differences in the rate of motion between the network formed from a sample with one modifying unit every 14 monomers (R7) and that formed from a sample with one modifying group every 20 isoprene units (R5) could be quite small.

Due to the highly polar nature of the modification, the slowing down effect is attributed to interchain hydrogen bonding, resulting in a network composed of virtual (i.e transient, non-chemical) crosslink points.

Results obtained from the three samples in dilute solution are shown in figure 4.6. The rate of motion of the chains would now appear to be identical in all three cases. By making the measurement in dilute solution, all intermolecular interactions are effectively removed, and only intramolecular effects will be observed. Since the three samples are now behaving as identical free chains, the intermolecular origin of the slowing down effect, attributed to interchain hydrogen bonding is now confirmed.

The solution data plotted in figure 4.6 show some systematic deviation from the theoretical Q^3 dependence predicted by equation (4.1). Since the measurements are being made in an intermediate frequency region ($Q\sigma \sim 1$), this deviation is not surprising, and indeed, such deviations at higher Q values have been observed by other workers[12 13]. Akcasu et al[90] have recently calculated the scattering from a polymer in dilute solution over the whole frequency range, through segmental motion (Zimm region) to local bond diffusion. The theory predicts that with increasing $Q\sigma$, the motion deviates from Q^3 Zimm behaviour towards a simple exponential form, typical of diffusive motion, which is in good agreement with the shape of the curve in 4.6.

It is believed that the data obtained shows conclusively the presence of interchain hydrogen bonding in the modified natural rubber samples, leading to the formation of a purely hydrogen bonded network.

4.5.2 Discussion of Polyester Network Results

Data obtained from the polyester network samples, N1 and N2 were again found to be best fitted by a Q^4 model scattering law. The variation of ΔE, for both samples, as a function of Q, is shown in figures 4.8 and 4.9, along with results obtained from the subtraction (N1-N2). Measurements made on N1 show the overall motion of the entire network, whereas N2 reflects motion of the crosslink points alone, and the spectra obtained by the subtraction (N1-N2) show the

motion of the chains between crosslink points.

It is immediately clear that the crosslink points are moving considerably more slowly than the bulk of the network. It would appear that the faster motion of the free chains, combined with the slower motion of the crosslink points give rise to the intermediate motion observed in the measurement of quasi-elastic spectra from N1. Investigation of the actual values of ΔE obtained indicates that the crosslink points are moving approximately half as fast as the overall network.

Figures 4.9 and 4.10 compare the results obtained from the subtraction (N1-N2), which is believed to represent the motion of the chains between crosslink points with results obtained under the same experimental conditions from a sample of high molecular weight polypropylene oxide, again using the Rouse model to obtain values of ΔE. Within experimental error the two sets of data are identical, indicating that the chains between crosslink points behave in exactly the same way as free chains in the melt, at least on the frequency scale of the neutron scattering experiments.

Shear modulus measurements indicated that the network samples were of rather low crosslink efficiency, and a question now arises regarding the role of the free ends in the network. Previous measurements made on urethane networks[18], as well as those discussed in the previous section, show clearly the importance of hydrogen bonding in modifying chain dynamics, and it seemed possible that an interaction involving hydrogen bonding between the carboxyl end groups and main chains could be occurring in these polyester networks. In order to investigate this possibility in detail, experiments using two modified samples of low molecular weight polypropylene oxide were performed. Neutron scattering measurements were made under exactly the same experimental conditions as for the polyester networks, and the results obtained assuming the application of the Rouse model shown in figure 4.11. Clearly some mechanism has caused the slowing down of the motion in the hydrogen succinate, and this is attributed to hydrogen bonding between the COOH

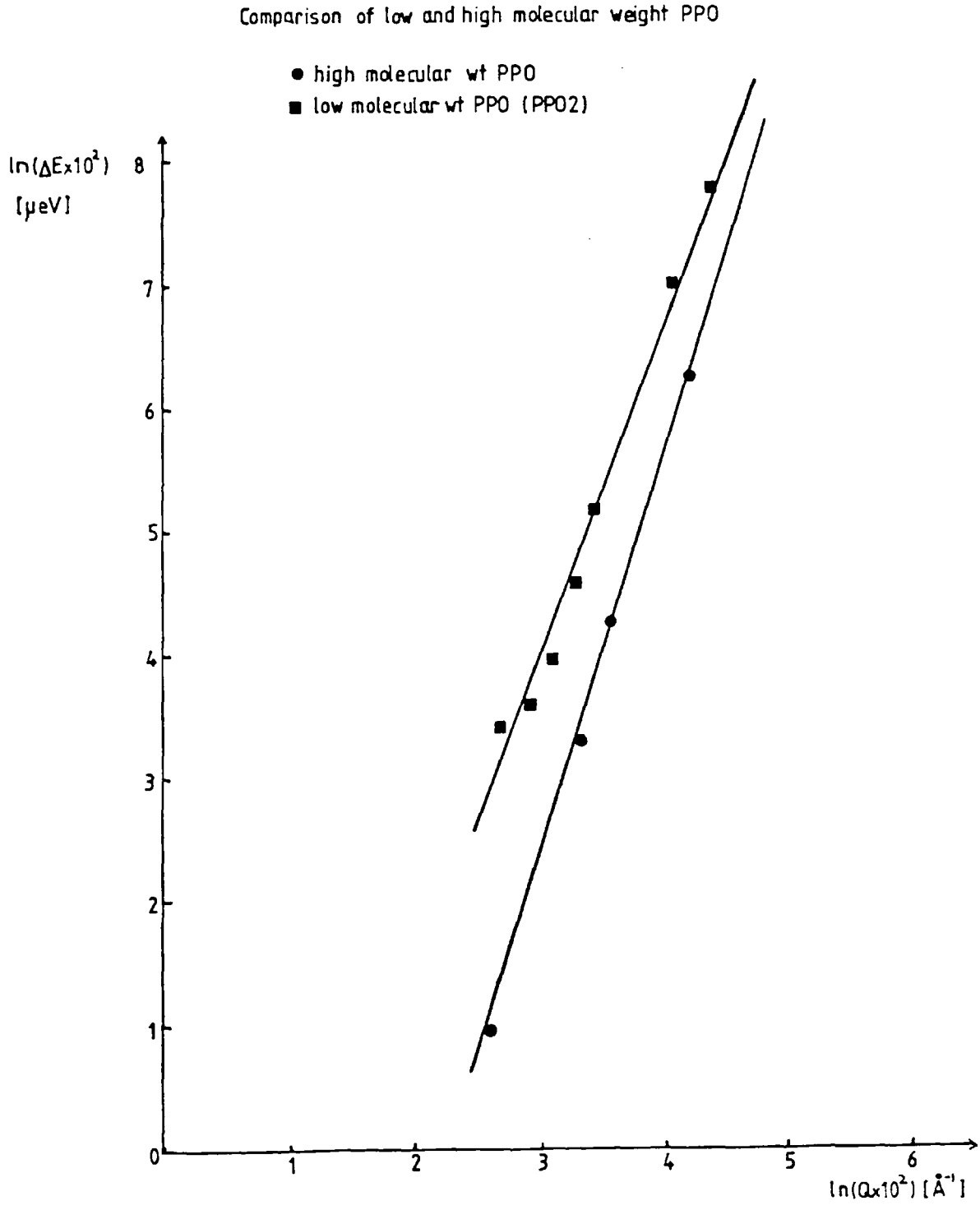
groups and main chains. It would suggest that the free ends present in the networks also form hydrogen bonds, creating temporary, or virtual crosslinks, so that on the timescale of a neutron scattering experiment there are no free ends, and a perfect network is being observed. If some consideration is given to the actual position of the hydrogen bonds, three possibilities arise. Firstly, a bond between the COOH group and somewhere in the middle of the chain between crosslink points may be formed. Secondly, a bond may be formed between the free carboxyl end group and the ester groups in the crosslink points, and finally, a bond may be formed between the two COOH free ends. Of the three, the third is probably the strongest bond, and the activation energy for this case is estimated to be 7-8 kcal/mol[91] . It is possible to calculate the lifetime (or frequency of formation) of a hydrogen bond, assuming an Arrhenius relationship of the form $\nu = \nu_0 \exp(-E_a/RT)$, where E_a is the activation energy, and ν_0 the vibrational frequency of the bond. If E_a is taken to be 7 kcal/mol, and ν_0 of the order of 200 cm^{-1} (a value obtained experimentally, and also predicted theoretically from thermodynamic considerations[91]), then the lifetime frequency is estimated to be of the order of 4.7×10^8 Hz. If E_a is assumed to be slightly higher, of the order of 8 kcal/mol, and ν_0 again 200 cm^{-1}, then a value of 8.7×10^7 Hz is btained for the frequency of formation of hydrogen bonds. These values are considered to be fairly generally applicable to the formation of hydrogen bonds in the network, and both fall in the upper limit of the timescale explored in a neutron scattering experiment ($\sim 10^{-10}$-10^{-7} sec), confirming that within the experimental timescale, a perfect network composed of both chemical and temporary, hydrogen-bonded crosslinks is being observed. This establishes beyond any doubt that the difference observed between the two samples N1 and N2 is not due to any physical difference, but genuinely to a slower motion of the crosslink points. Warner[19] has calculated the Rouse motion of a junction point in a polymer network of functionality γ. He shows that the Q dependence of ΔE is unaltered (i.e Q^4) but the rate of motion is slowed down relative to a freely moving point on the chain, by a factor of $2/\gamma$. Thus if the polyester networks under discussion here were perfect, their tri-

functional junctions would be expected to slow down by a factor of 2/3. The fact that the apparent experimental factor is not exactly 2/3 is not considered a major discrepancy, when the imperfections in the network and the experimental Q range are taken into account. As discussed above, the free ends at a crosslink point will make hydrogen bond junctions on the timescale of the neutron scattering experiment, but these will form at arbitrary points along the chain. Thus the effective functionality of the network is somewhat uncertain, and may even be greater than three. In addition, the Q range of these experiments falls at the upper limit of the region where Q^4 Rouse behaviour is predicted. This is demonstrated clearly by the Q dependence of the ΔE values themselves, which is found to be closer to Q^3 than Q^4. In this frequency range the assumptions of Warner's calculations, based on a Rouse model, break down, and the exact numerical factor of $2/\gamma$ should not necessarily be observed.

Figure 4.11 also shows the results obtained from the fully hydrogenous sample N1, and it is interesting to note, that on this timescale, the network formed due solely to hydrogen-bonding forming temporary crosslink points between chains in the linear polypropylene oxide is identical to the real network (N1) composed of both chemical and hydrogen-bonded crosslinks.

While chemical and hydrogen-bonded networks have a very similar rate of motion to free long chains, comparison of figures 4.10 and 4.11 shows a remarkable difference in the rate of motion observed between the low molecular weight polypropylene oxide (PPO2, MW $\sim$ 2000) and high molecular weight polypropylene oxide (MW $\sim 10^6$). To show this difference more clearly, the data are replotted in figure 4.14. Although at first sight it could be tempting to ascribe this faster motion of the low molecular weight chain to centre of mass diffusion, results obtained from poly (dimethyl siloxane) (PDMS) would present a more plausible explanation. Early low resolution experiments[4] on a series of linear and cyclic PDMS samples showed little change in

Fig 4.14


Comparison of low and high molecular weight PPO
● high molecular wt PPO
■ low molecular wt PPO (PPO2)
ln(ΔEx10²) [μeV]
8
7
6
5
4
3
2
1
0
1
2
3
4
5
6
ln(Qx10²) [Å⁻¹]

values of ΔE obtained above a molecular weight of about 1100, corresponding to 15 monomer repeat units. These results have recently been confirmed in a series of experiments at high resolution, using IN10. Since polypropylene oxide is a considerably stiffer molecule, it could not be expected to have faster centre of mass diffusion motion than PDMS of equivalent chain length. Instead, it is necessary to ascribe the decrease in frequency when the length increases from 30 units to infinity in the PPO samples to internal modes. Estimates of the chain length associated with one Rouse spring unit have been made from high resolution neutron scattering results for several polymers in dilute solution[13] . Because of its high flexibility, this chain length is only 4 to 5 monomers for PDMS, but is found to be much larger for other polymers (11 units for poly(tetrahydrofuran) and 55 units for polystyrene). Thus in terms of Rouse spring units, the short PPO chains may consist of only one or two segments, and the application of the Rouse model to describe the motion is not really justified. When these short chains hydrogen bond to form a network, the whole connected system sustains Rouse modes, and long chain behaviour is regained.

Chapter 5 Conclusions and Aims for Future Work

5.1 Conclusions from the Investigation of Local Dynamics in Poly(methyl methacrylate)

Quasi-elastic neutron scattering results show clearly that after accounting for coherent scattering effects, the rotational motion of both the α-methyl and ester methyl groups in PMMA may be described in terms of a series of jumps between three equivalent sites on a circle of radius 1.032 Å. This is exactly as predicted for the α-methyl group, and further shows that any kind of more complex motion proposed for the ester methyl group cannot be observed on the time-scale of the neutron scattering experiments performed on IN5 and IN6. Measurements of the widths of the quasi-elastic component of the rotational scattering law have allowed activation energies for both groups to be calculated, giving the following results. For the α-methyl group, a combination of quasi-elastic data from IN10 with NMR T_1 measurements gave an activation energy of 29.1 kJ/mol for an atactic sample. This may be compared with values of 23.3 kJ/mol and 15.8 kJ/mol for pure syndiotactic and pure isotactic PMMA respectively, obtained using NMR techniques. For the ester methyl group, quasi-elastic neutron scattering measurements gave a value of E_a of 7.6 kJ/mol for an approximately 50% syndiotactic sample. The achievement of a conclusive value of the activation energy for the ester methyl group is considered of major importance, since NMR and other neutron scattering experiments,to date, have yielded only rather speculative values. Furthermore, it is tentatively suggested that for the ester methyl group, E_a(syndiotactic) > E_a(isotactic) although activation energies for stereoregular samples have not yet been firmly established.

In general, quasi-elastic measurements of the EISF and rotational frequency were found to be in good agreement for the two instruments, IN5 and IN6.

Values of V_3, the barrier height to rotation, calc-

ulated using the above values of E_a, on the assumption of the presence of quantum mechanical tunnelling, were found to be in excellent agreement with those obtained directly from incoherent inelastic experiments. This excellent agreement between the two methods of obtaining V_3 was considered strong evidence for the presence of tunnelling in both methyl groups at low temperatures. For the α-methyl group, V_3 was found to be 33 kJ/mol for syndiotactic PMMA, and 23 kJ/mol for isotactic PMMA. V_3 for the ester methyl group in a sample consisting of 50% syndiotactic and 40% atactic sequences was found to be between 3.2 and 10.5 kJ/mol. The inelastic measurements also revealed useful information about other vibrational motions in the molecule, such as sidegroup and backbone bending and wagging, in good agreement with far infra-red measurements. Within experimental error, the frequency distribution function obtained for the various samples of PMMA were found to be identical for both IN6 and 4H5 measurements.

The structure factor, $S(\underline{Q})$, obtained from neutron diffraction measurements was found to be identical to that obtained from calculations based on the deviation of the observed EISF from the predicted values, and furthermore, both were in excellent agreement with the wide angle X-ray determination of $S(\underline{Q})$. Peak positions in $S(\underline{Q})$ were associated with different periodicities in the PMMA molecule, giving useful structural and conformational information about the amorphous polymer.

Inelastic measurements relating to the torsional motion of the α-methyl group have been found to be reproducible, and in good agreement with results obtained using NMR and quasi-elastic techniques, measuring related parameters. The dependence of barrier height and torsional motion on the polymer tacticity has been firmly established. It has been shown that the geometry of the rotational motion of the α-methyl group can be well described in terms of a simple three-fold jump model. These results are all considered conclusive, and it is believed that the motion of the α-methyl group is now well understood.

For the ester methyl group, however, the results obtained are not so complete, particularly relating to the effect of tacticity on the rotational motion of the group. Due to problems mentioned earlier, related to the appearance of crystalline backbone modes at low frequencies, it is considered unlikely that further inelastic measurements would give any really conclusive results, even with the use of partially deuterated samples to eliminate some of the vibrational modes. Instead, it is proposed that more useful information could be obtained from a more extensive study of the behaviour of the rotational frequency in stereoregular forms of PMMA over a range of temperatures, using quasi-elastic neutron scattering techniques. It has been shown that some problems with data analysis are encountered when using purely hydrogenous samples, so it is felt that for this study, partially deuterated stereoregular samples should be used, to eliminate excess elastic scattering. Since the activation energy for the ester methyl group in an atactic form of PMMA has already been established, this future work on stereoregular samples would conclude the investigation of rotational motion of the ester methyl group in PMMA.

5.2 Conclusions from the Investigation of the Local Dynamics of Rubber Networks

The first series of experiments described in chapter 4 showed clearly that the introduction of highly polar modifying groups into natural rubber samples gave rise to intermolecular hydrogen bonding, interpreted in terms of virtual or transient crosslink points, causing the formation of a network, on the timescale of a neutron scattering experiment. Although these virtual crosslinks obviously slowed down the motion of the chains in the rubber, no difference could be seen between the effect of a 5% modification and a 7% modification. However, since this difference is likely to be small, this is not altogether surprising. The results obtained are considered conclusive, and any further work probably unnecessary, unless a sample with a considerably higher degree of modification could be obtained, in which case it would be

of interest to see if the motion still appeared identical to that of a 5% or 7% modified sample, or if, as seems more reasonable, a greater number of virtual crosslinks are formed, and the motion slowed down still further.

The second set of experiments demonstrated that the crosslink points in a chemically bonded network move approximately half as fast as the free chains between crosslink points, which was found to be in good agreement with the behaviour predicted theoretically. In addition, it was found that the presence of free carboxyl end groups in a poor chemical network would again cause virtual hydrogen bond crosslinks, so that on the timescale of a neutron scattering experiment, a perfect network was being observed.

An interesting topic for possible future work arises from the supplementary experiments performed to study the formation of hydrogen bonds in low molecular weight sample of modified polypropylene oxide. A large difference in the rate of motion observed in a low molecular weight sample (MW $\sim$ 2000) and that of a high molecular weight sample (MW $\sim 10^6$) was found. This was explained in terms of the break-down of the Rouse model at low molecular weights, due to an insufficient number of bead-spring segments to describe the motion, and compared to a similar situation encountered in the study of main chain dynamics of poly(dimethyl siloxane) (PDMS). For PDMS, it was found that the rate of motion observed varies until the chains are of the order of fifteen monomer units long, when a limiting value of ΔE is reached, and no further change with increasing molecular weight is found. It would be interesting to repeat these experiments for polypropylene oxide, over a range of molecular weights from about 2000 to several hundred thousand, and see if a similar limiting value is obtained at a critical molecular weight.

5.3 Concluding Remarks

The results presented in this thesis have shown the usefulness of the application of incoherent quasi-elastic and inelastic neutron scattering specifically to the study of sidegroup motion in poly(methyl methacrylate), and to the investigation of main chain dynamics of polymer networks. However, further consideration of the neutron scattering technique suggests that the scope for similar experiments to study dynamic properties over a whole range of polymeric systems is enormous.

One of the major reasons for the success of neutron scattering studies on polymers is their large hydrogen content, combined with the possibility of partial deuteration. Since hydrogen is such a strong incoherent neutron scatterer, and deuterium a relatively weak one, the possibilities of selective deuteration to study different aspects of different sytems are virtually endless. Another major advantage offered by polymers is the dependence of the motion on temperature - thus by working below the glass transition temperature it is possible to 'freeze out' the backbone motion, allowing study of the sidechain motion only - and, of course, different sidegroups have very different responses to temperature, so that within a given system, different sidechains may be moving at quite different rates at a given temperature - and this leads to an important concept in neutron scattering - that of the timescale of the neutron scattering experiment, which is directly related to instrument resolution. Only the motions of a comparable frequency to the resolution will be observed - thus a suitable choice of instrument, combined with a suitable choice of temperature will allow a single sidegroup motion, or perhaps the backbone motion (if above T_g) only to be observed, due to the vastly different timescales involved.

It is this aspect of neutron scattering which allows it to essentially isolate the motion of a single component of the polymeric system, partly by selective deuteration,

and partly by suitable choice of resolution which makes it such a powerful tool in the study of polymer dynamics.

Limitations of the technique are due only to insufficient resolution to observe the slowest backbone motions - although with the advent of spectrometers of better and better resolution, this is scarcely a problem, and to limits of deuteration of the polymer, although for most common systems there is virtually no limit to what can be achieved.

In conclusion, it seems that quasi-elastic and inelastic neutron spectroscopy can offer a valuable contribution to the study of the dynamics of polymer chains.

References

1 Ed B.T.M.Willis, Chemical Applications of Thermal Neutron Scattering, OUP (1973)

2 T.Springer, Springer Tracts in Modern Physics, 64, Springer-Verlag (1977)

3 J.S.Higgins, Treatise on Materials Science and Technology, 15, 381 (1979)

4 G.Allen,P.N.Brier,G.Goodyear and J.S.Higgins, Faraday Symposium 6 (1972)

5 G.Allen,R.E.Ghosh,A.Heidemann,J.S.Higgins and W.S.Howells, Chem.Phys.Lett, 27, no.3, 308 (1974)

6 G.Allen,J.S.Higgins and C.J.Wright, J.Chem.Soc., Far.Trans.II, 70, 349 (1974)

7 P.E.Rouse, J.Chem.Phys., 24, 269 (1956)

8 P.de Gennes, Physics(Long Island City, N.Y) 3, 37 (1967)

9 G.Allen and J.S.Higgins, Macromolecules,10, 1006 (1977)

10 J.S.Higgins,R.E.Ghosh,W.S.Howells and G.Allen, J.Chem.Soc.,Far.Trans.II, 73, 40 (1977)

11 J.S.Higgins,L.K.Nicholson and J.B.Hayter, Polymer, 22, 163 (1981)

12 L.K.Nicholson,J.S.Higgins and J.B.Hayter, Polymer Preprints, 22, no.1, 86 (1981)

13 L.K.Nicholson,J.S.Higgins and J.B.Hayter, accepted by Macromolecules

14 L.K.Nicholson, to appear in Contemporary Physics

15 B.H.Zimm, J.Chem.Phys., 24, 269 (1956)

16 E.Dubois-Violette and P.de Gennes, Physics 3, no.4, 181 (1967)

17 H.Benoit, D.Decker, R.Duplessix,C.Picot,P.Rempp,J.Cotton, B.Farnoux,G.Jannink and R.Ober, J.Polym.Sci., Polym. Phys.Ed., 14, 2119 (1976)

18 D.J.Walsh,J.S.Higgins and R.H.Hall, Polymer 20, 951 (1979)

19 M.Warner, submitted to J.of.Phys.

20 G.Allen and J.S.Higgins, Molec.Spect., 261 (1971)

21 J.S.Higgins,G.Allen and P.N.Brier, Polymer 13, 157 (1972)

22 G.Allen,C.J.Wright and J.S.Higgins, Polymer 15, 319 (1974)

23 N.G.McCrum,B.E.Read and J.Williams, Chap.8, Anelastic and Dielectric Effects in Polymeric Solids, Wiley and Sons (1967)

24 J.G.Powles and P.Mansfield, Polymer 3, 336 (1962)

25 J.G.Powles,J.H.Strange and D.J.H.Sandiford, Polymer 4, 401 (1963)

26 T.M.Connor and A.Hartland, Phys.Lett., 23, no.11, 662, (1966)

27 J.A.Sauer, Polym.Sci.Symp., 32, 69 (1971)

28 T.Kawai, J.Phys.Soc.Japan, 16, 1220 (1961)

29 E.O.Stejskal and H.S.Gutowsky, J.Chem.Phys., 28, 388, (1958)

30 A.Eisenberg and S.Reich, J.Chem.Phys., 51, no.12, 5706, (1969)

31 J.Williams and A.Eisenberg, Macromolecules, 11, no.4, 700 (1978)

32 J.A.Sauer and R.G.Sabe, J.Molec.Sci., Chem. A3(7), 1217 (1969)

33 A.Leadbetter and R.E.Lechner, Chap.8, The Plastically Crystalline State, Ed. J.Sherwood, Wiley & Sons (1979)

34 H.Hervet,A.J.Dianoux,R.E.Lechner and F.Volino, J.de.Physique, 37, 587 (1976)

35 A.J.Dianoux,F.Volino and H.Hervet, Molec.Phys., 30, no.4, 1181 (1975)

36 A.B.Gardner,J.Howard and T.C.Waddington, to be published

37 F.Volino,A.J.Dianoux and H.Hervet, J.de.Physique, Colloque 3, sup to no.6, 37, C3-55 (1976)

38 A.J.Dianoux,F.Volino,A.Heidemann and H.Hervet, J.de Physique, 36, 275 (1975)

39 W.Marshall and S.Lovesay, Theory of Thermal Neutron Scattering, Clarendon Press (1971)

40 G.E.Bacon, Neutron Diffraction, OUP (1962)

41 V.E.Turchin, Slow Neutrons, Jerusalem:Israel Program for Scientific Translations (1965)

42 F.Volino and A.J.Dianoux,New Developments in Neutron Scattering for the Study of Molecular Systems:Structure and Diffusive Motions, Euchem Conference (1976)

43 J.S.Higgins and G.Allen, Reports in Progress on Physics, 36, no.9, 1073 (1973)

44 R.E.Lechner, The Multichopper,IN5, Scientific Status Report (1973)

45 R.E.Lechner, IN5-User's Manual, ILL Int.Report 74L201T, (1975)

46 A.Heidemann, IN10-User's Guide, ILL Int. Tech.Report 78HEI44T (1978)

47 A.H.Baston, The Collection and Processing of Data from Three Time-of-Flight Spectrometers, AERE Report, M2570 (1978)

48 A.H.Baston and D.H.C.Harris, Neutron Beam Instruments at Harwell,AERE-R9278 (1978)

49 A.J.Dianoux, IN6-Progress Report ILL Report 78DI2123 (1978)

50 A.J.Dianoux, IN6-Progress Report ILL Report 79DI17T, (1979)

51 M.Birr,A.Heidemann and B.Aleford, Nucl.Instrum. Methods, 95, 435 (1971)

52 W.S.Howells and A.Heidemann, User's Guide to Processing of IN10 data, ILL Report 78HOI89T (1978)

53 W.S.Howells, Fourier Transformation and Deconvolution of IN10 Data (Aug 1979)

54 A.J.Dianoux, IN5 Program Package (1975)

55 J.Howard and T.C.Waddington, Advances in IR Spectroscopy, Vol VII, Ed. R.E.Hester and R.J.H.Clark, Haydon (1980)

56 R.M.Richardson, Notes on Some Quasi-elastic Neutron Scattering Analysis Programs on the Rutherford Laboratory IBM 360/195, Rutherford Report R-L-79-095 (1979)

57 J.D.Barnes, J.Chem.Phys., 58, no.12, 5193 (1973)

58 R.E.Ghosh, Computer Programs for Analysis of Neutron T.O.F Data, Rutherford Report R-L-74/552 (1974)

59 J.White, Chap.3, Chemical Applications of Thermal Neutron Scattering, Ed.B.T.M.Willis, OUP (1973)

60 G.Allen, Chap.5, Chemical Applications of Thermal Neutron Scattering, Ed.B.T.M.Willis, OUP (1973)

61 S.Fewster, Ph.D. Thesis, Manchester University, Dept.of Chemistry (1970)

62 P.R.Sundajararajan and P.J.Flory, J.Amer.Chem.Soc., 96, 16, 5021 (1974)

63 R.Lovell and A.H.Windle, Polymer,22, 175 (1981)

64 S.Havriliak and N.Roman, Polymer, 7, 387 (1966)

65 Sadtler Guide to the NMR Spectra of Polymers

66 T.R.Mandley and C.G.Martin, Polymer, 12, 524 (1971)

67 H.Tadohoro,Y.Chatani, H.Kusanagi and M.Yokoyama, Macromolecules, 3, 441 (1970)

68 D.I.Page, Chap.8, Chemical Applications of Thermal Neutron Scattering, Ed.B.T.M.Willis, OUP (1973)

69 R.M.Richardson,A.J.Leadbetter,D.H.Bonsor,G.J.Kruger, Molec.Phys., 40, no.3, 741 (1980)

70 H.Hervet,F.Volino,A.J.Dianoux and R.E.Lechner, Phys.Rev.Lett., 34, 451 (1975)

71 see, for example, V.J.McBrierty, Polymer, 15, 503 (1974)

72 T.P.Das, J.Chem.Phys., 27, 763 (1957)

73 J.G.Powles and H.S.Gutowsky, J.Chem.Phys, 21, 1695 (1953)

74 F.Apaydin and S.Clough, J.Phys.C., 932 (1963)

75 R.B.Davidson and I.Mivagawa, J.Chem.Phys., 52, 1727 (1970)

76 M.Bloom, Pure Appl.Chem., 32, 99 (1972)

77 P.S.Allen, J.Phys.C., 7, 22 (1974)

78 A.Huller and D.M.Kroll, J.Chem.Phys., 63, 4495 (1975)

79 A.Odajima,A.E.Woodward and J.A.Sauer, J.Polym.Sci., 55, 181 (1961)

80 C.D.Knutson and D.M.Speitzer, J.Chem.Phys., 45, 407 (1960)

81 R.Kosfeld and U.von Mylius, Kolloid-Z, 250, 1081 (1972)

82 S.Clough and J.R.Hill, J.Phys.C., 7, 1, 20 (1974)

83 S.Clough and B.J.Mulady, Phys.Rev.Lett., 30, 161 (1973)

84 J.L.Carolan, J.Phys.C., 5, 631 (1972)

85 S.Clough, Phys.Rev.Lett., 33, 1257 (1974)

86 S.Clough,J.R.Hill and F.Poldy, J.Phys.C., 5, 518 (1972)

87 J.S.Higgins to be submitted to J.Chem.Soc.

88 G.T.Knight, M.J.R.Loadman,B.Saville and J.Wildgoose, J.C.S.Chem.Comm., 193 (1974)

89 R.H.Hall,J.S.Higgins and K.Ma, in preparation

90 A.Z.Akcasu,M.Benmouna and C.C.Han, accepted by Polymer

91 P.Hadzi, Hydrogen Bonding, Pergamon Press (1957)

92 F.Heatley, Private communication

93 F.Heatley and A.Begum, Polymer, 17, 399 (1976)

94 G.Albernese,A.Deriu and C.Ghezzi, Il Nuovo Cimento, 51B , no.2 (1979)

95 G.Plazcek, Phys.Rev., 86, 377 (1952)

96 G.S.Rushbrooke, Introduction to Statistical Mechanics, OUP (1949)

97 C.Brot, Chem.Phys.Lett., 3, 319 (1969)